DESIGN AND SYNTHESIS OF NOVEL FLUORESCENCE CONSTRUCTS FOR THE DETECTION OF ENVIRONMENTAL ARSENIC

by

VIVIAN CHIBUZO EZEH

(Under the Direction of TODD C. HARROP)

ABSTRACT

Arsenic compounds are classified as group 1 carcinogens and the maximum contamination level in drinking water is set at 10 ppb by the United States Environmental Protection Agency. Methods currently approved for monitoring environmental arsenic are classified as colorimetric and instrumental methods. However, toxic byproducts (arsine gas and mercury) are formed in colorimetric methods, while instrumental methods require high maintenance costs. Therefore developing a sensitive, safe, and less expensive detection technique for arsenic is needed. One strategy involves the development of new imaging tools using small molecule fluorescent sensors, which will offer a sensitive and inexpensive method of arsenic detection in environmental samples. Emphasis will be on As(III) compounds because they are prevalent in the environment. To accomplish this goal, the coordination chemistry of As(III) was studied to discover new As(III) chemistry/preference for thiols. One finding from this work is the As(III)-promoted redox rearrangement of a benzothiazoline-containing compound to afford a four-coordinate As(III) complex and the benzothiazole analog. The knowledge gained was used to design two fluorescent chemodosimeters for As(III). The first generation sensors, named ArsenoFluors (AFs), were designed to contain a benzothiazoline functional group appended to a

coumarin fluorescent reporter and were prepared in high yield by multi-step organic synthesis. The sensors react with As(III) to afford a highly fluorescent coumarin-6 dye (benzothiazole analog), which results in a 20 – 25 fold increase in fluorescence intensity and 0.14 – 0.23 ppb detection limit for As(III) in THF at 298 K. In addition, the reaction is complete within 30 min and is selective for As(III) over other toxic ions such as Hg(II) and Pb(II). The sensors also react with a common environmental species of As(III), namely sodium arsenite, in a THF/CHES (1:1, pH 9) buffer mixture. However, the reaction is slower (time > 5 h) and the enhancement of fluorescence is modest (1.5- to 3- fold) due to the quenching of the coumarin dye in a high polarity solvent. Finally, the mechanism for the As(III)-promoted formation of the fluorescent benzothiazole compounds from the benzothiazolines is proposed.

INDEX WORDS: Arsenic, Fluorescence Detection, Environment, Sulfur

DESIGN AND SYNTHESIS OF NOVEL FLUORESCENCE CONSTRUCTS FOR THE DETECTION OF ENVIRONMENTAL ARSENIC

by

VIVIAN CHIBUZO EZEH

B.Sc, University of Ibadan, Nigeria, 2006

A Dissertation Submitted to the Graduate Faculty of The University of Georgia in Partial Fulfillment of the Requirements for the Degree

DOCTOR OF PHILOSOPHY

ATHENS, GEORGIA

2013

DESIGN AND SYNTHESIS OF NOVEL FLUORESCENCE CONSTRUCTS FOR THE DETECTION OF ENVIRONMENTAL ARSENIC

by

VIVIAN CHIBUZO EZEH

Major Professor:	Todd C. Harrop
Committee:	Michael K. Johnson
	Jason Locklin

Electronic Version Approved:

Maureen Grasso
Dean of the Graduate School
The University of Georgia
August 2013

DEDICATION

I dedicate this work to Prof. Kehinde Okonjo, for motivating me to pursue a career in Chemistry.

ACKNOWLEDGEMENTS

I owe the successful completion of my graduate studies to the role of several people that have assisted me along the way. I appreciate Prof. Todd Harrop for the opportunity to work in his research group and for being an amazing teacher and mentor. Members of my advisory committee, Prof. Michael Johnson and Prof. Jason Locklin, provided useful feedback that helped me improve on my research, writing and presentation skills. Thank you.

Former and present members of the Harrop's research group; Dr. Ashis Patra, Dr. Eric Gale, Wren Cheatum, Koustubh Dube, Brian Sanders, Melody Rhine, Phan Truong, Ellen Broering, Ramsey Steiner and Emily Betchy, thank you for creating a collegial work environment where I could thrive in my studies. Furthermore, I thank the Chemistry Department at the University of Georgia for an excellent education and the faculty and staff for support and assistance during my studies.

I thank my parents; Mr. and Mrs. Ezeh, my brothers; Chinedu and Chike, and extended family for their support. Also, my friends: Barr. Funmi Alonge, Dr. Bo Zhang, Dr. Simon Owino, etc. for providing companionship and assistance during my graduate studies program.

Finally, financial support for my research was provided by the University of Georgia Research Foundation and National Research Foundation. Dissertation year support was provided by Kenyon College, where I was provided the space to write my dissertation. Thank you.

TABLE OF CONTENTS

Page

LIST OF TABLES

Page

LIST OF FIGURES

Page

CHAPTER 1

INTRODUCTION AND LITERATURE REVIEW

1.1 General Introduction to Arsenic

1.1.1 Brief history and discovery of arsenic

The name arsenic is derived from the Greek word "arsenikon," which means 'potent' or 'masculine' and is inspired from the extensive use of arsenicals in ancient medicine and other materials.[1] Arsenic played an important role in ancient alchemy and metallurgy. For example, in the Bronze Age copper-alloys containing arsenic minerals were sought after because of their higher ductility and the silvery sheen of the finished product.[2] Other ancient applications of arsenic compounds include their use as depilatories in the leather industry, in pigments to achieve a gold/yellow or red color and as an active ingredient in most ancient medicines.[1] The German alchemist, Albert Magnus (1193 – 1280) is credited with the first discovery of elemental arsenic, which he achieved by heating soap and arsenic trisulfide (As_2S_3) in 1250.[3] Other scientist's that have contributed to the discovery of arsenic compounds include, (i) Geber (Jabir ibn-Hayyan, 760 - 815), an Arabian alchemist that discovered arsenic trioxide (As_2O_3) by heating arsenic trisulfide (As_2S_3),[4] (ii) Avicenna (Ibn-Sina, 980 – 1037), a Persian polymath who described the difference between white (As_2O_3), yellow (As_2S_3), and red (As_2S_2) arsenic minerals, and (iii) Vannoccio Biringuccio (1480 –c.1539), an Italian metallurgist who made a clear distinction between elemental arsenic and arsenic minerals.[4] The discovery of arsine gas (AsH_3) by Swedish chemist Carl Willhelm Scheele in 1775 was the basis for the later development of the Marsh test for detecting arsenic compounds. The discovery of arsenic

compounds by these scientists was a hazardous process as many of them paid a toll with their health.[1]

1.1.2 Occurrence and general properties of arsenic

Arsenic (As) is a member of the pnictogens (pnictogens is derived from the Greek word "pnigein" which means "to choke" from breathing pure $N_2(g)$[3]) found in group 15 of the periodic table. The element exists in several different allotropes, with the common ones being metallic grey, yellow, and black arsenic.[5] Arsenic has one stable isotope, ^{75}As, which occurs in 100% abundance in all natural sources.[6] Its abundance in the crust of the earth is estimated at 2 ppm and it is commonly found associated with chalcogens (S, Se and Te) rather than oxides and silicates.[7] Ores of arsenic are not mined specifically for the element, but are obtained as a by-product of the mining of Cu, Ag, Au, etc. Common minerals include the sulfides: realgar (As_4S_4), orpiment (As_2S_3) and arsenopyrite (FeAsS); the oxide, arsenolite (As_2O_3) and arsenides, löllingite ($FeAs_2$) and domeykite (Cu_3As).[8-9]

1.1.3 Atomic and orbital properties of arsenic

One of the defining characteristics of the pnictogens is their valence electronic configuration i.e. five electrons in their outermost shell for an ns^2np^3 configuration. Arsenic (atomic mass = 74.9216 g/mol) has atomic number 33 and its electronic configuration is $1s^22s^22p^63s^23p^63d^{10}4s^24p^3$. Much of the chemistry of arsenic can be interpreted on the basis of its $4s^24p^3$ (^4S term symbol) three singly-occupied orbital in its ground-state electronic configuration.[10] The common oxidation states are -3, 0, +3 and +5, though other oxidation states like +1 and +2 have also been reported.[11-14] The first ionization energy of 947 kJ/mol is high and expected since the valence *p* electrons are in separate orbitals according to Hund's rule of maximum spin multiplicity which results in a half-filled subshell.[10] The electron affinity of 78

kJ/mol and Pauling scale electronegativity values of 2.18 reflects the metalloid character of As.[15] The observed or calculated atomic, covalent and ionic radii of As depends on the oxidation state and are listed in Table 1.[7, 16-17]

Table 1. Size properties of arsenic (Å)

Atomic radius (Calculated value)[18]	1.15 (1.14)
Covalent radius (2008 values)[19]	1.19
Molecular single bond covalent radius (CN = 3)	1.21
Molecular double bond covalent radii	1.14
Molecular triple bond covalent radii	1.06
van der Waals radius	1.85
Ionic radius (three-coordinate, trigonal-pyramidal As(III))	0.58
Ionic radius (six-coordinate, O_h As(III))	0.72
Ionic radius (four-coordinate, T_d As(V))	0.48
Ionic radius (six-coordinate, O_h As(V))	0.60

1.1.4 Chemical Properties

Arsenic has chemical properties that are between that of metals and non-metals, hence they are classified as metalloids. The arsenic-oxides are acidic in nature as expected for a non-metal. For example, arsenate [H_3AsO_4] is a tribasic acid with a $pKa_1 = 2.2$. Furthermore, As can form binary compounds with various metals (e.g. Na_3As) which are named arsenides. In these intermetallic compounds, As acts as the electron acceptor and ligand.[17] Conversely, As readily forms strong covalent bonds to most non-metals (oxides, halides, sulfides, carbon-based ligands, etc.), as seen from some experimentally determined bond dissociation energies of As-element diatomic species in the gas phase (Table 2). Although the As-center is assigned a positive oxidation number in compounds with non-metals, free As-cations (As^{3+} or As^{5+}) do not exist in solution.[16] The difference in electronegativity compared to non-metal ligands results in polarization of the covalent bond ($As^{\delta+}$---$X^{\delta-}$), thus making As the electropositive element.[20]

Table 2. Experimentally determined As – Element bond energies in the gas phase (kJ/mol)[17]

As – H	274 ± 2.9	As – S	379.5 ± 6.3
As – N	489 ± 2.1	As – Cl	448
As – O	484 ± 8	As – As	385.8 ± 10.5
As – F	410	As – I	296.6 ± 24
As – P	433.5 ± 12.6		

1.1.5 Structure and Bonding

As is dominantly a trivalent ion and forms three electron-pair bonds with its 4p orbitals, leaving the $4s^2$ lone pair in a non-bonding orbital.[10] Hybridization of the 4s and 4p orbitals are not common because of the spatial incompatibility of these orbitals. Hence, the bond angles in the tri-coordinate As-compounds are closer to 90° which represent pure p-orbital overlap.[21] When hybridization occurs, the number of bonds to the As-center increases and results in compounds with trigonal-bipyramidal, square pyramidal or octahedral geometries.[10] A representation of possible bonding environments for the As-center is depicted in Chart 1. While structures A – C are common for As(III), structures D – F are primarily observed in As(V) compounds.

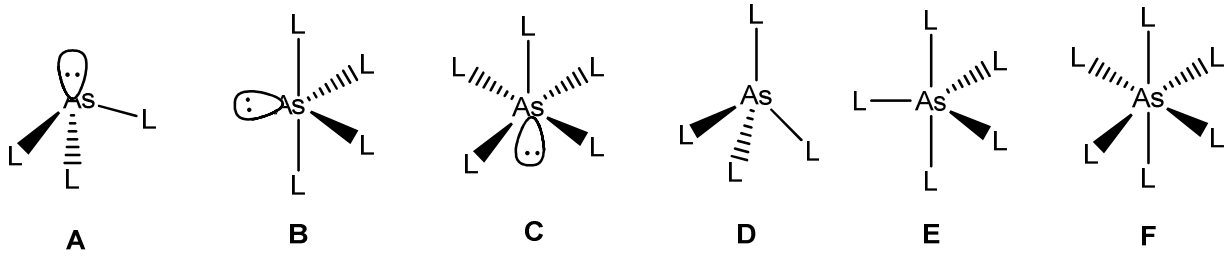

Chart 1. Structural depiction of geometries observed in As-compounds. A = trigonal pyramidal, B = pseudo trigonal bipyramidal, C = square-based pyramidal, D = tetrahedral, E = trigonal bipyramidal and F = octahedral.

1.1.6 Classification of arsenic compounds

Compounds of As (often times referred to as arsenicals) are generally classified as either inorganic (iAs) or organic in nature based on the type of ligand bound to the As center.

Organoarsenicals have at least one bond to a carbon-based ligand such as a methyl or phenyl group while iAs have no carbon-based ligand but contain ligands with chalcogen or halide groups (e.g. O^{2-}, S^{2-}, RS^{-}, X^{-}). Another difference is that while most iAs occur naturally in the environment (e.g. arsenite [$As(OH)_3$] and arsenate [$O=As(OH)_3$]), the organoarsenicals are formed as metabolic products of iAs by bacteria, fungi, plants and even higher animals.[20, 22-24] Chart 2. gives the structure of some common As compounds found in the environment.

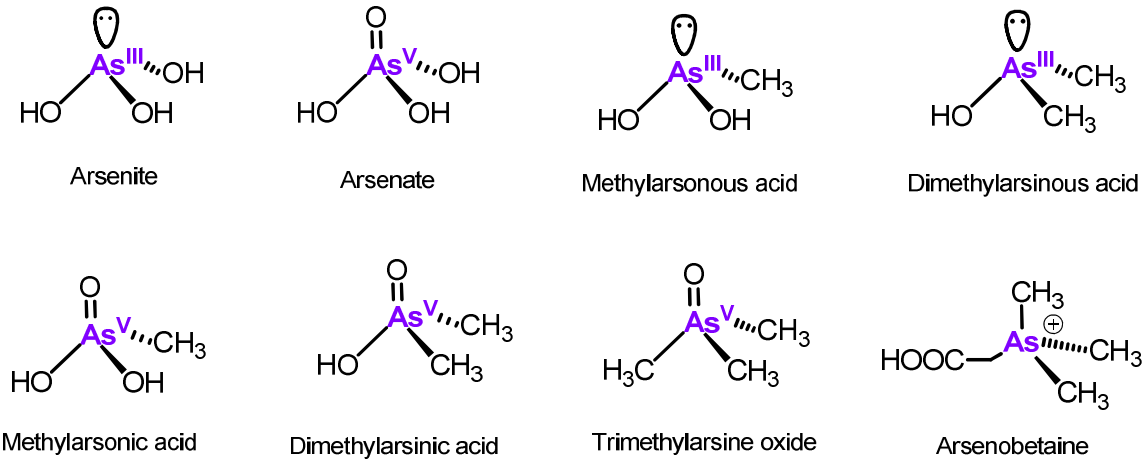

Chart 2. Examples of arsenicals found in the environment.

1.1.7 Uses of Arsenic compounds

1.1.7.1 Medicine. Arsenicals have been used since ancient times for the treatment of several ailments. In 1786, Thomas Fowler, an English physician proposed the use of a 1% solution of $KAsO_2$ (now known as Fowler's solution) for the treatment of skin diseases, blood diseases (anemia, leukemia and Hodgkin's disease), malaria and several other ailments.[25] The use of Fowler's solution was discontinued in the United States in the late 1950's because of its side effects, which include cirrhosis of the liver/bladder and skin cancers. In the 19th century, the focus turned to using organoarsenicals in medicine because they were thought to be less toxic than inorganic arsenicals. For example, arsenate analogs such as sodium cacodylate

($Na[(CH_3)_2AsO_2]$) and atoxyl (see Chart 3), were used in place of Fowler's solution for the treatment of malaria, sleeping sickness and pellagra, but were later found to be very toxic.[25] Inspired by the effectiveness of atoxyl but seeking a drug that will have minimal effects on body tissue, Paul Ehrlich and coworkers designed and synthesized various organoarsenicals in a quest to discover a silver bullet against syphilis.[26]

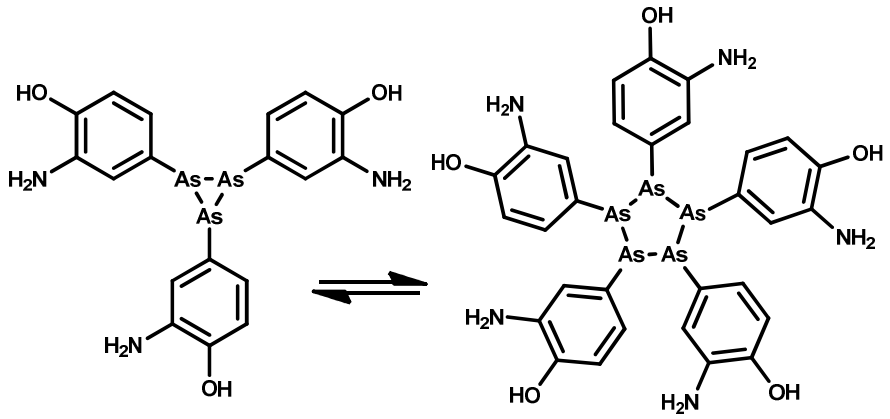

Arsphenamine is proposed to be a mixture of cyclic trimers and pentamers

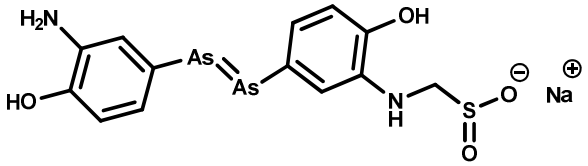

Neoarsphenamine

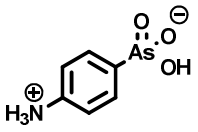

Atoxyl

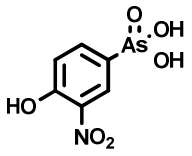

Roxarsone

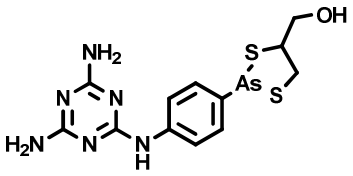

Melarsoprol

Chart 3. Organoarsenicals used in medicine and agriculture.

In 1907, Ehrlich's compound 606 called arsphenamine (also called salvarsan, see Chart 3) was found to be very effective against syphilis. However, it was not very water soluble and the solution was unstable in air. Neoarsphenamine (neosalvarsan, see Chart 3) was later

introduced, it was more water soluble but less effective compared to arsphenamine. Injections of arsphenamine/neoarsphenamine in combination with bismuth were used for the treatment of syphilis and yaws before the advent of penicillin in the 1940's.[27] Indeed, the advent of chemotherapy is attributed to the work of Ehrlich and coworkers to improve the efficacy of a drug by systematic chemical modification.[27] Despite the side effects associated with arsenic drugs, some are the last line of defense against a number of human and veterinary ailments. For example, a proprietary formula of arsenic trioxide (As_2O_3) is used to treat acute promyelocytic anaemia,[28] while atoxyl and melarsoprol are used for treating trypanosomiasis (sleeping sickness) and Chagas disease.[29]

1.1.7.2 Agriculture. The use of arsenic compounds as insecticides and herbicides was important for the advancement of agriculture. Arsenicals were popular because of their toxicity to a wide variety of insects, bacteria, fungi, weeds and were obtained cheaply as by-products of mining.[1] Inorganic arsenicals such as copper arsenate (Paris Green), calcium arsenate and lead arsenate were used extensively as insecticides, but were later replaced by dicholordiphenyltrichloroethane (DDT) in 1947 because the pests developed resistance to these arsenicals.[30] The organoarsenicals, monosodium methylarsonate ($Na[H_2AsO_4]$) and disodium methylarsonate ($Na_2[HAsO_4]$) were also used as herbicides especially in cotton plantations.[31] Although the toxicity of these organoarsenicals is low, they are ultimately biodegraded into the more toxic inorganic form.[32] Over the years, the spraying of over 1 billion pounds of arsenical pesticides on American crops has left a legacy of contaminated soils and groundwater.[1] Arsenicals were also used in animal husbandry from the early 20th century, organoarsenicals such as roxarsone and atoxyl (Chart 3) were added to animal feeds to promote growth by eradicating parasites and preventing dysentery.[32-33] This practice, which was only discontinued

recently in 2011, has created concern over As contamination the in environment as an estimated 20-50 metric tons of roxarsone in chicken litter has been used as fertilizer.[34]

1.1.7.3 Military. Compounds of arsenic have also played a major role as effective war agents. Lewisite ($ClCHCHAsCl_2$) was used as a highly effective killing agent in World War I. It hydrolyzes to produce HCl, which caused blisters that were difficult to heal.[35] Agent Blue (a mixture of cacodylic acid, ($[(CH_3)_2HAsO_2]$) and sodium cacodylate, ($Na[(CH_3)_2AsO_2]$)) was used to defoliate and dessicate forests in the Vietnam War.[36] As is also popular for its role as an inheritance poison. Arsenic oxide (As_2O_3) was used as the ideal murder or suicidal weapon in the middle ages. Poisoning from this tasteless and odorless powder showed symptoms that were similar to cholera thereby masking the true cause of death. This practice was discouraged by the introduction of the Marsh test for detecting low levels of arsenic in 1836.[37]

1.1.7.4 Electronics. Alloys of As with Pb, Cu, Ga, Si or Al have several important uses in the electronics industry. For example, the lead storage battery used in cars and trucks contain alloys of lead and arsenic. Also, GaAs and As-doped silicon are very important semiconductor materials, which are used extensively in communication products such as mobile phones, GPS navigation units and light emitting diodes (LEDs).[38-40]

1.1.7.5 Wood Treatment. Arsenicals are also utilized to preserve wooden structures from fungi and wood attacking insects such as termites and marine borers. Examples of arsenicals used for this purpose include chromate copper arsenate (CCA, a mixture of CuO, As_2O_5 and CrO_3 in varying ratios) and ammoniacal copper arsenate. Wooden structures treated with these arsenicals are referred to as pressure-treated and are durable. However, in acidic environments the arsenic can leach and thus contaminate the soil.[41] The use of pressure-treated wood is now discouraged in residential and playground structures in order to minimize its toxicity.[42]

1.1.7.6 Analytical Chemistry. Arsenicals have been used as dyes for the spectrophotometric analysis of various analytes. Arsenazo I and III (see Chart 4) are As-based metallochromic indicators that were utilized for the detection of various metal ions such as Zn(II), Ca(II), and U(VI).[43-47] The dyes react with the metal ions and give rise to intensely colored metal complexes that can be measured with a spectrophotometer. For example, aqueous solutions of Arsenazo III has an absorption maxima at 550 nm (pH 2 – 10) with molar absorptivity values of ~ 30,000 $M^{-1}cm^{-1}$.[44] Upon reaction with Zn(II), a blue 1:1 complex with absorption maxima at 590 nm (pH 9) results with a linear detection range of 0.14 – 1.26 ppb.[45] Development of new colorimetric/fluorescent metal sensors has led to decline in the use of Arsenazo I and III.

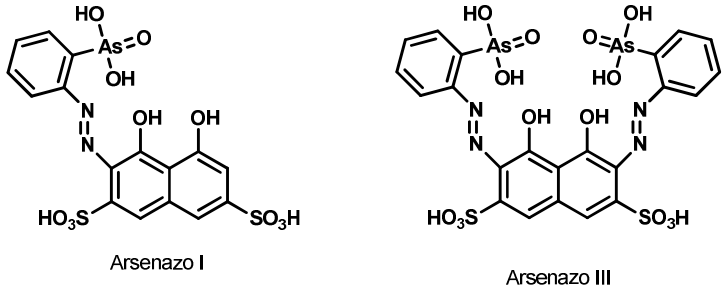

Chart 4. Structural depiction of Arsenazo I and III used as metallochromic dyes in analytical chemistry.

Another important analytical application is the use of the As-based fluorophores, FlAsH-EDT_2 and ReAsH-EDT_2 (see Chart 5), to label proteins tagged with a tetracysteine (CCXXCC, where X is a non-cysteine amino acid) sequence.[48-49] The dyes contain either a fluorescein or resourfin group bound to As(III) while the 1,2-ethanedithiol acts as a protecting group for As(III). The dyes are non-fluorescent (e. g. Φ_f (FlAsH-EDT_2) = 0.0005), but when they react with an appropriately tagged protein, the 1,2-ethanedithiol group is exchanged to form a brightly emissive dye-protein complex (e. g. Φ_f (FlAsH-protein) = 0.49, λ_{ex} = 508 nm and λ_{em} = 528

nm).[48] Some advantages of using FlAsH-EDT_2, ReAsH-EDT_2 and their analogs include: (i) the small size doesn't perturb the protein folding significantly; (ii) the high affinity for the tetracysteine tag; and (iii) the dyes are membrane-permeble.[49] FlAsH-EDT_2, ReAsH-EDT_2 and their analogs are applied to the study of protein folding, protein-protein interactions and fluorescence anisotropy measurements.[50]

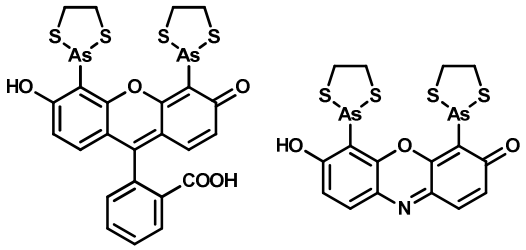

FlAsH-EDT_2 ReAsH-EDT_2

Chart 5. Structural depiction of FlAsH-EDT_2 and ReAsH-EDT_2.

1.2 Arsenic in the Environment

1.2.1 Arsenic cycle

Arsenic is ubiquitous in the environment and the speciation of arsenic compounds depends on the redox potential, pH and microorganism activities.[51] In aquatic systems, arsenicals are interconverted by a series of oxidation-reduction, ligand exchange, precipitation and adsorption reactions. These processes contribute to make the concentration of As species in the environment dynamic.[52]

An E_h-pH (E_h = the redox potential of an environment vs SHE) diagram obtained from available thermodynamic data shows the predominant iAs species in aqueous environments under different conditions (Figure 1). In oxygenated waters with high E_h values, analogs of the As(V) compound arsenate are prevalent and stable.[20, 53-55] When environmental conditions become slightly reducing and anoxic, the As(III) compound arsenite dominates. The As

oxyanions readily interconvert and hence the common arsenicals present in drinking water (neutral pH and $E_h \geq 0$ V) are the mono and di protonated versions of arsenate ($H_2AsO_4^-$ and $HAsO_4^{2-}$) and arsenite ($As(OH)_3(aq)$).[8, 56] In a highly reducing environment ($E_h \leq -0.1$ V at pH $\leq$ 7), arsine ($AsH_3(aq)$) can be formed.

The presence of hydrated manganese, aluminum and especially iron oxides in sediments has an effect on the mobility of arsenate species in aqueous environments. Minerals like ferrihydrite and alumina are known to adsorb arsenate species, thus making them less mobile compared to arsenite species.[37, 57-58] However, bacterial reduction of Fe(III) to Fe(II) can release the bound arsenate, making it available for further chemical or biological reactions and contamination of water sources.[59]

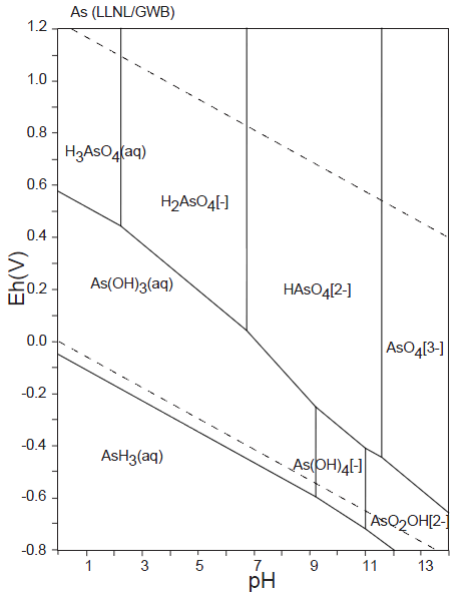

Figure 1. E_h-pH diagrams of inorganic arsenic compounds in aqueous systems at 298.15 K and 10^5 Pa based on data from the Lawrence Livermore National Lab using the Geochemist's Workbench. Total concentration of elements is 10^{-10} mole/kg. Dashed lines are the stability fields of water at 298 K, 10^5 Pa.[60]

Although arsenic compounds are toxins for most organisms, some microbes utilize arsenate as their respiratory oxidant.[61] For example, two closely related ε-Proteobacteria, *S.*

arsenophilum and *S. barnesii*, couple the reduction of As(V)-to-As(III) to the oxidation of lactate as an energetically favorable process (ΔG^o = -295 kJ/mol lactate).[37] The enzyme involved in respiration is a molybdenum enzyme of the DMSO reductase family.[37, 55, 62] Conversely, several microbes couple the oxidation of arsenite to the reduction of either oxygen or nitrate and use the energy derived to fix CO_2 into organic cellular materials and achieve growth.[37] Microbes also play an important role in the cycling of organoarsenicals in the environment (Figure 2). Methylated arsenic compounds like monomethylarsonic acid and dimethylarsonic acid (see Chart 2), are formed when arsenite accepts a methyl group from S-adenosylmethionine.[63] This detoxification pathway, present in some bacteria and higher eukaryotes, is catalyzed by the enzyme As(III)-methyltransferase (*AS3MT*).[63-64] Other microbes reverse the process and degrade organoarsenicals to iAs.[65] In marine animals and algae, iAs is converted to arsenobetaine, arsenocholine and arsenic-containing sugars; these organoarsenicals are benign compounds.[8, 20, 66-68] In summary, the cycling of As is a complex process and poses a challenge to predicting the behavior of As in the environment, which is important for applying an effective remediation methodology.

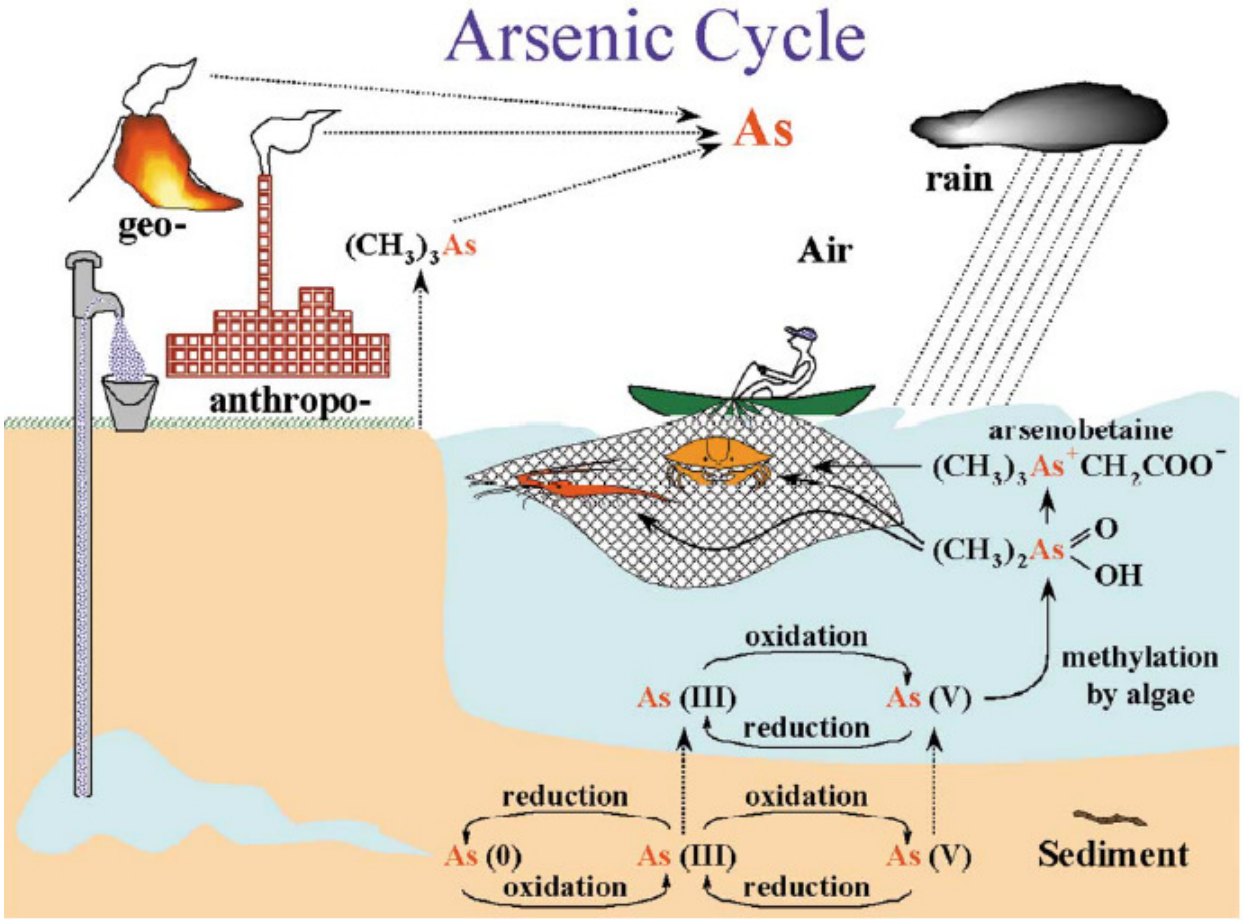

Figure 2. Arsenic global geocycle (Reprinted by permission of John Wiley and Sons).[69]

1.2.2 Sources of contamination

Contamination of the environment by arsenicals emanate from both natural and anthropogenic sources. The high levels of As in saline lakes such as Mono Lake in California are results of hydrothermal activities. Hydrothermal fluids originate in the subsurface with a temperature range of 50 – 600 ^{o}C and extracts As from magma and hot subsurface rocks. As the temperature of the fluid cools below 50 ^{o}C, the As compounds are deposited and thus contaminate the groundwater.[70] In Bangladesh and West Bengal, the high incidence of As-poisoning is a result of the high levels (up to 2000 ppb) of arsenicals in groundwater used as a source of drinking water. It is proposed that the microbial activities in the As and Fe-rich alluvial

aquifers is the source of the high levels of As.[71] Anthropogenic sources of As include mining,[51] industrial operations[72] and agricultural activities. Arsenicals are the unintended by-product of Cu and Fe mining introducing approximately 62,000 tons of As annually into the environment.[22, 73] These activities explain the high concentration of As in the soil and water of mining communities.[58, 74-75] Industrial operations such as coal combustion, hide-tanning and pressure-treating wood also serve as a source of environmental As contamination.[22] Additionally, the former use of arsenicals as insecticides and pesticides was a significant source of As contamination. Approximately 10,000 metric tons/yr of calcium arsenate and dimethylarsonate were used as pesticides from 1930 – 1980.[76] Roxarsone (see Chart 3), for many years was used as an addictive in swine and chicken feed to prevent intestinal worms. This practice was only recently discontinued in 2011.[32-33] It has been estimated that the poultry industry on the east coast of the United States used 20 to 50 metric tons of roxarsone annually.[77] Roxarsone is excreted mostly unchanged and is a source of As when the waste is used in fertilizers as it is eventually biodegraded in the environment to give iAs compounds.[32-33, 78-82]

1.2.3 Levels in the environment

The concentration of arsenicals in the environment varies considerably with the geological composition and level of anthropogenic input in the location.[83] Levels of As in soils can range between 100 – 40,000 ppb (1 ppb = 1 μg/kg) depending on the geographic location (Table 3).[84] Unpolluted freshwater As levels vary from 1 – 10 ppb (1 ppb = 1 μg/L) and can increase to 100 – 500 ppb in areas with mining activities.[75, 84-85] Levels in seawaters are generally lower and can range from 1 – 8 ppb.[86] In many communities groundwater has increasingly become a source of drinking water, but this water source can also be contaminated with As. For example, a survey of approximately 31,000 private wells in the U. S. by the U. S. Geological

Survey (USGS) shows the average concentration of As in the groundwater system (Figure 3).[87] The levels reflect the different geological make-up of the environment with levels up to 50 ppb in places with high hydrothermal activities such as California.[76]

Table 3. Arsenic content in the soils of various countries.[84]

Countries	Sample size	Range (ppb)	Mean (ppb)
United States	1215	1,600 – 72,000	7,500
Bangladesh	10	9,000 – 28,000	22,100
West Bengal, India	2235	10,000 – 196,000	-
Italy	20	1,800 – 60,000	20,000
Japan	358	400 – 70,000	11,000
Mexico	18	2,000 – 40,000	14,000
China	4095	10 – 626,000	11,200

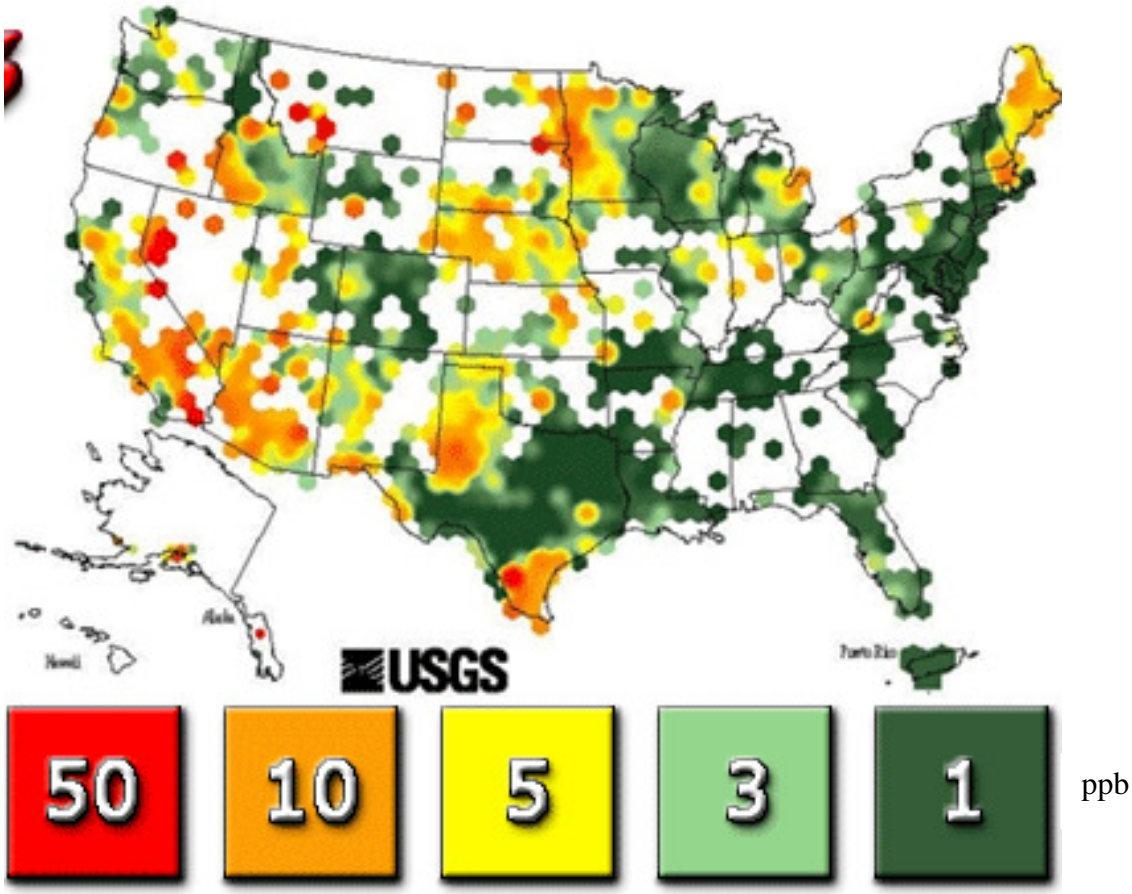

Figure 3. USGS map of arsenic in groundwater of the United States.[87]

1.3 Toxicity of Arsenic Compounds

1.3.1 Toxicity of As(III) compounds

The toxicity of As(III) compounds (e.g. $[As(OH)_3]$ and $[CH_3As(OH)_2]$) can be attributed to the strong bond the soft metalloid forms with thiol functional groups.[37, 88] The binding constants (β) of arsenite and monomethylarsonous acid with common thiol-containing biomolecules (Chart 6) have been obtained by spectrophotometric titration measurements and are listed in Table 4.[89] Arsenite is transported into the cell as a neutral molecule at pH 7 by transport proteins such as aquaglyceroporins (AQPs) in microbes and mammals or nodulin26-like intrinsic proteins (NIPs) found in plants.[90-94] Analysis of EXAFS data indicate that at pH 7, $[As(OH)_3]$ retains its coordination to three hydroxide ligands during cellular uptake.[95] Inside the cell, $[As(OH)_3]$ can form complexes with a variety of biomolecules that can either enhance its toxicity or aid in its expulsion from the cell. For example, glutathione (GSH), an abundant tripeptide (mM) that aids in maintaining cellular redox balance, contains a thiol group that can displace the hydroxyl donors in arsenite to form the tri-coordinate complex, $[As(SG)_3]$ (see Chart 1 for general coordination geometry).[96] Furthermore, the activity of proteins with key Cys residues or dithiolate cofactors are inhibited upon reaction with $[As(OH)_3]$.[97-99] For instance, pyruvate dehydrogenase contains dihydrolipoic acid (see Chart 6) as a cofactor and catalyzes the transformation of pyruvate to acetyl-CoA. A strong complex is formed between $[As(OH_3)]$ and dihydrolipoic (Scheme 1) with a measured stability constant of log $\beta_{2:3}$ = 18.6. Inhibition by micromolar concentrations of As(III) can affect energy production in the cells. Other effects of As(III) toxicity include: misfolding of proteins with key Cys residues, changes in cellular redox levels leading to an increase in oxidative stress, and prevention of DNA repair.[98, 100-101] Organic As(III) compounds such as monomethylarsonous acid are generally more toxic compared to

arsenite because they form slightly stronger bonds with thiol-containing biomolecules.[99, 102] The toxicity of these arsenicals is most evident in their LD_{50} values of 4.5 mg/kg (mouse) and 3.6 mg/kg (hamster) for arsenite and $CH_3As(OH)_2$, respectively.[93]

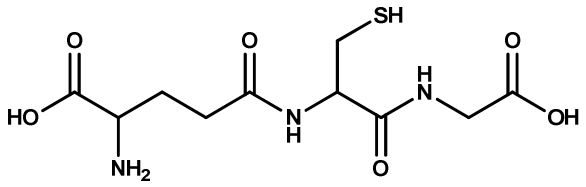

Glutathione

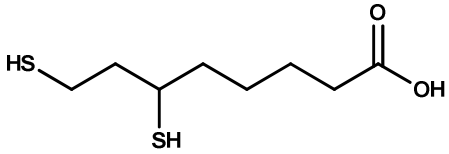

Dihydrolipoic acid

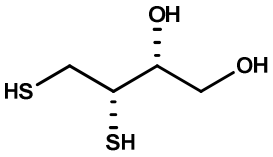

Dithiothreitol

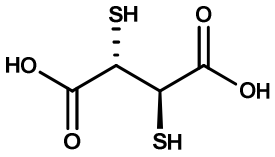

Meso-2,3-dimercaptosuccinic acid

Chart 6. Structures of common thiol-containing biomolecules that bind As(III).

Table 4. Overall Stability Constants of As(III)-thiolate Complexes Obtained from Best Fits of Near-UV Spectral Titration.[89]

	Arsenite		Monomethylarsonous acid	
Thiol Biomolecules	logβ	Ratio (As:RSH)	logβ	Ratio (As:RSH)
Glutathione	7	1:3	7.36	1:2
Dimercaptosuccinic acid	9.70	1:2	5.43	1:1
Dihydrolipoic acid	18.60	2:3	6.51	1:1
Dithiothreitol	6.04	1:1	6.30	1:1

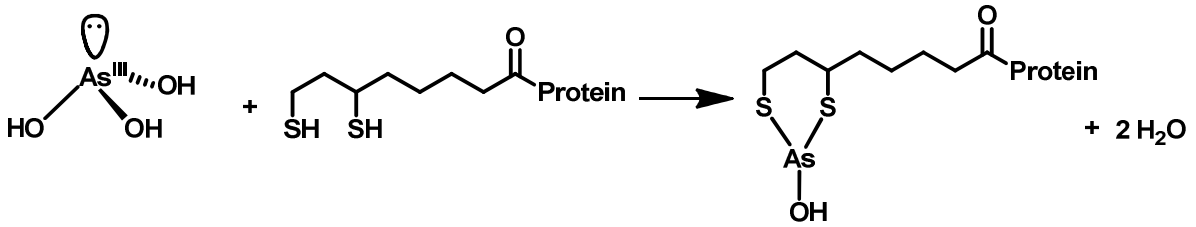

Scheme 1. Reaction of arsenite and dihydrolipoic acid, the reduced cofactor in pyruvate dehydrogenase complex, to form the inactivated protein complex.

1.3.2 Toxicity of As(V) compounds

Arsenate is a molecular analog of phosphate and enters the cell via phosphate transporters.[93] The toxicity associated with arsenate can be explained by two mechanisms. First, arsenate can be reduced to the more toxic arsenite by arsenate reductases[93, 103-104] or thiol biomolecules such as lipoic acid.[96, 105-107] Conversely, arsenate inhibits glycolysis, which is life's main energy generation system by replacing one phosphate group in the formation of 1,3-bisphosphoglycerate. The 1-arseno-3-phosphoglycerate formed is quickly hydrolyzed without generating ATP (Scheme 2).[108] The LD_{50} value for arsenate in mouse is estimated at 14 – 18 mg/kg.[93]

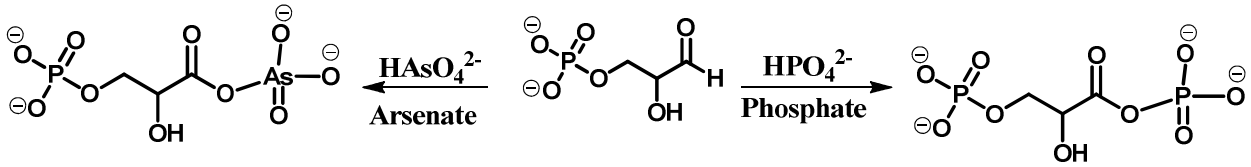

1-Arseno-3-phosphoglycerate
Nonenzymatic spontaneous hydrolysis preventing ATP formation

Glyceraldehyde-3-Phosphate

1,3-Diphosphoglycerate
Additional process leading to formation of ATP

Scheme 2. Arsenate can temporarily replace phosphate thereby reducing energy production via glycolysis.

1.3.3 Health problems associated with arsenic toxicity

Arsenic compounds are classified as group 1, nonthreshold carcinogens because there is no estimated safe dose.[109] The effect on human health depends if arsenic exposure is acute or chronic. Acute ingestion of arsenicals can lead to multisystem organ failure and eventually death as soon as 30 min after exposure.[72, 110] Chronic exposure, which involves ingestion of small amounts of arsenic over a long period of time, increases the risk of cancer of the liver, bladder and lungs. Arsenicosis, a skin condition which manifests as patches on the skin, as well as

hardening and lesions, is also caused by prolonged exposure to arsenic.[72] Effects on the gastrointestinal tract, respiratory tract, skin, liver, cardiovascular system, hematopoietic system, nervous system etc. are also observed.[84]

1.4 Coordination Chemistry of As(III)

Most of the toxicity associated with As relates to exposure to As(III) compounds. Hence, knowledge of the coordination properties of As(III) will aid in the design of appropriate receptor molecules for this metalloid. As(III) forms various types of coordination compounds. Being a soft metalloid, most of these complexes contain ligands with soft donors such as sulfur. In recent years, new and interesting complexes of As(III) have been reported in the chemical literature. These studies which are fascinating from a structure and bonding point of view also give insight into the *in vivo* interaction of As(III) with biological ligands.

The coordination number in As(III) complexes can range from one to six. The nature of the ligands used in the coordination chemistry studies plays an important role on the type of coordination geometry observed. The geometries reported from X-ray structural analysis include: linear (one-coordinate), bent (two-coordinate), trigonal-pyramidal (three-coordinate), Ψ-trigonal-bipyramidal (four-coordinate; Ψ = pseudo, because the lone pair is considered in determining the geometry) and octahedral (six-coordinate).[12-13, 15, 111-120]

The most common coordination geometry is trigonal-pyramidal, where the ligands occupy the trigonal base with the As(III) $4s^2$ lone pair in the apical position where it plays a role in controlling the geometry, i.e. a stereochemically active lone pair (Chart 1).[117-118] This geometry is used to describe complexes between As(III) and monodentate thiolate ligands such as cysteine or glutathione (GSH), $[As(SR)_3]$. Previous work has shown, that $[As(SG)_3]$ is

preferentially formed when As(III) reacts with GSH, and this complex has been characterized by ^{1}H and ^{13}C NMR, MS, UV-vis, potentiometry and calorimetric methods.[89, 96, 105, 121-124] The UV-vis spectrum of [$As(SR)_3$] complexes (where SR = Cys or GS) feature a broad peak between 260 – 320 nm in pH ~ 7 buffered solutions with ε ~ 500 – 2000 $M^{-1}cm^{-1}$.[121, 124] This peak has been assigned as a sulfur-to-arsenic charge-transfer and its near-UV maxima account for the pale-to-yellow solution color of As(III)-thiolate complexes.[89, 121, 124] Although, As(III) has a high affinity for monothiols (for example, formation constant of [$As(SG)_3$] is log β_3 = 7.0),[89] the ligands are readily exchanged for dithiol groups especially when a chelate or an insoluble complex is the end-product; this process is labeled as transthiolation.[89, 106, 125-126]

The reported crystal structures of As(III) complexes with dithiol ligands such as dithioerythritol (dte) and dithiothreitol (dtt) provides insight to how As(III) binds to dithiols such as lipoic acid *in vivo* (Figure 4 shows the structure of [$As(H_{-3}dte)$]). The geometry of these complexes is described as trigonal-pyramidal with the –S and –O donors in the trigonal plane. The As-S (~ 2.25 Å) and As-O (~1.83 Å) bond lengths are consistent with single bonds while the bond angles within the trigonal base approaches 90º, which indicates repulsion between the lone pair and bond pairs (see Figure 4).[121, 127] This X-ray structure shows that a ligand poised to bind As(III) in its preferred trigonal-pyramidal geometry will form strong complexes with the metalloid.

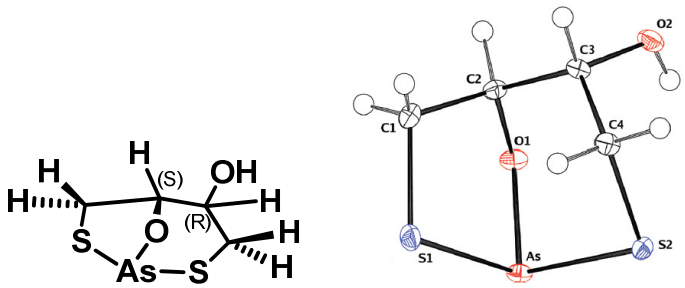

Figure 4. Structural depiction (left) and ORTEP diagram (right) of [As(H_{-3}dte)], where dte = dithioerythritol. Selected bond lengths (Å) and angles (º): As – S1: 2.2524(4); As – S2: 2.2579(4); As – O1: 1.8200(8); S1 – As – S2: 100.08(1); S1 – As – O1: 90.12(2); S2 – As – O1: 96.01(2) (Reprinted by permission of American Chemical Society).[121]

For As(III)-complexes with coordination numbers greater than three, secondary bonding interactions (SBIs) begin to play a role in the stability and geometry of the complexes. SBIs are weak attractive forces between main group metals and heteroatoms such as O, N, S, halogens or phenyl groups with interatomic distances less than the sum of the corresponding van der Waals radii (2.7 – 3.2 Å).[128-130] For example, the effect of SBIs can be observed in the As(III) complex, [$S(C_6H_4S)_2AsX$], where $S(C_6H_4S)_2$ = 2,2'-thiodibenzenethiolate and X = Cl, Br, I (Figure 5).[120] The distance between the thioether-S and As(III) is 2.705 (3) Å in the chloride complex, which is less than the sum of the van der Waals radii (3.8 Å), hence it is proposed to be an SBI. The geometry of this four-coordinate complex is described as distorted Ψ-trigonal-bipyramidal, where the halogen and SBI occupies the axial position and the equatorial position is occupied by two thiolate ligands and the lone pair.[120]

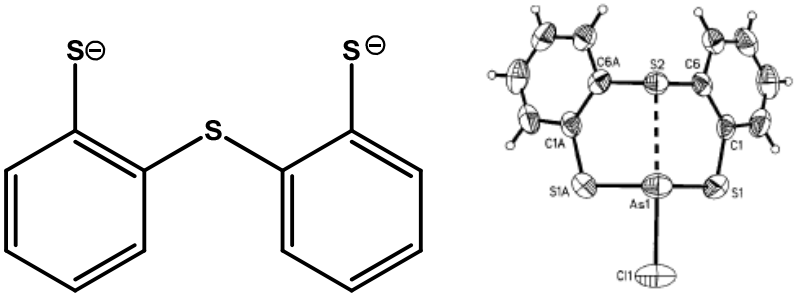

Figure 5. Structural depiction of $S(C_6H_4S)_2$ ligand (left) and ORTEP diagram of $S(C_6H_4S)_2AsCl$ (right). Selected bond lengths (Å) and angles (º): S2→As: 2.705(3), S1 – As: 2.268(2), As – Cl: 2.29(2), S1 – As – S2: 84.55(6) (Reprinted by permission of John Wiley and Sons).[120]

The affinity of As(III) for thiol ligands and its potential to form SBIs have been utilized extensively in designing ligands/chelators for this metalloid. For example, efforts to obtain self-assembled supramolecular coordination compounds of As(III), its reaction with 1,4-phenylenedimethanethiolate afforded the complex shown in Figure 6. The As(III) center is coordinated to three thiolate ligands with a trigonal-pyramidal geometry showing an As(III)-C_{Aryl} distance between 3.18 – 3.33 Å indicating a SBI between the lone pair and phenyl ring of the ligands (Figure 6).[131-132] Interestingly, when a $CHCl_3$ solution of the complex was subjected to reflux in the presence of excess strong acids such as trifluoroacetic acid or *p*-toluenesulfonic acid, no changes were observed in the repeated ^1H NMR spectrum of the complex. This result shows that the complex is robust and resists decomposition when subjected to such harsh conditions. The stability of the complex is possibly because of the strong As-thiolate bond enhanced by the SBIs within the complex. Such knowledge can be applied to the rational design of ligands that can selectively bind As(III).

In summary, As(III) prefers a trigonal-pyramidal geometry and binds strongly to soft donor groups. Designing ligands that utilize this binding preference in addition to having options for SBIs can lead to As(III)-complexes that are less prone to hydrolysis or decomposition as seen in the $[As_2(L)_3]$ (L = 1,4-phenylenedimethanethiolate) complex depicted in Figure 6.

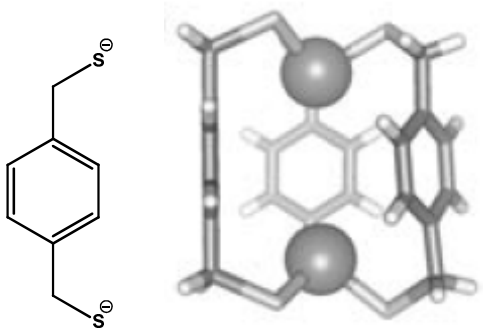

Figure 6. Structural depiction of 1,4-phenylenedimethanethiolate (left) and wireframe representation of the structure of $[As_2(L)_3]$, where L = 1,4-phenylenedimethanethiolate. This structural orientation shows the As(III) lone pairs directed towards the inside of the cavity of the complex (Reprinted by permission of John Wiley and Sons).[131]

1.5 Regulation and Detection of Arsenic Compounds

1.5.1 Regulation of arsenic in drinking water

To reduce the public health risk of chronic exposure to As in drinking water, the United States Environmental Protection Agency (EPA) revised the acceptable levels of As in community water systems from 50 ppb to 10 ppb in 2001.[133] The World Health Organization (WHO) has also recommended the same maximum contamination level (MCL) goal of 10 ppb for drinking water, but each country has a set level depending on its needs.[133] For example, the acceptable level in Bangladesh is still 50 ppb because of the huge cost associated with complying with a lower As level.[134] Presently there is no regulation for As levels in food, but as food becomes a significant source of As exposure, a level may be set soon.

1.5.2 Methods of detecting arsenic.

The initial driving force to develop methods for the determination of As was due to the numerous homicides that were committed all over Europe during the Middle Ages with the help of arsenic trioxide.[135] To meet this need, James Marsh devised the first chemical test of As in body tissue or fluid samples.[37] The sample is treated with Zn(s)/HCl in a closed vessel and any

As_2O_3 present is reduced to arsine ($AsH_3(g)$). The $AsH_3(g)$ formed in the reaction is ignited to form elemental As and H_2O. The elemental As thus formed is then deposited as a silvery-black film on a cold ceramic bowl held over the flame (see Equation 1). Finally, the intensity is compared to films of known As_2O_3 concentration. A detection limit of 20 ppb was obtained for this method.[136] Since the Marsh test, several other methods have been developed for detecting As in the environment. Each method will be discussed below and their advantages and disadvantages highlighted

$$As_2O_3(s) + 6\,Zn(s) + 12\,HCl(aq) \longrightarrow 2\,AsH_3(g) + 6\,ZnCl_2(aq) + 3\,H_2O(l)$$

$$\downarrow \Delta$$

$$2\,As(s) + H_2O(l)$$

Silvery-black
film on ceramic

Equation 1. Marsh's test for detecting As_2O_3.

1.5.2.1 Colorimetric test kits. Commercial test kits have been developed based on the Gutzeit method.[137-138] Inspired by Marsh, an acidified water sample is treated with a reducing agent to reduce the arsenic present to $AsH_3(g)$. The $AsH_3(g)$ formed is exposed to a paper impregnated with mercuric bromide to produce a highly colored compound where the concentration of As can be approximated with a calibrated color scale with a detection limit of 10 ppb (Equation 2 and Figure 7).[110] These test kits have been used extensively to monitor arsenic levels in the field because it is inexpensive and can be carried out by minimally trained personnel. The limitations include a lack of consistency in the results obtained from all commercial test kits and in some instance incorrect results when compared to laboratory test methods.[137] Additionally, the operator can be exposed to $AsH_3(g)$ generated during the test and the paper strip can serve as a source of mercury in the environment.[134, 137]

$$As_2O_3(s) + 6\,Zn(s) + 12\,HCl(aq) \longrightarrow 2\,AsH_3(g) + 6\,ZnCl_2(aq) + 3\,H_2O(l)$$

$$\downarrow HgBr_2\ (white)$$

$HAs(HgBr)_2$ (yellow) or $As(HgBr)_3$ (brown) or Hg_3As_2 (black)

The compound/color formed depends on the concentration of AsH_3 in the sample.

Equation 2. Gutzeit's reaction used in developing As test kits.

Figure 7. Arsenic Quick II Water Test Kit sold by Industrial Test Systems.[139]

1.5.2.2 Molybdenum Blue Method. Inspired by the detection method for phosphate, this test involves treating the water sample with oxidizing acids such as HNO_3 to convert all arsenic species to arsenate. The arsenate is then reacted with molybdenum oxide in an acidic medium to form an arsenate polyoxomolybdate that can be reduced with stannous chloride, hydrazine or ascorbic acid to yield the intense blue arsenomolybdate anion (Equation 3). Spectrophotometric measurement of these solutions allows for quantitative analysis. A detection limit of 20 ppb has been established with natural water samples. This method is relatively inexpensive and molybdenum has a low toxicity. However, the molybdenum blue method is not applicable for field studies because phosphate, iron and silicate interfere with the measurement and sample

preparation is complex requiring all As compounds to be converted to arsenate. Incorporating ion exchange chromatography can remove interferences and improve the detection limit to approximately 1 ppb.[137, 140]

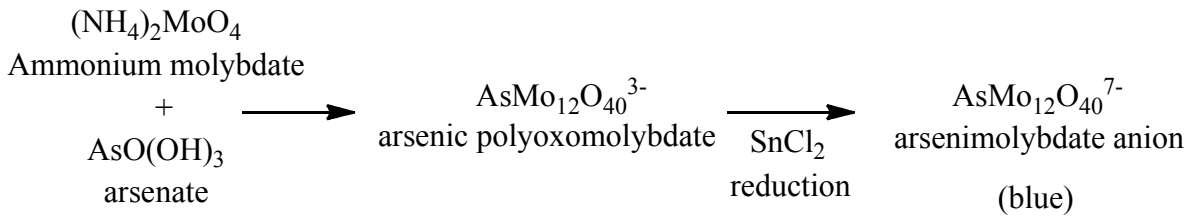

Equation 3. Molybdenum blue method for detecting As compounds.

1.5.2.3 Fixed Laboratory Assays. More commonly, laboratory-based techniques are used to accurately measure As in an environmental sample. Analytical methods used include: atomic fluorescence spectroscopy (AFS), graphite furnace atomic absorption (GFAA), hydride generation atomic absorption spectroscopy (HGAAS), inductively coupled plasma-atomic emission spectrometry (ICP-AES), and inductively coupled plasma-mass spectrometry (ICP-MS). The sample preparation step is very important to obtain a reliable result with these methods. All arsenic compounds have to be converted to iAs with minimal loss of analyte. This conversion can be achieved by dry ashing with inorganic oxidants such as $Mg(NO_3)_2$/magnesium oxide mixture or wet ashing with oxidizing acid mixtures. A separation step utilizing different chromatographic techniques can be applied to improve the detection limit or for studying the speciation of arsenicals. These methods are sensitive and a reliable detection limit of 0.003 ppb has been obtained.[141] However, these instrumental methods are expensive to maintain and operate, and require a well-trained technical staff to perform and analyze measurements involving extensive sample preparation step.

1.5.2.4 Portable X-ray Fluorescence (XRF). A hand-held X-ray fluorescence device can be used to measure As levels in soil samples without aqueous extraction. A sealed ^{109}Cd radioisotope is used to irradiate the sample and the characteristic X-ray fluorescence from the As in the sample is measured. The detection limit of XRF is 60 ppm and the main interferences are lead compounds, variation in particle size, and moisture.[137]

1.5.2.5 Anodic Stripping Voltammetry (ASV). This method can be used to measure total dissolved iAs at a potential of +145 mV vs. SCE with a conditioned gold-plated electrode. Portable ASV instruments have been developed and a detection limit of 0.1 ppb can be achieved. The downside of ASV is electrode fragility, the need for well trained personnel to operate and interpret data, and positive interference from antimony, bismuth, copper, mercury and zinc.[137]

1.5.2.6 Biological Assays. More recent advances (1997) in developing an As detection method involves the use of bacteria or plants for As detection. In *E. coli* and some other bacteria, the ability to detoxify As is conferred by the *ars* operon.[90, 142-143] Bacterial biosensors have been developed by linking genes that produce fluorescence reporter proteins such as luciferase or green fluorescent protein to the As detoxification genes. When As is present, the detoxification mechanism is switched on and at the same time the fluorescent protein is produced, which can be measured and correlated to the amount of As present.[144-151] This strategy has been utilized in developing a test kit with non-pathogenic *E. coli;* a field test in Bangladesh afforded a detection limit of 4 ppb.[151] Certain plants such as Brake Fern (*Pteris vittata*) and rootless duckweed (*Wolffia globosa*) are able to extract iAs from contaminated soil and accumulate it in its above ground biomass.[152-153] Research efforts have been carried out to use these plants to detect As by pigment change and in the bioremediation of As-contaminated sites.[137]

1.5.2.7 Fluorescence Methods The use of small molecule fluorescent dyes for the detection of As(III) is a recent research endeavor. Interest in developing fluorescence detection methods for As(III) have been inspired by the successful use of this method for other analytes, e.g. fluorescent dyes are now used extensively to probe calcium levels in biological systems.[154] The advantages include the high sensitivity of fluorescence in addition to giving a real-time and non-destructive report of the analyte. Developing As(III) fluorescent dyes will be useful in measuring concentration of the As(III) in environmental and biomedical samples.

In the design of As(III) fluorescent dyes, one strategy is to incorporate a fluorescent reporting group onto a biomolecule with high affinity for As(III). In the work of Parker et al. a naphthyl group was covalently attached to phytochelatins.[155] Phytochelatins contain a large number of cysteine residues and are produced by plants to combat heavy metal toxicity.[156] A change in fluorescence properties (2-fold decrease) of the naphthyl-phytochelatin dye is observed only when 100 mol-equiv of As(III) is present. However, other heavy metals such as Pb(II) also elicits fluorescence quenching of the dye. Although the naphthyl-phytochelatin dye forms strong bonds with As(III), there is no significant and selective change in fluorescence properties making it an inadequate dye for As(III). Another example is reported by Baglan et al. in which a tetraphenylethene group is attached to a cysteine amino acid residue (Chart 7).[157] The dye reacts with [$As(OH)_3$] to form the [$As(Cys\text{-}TPE)_3$] complex in the preferred trigonal-pyramidal geometry of As(III). After complex formation, the bond angle in the trigonal plane places the TPE groups in close proximity. This aggregation thus increases the hydrophobic environment within the complex which leads to an increase in fluorescence intensity and a detection limit of 0.5 ppb for [$As(OH)_3$]. However, other ions such as Cu(II), Zn(II) and Hg(II) also elicit some fluorescence intensity increase albeit at a lower intensity compared to As(III).

While TPE-Cys is a sensitive dye for As(III) in aqueous media, it is not a selective dye possibly because the Cys group forms complexes with the other ions. Hence, a better strategy will be to design small molecule sensors inspired by the binding preference of As(III) in order to achieve both sensitivity and selectivity during detection.

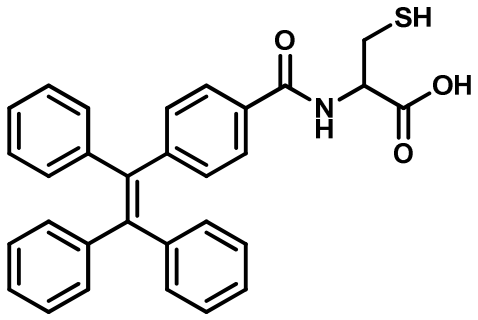

Chart 7. Structural depiction of tetraphenylethene appended cysteine (TPE-Cys).

1.6 Introduction to Fluorescence Spectroscopy

Fluorescence spectroscopy is a highly sensitive analytical tool that will be employed in designing a fluorescent detection method for As(III) in this work. Fluorescence is the emission of light from a substance as an excited electron returns to the ground state from the first excited singlet state.[158] When a substance interacts with light energy several events can happen and some of these processes are depicted in a Jablonski diagram (Figure 8). The electronic absorption transitions between the ground electronic state (S_0) and any of the excited electronic states (S_1, S_2, etc.) are depicted by vertical lines to illustrate the instantaneous electronic transition (10^{-15} s) without significant displacement of the nuclei as explained by the Franck-Condon principle.[159-160] Due to the large energy difference between S_0 and S_1, light rather than heat energy is used to populate the excited states. Following light absorption, the electron is usually excited to some higher vibrational level of either S_1 or S_2. A rapid relaxation (~10^{-12} s) to the lowest vibrational

level of S_1 usually follows and this process is called an internal conversion. Emission of light energy as the electron relaxes from the first excited state to the ground state ($S_1 \rightarrow S_0$) is termed fluorescence. The rate of light emission is rapid, typically 10^8 s^{-1} because it is a spin-allowed transition. Also, the typical fluorescence lifetime, which is the average time between the excited state and return to the ground state of a fluorophore, is between $10^{-5} - 10^{-8}$ s.[158] The process of an electron spin-flip from the singlet to the triplet state is named intersystem crossing. Emission of light as the electron returns to the ground state from the triplet state is a spin-forbidden transition and slow process ($10^3 - 10^{10}$ s^{-1}), that is called phosphorescence.

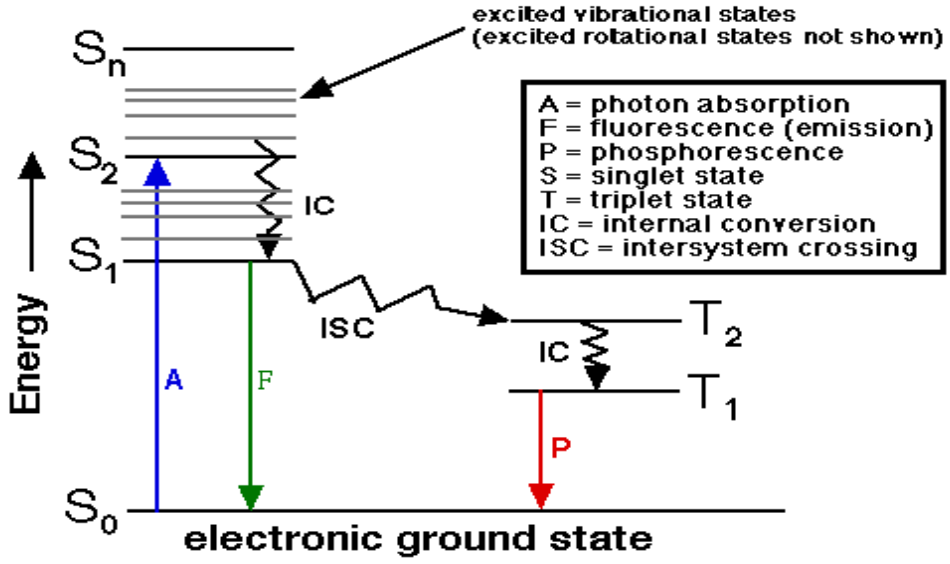

Figure 8. Jablonski diagram.[161]

The Jablonski diagram can be used to illustrate some of the general characteristics observed in the fluorescence process. For example, the energy of the emitted light is typically less than that of absorption ($\lambda_{abs} < \lambda_{em}$). This difference in λ, which is consistent with the $S_1 \rightarrow S_0$ transition is called the Stokes shift after Sir G. G. Stokes who first observed this phenomenon.[162] Another general property of fluorescence is based on Kasha's rule, which shows that

fluorescence emission is usually independent of the excitation wavelength.[163] The internal conversion process (10^{-12} s) ensures a quick dissipation of the excess energy and rapid relaxation to the S_1 level, from where emission takes place. Hence, a fluorescence spectrum is typically red-shifted compared to the absorption spectrum because of the Stokes shift and at $\lambda_{em} > \lambda_{abs}$ is due to Kasha's rule.

The measurement of the fluorescence properties of a compound can be used as an analytical tool. Two classes of fluorescence measurements can be made: (i) steady-state and (ii) time-resolved measurements. In steady-state measurements, the intensity of emitted light is measured after illumination, while in time-resolved experiments the decay of emission is measured. Most fluorescence experiments are steady-state measurements, since steady-state conditions are achieved quickly due to the nanosecond timescale of fluorescence processes. A typical fluorescence or emission spectrum is a plot of the fluorescence intensity versus wavelength (nm) or wavenumber (cm^{-1}).[158] Also, emission spectra vary widely and are dependent upon the chemical structure of the fluorophore and the solvent in which the measurement is performed.

Fluorescence spectroscopy is applied in a variety of fields such as biotechnology, flow cytometry, genetic analysis, forensics and chemical sensing. This active area of research is driven by the need for rapid and low-cost testing methods for a wide range of clinical, bioprocess and environmental applications.[164-166] One advantage of fluorescence spectroscopy is its high sensitivity; this advantage is due to measurement of the emitted light relative to a dark background as compared to the bright reference beam in an absorbance measurement.[158] As seen from the equation, $I_f = 2.303k\Phi_f P_o \varepsilon bc$ when $\varepsilon bc < 0.01$ (I_f = fluorescence intensity; k = constant; Φ_f = quantum yield; P_o = incidence light; ε = molar absorptivity; b = path length and C =

concentration),[167] the intensity of emitted light depends directly on the incident light rather than a ratio with transmitted light as is the case in electronic absorption (A = εbc). The high sensitivity has led to the application of fluorescence spectroscopy for sensing trace amounts of analytes in biological systems (e.g. Zn^{2+}, NO, pO_2) and environment systems (Hg^{2+}).[168-176] Additionally, fluorescence is a relatively inexpensive analytical tool. Improvements in instrument design have made spectrofluorometers compact in size without the need for constant maintenance. Moreover, hand-held spectrofluorometers make the technique amenable to field application. However, to ensure success in fluorescence measurements certain experimental details need to be considered. For example, the samples should not be very concentrated in order to prevent or minimize reabsorption of emitted light (inner filter effects) or light scattering. Also, adequate cleaning of sample holders is important to prevent interference from residual fluorescent compounds.

The measurement of fluorescence is possible only when the substance contains a light emitting unit or fluorophore. There are two classes of fluorophores: (i) intrinsic and (ii) extrinsic fluorophores. The amino acid tryptophan absorbs and emits at 280 nm and 340 nm, respectively, and is an example of an intrinsic fluorophore since the fluorescence-sensitive indole group is an integral part of the tryptophan structure. Compounds without an inherent fluorescence can still be studied by labeling with fluorescent dyes, these are called extrinsic fluorophore. Examples of compounds that are used as extrinsic fluorophores include 1-dimethylamino-5-naphthylsulfonyl chloride (dansyl chloride), fluorescein isothiocyanate (FITC), Bodipy (see Chart 8) etc. Most of the research in the field of fluorescence spectroscopy involves combining extrinsic fluorophores and analyte receptor groups in novels ways to afford fluorescent dyes that can be used for sensing various analytes. In summary, fluorescence spectroscopy is an attractive analytical tool to be applied to the challenge of developing a new detection method for As(III) because it will be

sensitive near or below the MCL of 10 ppb and the method is amenable to use in the field with little or no sample preparation.

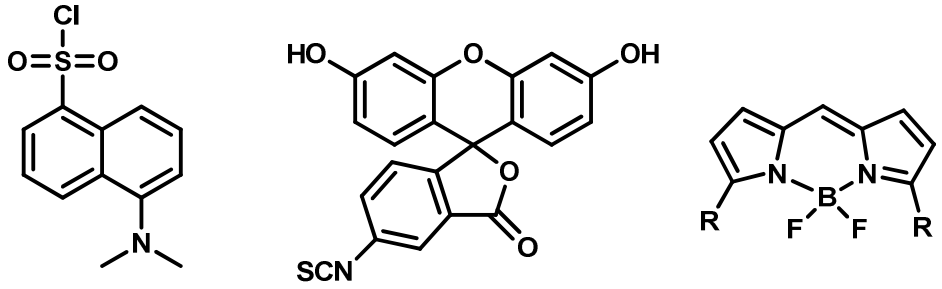

Dansyl chloride FITC Bodipy

Chart 8. Structural depiction of Dansyl chloride, FITC and Bodipy fluorophores.

1.7 Intent of Research

Complying with the recommended levels of As in drinking water set by the U. S. EPA is a challenging endeavor. Municipal water treatment plants in the U. S. have a mandate to maintain As levels below 10 ppb in the drinking water supply. However, the water treatment steps of flocculation, sedimentation and disinfection are not effective in removing As from water.[177] Treatment steps for As removal include adsorption, chemical precipitation, ion exchange, and so forth. Choosing the best treatment method and monitoring the progress of As removal depends on having appropriate methods to detect arsenicals.[177] Although fixed instrumental methods such as ICP-MS are effective for monitoring As levels, the cost and instrument maintenance makes this method inaccessible to many water treatment plants and owners of private wells. Hence, research in the field of As detection is ongoing with the aim of developing safe, sensitive, selective, relatively inexpensive, and field deplorable methods for detection and monitoring As concentration in water supply systems. Our approach is to apply fluorescence spectroscopy as an analytical tool for the detection of As(III) compounds. This

fluorescence based method is proposed to combine the sensitivity and selectivity of fixed laboratory methods, while being field deplorable and inexpensive like the colorimetric method. The overall goal of this research is to develop fluorescent dyes for As(III) compounds that can be utilized for monitoring As levels in the environment. Emphasis will be placed on dyes for As(III) compounds because they are more toxic compared to As(V) compounds. Also, As(III) compounds such as [$As(OH)_3$] are more mobile and prevalent in the environment since they are not easily adsorbed onto sediments like the As(V) compounds.[37] To achieve the goal of developing a fluorescence detection method for As(III), the coordination chemistry of As(III) as a central acceptor metalloid will be studied in this work. The objective is to uncover new chemistries that are unique to As(III) and to obtain ligands that have a high affinity for As(III). This study is important to the design of fluorescent dyes for As(III) because it impacts selectivity for As(III) that will prevent false results when such dyes are used to detect As(III) in the presence of other analytes. The knowledge gained from the coordination chemistry will be utilized to design and develop small molecule sensors for the fluorescent detection of As(III)-compounds. Fluorescent probes usually involve incorporating an extrinsic fluorophore to a receptor molecule that is known to react with the analyte of interest. Hence, when the dye and analyte react it will result in measurable fluorescence changes. Extrinsic fluorophores such as dansyl and coumarin groups will be used in the design of As(III) fluorescent probes because of their high sensitivity to changes in their environment.

Interesting discoveries on As(III) chemical reactivity will be presented in this work. A redox rearrangement of the benzothiazoline functional group promoted by As(III) is presented in chapter 2. In chapter 3, the chemistry with the benzothiazoline group coupled to a coumarin fluorophore is applied in designing chemodosimeter dyes that respond to As(III) compounds

with remarkable changes in fluorescence properties. Finally, Appendix A will cover various chemosensor dyes that respond by modest fluorescence changes to As(III).

CHAPTER 2

SYNTHESIS AND CHARACTERIZATION OF S-BASED LIGANDS FOR RECEPTOR DESIGN IN As(III) SENSORS

2.1 Abstract

Understanding the fundamental coordination of As(III) is important in the construction of As(III) sensors. In general, As(III) prefers the trigonal-pyramidal geometry in coordination compounds with a stereochemical active lone pair occupying the apex of this pyramid. Studies of As(III) coordination chemistry have revealed that other geometries can also be accessed by appropriately designed ligands. This work contributes to this quest by designing ligands with different donor groups and donor strength to enable structural and spectroscopic characterization of new As(III)-compounds. In this work, coordination studies with N-acetyl-L-cysteine methyl ester ($SNAc^{OMe}$) revealed a preferential binding via the thiol group to afford a three-coordinate complex of formula $[As(SNAc^{OMe})_3]$, confirming prior reports of tri-thiolate ligated As(III) compounds. Additionally, a set of ligands that can form supramolecular coordination compounds with As(III) were prepared, comprised of thioether-S donor groups and varying options for SBIs such as imine-N. However, no reaction was observed under the conditions utilized. Finally, a set of ligands containing the benzothiazoline functional group was prepared and studied. An interesting redox-rearrangement of the benzothiazoline functional group to afford the benzothiazole with the formation of a four-coordinate As(III)-complex containing deprotonated amine. The geometry observed in the four-coordinate complex is a Ψ-trigonal-bipyramidal

geometry, which is not commonly observed in As(III) complexes. All compounds were probed by various forms of spectroscopy including UV-vis, ^{1}H NMR, ESI-MS, FTIR, and in some cases X-ray crystallography.

2.2 Introduction

In an effort to generate ligands that will be incorporated into As(III)-specific dyes, several ligands with different structural motifs were designed and synthesized. All the ligands used in this study contain a sulfur donor group, inspired by the thiophilic nature of As(III). Furthermore, to take advantage of the stability achieved by SBIs, functional groups that can promote SBIs were incorporated into the ligand design. The ligand, $SNAc^{OMe}$ (Chart 9) contains a thiol group and is expected to form a complex with As(III) similar to [As(Cys)$_3$]. Ligands **L1** – **L5** (Chart 9) are inspired from supramolecular chemistry studies that show As(III) will form self-assembled complexes with appropriately designed ligands.[130-132, 178] The S-donors in **L1** – **L3** are thioether-S groups, which are incorporated into the ligands to determine if they are good ligands for As(III). Another advantage to using the thioether functional group is to protect the sulfur from reacting during the fluorophore attachment reaction. In addition to the phenyl group, the other SBI group was varied from amide-N, imine-N and amine-N in **L1** – **L3** to study the effect of varying the donor ability of the N-group on the stability of the As(III) complex formed. **L4** – **L5** contains thiol-S, which are protected as the benzothiazoline functional group.

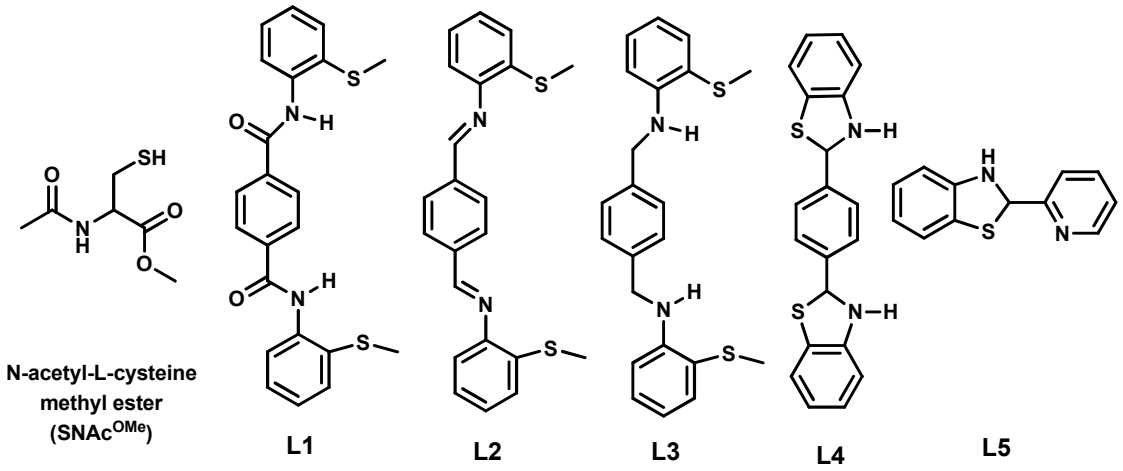

Chart 9. Ligands used in As(III) coordination chemistry study.

The principal goal of this chapter is to expand the understanding of the coordination chemistry of As(III) for future receptors in As(III) fluorescent probes. The complexes obtained with the designed ligands were fully characterized. Analysis of this spectroscopic data has provided insight into the ease of formation and stability of As(III) coordination complexes with S-ligands. This information will be applied to the design and synthesis of fluorescent sensors for As(III).

2.3 Results and Discussion

2.3.1 Synthesis and Characterization of As(III)-SNAc^{OMe} complex

Since As(III) has a known affinity for thiolates, we started by exploring the coordination chemistry with Cys-based ligands. The reaction of $AsCl_3$ or AsI_3 with three mol-equiv of $SNAc^{OMe}$ in THF in the presence of Et_3N (general base) resulted in an off-white solid (Scheme 3). Comparison of the ^1H NMR spectrum of the off-white solid obtained in the reaction to the ^1H NMR spectrum of $SNAc^{OMe}$ shows a slight downfield shift of all the signals upon complexation to As(III). The most significant shift is the $–CH_2–$ closest to the thiol functionality with a change of +0.32 ppm (Figure 9). This shows that $SNAC^{OMe}$ binds to As(III) via the S-donor of

$SNAC^{OMe}$. The ESI-MS characterization of the white solid shows a peak at m/z = 604.0 in the positive mode which can be assigned to $[As(SNAc^{OMe})_3 + H]^+$, and supports the formation of the tri-coordinate As(III)-$SNAc^{OMe}$ complex. Furthermore, the base peak at m/z = 427, assigned to $[As(SNAc^{OMe})_2]^+$ indicates that one of the ligands dissociates either in solution or when obtaining the MS. Further support for the formation of $[As(SNAc^{OMe})_3]$, is obtained by comparing the FTIR of $SNAc^{OMe}$ and $[As(SNAc^{OMe})_3]$, which shows the disappearance of the S-H stretch at 2575 cm^{-1} (Figure 10). There is also a general broadening of all the peaks in the $[As(SNAc^{OMe})_3]$ spectrum compared to the FTIR spectrum of free $SNAc^{OMe}$. This is possibly due to having three $SNAc^{OMe}$ in close proximity to each other and engaging in intermolecular H-bonding. Attempts to obtain a single crystal suitable for X-ray diffraction resulted in oily globular precipitates, thus preventing structural characterization of $[As(SNAc^{OMe})_3]$. UV-vis studies of the $[As(SNAc^{OMe})_3]$ compound in CH_2Cl_2, MeOH or THF shows broad absorption bands between 260 – 300 nm (Figure 11), presumably due to S-As(III) charge transfer transitions. This electronic property is consistent with that observed for other As(III)-alkyl thiolate complexes and accounts for the off-white color of the isolated solid. In conclusion, though X-ray characterization wasn't possible, other spectroscopic data point to the formation of the tri-coordinate As(III) compound in a variety of different solvents suggestive of the stability of the AsS_3 coordination sphere.

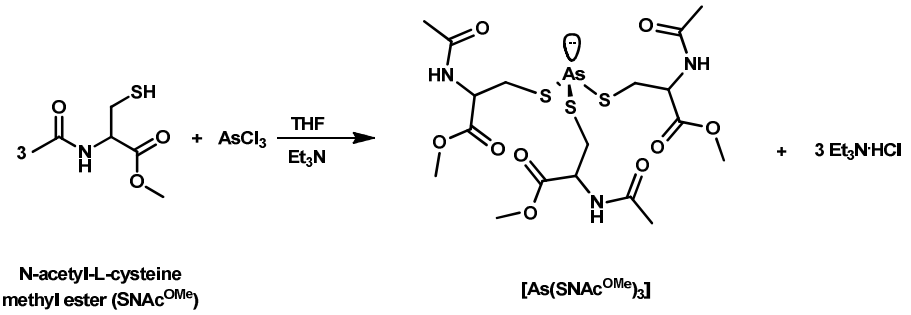

Scheme 3. Reaction of $SNAc^{OMe}$ and $AsCl_3$ to give $[As(SNAc^{OMe})_3]$.

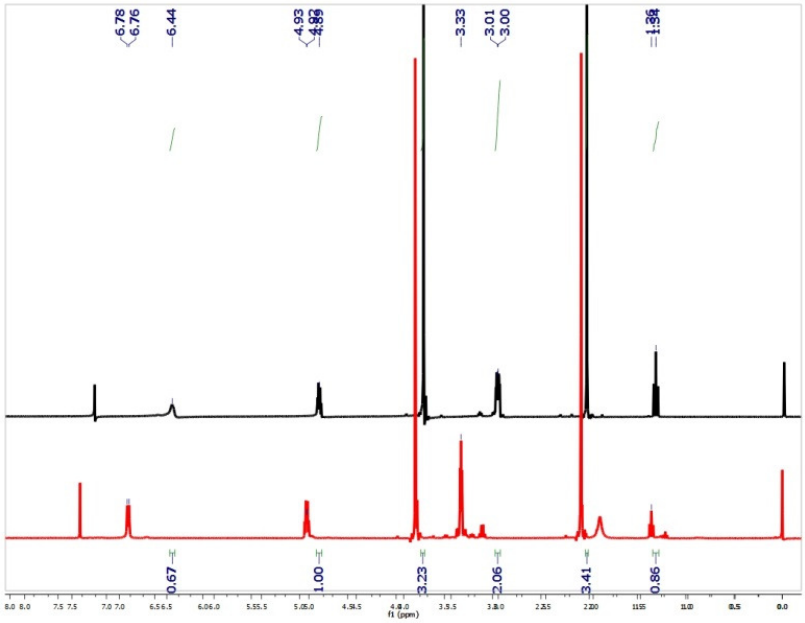

Figure 9. ^{1}H NMR spectrum of SNAc^{OMe} (black trace) and [As(SNAc^{OMe})$_3$] (red trace) in $CDCl_3$ at 298 K.

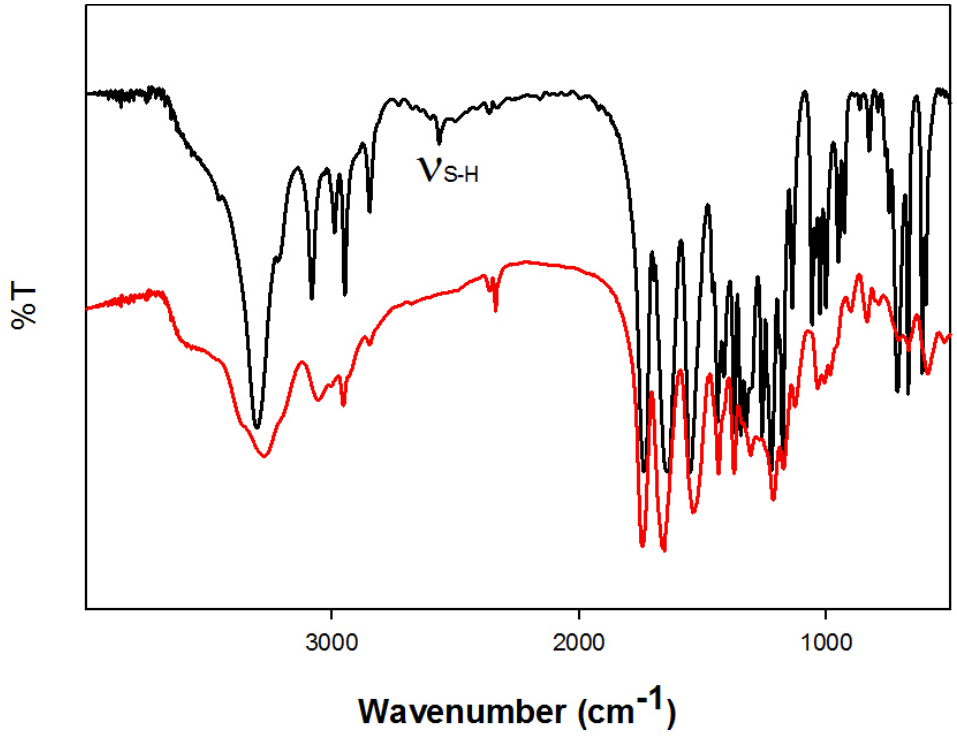

Figure 10. FTIR spectrum (KBr) of SNAc^{OMe} (black trace) and [As(SNAc^{OMe})$_3$] (red trace).

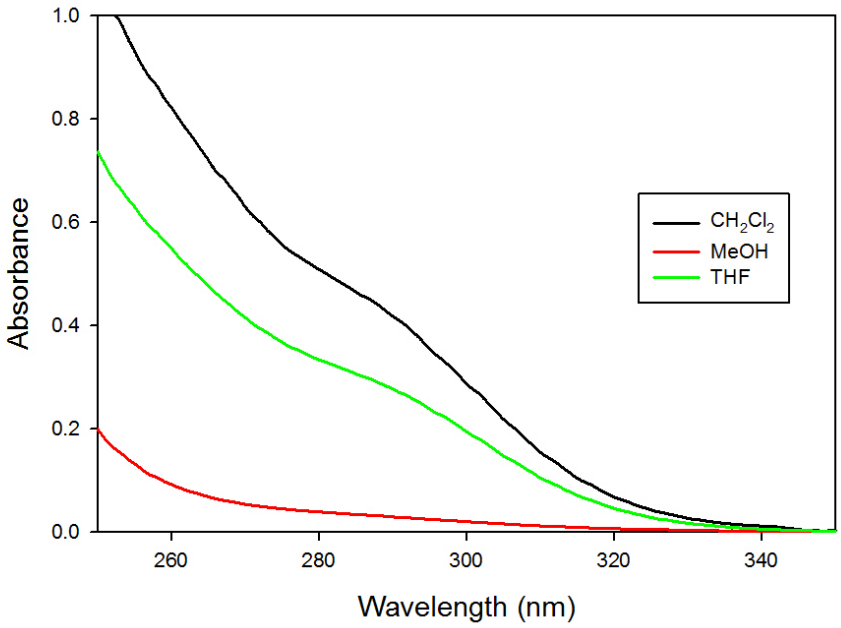

Figure 11. UV-vis spectrum of a 0.16 mM solution of [As(SNAc^{OMe})$_3$] in CH_2Cl_2 (black trace), MeOH (red trace) and THF (green trace) at 298 K.

2.3.2 Synthesis and Characterization of As(III)-thioether complexes

The ligands: **L1**, **L2** and **L3** (Chart 9) were designed to maximize the interaction with As(III) via SBIs. Since the preferred geometry for As(III) is trigonal-pyramidal, the proposed structure consist of a three-coordinate [$As_2(L)_3$] complex with the thioether-S as the point of attachment (see Chart 10).[131-132, 178]

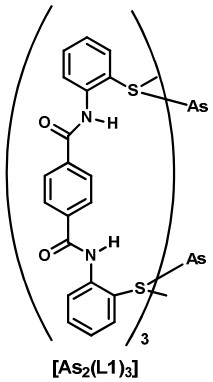

Chart 10. General structural depiction of proposed As(III)-complex with thioether ligands, using ligand **L1** as an example.

The syntheses of the ligands, L1 – L3 are described in schemes 4 – 5. The Ligand, **L1**, containing carboxamide groups for SBIs, was synthesized by reaction between terephthaloyl chloride and two mol-equiv of 2-(methylthio)aniline in 50% yield (Scheme 4). The ^{1}H NMR shows seven signals which integrates to the expected 20 hydrogen atoms in **L1**. The signal for the amide N-H is deshielded and resonates at 9.31 ppm. The ^{13}C NMR shows ten signals which corresponds to the number of unique carbon atoms and the symmetry in **L1**. Further confirmation for the formation of **L1** is obtained from the ESI-MS, which shows a parent peak at *m/z* = 409.2 that can be assigned to [**L1** + H]$^{+}$. **L2**, containing imine groups for SBIs, was synthesized in 70% yield following a literature procedure and the purity was confirmed by ^{1}H, ^{13}C NMR, FTIR, ESI-MS and X-ray crystallography.[179] Reduction of **L2** with $NaBH_4$ in THF afforded **L3** (amine SBI donor) in 75% yield (Scheme 5). The ^{1}H NMR shows a broad signal at 5.35 ppm which disappears when D_2O is added to the $CDCl_3$ solution, suggestive of an exchangeable NH proton in **L3**. A total of eight signals were present in the ^{1}H NMR spectrum accounting for the expected 24 hydrogen atoms in **L3**. The presence of the NH is further supported by a signal at 3360 cm^{-1} in the FTIR. A peak at *m/z* = 381.2 in the ESI-MS supports the formation of **L3**.

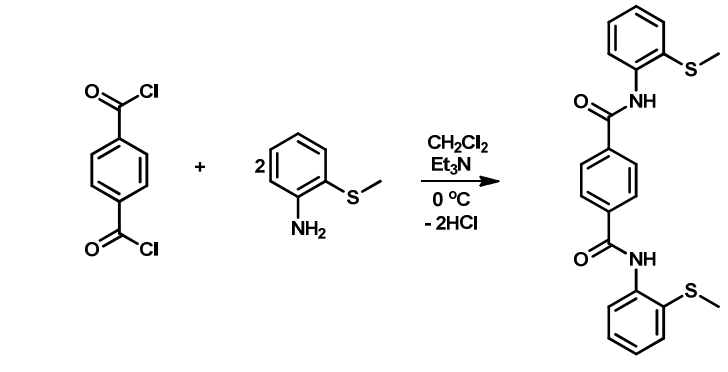

Terephthaloyl chloride 2-(methylthio)aniline **L1**

Scheme 4. Synthesis of **L1**.

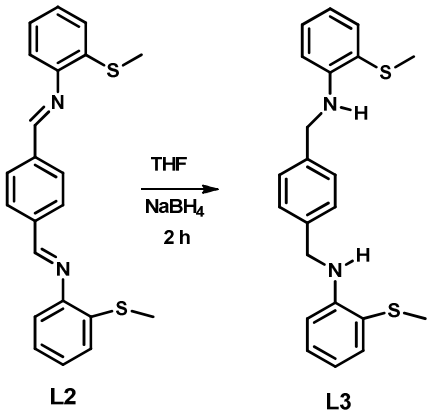

Scheme 5. Synthesis of **L3**.

The coordination chemistry of **L1**-**L3** with As(III) was then studied using $AsCl_3$ as the source of As(III) ions because of its solubility in organic solvents. In a typical reaction, a solution of the ligand in CH_2Cl_2 or THF was stirred with two mol-equiv of $AsCl_3$ at RT. The products obtained were off-white or yellow in color; however, ^{1}H NMR analysis of the isolated solid formed from the reaction with **L3** showed that the HCl salt of the ligand was formed as the spectrum was comparable to the ^{1}H NMR of independently synthesized **L3**·HCl. Further confirmation was obtained from the X-ray structure of a crystal obtained from the reaction of $AsCl_3$ and **L3**, which was shown to be **L3**·HCl (Figure 12). Based on these observations and literature precedence,[180] it was determined that high purity $AsCl_3$ contains between 0.1 – 1 M water, which can cause hydrolysis to form HCl and As_2O_3, the HCl then protonates any Lewis basic ligand thus limiting its coordination ability. Repeating the reaction in the presence of 3 Å molecular sieves to remove any traces of water resulted in no reaction, indicating thioether groups are not ideal donor groups for As(III) under these reaction conditions. Similar results were obtained for **L1** and **L2**.

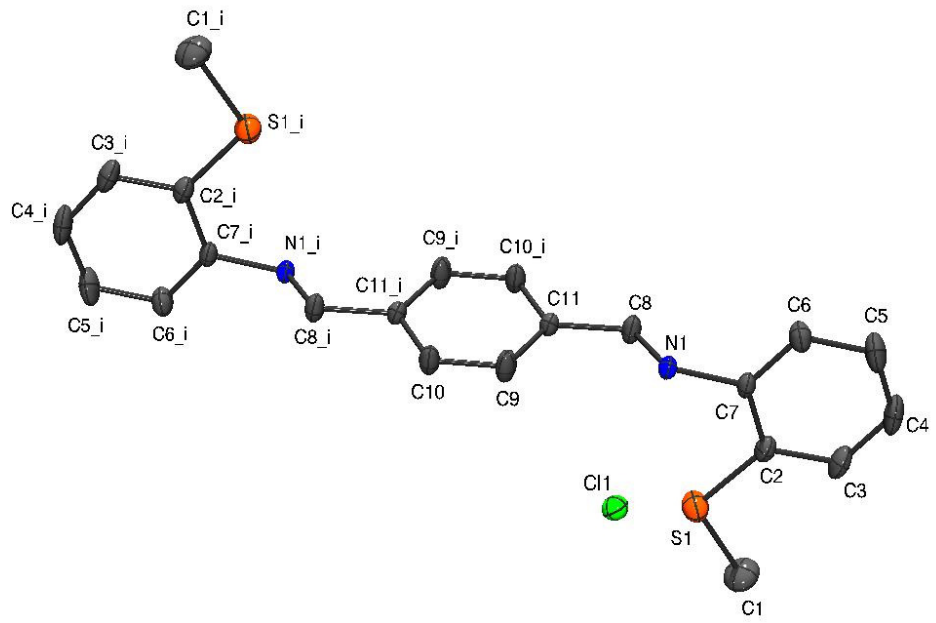

Figure 12. ORTEP diagram showing 30% thermal ellipsoids of **L3**·HCl obtained from the reaction of $AsCl_3$ and **L3**. Selected bond lengths (Å): N1 – C7: 1.4693(15), N1 – C8: 1.4982(17), S1 – C1: 1.778(2).

Coordination compounds of As(III) with thioether ligands have been reported in the literature. The first As(III)-thioether complex reported was a 1:1 adduct of AsI_3 and 1,3,5,7-(tetramethyl)-2,4,6,8,9,10-(hexathia)-adamantane (Figure 13).[181] This complex was obtained when a mixture of an aqueous solution of thioacetic acid and powdered AsI_3 was held in a closed vessel for four weeks. In acidic media, thioacetic acid analogs are known to react and form the hexathia-adamantane unit.[182] The formation of the hexathia-adamantane in this reaction is proposed to be catalyzed by the HI formed from the hydrolysis of AsI_3.[181] The coordination geometry around As(III) is best described as a distorted octahedron with three thioether-S and three I ligands.[181]

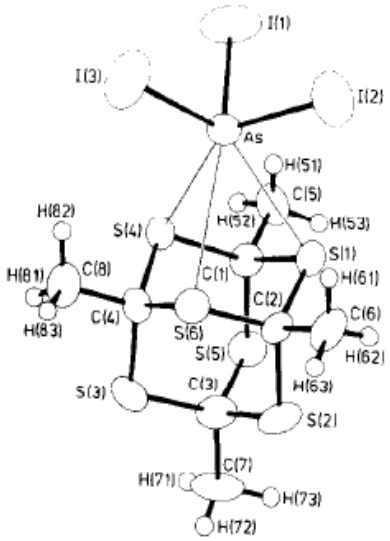

Figure 13. Molecular structure of the 1:1 adduct of AsI_3 with 1,3,5,7-(tetramethyl)-2,4,6,8,9,10-(hexathia)-adamantane. Selected bond lengths (Å) and angles (º): As – I: 2.575 – 2.577, As – S: 3.274 – 3.310, I – As – I: 98.4 – 100.3, I – As – S: 89.5 – 111.7(Reprinted by permission of Elsevier).[181]

Other As(III)-thioether complexes have been reported by Reid and coworkers.[183] These complexes were prepared by reacting CH_2Cl_2 solutions of AsX_3 (where X = Cl, Br or I) with one mol-equiv of the polydentate and macrocyclic thio- and selenoether depicted in Figure 14. Single crystals of the various complexes were obtained by slow evaporation of layered solutions of the reactants in anaerobic CH_2Cl_2 to confirm the formation of these six-coordinate As(III)-thioether complexes (Figure 14). However, the ^1H NMR of the solids in $CDCl_3$ or CD_2Cl_2 were similar to the resonance of the free ligands, revealing that *there was extensive dissociation or fast exchange of ligands in these complexes in solution*.[183] This result, combined with our findings further confirm the weak coordination of thioether groups to As(III).

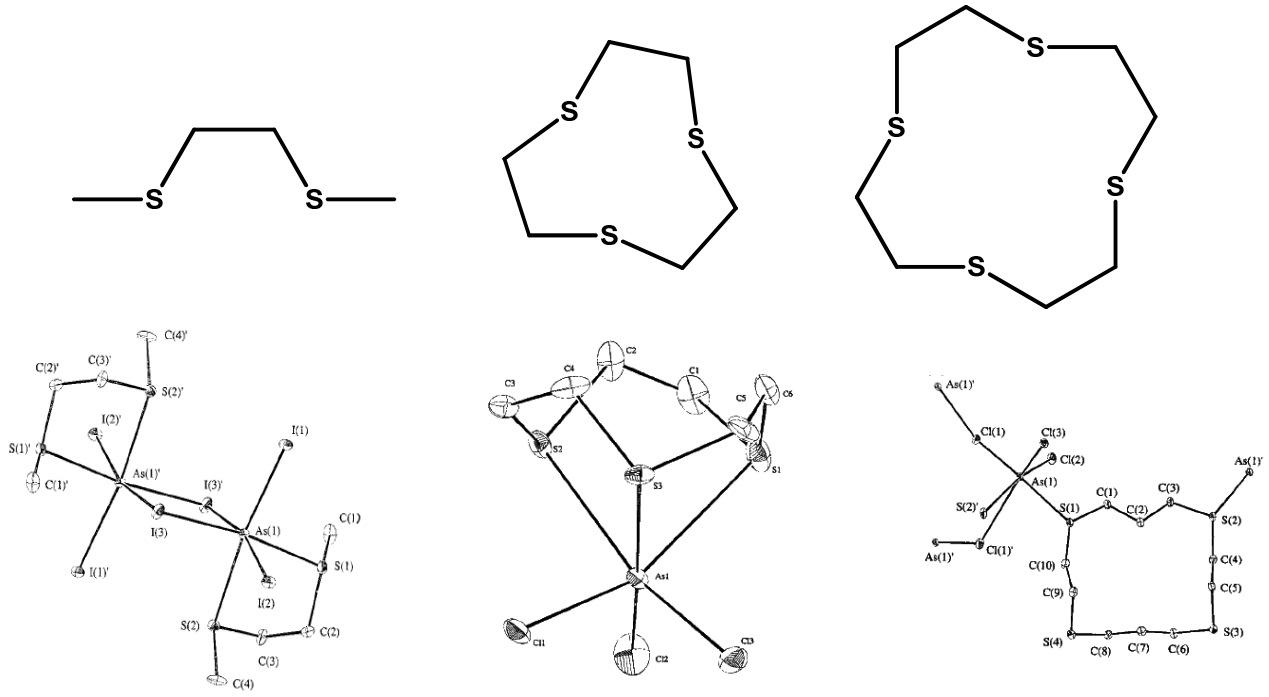

Figure 14. Structural depiction of thioether ligands (top) and ORTEP diagram (bottom) of $[AsI_3(CH_3S(CH_2)_2SCH_3)]$ (left), $[AsCl_3([9]aneS_3)]$ (middle) and $[AsCl_3([14]aneS_4)]$ (right) (Reprinted by permission of American Chemical Society).[183]

Although no reaction was observed with As(III) and the ligands in this study, some insight has been obtained with respect to ligand design for As(III). The weak Lewis acidity of As(III) coupled with the weak Lewis basicity of the ligands leads to no complexation even in non-coordinating solvents such as CH_2Cl_2. While it is possible that single crystals would have been obtained after an extended period of time, as observed from the thioether complexes discussed above the complexes would have easily dissociated in solution. This type of coordination would not be beneficial in a sensing experiment. This study also highlights the importance of maintaining strict anhydrous conditions when working with As(III)-halides. Hydrolysis of the halide salts leads to the formation of As(III)-oxides, As_2O_3, which is very stable. Finally, **L1**, **L2** and **L3** will not be ideal platforms to design As(III)-specific sensors due to the low affinity to these ligands for As(III) in solution.

2.3.3 Synthesis and Characterization of As(III)-thiolate complexes

Motivated by the high affinity of As(III) for thiolate-S-containing compounds, **L4** and **L5** (Chart 9) were constructed as they were expected to form stable As(III) complexes. **L4** was synthesized by a condensation reaction between 2-aminothiophenol and terephthalaldehyde in EtOH to give an off-white colored solid in ~ 40% yield (Scheme 6).

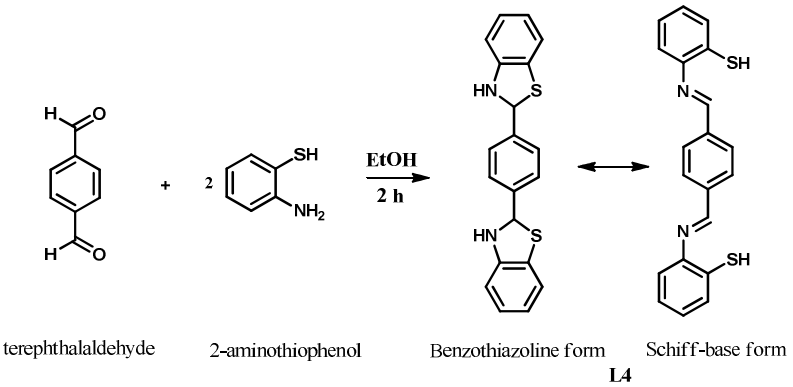

Scheme 6. Synthesis of **L4** (racemic mixture) and its resonance forms.

Two tautomeric forms are possible for **L4**; the ring open Schiff-base form or the benzothiazoline form (Scheme 6).[184] The ^{1}H NMR spectrum of isolated **L4** shows a signal at 4.36 ppm that disappears when D_2O is added to the sample. This signal can be assigned to an N-H functional group, which is further supported by the ν_{NH} peak at 3306 cm^{-1} in the FTIR of the solid. The ^{1}H NMR and FTIR data indicate that **L4** exists solely in the benzothiazoline form in both solid- and solution-states, which is an excellent form of protecting the thiol functionality from reacting before As(III) is present. Furthermore, the formation of **L4** is confirmed by a peak at *m/z* = 349.2 in the ESI-MS which corresponds to the [**L4** + H]$^{+}$. **L5** was synthesized according to a literature procedure and was isolated as an off-white solid in ~ 44% yield. Characterization by ^{1}H, ^{13}C NMR, FTIR and ESI-MS confirmed the purity of the ligand which also exists solely in the benzothiazoline form.

We predicted that the reaction of these ligands, when deprotonated, would result in the preferred trigonal-pyramidal As(III)-thiolate coordination complexes as depicted in Chart 11. When deprotonated **L4** (with NaH) was reacted with As(III) (3:2 ratio); the THF reaction turned yellow with appearance of a white precipitate. The white precipitate obtained after filtration was assigned to be NaCl because of the absence of IR peaks and its water solubility. The filtrate was concentrated to give an orange colored solid, which was characterized by various spectroscopic methods. The ^{1}H NMR showed multiple peaks both in the aliphatic and aromatic regions; none of the peaks could be assigned to the starting material and attempts to assign the spectrum to possible products was challenging. No insight was gained from the FTIR data which displayed a broad peak at 3343 cm^{-1} that could be water. The ESI-MS data showed major peaks with *m/z* = 316, 339 and 465 that couldn't be assigned to known combinations of **L4** and As(III). These data shows that **L4** does react with As(III), because characterization data that belong to **L4** are not present in the reaction product. However, rather than forming a discreet [As_2(**L4**)$_3$] complex, the product of the reaction is likely polymeric in nature.

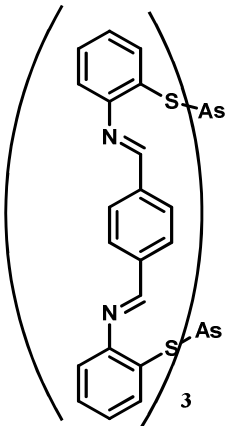

Chart 11. Proposed product of the reaction of **L4** and As(III).

Due to the difficulty in characterizing the product formed between **L4** and As(III), **L5** was used because of the one benzothiazoline unit and an additional pyridine donor group. The

reaction of **L5** with As(III) in various stoichiometries was studied; however, the product of the **L5**:As(III) (2:1) ratio was the easiest to characterize. To carry out the reaction, **L5** was first treated with NaH in THF to give a purple solution. After stirring for 20 min, 0.5 mol-equiv of $AsCl_3$ in THF was added to the deprotonated **L5** to give a yellow-orange solution with the formation of an off-white solid. The off-white solid was identified to be NaCl based on the absence of peaks in the IR spectrum and water solubility. The ^{1}H NMR spectrum of the solid obtained after removing the THF revealed an equal mixture of benzothiazole analog and [As(**L5**)Cl] (Scheme 7). Utilizing the Et_2O solubility of the benzothiazole product, the compounds were separated by recrystallization to give pure [As(**L5**)Cl]. The [As(**L5**)Cl] complex, contains As(III) coordinated by the most reduced and dianionic form of the deprotonated **L5**. Support for this assignment was obtained from ^{1}H NMR spectroscopic data and X-ray crystallography of the iodide analog, [As(**L5**)I]. The ^{1}H NMR spectrum of [As(**L5**)Cl] in $CDCl_3$ shows a singlet at 5.16 ppm which integrates for two methylene $–CH_2–$ protons. This resonance shifts to 4.83 ppm in the iodide analog. Also, an intense peak at m/z = 289.0 was observed for both [As(**L5**)Cl] and [As(**L5**)I] in the ESI-MS experiment, which can be assigned to the compound that results from the loss of a halogen ion $[As(\mathbf{L5})]^+$. To confirm this structure a DEPT (Distortionless Enhancement by Polarization Transfer) experiment was performed, which indicated the presence of one carbon with two H attached (see Figure 15). The presence of the $–CH_2–$ group rather than a –C=N– group is further supported by the absence of a strong $\nu_{C=N}$ stretch in the 1640 – 1690 cm^{-1} region in the FTIR.

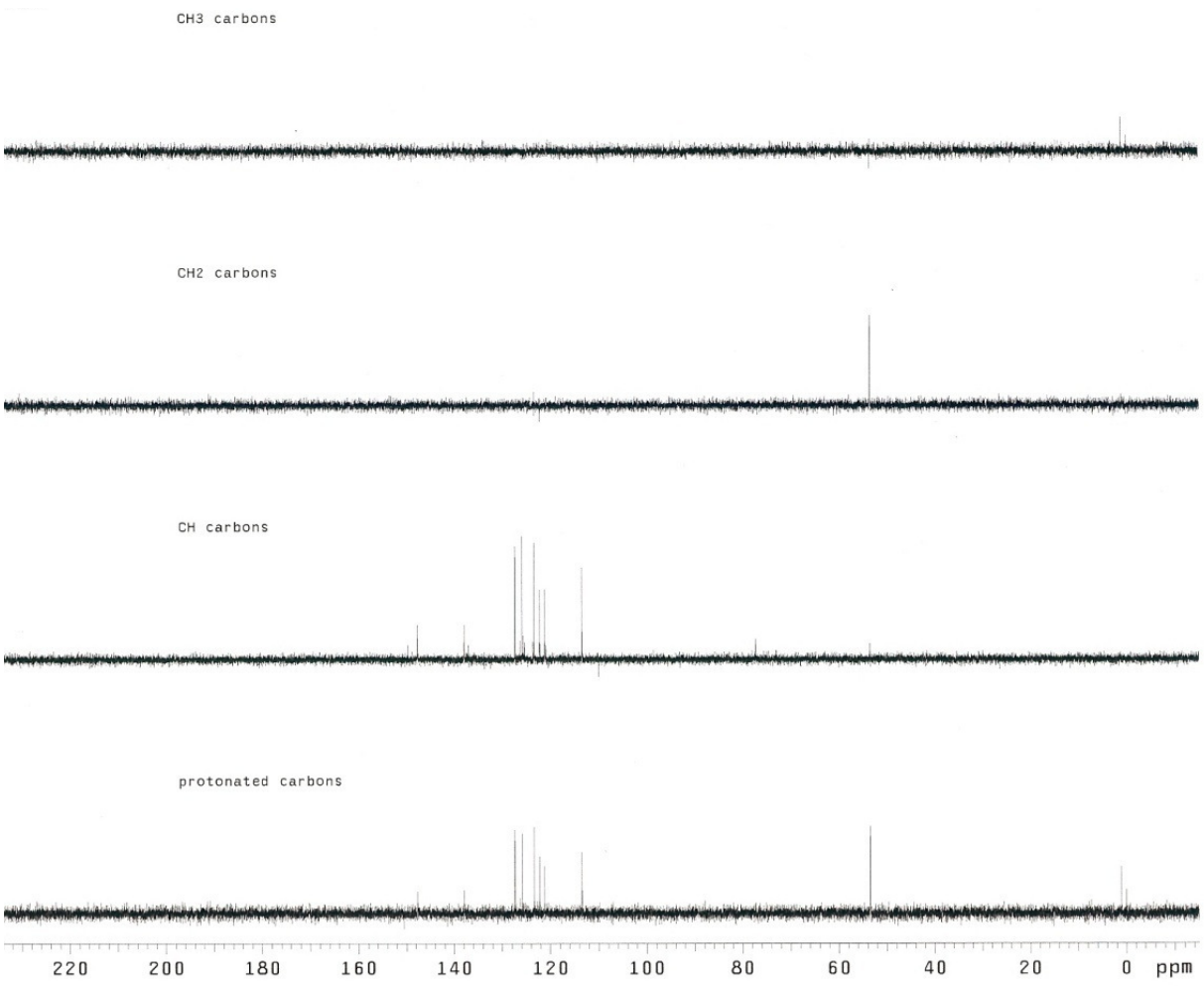

Figure 15. DEPT experiment of [As(**L5**)Cl] in $CDCl_3$ at 298 K. The second panel reveals the presence of one $–CH_2–$ group in the complex.

Performing a salt metathesis with NaI resulted in a near stoichiometric conversion of [As(**L5**)Cl] to [As(**L5**)I] (see Scheme 7). A diffraction quality crystal of [As(**L5**)I] was obtained by diffusion of pentane into a CCl_4 solution of [As(**L5**)I], which further confirmed the structure proposed from spectroscopic studies. The deprotonated **L5** ligand binds to the As(III) center as a tridentate ligand forming two five-member chelate rings from the N_2S donor atoms. The structure can be viewed as an AB_4E system on the basis of VSEPR (where, A = As(III), B = N, N, S, I and E = lone pair). The geometry about the As(III) center can be described as an

equatorially vacant trigonal-bipyramidal structure.[5] The equatorial plane consists of N1, I1 and the stereochemical lone pair, while the axial positions are occupied by S1 and N2 (see Figure 16). The As-S bond distance (As1-S1: 2.292 Å) is similar to other reported As(III)-thiolate bonds.[114, 121, 127, 185] Though As-N bonds are not very common, the bond length observed in [As(**L5**)I] (As1-N1, 1.846(5) and As1-N2, 2.411(6) Å) is within the range of reported As(III)-amide and As(III)-py complexes.[114, 186-187]Additionally, the N1-C7 bond distance of 1.441 (8) is consistent with a single C—N bond rather than a double C =N bond between N1 and C7.

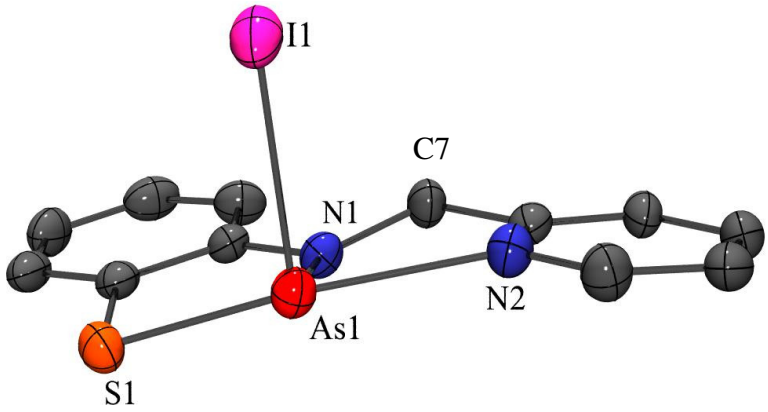

Figure 16. ORTEP diagram of [As(**L5**)I] showing 30% thermal probability ellipsoids. H atoms are omitted for clarity. Selected bond distances (Å) and angles (deg) for [As(**L5**)I]: As1-I1, 2.737(2); As1-N1, 1.846(5); As1-S1, 2.292(2); As1-N2, 2.411(6); N1-C7, 1.441 (8); N1-As1-S1, 87.71(2); N1-As1-I1, 97.86(2); S1-As1-N2, 162.69(2); N1-As1-N2, 76.64(2).

UV-vis studies of [As(**L5**)Cl] and [As(**L5**)I] were carried out in both donor and non-donor solvents to determine the effect of different solvents on the stability of this four-coordinate complex. In a non-donor solvent such as CH_2Cl_2, the 298 K UV-vis spectrum of [As(**L5**)Cl] displays a peak at 310 nm (ε = 4600 $M^{-1}cm^{-1}$) with a shoulder at 260 nm. In donor solvents such as MeCN, λ_{max} is essentially the same at 313 nm, but has a lower molar absorptivity value (ε = 2300 $M^{-1}cm^{-1}$). The similarity in the absorption profile of [As(**L5**)Cl] in both donor and non-

donor solvents indicates that the complex retains its four-coordinate structure in solution (Figures 17 – 18).

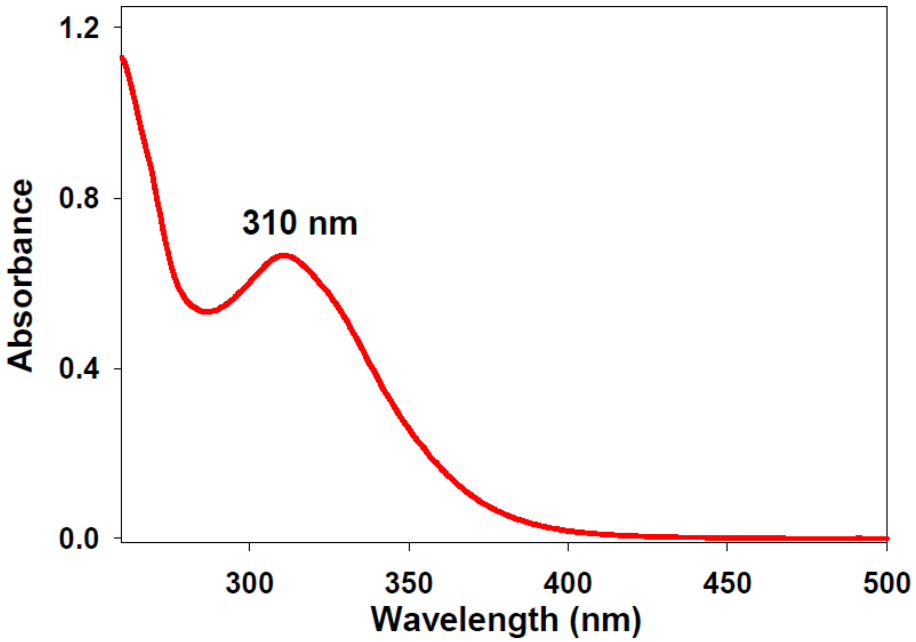

Figure 17. UV-vis spectrum of a 0.14 mM CH_2Cl_2 solution of [As(**L5**)Cl] at 298 K.

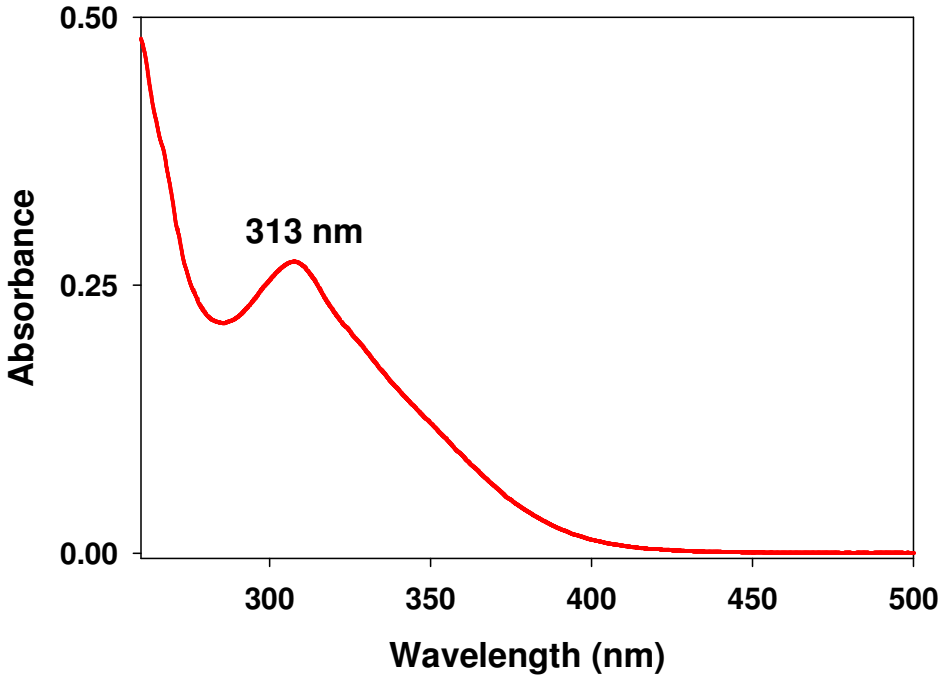

Figure 18. UV-vis spectrum of a 0.14 mM MeCN solution of [As(**L5**)Cl] at 298 K.

The UV-vis spectrum of [As(**L5**)I] was measured in CH_2Cl_2, MeCN and THF and shows two maxima; a shoulder is also observed in MeCN and CH_2Cl_2. The peaks are centered at 294 nm (2830 $M^{-1}cm^{-1}$) and 382 nm (4800 $M^{-1}cm^{-1}$) in CH_2Cl_2, the 294 nm (775 $M^{-1}cm^{-1}$) peak is retained and a blue-shift to 362 nm (505 $M^{-1}cm^{-1}$) is observed in THF. Additionally both peaks are blue-shifted to 290 nm (1035 $M^{-1}cm^{-1}$) and 356 nm (625 $M^{-1}cm^{-1}$) in MeCN (Figures 19 – 21). The peak at 290 nm – 313 nm has been assigned as a S-to-As charge transfer and this assignment is supported by a similar peak in other spectroscopically-characterized As(III) thiolates.[89, 121, 124] The additional lower energy peak at 356 nm – 382 nm has been tentatively assigned to a I-to-As charge transfer and the lower molar absorptivity of these bands in donor solvents is possibly due to the ease of dissociation of the As-I bond.[188]

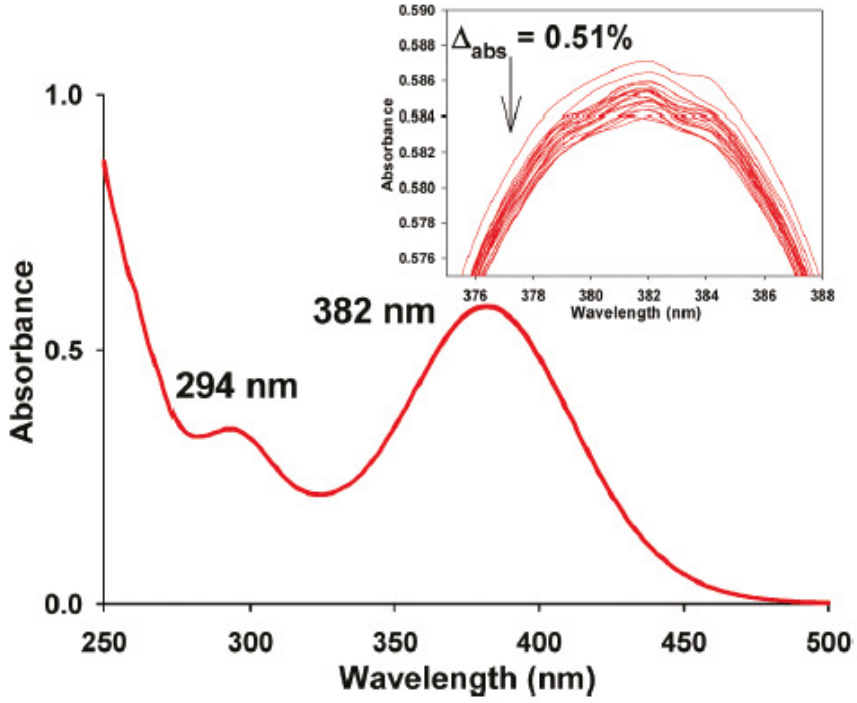

Figure 19. UV-vis spectrum of a 0.12 mM CH_2Cl_2 solution of [As(**L5**)I] at 298 K. Inset: Spectral changes upon direct purging of O_2(g) at 298 K (traces recorded at 3 min intervals; total time = 1 h; Δ_{abs} = 0.003 = 0.51% change).[188]

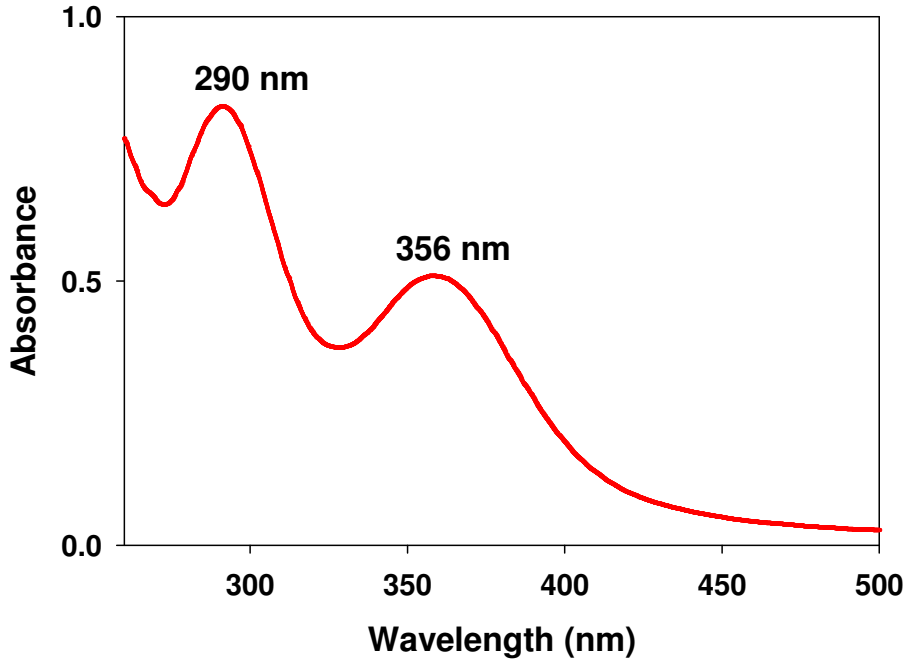

Figure 20. UV-vis spectrum of a 0.78 mM MeCN solution of [As(**L5**)I] at 298 K.

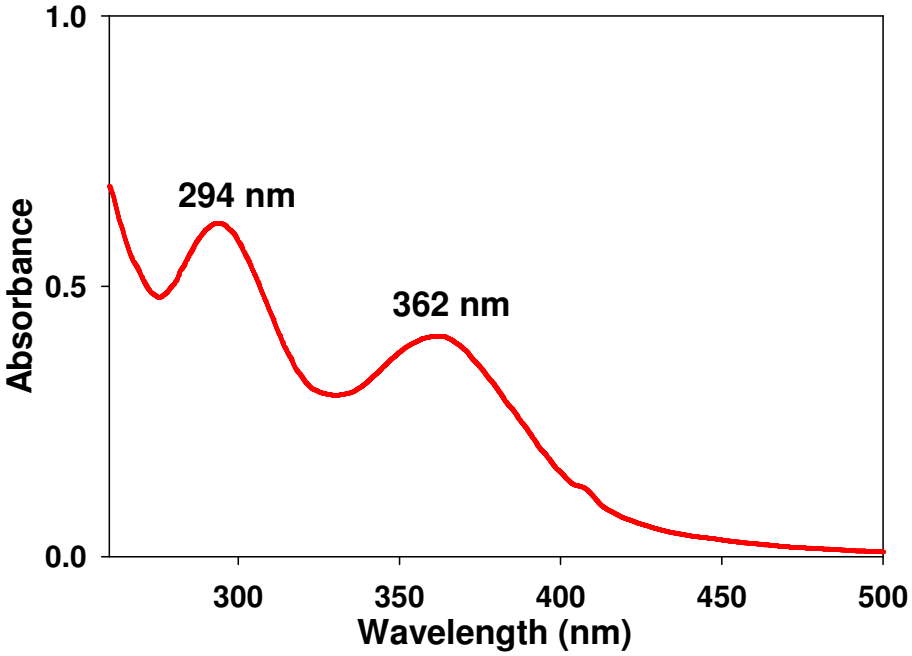

Figure 21. UV-vis spectrum of a 0.78 mM THF solution of [As(**L5**)I] at 298 K.

Furthermore, the complexes are stable in aerobic conditions, purging solutions of [As(**L5**)I] with pure O_2 or exposure to ambient atmospheric conditions for 5 min resulted in no significant change in the ESI-MS, ^{1}H NMR and UV-vis (see inset in Figure 19). The O_2-stability is further supported by the lack of any redox event between +2.0 to -2.0 V vs Ag/AgCl in THF at room temperature. However, the complexes are easily hydrolyzed as dissolution of the compound in pH 7.2 water (phosphate buffer) resulted in an oily substance.

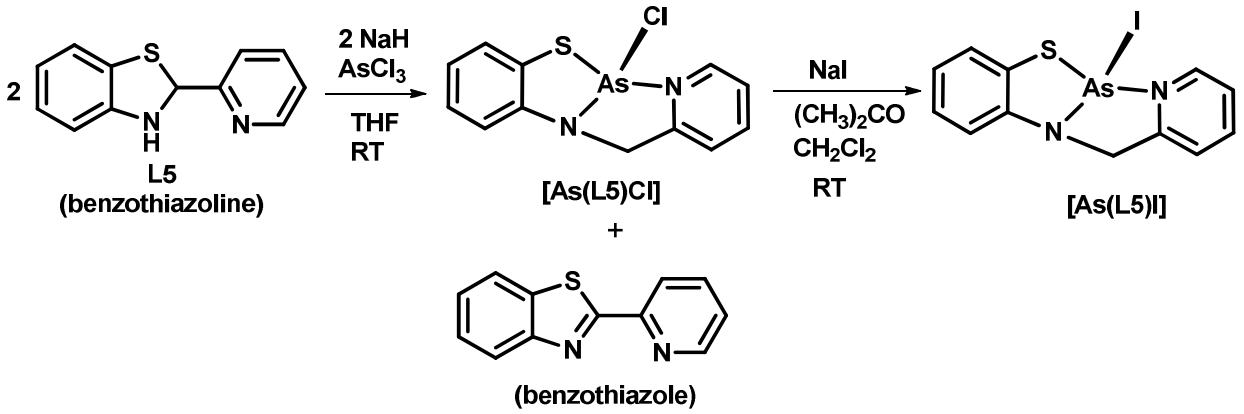

Scheme 7. Reaction of **L5** and As(III) to give [As(**L5**)Cl] and benzothiazole, then salt metathesis to give [As(**L5**)I].

In summary, the reaction of **L5** with As(III) in the presence of a base leads to the disproportionation of **L5** to give the benzothiazole analog and the ring-open reduced form which yields a four-coordinate complex with As(III) (Scheme 7 and Figure 16). This newly observed chemistry is interesting in many aspects. First, this new structure contributes to the small number of structurally characterized As(III)-four-coordinate complexes.[11, 119, 186, 189-191] The stability of [As(**L5**)Cl] and [As(**L5**)I] in solution in the presence of excess oxygen indicates the possibility and stability of such binding mode in biological systems and for sensing purposes. Indeed, a 2.3 Å resolution structure of an As(III) extrusion protein (named ArsA ATPase) found in *E. coli*, has

a metal binding site that contains both Cys-S and His-N residues.[192] The structure of this protein was obtained with Sb(III) exhibiting an N,S-chelation as further proof that this coordination mode is possible for As(III) *in vivo*. Finally, **L5** forms complexes with several transition-metals as the Schiff-base form;[184, 193] the observed redox-rearrangement with As(III) is a rare event (only reported for Re(V)[194]) and will be utilized in designing a chemodosimeter-based fluorescent dye for As(III).

2.4 Conclusion.

The coordination chemistry of As(III) with various types of ligands containing different S-based topologies was studied. The thioether-based ligands, **L1 – L3** appear to be poor ligands for As(III) because any complex formed is readily dissociated in solution. Spectroscopic evidence indicate the formation of the tri-coordinate complex with N-acetyl-L-cysteine methyl ester, used here as an analog for cysteine suggesting that monodentate thiolate ligands may serve as effective ligands for As(III). Finally, the reaction of As(III) and a benzothiazoline-containing ligand, **L5**, led to the formation of a four-coordinate As(III) complex and benzothiazole by-product. This redox rearrangement of the benzothiazoline functional group is the first to be reported for a main group element and could serve as an As(III) specific response in future sensor platforms.

2.5 Experimental Section

General Information. All reagents were purchased commercially and used as received unless otherwise noted. Acetonitrile (MeCN), methylene chloride (CH_2Cl_2), tetrahydrofuran (THF), diethyl ether (Et_2O) and pentane were purified by passage through activated alumina columns

using an MBraun MB-SPS solvent purification system and stored under a dinitrogen (N_2) atmosphere before use. Ethanol (EtOH) was dried by distilling from $Mg(OEt)_2$ under N_2 atmosphere and acetone was distilled from $CaSO_4$. Both solvents were degassed by three freeze-pump-thaw cycles. Anhydrous carbon tetrachloride (CCl_4) was procured from Aldrich and used as received. Oxygen gas (99.95%) was purchased from Airgas and used without further purification. Reactions that required anaerobic conditions were performed in an MBraun Unilab glovebox under an atmosphere of purified N_2. The ligands, (*N,N'E,N,N'E*)-*N,N'*-(1,4-phenylenebis(methanylylidene))bis(2-(methylthio)aniline) (**L2**) and racemic 2-(pyridin-2-yl)-2,3-dihydrobenzo[d]thiazoline (**L5**) were synthesized according to published procedures.[179, 195]

Physical Measurements. ^1H and ^{13}C NMR spectra were recorded in deuterated solvents on either a Varian Unity Inova 500 MHz or Varian Mercury plus 400 MHz NMR spectrometer at 298 K with chemical shifts referenced to tetramethylsilane (TMS) or residual protio signal of the deuterated solvent.[196] FTIR spectra were collected on a ThermoNicolet 6700 spectrometer running the OMNIC software. Samples were run as solids either in a KBr matrix or ATR diamond transmission window. Electronic absorption spectra were run at 298 K using a Cary 50 spectrophotometer equipped with a Quantum Northwest TC 125 temperature control unit. UV-vis samples were prepared in gas-tight Teflon-lined screw cap quartz cells with an optical pathlength of 1 cm. Cyclic voltammetry measurements were performed with a PAR Model 273A potentiostat using a Ag/AgCl reference electrode, Pt counter electrode and a Glassy Carbon working electrode. Measurements were performed at ambient temperature using 2.0 – 5.0 mM analyte in THF under N_2 containing 0.1 M $^nBu_4NPF_6$ as the supporting electrolyte. Low resolution ESI-MS data were collected on a Perkin-Elmer Sciex API-I Plus quadrupole mass spectrometer. Elemental analysis was performed by Quantitative Technologies Inc in

Whitehouse, N.J. FTIR and UV-vis data were plotted using the SigmaPlot 10.0 software package and NMR data were plotted with MestReNova Lite.

Synthesis Safety Note. Caution! Compounds containing arsenic (As) are toxic and should be handled with extreme care.

Reaction of N-acetyl-L-Cysteine methyl Ester ($SNAc^{OMe}$) and $AsCl_3$, [$As(SNAc^{OMe})_3$]. A solid batch of $SNAc^{OMe}$ (0.6243 g, 3.52 mmol) was dissolved in 4.5 mL of THF to give a clear solution, and then a 1.5 mL THF solution of Et_3N (0.4043 g, 3.99 mmol) was added and the solutions was stirred for 20 min with no observable changes. Then a 6 mL THF solution of $AsCl_3$ (0.2189 g, 1.21 mmol) was added to the deprotonated $SNAc^{OMe}$ resulting in the immediate formation of an off-white precipitate (presumably $Et_3N{\cdot}HCl$). After 2 h, the reaction was filtered to give an off-white residue (identified to be $Et_3N{\cdot}HCl$), and a clear filtrate, which was concentrated to an off-white solid. The solid was treated with 3 mL of Et_2O and dried under vacuum to give the complex of interest (0.2244 g, 31%). ^1H NMR (400 MHz, $CDCl_3$, δ from TMS): 2.08 (s, 3H), 3.33 (t, 2H), 3.79 (s, 3H), 4.92 (m, 1H), 6.77 (d, 1H, NH). ^{13}C NMR (100 MHz, $CDCl_3$, δ from TMS): 23.1, 34.1, 52.8, 53.3, 170.3, 170.7. FTIR (KBr) ν_{max} (cm^{-1}): 3306 (vs, N-H), 3050 (m), 2950 (m), 2929 (m), 2839 (m), 1740 (vs), 1647 (vs), 1533 (vs), 1437 (s), 1372 (s), 1343 (s), 1314 (s), 1295 (s), 1271 (s), 1247 (s), 1211 (s), 1169 (s), 1008 (m), 668 (m), 589 (m). LRMS-ESI (*m/z*), $[M + H]^+$ calcd for $C_{18}H_{30}AsN_3O_9S_3$, 604.0; found, 604.0. Anal calcd for $C_{18}H_{30}AsN_3O_9S_3$: C, 35.82; H, 5.01; N, 6.96. Found: C, 34.02; H, 4.92; N, 6.96. UV-vis (MeOH, 298 K) λ_{max}, nm (ε, M^{-1} cm^{-1}): 260 – 320 (broad peak).

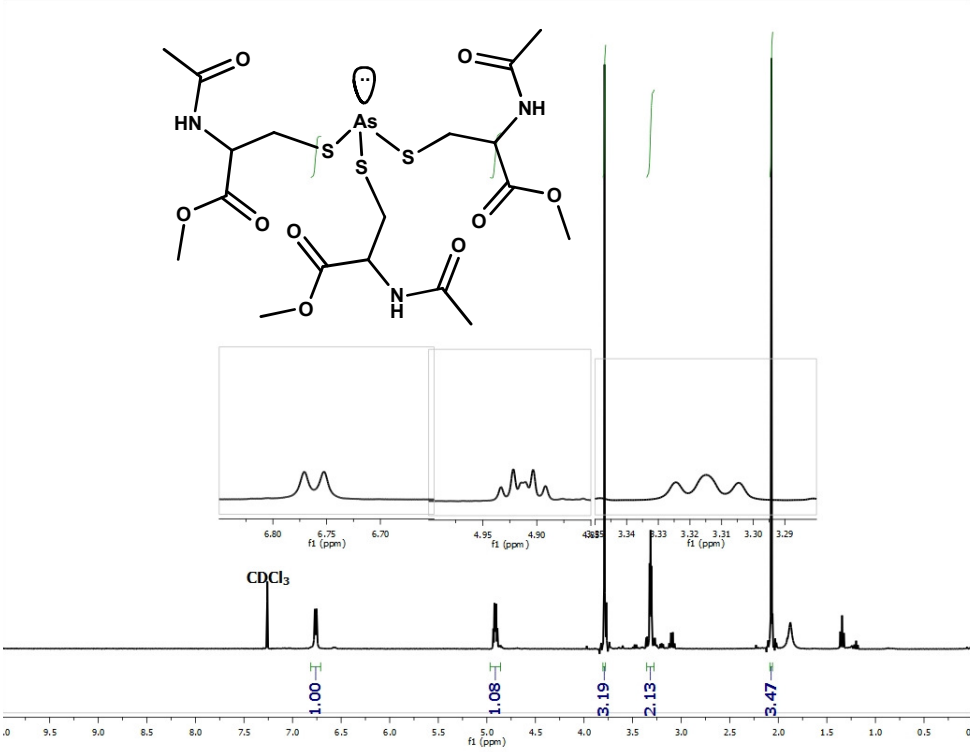

Figure 22. ^{1}H NMR spectrum of [As(SNAc^{OMe})$_3$] in $CDCl_3$ at 298 K. Inset: proposed structure of [As(SNAc^{OMe})$_3$].

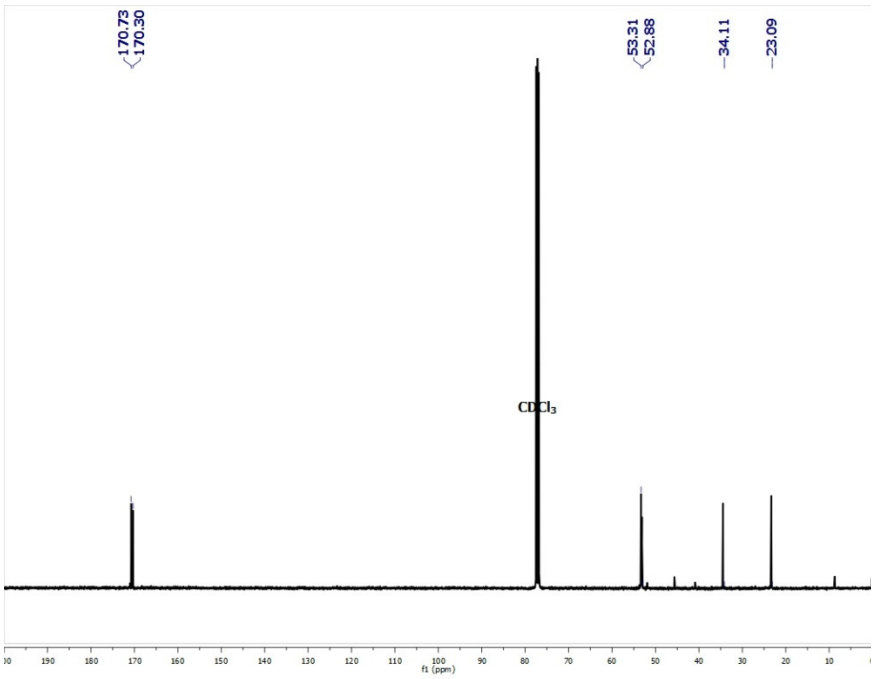

Figure 23. ^{13}C NMR spectrum of [As(SNAc^{OMe})$_3$] in $CDCl_3$ at 298 K.

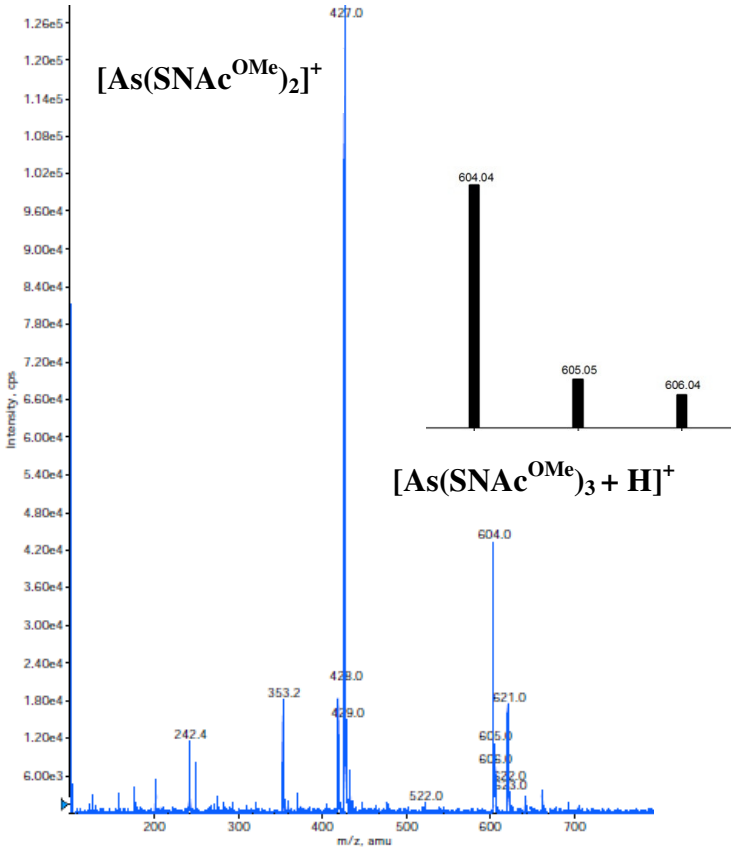

Figure 24. Positive mode LRMS-ESI-MS of [As(SNAc^{OMe})$_3$] showing the parent peak at *m*/*z* = 604.0. Inset: calculated molecular weight and isotopic distribution of [As(SNAc^{OMe})$_3$].

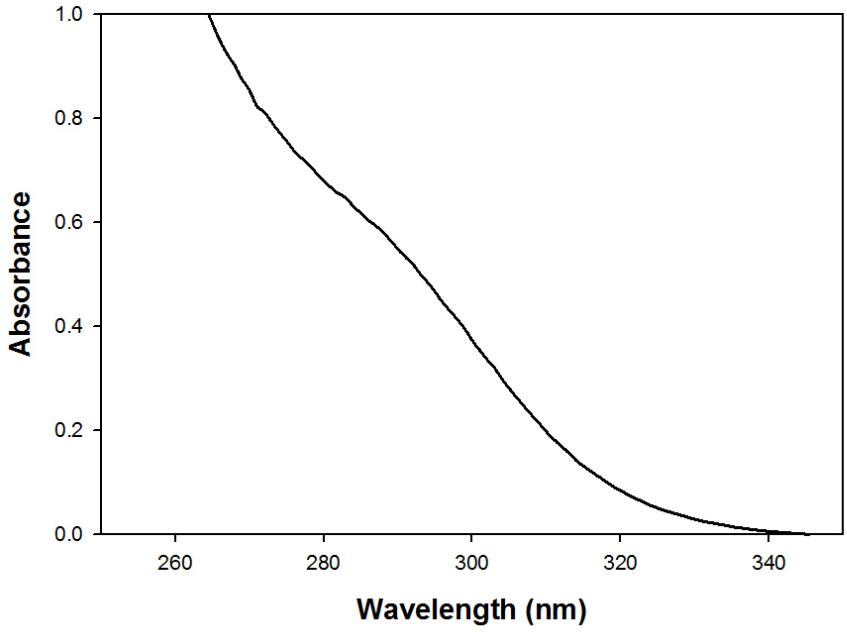

Figure 25. UV-vis spectrum of a 0.77 mM solution of [As(SNAc^{OMe})$_3$] in MeOH at 298 K.

Synthesis of N^1,N^4-bis(2-(methylthio)phenyl)terephthalamide (L1). A batch of 2-(methylthio)aniline (0.5220 g, 3.749 mmol) and Et_3N (1.9226 g, 19.000 mmol) was dissolved in 10 mL of CH_2Cl_2 to give a yellow solution. This solution was added dropwise to a flask maintained at 0 ^oC with an ice bath containing a clear solution of terephthaloyl chloride (0.3863 g, 1.900 mmol) dissolved in 12 mL of CH_2Cl_2. The reaction turned yellow after the first few drops and was left to stir for 24 h at RT. An off-white precipitate was observed within 12 h of the reaction. CH_2Cl_2 (100 mL) was added to dissolve the precipitate and the resulting solution was washed twice with saturated $NaHCO_3$ solution, once with DI water and twice with saline solution. The organic layer was dried with $MgSO_4$, filtered and concentrated on a rotavap to afford an off-white solid. The product was further purified by trituration with Et_2O, filtered and dried to afford 0.4040 g (52%) of product as an off-white solid. ^1H NMR (500 MHz, $CDCl_3$ δ from TMS): 2.44 (s, 6H), 7.15 (t, 2H), 7.39 (t, 2H), 7.57 (d, 2H), 8.11 (s, 4H), 8.54 (d, 2H), 9.31 (s, 2H). ^{13}C NMR (100 MHz, $CDCl_3$ δ from TMS): 19.48 (CH_3), 120.60, 124.99, 125.78, 127.87, 129.43, 133.52, 137.98, 138.40, 164.22. FTIR (KBr, powder) ν_{max} (cm^{-1}): 3273 (m, N-H), 3057 (w), 2978 (w), 2916 (w), 2677 (w), 2603 (w), 2492 (w), 1940 (w), 1682 (vs), 1578 (vs), 1522 (vs), 1473 (vs), 1435 (vs), 1401 (s), 1308 (s), 1183 (m), 1117 (m), 1086 (vs), 1066 (m), 1052 (m), 1038 (m), 1015 (m), 969 (m), 955 (m), 922 (m), 906 (m), 863 (m), 825 (m), 749 (m), 724 (m), 675 (m), 597 (m), 546 (m), 467(m), 449(m). LRMS-ESI (*m/z*), $[M + H]^+$ calcd for $C_{22}H_{20}N_2O_2S_2$, 409.5; found, 409.2.

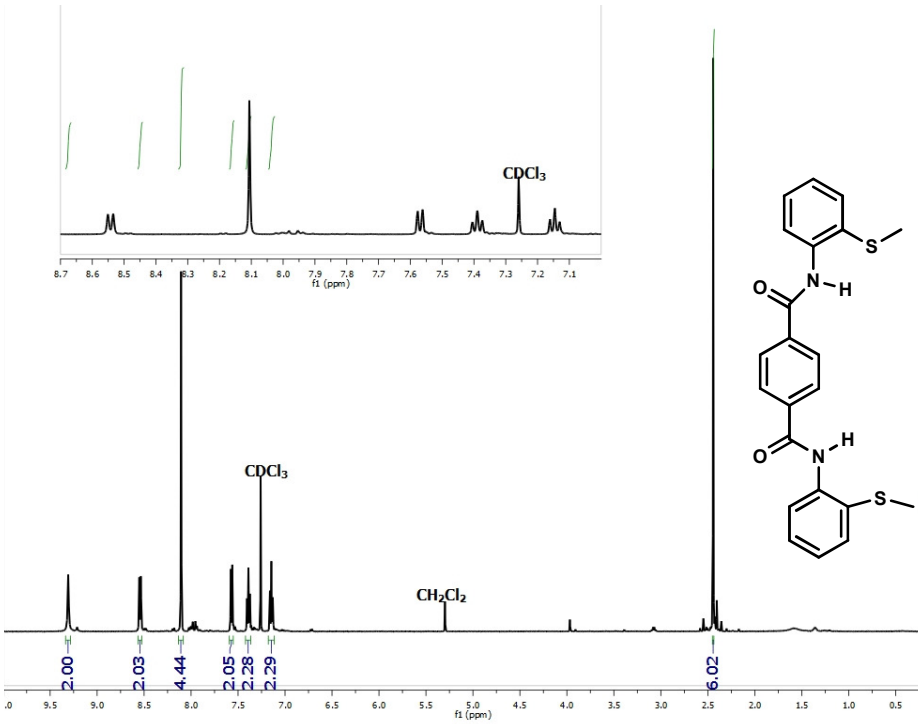

Figure 26. ^{1}H NMR spectrum of **L1** in $CDCl_3$ at 298 K. Inset: structural depiction of **L1**.

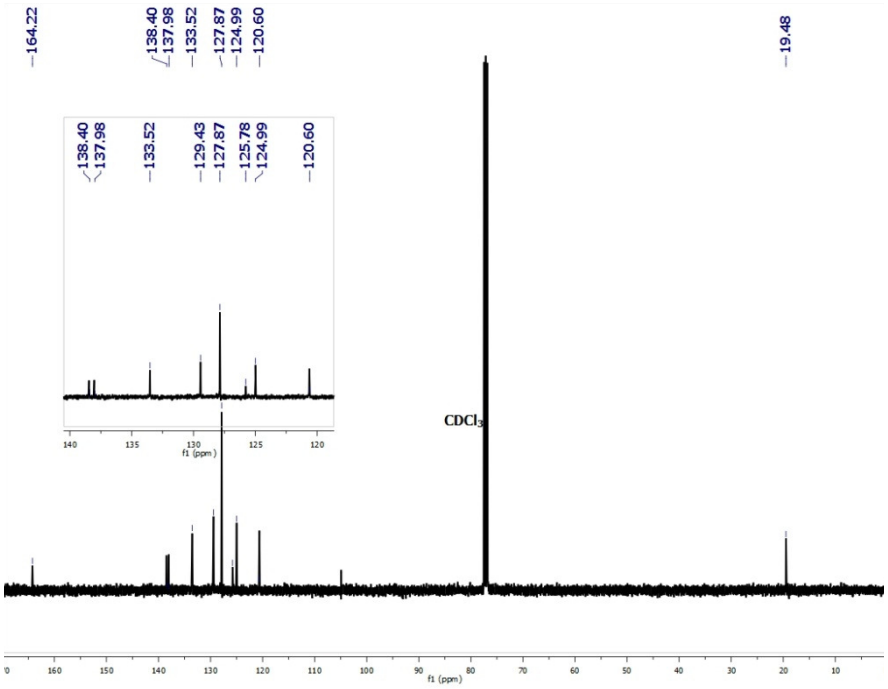

Figure 27. ^{13}C NMR spectrum of **L1** in $CDCl_3$ at 298 K.

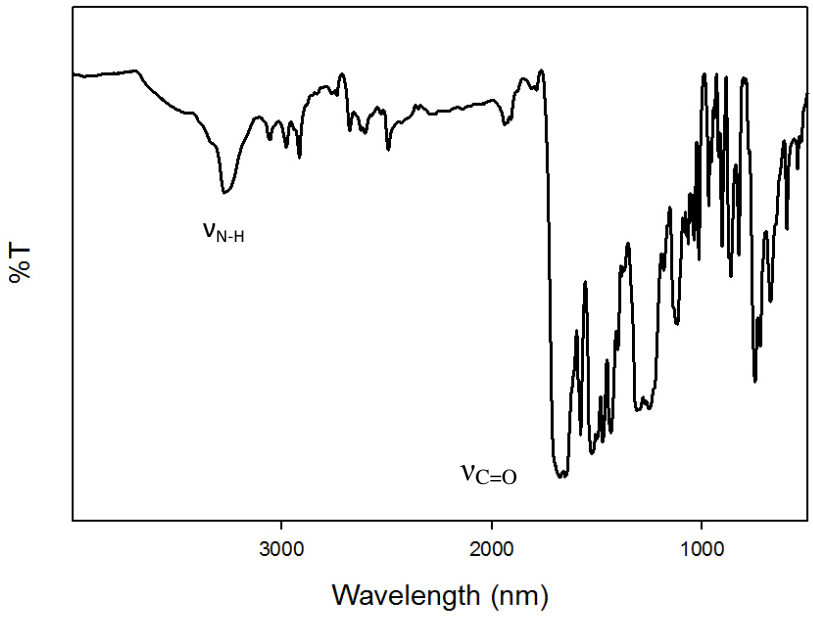

Figure 28. Solid-state FTIR spectrum (KBr) of **L1**.

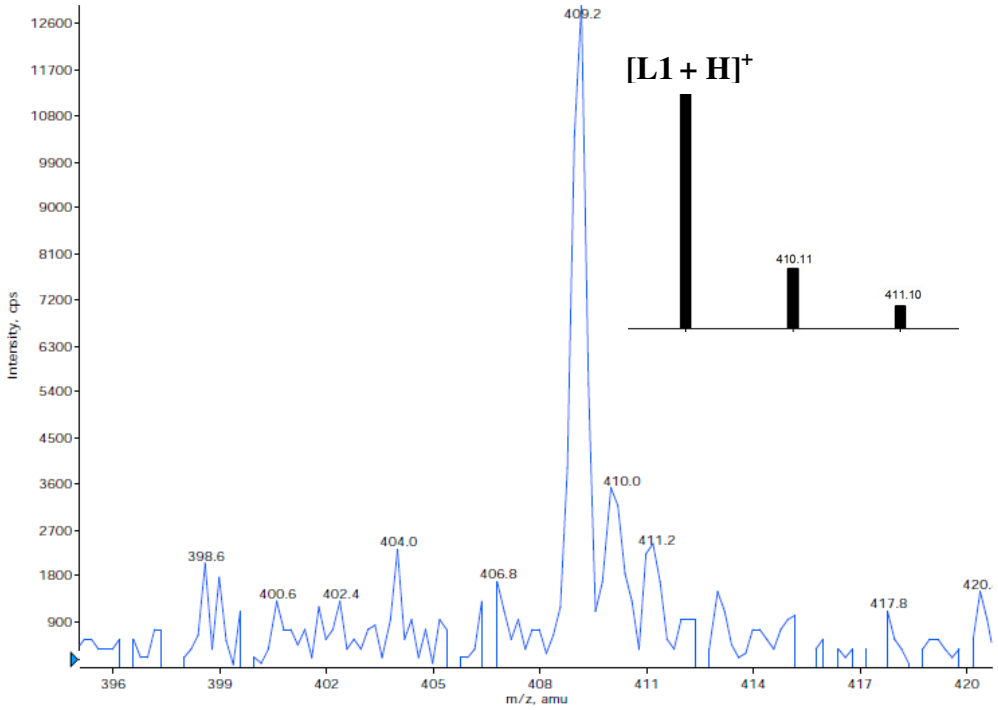

Figure 29. Positive mode LRMS-ESI-MS of **L1** showing the parent peak at *m*/*z* = 409.2. Inset: calculated molecular weight and isotopic distribution of **L1**.

Synthesis of *N*,*N*'-(1,4-phenylenebis(methylene))bis(2-methylthio)aniline) (L3). A batch of $NaBH_4$ (2.1001 g, 55.5141 mmol) was added portionwise to a solution of **L2** (2.0242 g, 5.3819 mmol) in 100 mL of THF. The reaction was refluxed for 2 h and 2 mL of DI water was then added. On addition of DI, the reaction boiled vigorously for several minutes. The reaction was left to reflux for an additional 2 h until the yellow color of **L2** disappeared. The THF was then removed using the rotavap and 100 mL of DI water was added to quench the $NaBH_4$. The product was then extracted with 100 mL of CH_2Cl_2, the organic layer was dried with $MgSO_4$ and concentrated to give a clear oil. Et_2O (10 mL) was added to the oil and after stirring for 5 min a white crystalline solid (1.5247 g, 74%) was obtained. ^{1}H NMR (400 MHz, $CDCl_3$, δ from TMS): 2.34 (s, 6H), 4.40 (d, 4H), 5.35 (s & br, 2H), 6.58 (d, 2H), 6.66 (t, 2H), 7.15 (t, 2H), 7.34 (s, 4H), 7.41 (d, 2H). ^{13}C NMR (100 MHz, $CDCl_3$, δ from TMS): 18.32 (CH_3), 47.92 (CH_2), 110.54, 117.41, 127.65, 129.59, 134.18, 138.36, 148.24. LRMS-ESI (*m/z*), $[M + H]^+$ calcd for $C_{22}H_{24}N_2S_2$, 381.6; found, 381.2. FTIR (ATR-diamond, powder) ν_{max} (cm^{-1}): 3360 (m, N-H), 3060 (w), 3021 (w), 2986 (w), 2941 (w), 2918 (w), 2848 (m), 1908 (m), 1879 (w), 1814 (w), 1786 (w), 1731 (w), 1694 (w), 1584 (vs), 1567 (s), 1514 (w), 1493 (vs), 1664 (s), 1447 (s), 1412 (s), 1311 (m), 1281 (m), 1269 (m), 1236 (m), 1214 (w), 1160 (w), 1132 (w), 1107 (w), 1084 (w), 1035 (m), 1018 (m), 967 (m), 941 (m), 880 (m), 847 (w), 819 (m), 785 (m), 750 (vs).

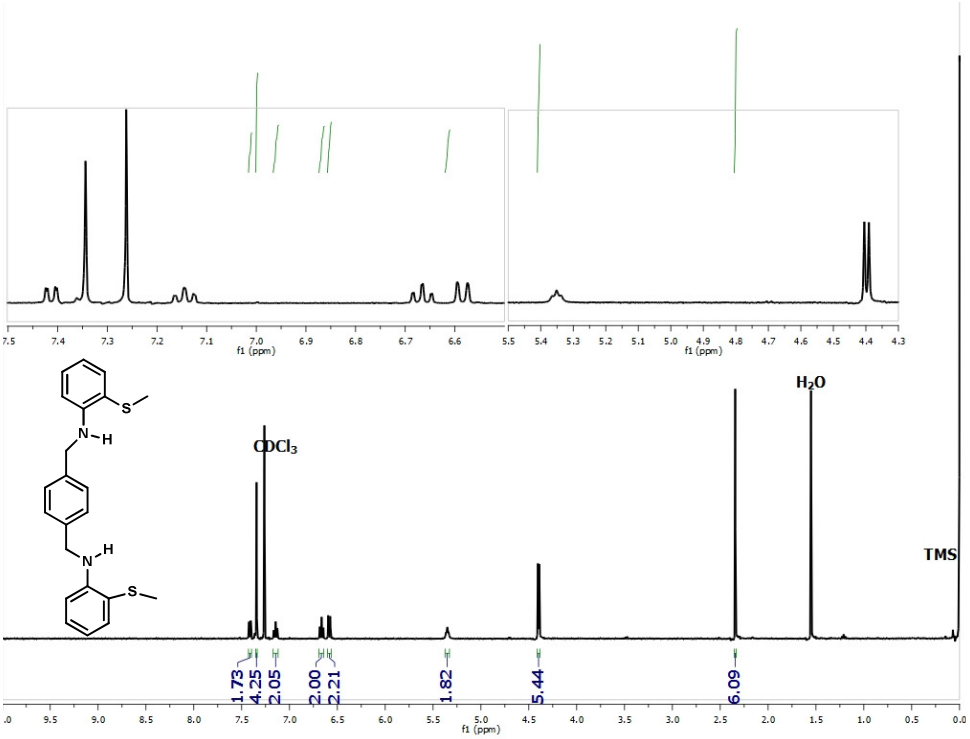

Figure 30. ^{1}H NMR spectrum of **L3** in $CDCl_3$ at 298 K. Inset: structural depiction of **L3**.

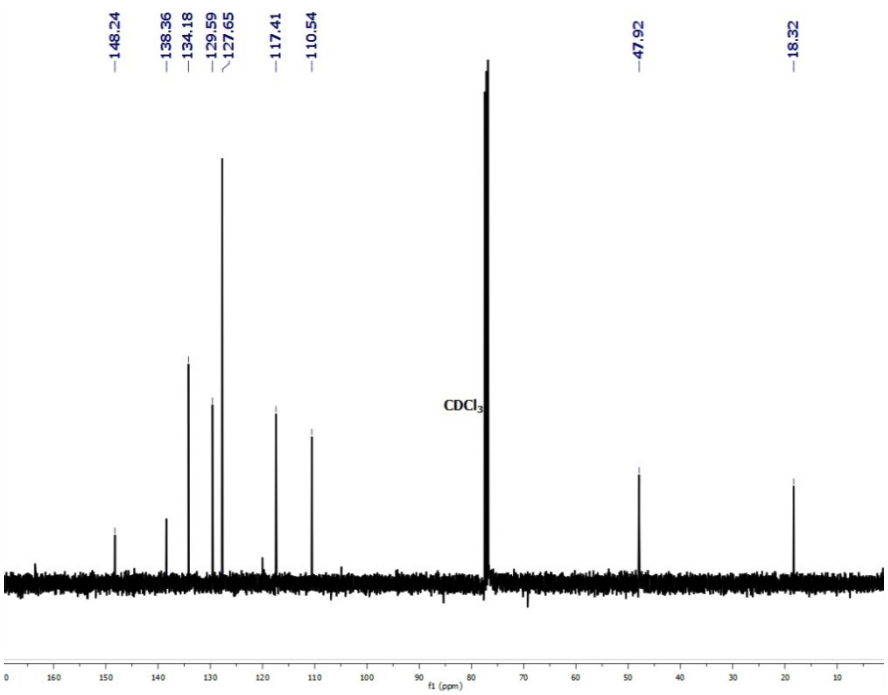

Figure 31. ^{13}C NMR spectrum of **L3** in $CDCl_3$ at 298 K.

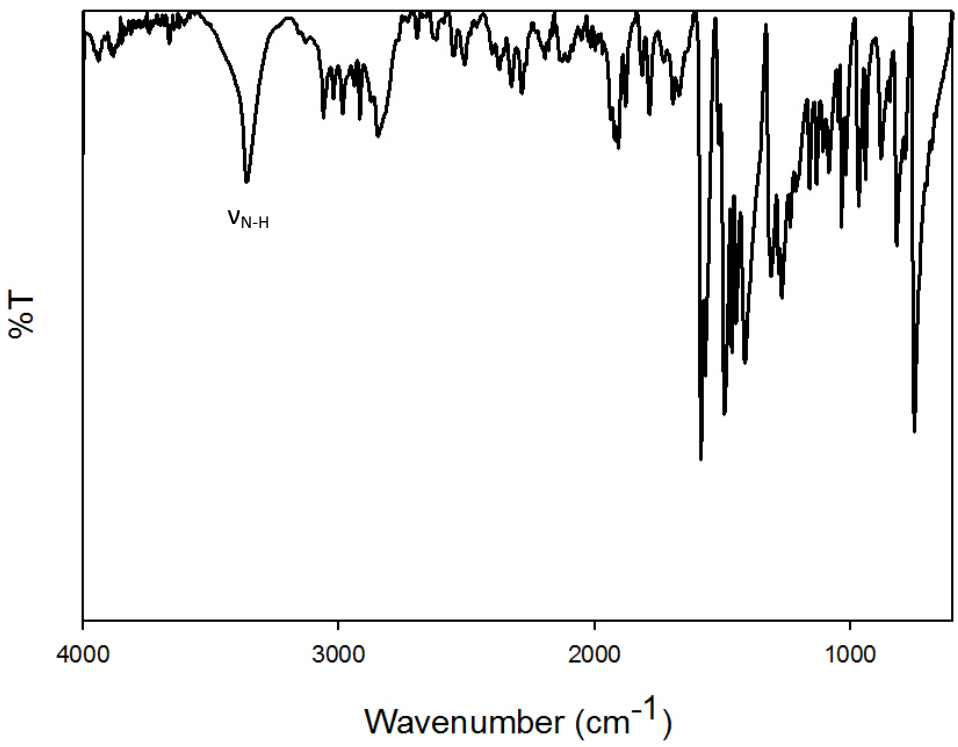

Figure 32. Solid-state FTIR spectrum (ATR-Diamond) of **L3**.

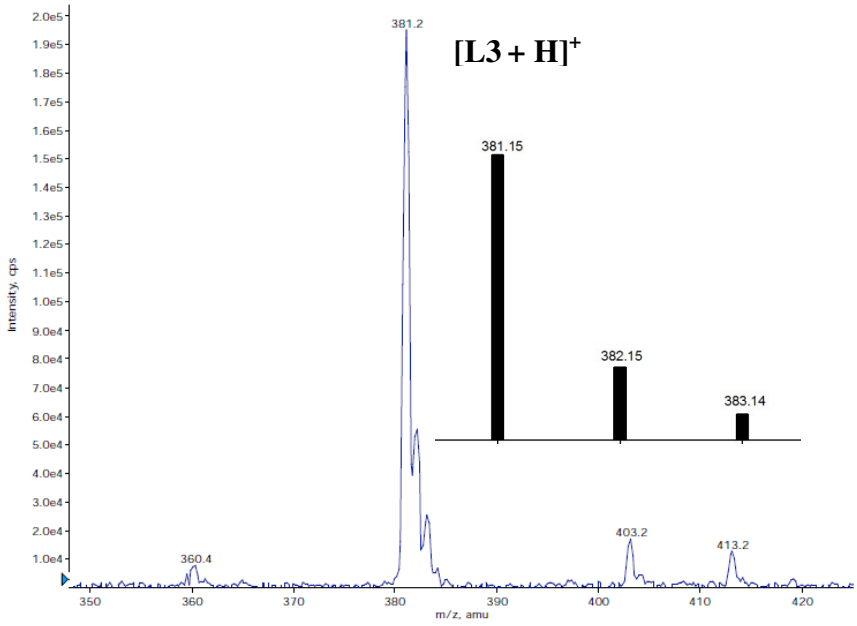

Figure 33. Positive mode LRMS-ESI-MS of **L3** showing the parent peak at *m*/*z* = 381.2. Inset: calculated molecular weight and isotopic distribution of **L3**.

Reaction of L1 and $AsCl_3$, attempted synthesis of $[As_2(L1)_3]$. A solid batch of **L1** (0.4211 g, 1.0321 mmol) was dissolved in 90 mL of CH_2Cl_2 and left to stir for 1 h in 3 Å sieves. A solution of $AsCl_3$ (0.1348 g, 0.7436 mmol) in 10 ml CH_2Cl_2 was then added and the solution was left to stir overnight, but no change was observed. The solvent was removed under vacuum to give an off-white solid (0.4001 g) whose ^1H NMR was consistent with that of unreacted **L1**. ^1H NMR (400 MHz, $CDCl_3$, δ from TMS): 2.44 (s, 6H), 7.15 (t, 2H), 7.39 (t, 2H), 7.57 (d, 2H), 8.11 (s, 4H), 8.54 (d, 2H), 9.31 (s, 2H).

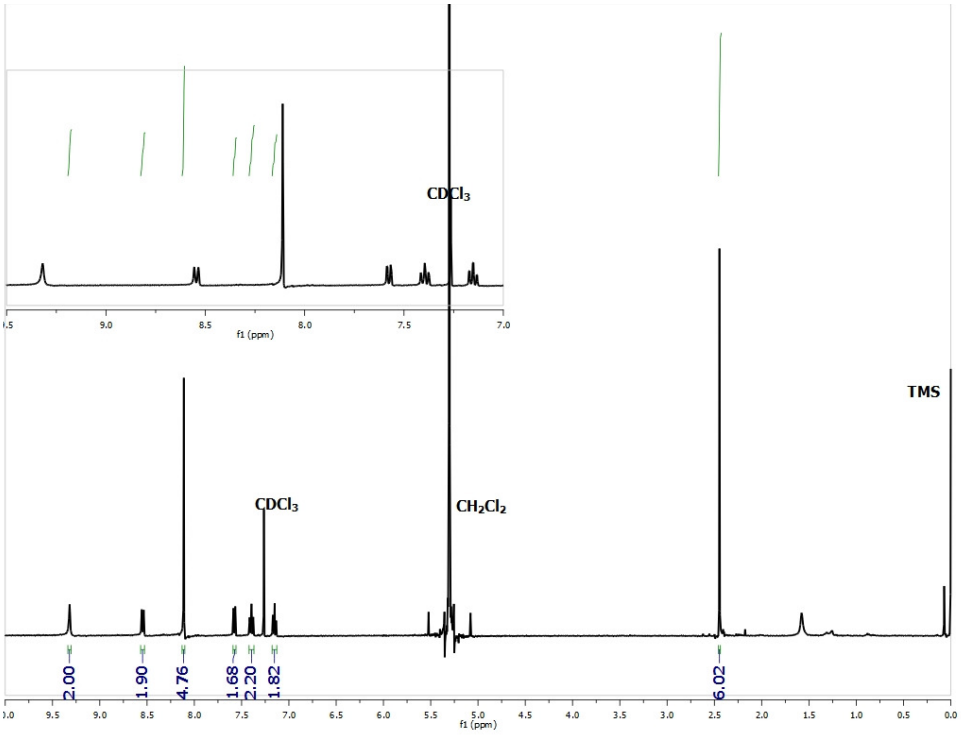

Figure 34. ^1H NMR spectrum of the reaction of **L1** and $AsCl_3$ in $CDCl_3$ at 298 K.

Reaction of L2 and $AsCl_3$, attempted synthesis of $[As_2(L2)_3]$. A solid batch of **L2** (0.9031 g, 2.4011 mmol) was dissolved in 50 mL of CH_2Cl_2 in a Schlenk flask and left to stir in sieves for 1 h. On adding a 10 mL CH_2Cl_2 solution of $AsCl_3$ (0.3177 g, 1.7525 mmol), the color of the reaction changed from yellow to orange and was left to stir for 5 h at RT. Filtration to remove

insolubles was performed and the filtrate was concentrated under vacuum to afford a yellow solid, which turned orange on further drying (1.0011 g) consistent with unreacted **L2**. ^{1}H NMR (400 MHz, $CDCl_3$, δ from TMS): 2.42 (s, 6H); 7.03 (d, 2H); 7.19 (m, 6H); 8.06 (s, 4H); 8.48 (s, 2H).

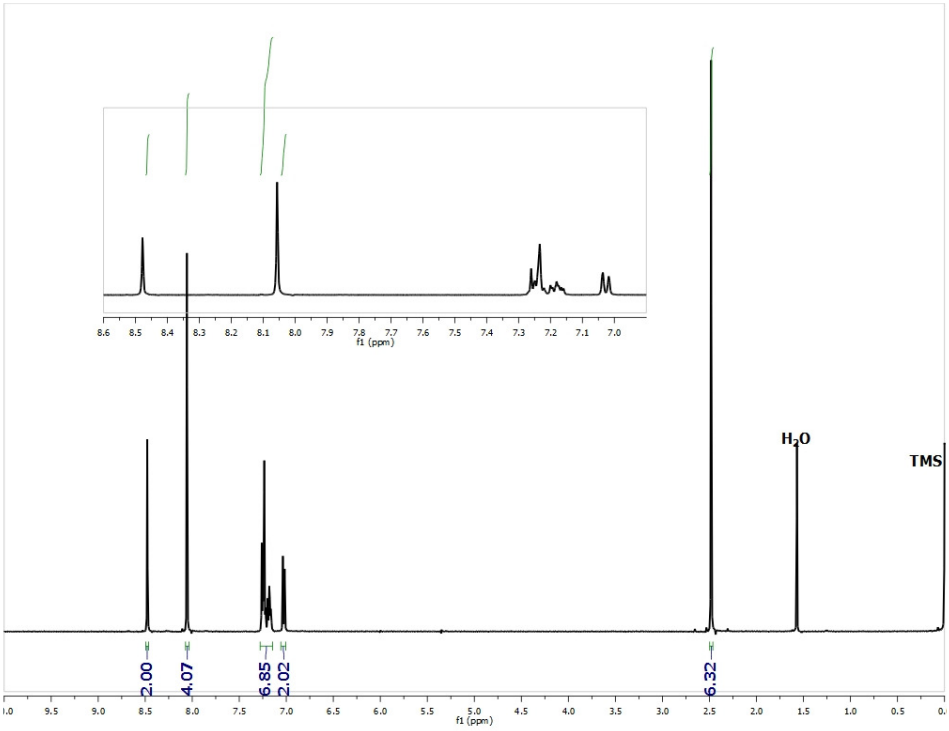

Figure 35. ^{1}H NMR spectrum of the reaction of **L2** and $AsCl_3$ in $CDCl_3$ at 298 K.

Reaction of L3 and $AsCl_3$, attempted synthesis of [As_2(L3)$_3$]. *Reaction A*: A solid batch of **L3** (0.2180 g; 0.5737 mmol) was dissolved in 20 mL of CH_2Cl_2 and a solution of $AsCl_3$ (0.0692 g, 0.3817 mmol) in 10 mL of CH_2Cl_2 was added. The reaction was clear at first but gradually turned cloudy within 1 h. The reaction was left to stir for 2 days at RT, and then the solvent was removed under pressure to give an off-white solid (0.2008 g). Single crystals were obtained by diffusion of Et_2O into a CH_3OH solution of the white solid obtained. ^{1}H NMR (500 MHz, CD_3OD, δ from TMS): 2.43 (s, 6H), 4.54 (s, 4H), 6.93 (d, 2H), 7.11 (t, 2H), 7.21 (t, 2H), 7.40 (s,

4H), 7.54 d, 2H). FTIR (ATR-diamond, powder) ν_{max} (cm^{-1}): 3361 (m, N-H), 2918 (w), 2850 (w), 2624 (w), 2517 (m), 2393 (m), 2351 (w), 1585 (vs), 1566 (vs), 1531 (w), 1494 (s), 1482 (s), 1465 (m), 1441 (s), 1416 (s), 1372 (m), 1313 (m), 1281 (m), 1258 (m), 1196 (w), 1160 (m), 1133 (m), 1068 (m), 1035 (m), 1018 (m), 991 (m), 967 (m), 949 (m), 881 (m), 866 (m), 800 (m), 770 (w), 751 (s), 588 (m), 532 (w) . *Reaction B* (In presence of 3 Å mol-sieves): A solid batch of **L3** (0.1994 g, 0.5245 mmol) was dissolved in 4 mL of CH_2Cl_2 and stirred in sieves for 1 h to remove all traces of water. Then a solution of $AsCl_3$ (0.0682 g, 0.3762 mmol) in 2 mL of dry CH_2Cl_2 was added resulting in a clear solution that slowly turned cloudy over 5 h. The reaction was left to stir further at RT for 10 h resulting in no change. The solvent was removed via short path vacuum distillation to give a sticky white solid, which was dried further under high vacuum to give an off-white solid (0.1668 g). ^1H NMR (500 MHz, CD_3OD, δ from TMS): 2.46 (s, 6H); 4.57 (s, 4H); 7.02 (d, 2H); 7.22 (m, 4H); 7.41 (s, 4H); 7.57 (d, 2H). FTIR (ATR-diamond, powder) ν_{max} (cm^{-1}): 3361 (m, N-H), 3060 (w), 2986 (w), 2918 (w), 2849 (w), 2363 (w), 1907 (w), 1878 (w), 1813 (w), 1785 (w), 1692 (w), 1585 (vs), 1568 (s), 1514 (w), 1493 (vs), 1464 (s), 1448 (s), 1412 (s), 1312 (m), 1281 (m), 1261 (m), 1236 (m), 1160 (w), 1132 (w), 1084 (w), 1049 (w), 1035 (w), 1018 (w), 968 (w), 941 (w), 880 (w), 819 (m), 751 (s).

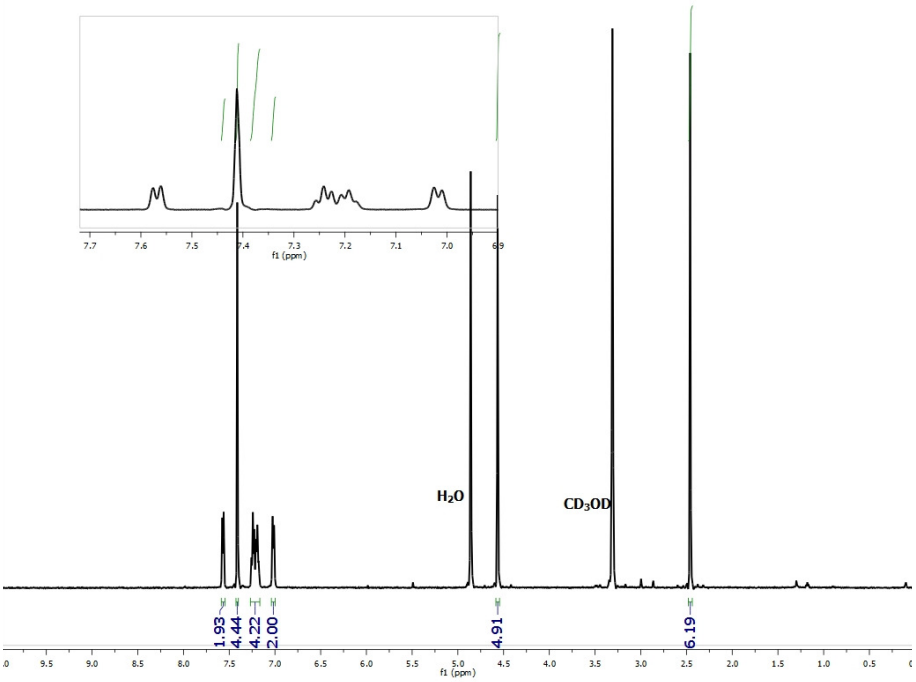

Figure 36. ^{1}H NMR spectrum of the reaction of **L3** and $AsCl_3$ without sieves (*reaction A*) in CD_3OD at 298 K.

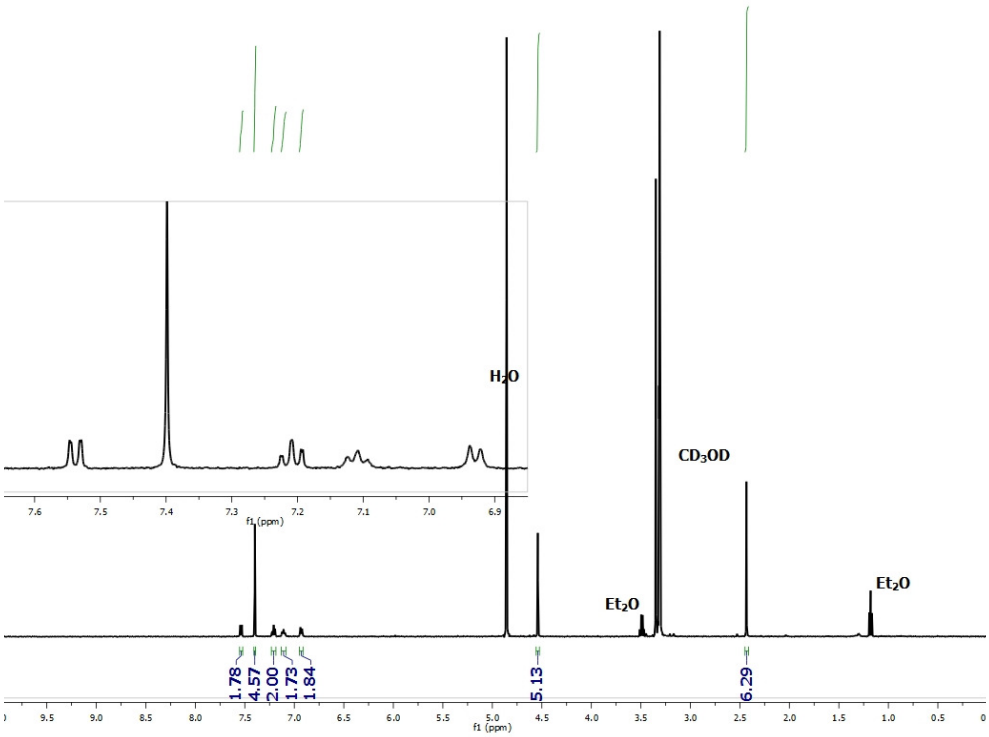

Figure 37. ^{1}H NMR spectrum of reaction of **L3** and $AsCl_3$ with 3 Å sieves (*reaction B*) in CD_3OD at 298 K.

Synthesis of L3·2HCl. A portion of **L3** (0.1048 g, 0.2758 mmol) was dissolved in 2 mL of THF resulting in a yellow colored solution. In a separate flask, NaCl (2.5866 g, 44.2608 mmol) was placed in a three-necked flask and approx 1.2 mL of H_2SO_4 was added to the flask. A line that connects the three-necked flask and the round bottom flask that contains the solution of **L3** was used to transfer the HCl gas formed. As the HCl bubbled into the flask, a white precipitate gradually formed. The reaction was filtered to give 0.1100 g of white solid (88%). ^{1}H NMR (400 MHz, CD_3OD, δ from TMS): 2.48 (s, 6H), 4.58 (s, 4H), 7.07 (d, 2H), 7.25 (t, 4H), 7.42 (s, 4H), 7.59 (d, 2H).

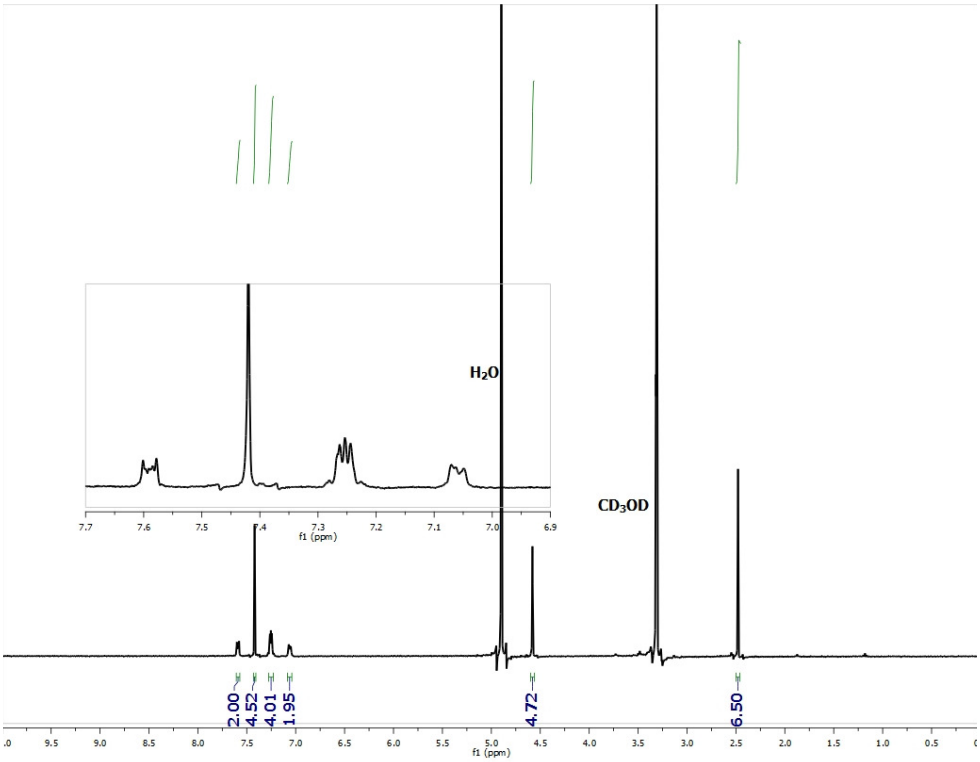

Figure 38. ^{1}H NMR spectrum of **L3·2HCl** in CD_3OD at 298 K.

Synthesis of 1,4-bis(2,3-dihydrobenzo[*d*]thiazol-2-yl)benzene (L4). A solution of 2-aminothiophenol (0.2977 g, 2.3780 mmol) in 2 mL of EtOH was added to a Schlenk flask and a

slurry of terephthalaldehyde (0.1591 g, 1.1862 mmol) in 10 mL of EtOH was added. The reaction was stirred under an atmosphere of N_2 for 2 h. Within 15 min, the reaction changed color from yellow to off-white. Anaerobic filtration of the reaction mixture afforded an off-white residue and a yellow filtrate. The residue was recrystallized by layering pentane over a CH_2Cl_2 solution of the residue. Filtration and drying of the precipitate obtained gave an off-white solid (0.1616 g, 40%). ^{1}H NMR (400 MHz, $CDCl_3$, δ from TMS): 4.36 (s, 2H), 6.37 (d, 2H), 6.67 (d, 2H), 6.76 (t, 2H), 6.95 (t, 2H), 7.04 (d, 2H), 7.53 (s, 4H). ^{13}C NMR (100 MHz, $CDCl_3$, δ from TMS): 69.31, 110.03, 121.97, 121.85, 125.56, 126.97, 128.24, 142.51, 146.24. FTIR (ATR-diamond, powder) ν_{max} (cm^{-1}): 3306 (m, N-H), 2873 (w), 1579 (m), 1503 (w), 1471 (m), 1457 (m), 1425 (m), 1392 (m), 1361 (m), 1331 (m), 1303 (m), 1253 (m), 1217 (m), 1192 (m), 1118 (m), 1103 (m), 1064 (m), 1035 (m), 1016 (m), 921 (m), 897 (m), 837 (m), 808 (m), 755 (s), 736 (vs), 714 (m), 697 (m), 658 (s), 587 (m), 558 (m). LRMS-ESI (*m/z*), $[M + H]^+$ calcd for $C_{20}H_{16}N_2S_2$, 349.5; found, 349.2

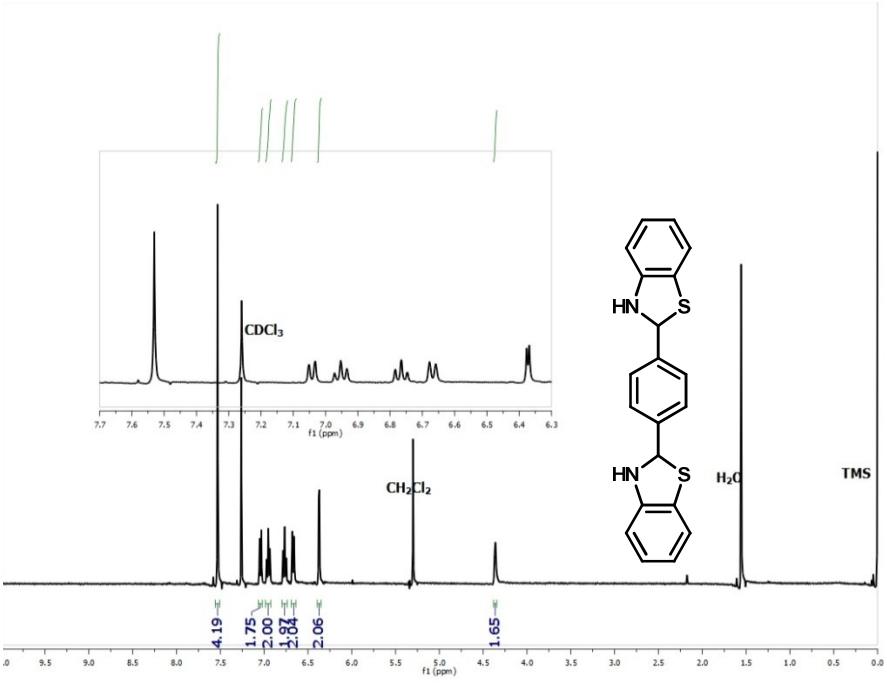

Figure 39. ^{1}H NMR spectrum of **L4** in $CDCl_3$ at 298 K. Inset: structural depiction of **L4**.

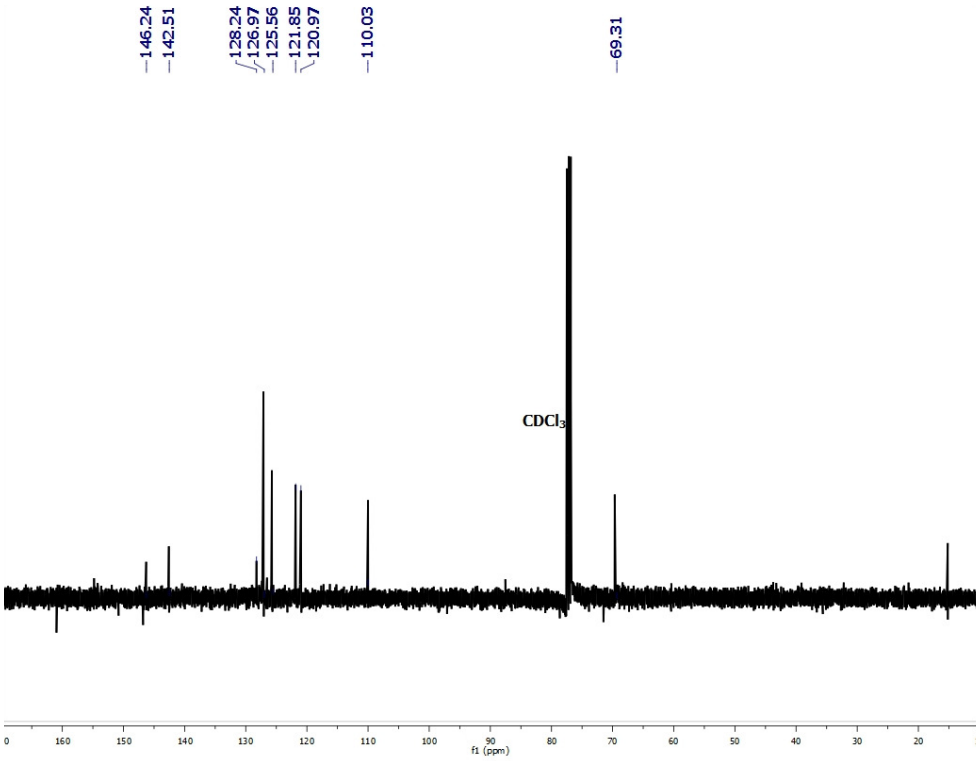

Figure 40. ^{13}C NMR spectrum of **L4** in $CDCl_3$ at 298 K.

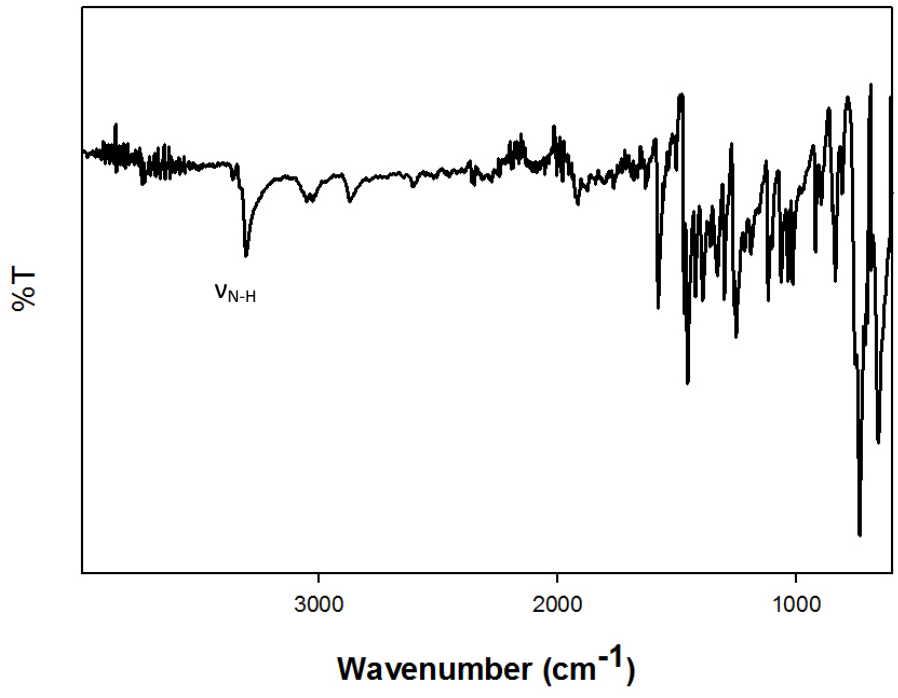

Figure 41. Solid-state FTIR spectrum (ATR-Diamond) of **L4**.

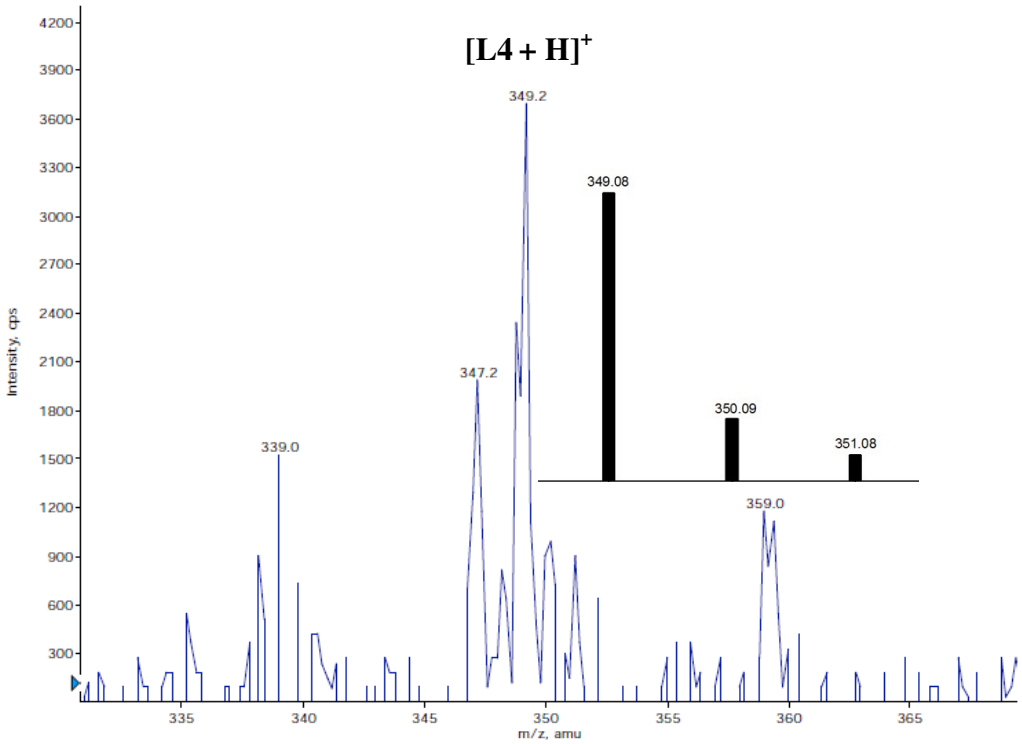

Figure 42. Positive mode LRMS-ESI-MS of **L4** showing the parent peak at *m*/*z* = 349.2. Inset: calculate molecular weight and isotopic distribution of **L4**.

Reaction of $AsCl_3$ and L4. A solid batch of **L4** (0.1068 g, 0.3065 mmol) was dissolved in 4 mL of THF and stirred in 4 Å sieves. To this solution was added a slurry of NaH (0.0146 g, 0.6083 mmol) in 4 mL of THF which was stirred for 20 min. The mixture turned slightly cloudy indicative of deprotonation. $AsCl_3$ (0.03693 g, 0.2037 mmol) was then added and the reaction turned light yellow. After stirring at RT for 2 h, the reaction was filtered to remove NaCl. The yellow filtrate was then concentrated via short-path vacuum distillation to give an orange solid (0.0563 g). ^{1}H NMR (400 MHz, $CDCl_3$, δ from TMS): 6.65 – 8.24 (multiple peaks); peaks in the aliphatic region have not been assigned. FTIR (ATR-diamond, powder) ν_{max} (cm^{-1}): 3343 (m & br), 2919 (w); 2850 (w), 1760 (w), 1748 (w), 1714 (w), 1600 (w), 1574 (m), 1556 (w), 1538 (w), 1504 (w), 1463 (s), 1455 (s), 1441 (s), 1417 (m), 1360 (m), 1287 (m), 1256 (m), 1086 (m), 1033

(s), 1018 (s), 963 (m), 841 (m), 799 (s), 739 (vs), 698 (s), 667 (m), 627 (m), 551 (m). LRMS-ESI (*m/z*): 316, 339, 465.

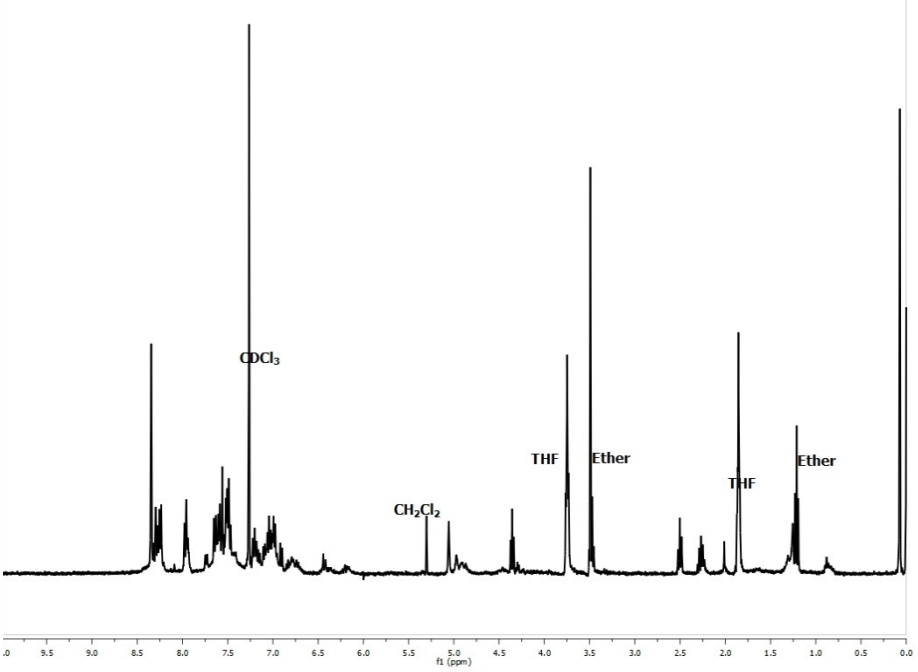

Figure 43. ^{1}H NMR spectrum of the reaction of **L4** and $AsCl_3$ in $CDCl_3$ at 298 K.

Reaction of $AsCl_3$ and L5, [As(L5)Cl]. An anaerobic THF solution (12 mL) of **L5** (1.211 g, 5.651 mmol) was allowed to stir in the presence of 4 Å molecular sieves to ensure a completely anhydrous reaction environment affording a yellow solution. To this mixture was then added a 5 mL THF slurry of NaH (0.136 g, 5.667 mmol) to generate a purple heterogeneous solution with significant effervescence (H_2 formation). The reaction mixture was left to stir for 20 min at RT to ensure complete deprotonation. To the deprotonated ligand was added a 3 mL THF solution of $AsCl_3$ (0.516 g, 2.846 mmol) dropwise causing the color to gradually turn yellow within ~5 min with the appearance of an off-white solid dispersed throughout the solution. The reaction was left to stir for 5 h at RT, filtered to remove the off-white residue and sieves, and the yellow filtrate was concentrated to give a yellow oil. The oil was triturated with 3 mL of dry Et_2O to afford a

yellow solid, which was filtered and dried to yield 0.688 g of products ([As(**L5**)Cl] and benzothiazole, see Scheme 7), which contained a 1:1 distribution of the two products (0.344 g, 1.060 mmol, 38% yield of [As(**L5**)Cl]) based on integration of the ^{1}H NMR signals of the product mixture. Recrystallization of the mixture from Et_2O afforded [As(**L5**)Cl] as the sole product (by NMR). ^{1}H NMR (400 MHz, $CDCl_3$, δ from TMS): 5.16 (s, 2H), 7.01 (m, 2H), 7.19 (t, 1H), 7.34 (t, 1H), 7.43 (d, 1H), 7.53 (d, 1H), 7.78 (t, 1H), 8.67 (d, 1H). FTIR (ATR-diamond, solid), ν_{max} (cm^{-1}): 3051 (w), 2968 (w), 1585 (m), 1569 (m), 1463 (s), 1433 (s), 1376 (m), 1284 (m), 1242 (m), 1135 (w), 1109 (w), 1087 (m), 1042 (m), 1012 (m), 992 (w), 931 (w), 738 (s), 663 (w), 644 (w), 633 (w), 615 (w), 592 (w), 562 (w). LRMS-ESI (*m/z*), $[M - Cl]^+$ calcd for $C_{12}H_{10}N_2SAs$, 289.0; found, 289.0. Anal calcd for $C_{12}H_{10}N_2SClAs$•0.2 Et_2O: C, 45.29; H, 3.56; N, 8.25. Found: C, 45.99; H, 3.46; N, 8.57. UV-vis (CH_2Cl_2, 298 K) λ_{max}, nm (ε, $M^{-1}cm^{-1}$): 260 (7900, sh), 310 (4600). UV-vis (MeCN, 298 K) λ_{max}, nm (ε, M^{-1} cm^{-1}): 255 (4000, sh), 313 (2300).

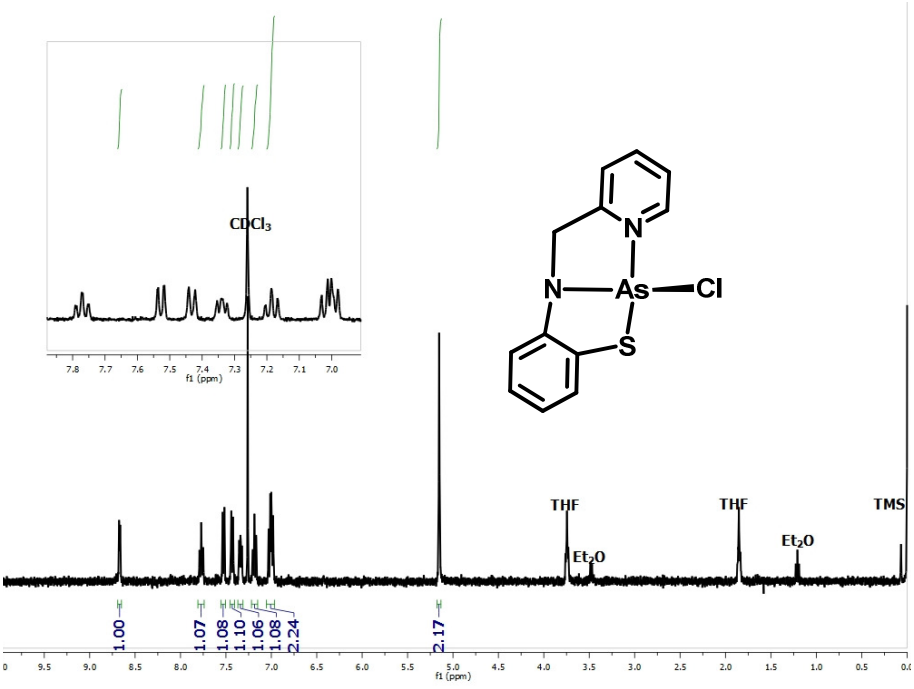

Figure 44. ^{1}H NMR spectrum of [As(**L5**)Cl] in $CDCl_3$ at 298 K.

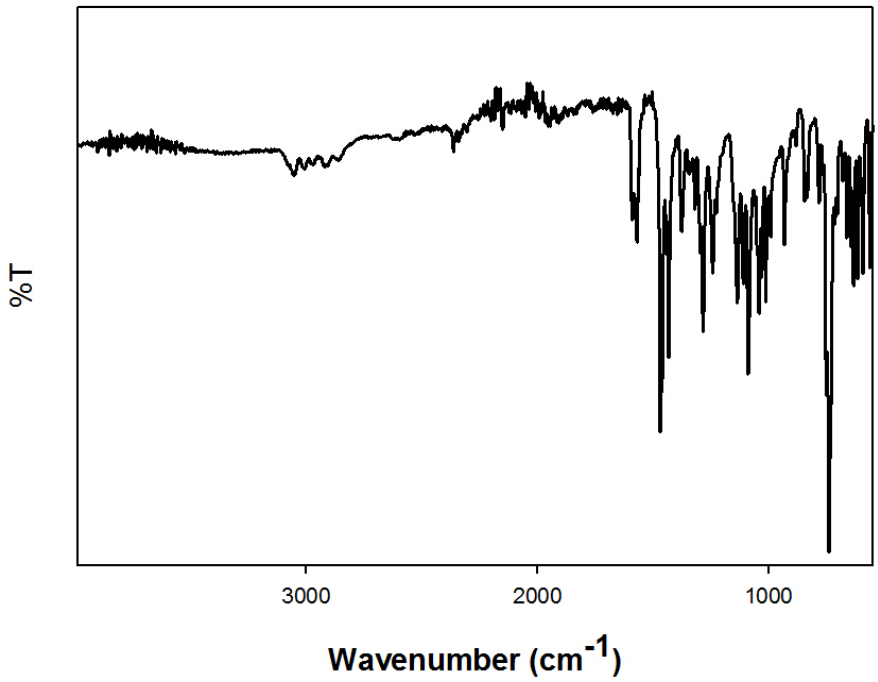

Figure 45. Solid-state FTIR spectrum (ATR-diamond) of [As(**L5**)Cl].

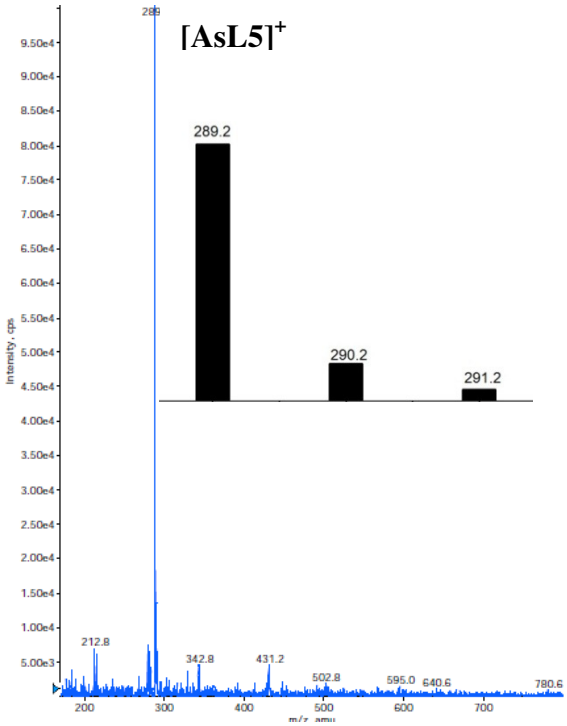

Figure 46. Positive mode LRMS-ESI-MS of [As(**L5**)Cl] showing parent peak at *m/z* = 289 which is assigned to [As(**L5**)]$^+$. Inset: calculated molecular weight and isotopic distribution of [As(**L5**)]$^+$.

Synthesis of [As(L5)I]. A batch of [As(**L5**)Cl] (0.253 g, 0.779 mmol) was dissolved in 10 mL of CH_2Cl_2 to generate a green-yellow solution. To this solution was added a 6 mL acetone solution of NaI (0.167 g, 1.114 mmol) and the reaction became orange in color with the appearance of an off-white solid (identified as NaCl). The reaction was left to stir for 4 h at RT. The solution was then filtered through a bed of Celite to remove insolubles affording an orange solution. This solution was concentrated in vacuo giving an orange solid, which was recrystallized by slow diffusion of pentane into a CCl_4 solution of [As(**L5**)I] at -15 ^oC (0.288 g, 0.69 mmol, 88%). ^1H NMR (500 MHz, $CDCl_3$, δ from TMS): 4.83 (s, 2H), 7.10 (m, 2H), 7.21 (t, 1H), 7.36 (t, 1H), 7.46 (d, 1H), 7.54 (d,1H), 7.81 (t, 1H), 8.68 (d, 1H). FTIR (ATR-diamond, solid), ν_{max} (cm^{-1}): 3043 (w), 2829 (w), 1595 (m), 1574 (w), 1428 (m), 1416 (m), 1286 (m), 1252 (m), 1147 (m), 1137 (m), 1090 (m), 1038 (m), 1010 (m), 905 (m), 763 (s), 751 (s), 718 (s), 649 (m), 632 (s), 611 (s), 565 (m). LRMS-ESI (*m/z*), $[M - I]^+$ calcd for $C_{12}H_{10}N_2SAs$, 289.0; found, 289.0. Anal calcd for $C_{12}H_{10}N_2SIAs$•0.05 CCl_4: C, 34.15; H, 2.38; N, 6.61. Found: C, 34.25; H, 2.18; N, 6.58. UV-vis (THF, 298 K) λ_{max}, nm (ε, M^{-1} cm^{-1}): 254 (990, sh), 294 (775), 362 (505). UV-vis (MeCN, 298 K) λ_{max}, nm (ε, M^{-1} cm^{-1}): 249 (1140, sh), 290 (1035), 356 (625). UV-vis (CH_2Cl_2, 298 K) λ_{max}, nm (ε, M^{-1} cm^{-1}): 294 (2830), 382 (4800).

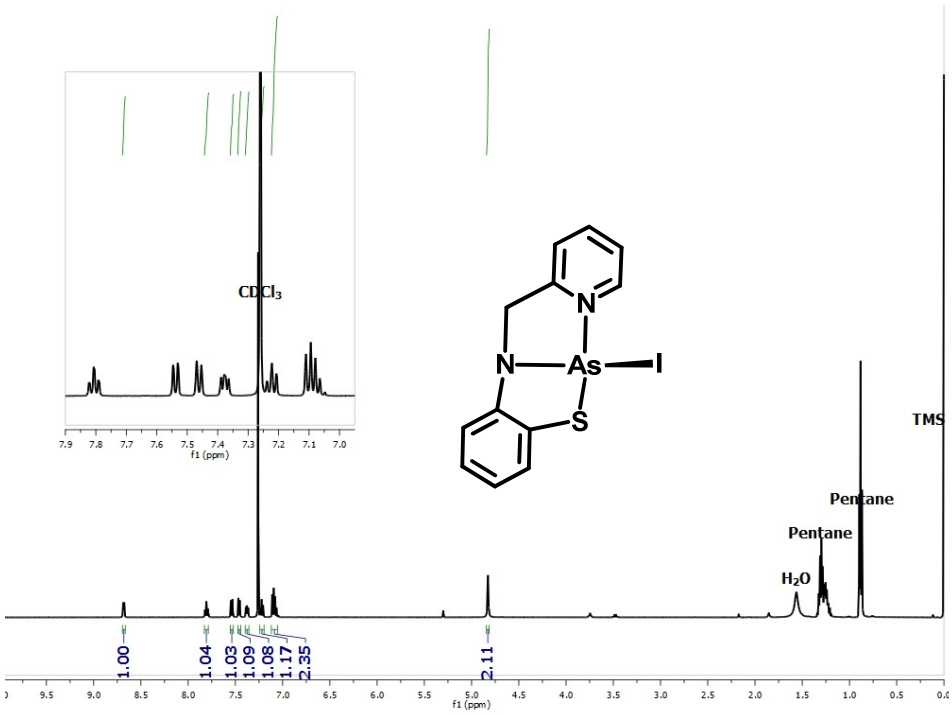

Figure 47. ^{1}H NMR spectrum of [As(**L5**)I] in $CDCl_3$ at 298 K.

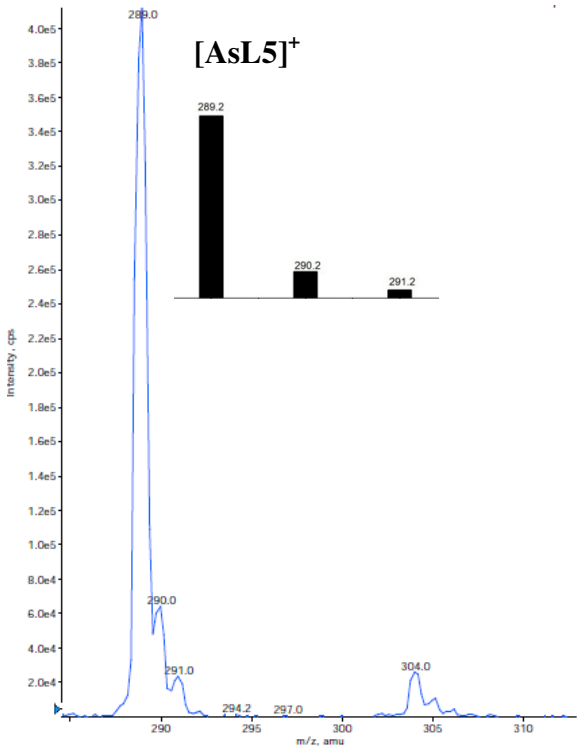

Figure 48. Positive mode LRMS-ESI-MS of [As(**L5**)I] showing parent peak at *m/z* = 289 which is assigned to [As(**L5**)]$^{+}$. Inset: calculated molecular weight and isotopic distribution of [As(**L5**)]$^{+}$.

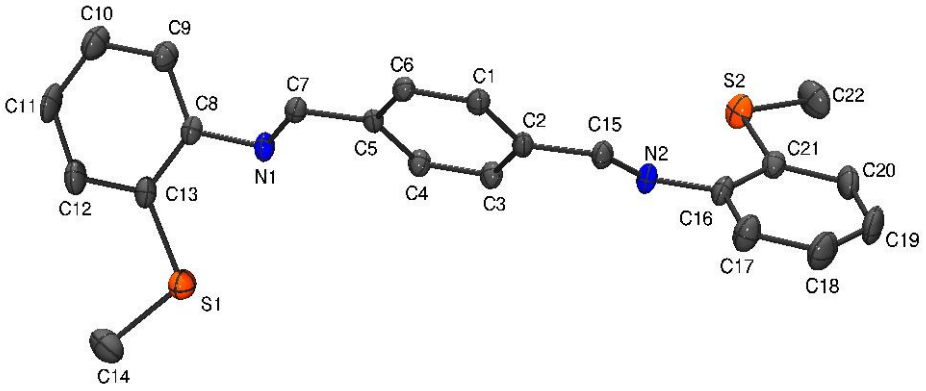

Figure 49. ORTEP diagram of **L2** showing 30% thermal probability ellipsoids. H atoms are omitted for clarity. Selected bond distances (Å) and angles (deg) for **L2**: N1-C7, 1.271(6); N2-C15, 1.254(6); S1-C14, 1.755(5); S2-C22, 1.789(6); C7-N1-C8, 118.3(4); C15-N2-C16, 120.2(4); C13-S1-C14, 103.4(3); C21-S2-C22, 103.9(3).

X-ray Data Collection and Structure Solution Refinement. Single crystals for X-ray structural studies of **L3·HCl**, **L2** and [As(**L5**)I] were obtained as follows. **L3·HCl**: diffusion of Et_2O into a MeOH solution of **L3·HCl**; **L2**: slow evaporation from a solution of **L2** in $CDCl_3$ and [As(**L5**)I]: diffusion of pentane into saturated solution of [As(**L5**)I] in CCl_4 at -15 ^oC under anaerobic conditions. Suitable crystals were mounted and sealed inside a glass capillary. All geometric and intensity data were measured at 293 K on a Bruker SMART APEX II CCD X-ray diffractometer equipped with graphite-monochromatic Mo Kα radiation (λ = 0.71073 Å) with increasing ω (width 0.5^o per frame) at a scan speed of 10 s/frame controlled by the SMART software package.[197] The intensity data were corrected for Lorentz-polarization effects and for absorption[198] and integrated with the SAINT software. Empirical absorption corrections were applied to structures using the SADABS program.[199] The structures were solved by direct methods with refinement by full-matrix least-squares based on F^2 using the SHELXTL-97 software[200] incorporated in the SHELXTL 6.1 software package.[201] The hydrogen atoms were

fixed in their calculated positions and refined using a riding model. All non-hydrogen atoms were refined anisotropically. Selected crystal data and metric parameters are summarized in Tables 5 – 8, respectively. Perspective views of the complex were obtained using ORTEP.[202]

Table 5. Summary of crystal data and intensity collection and structure refinement parameters for **L3·HCl**, **L2** and [As(**L5**)I]

Parameters	**L3·HCl**	**L2**	[As(**L5**)I]
Formula	$C_{22}H_{25}ClN_2S_2$	$C_{22}H_{20}N_2S_2$	$C_{12}H_{10}N_2SIAs$
Formula weight	416.11	376.11	416.11
Crystal system	Triclinic	Triclinic	Monoclinic
Space group	P_{-1}	P_{-1}	$P\ 2_1/n$
Crystal color, habit	White, rectangle	Orange, needle	Orange, rectangle
a, Å	7.8714(6)	6.794(4)	8.724(7)
b, Å	8.0241(7)	9.472(8)	10.984(9)
c, Å	9.8134(7)	15.289(8)	14.343(11)
α, deg	92.5270(10)	85.864(8)	90
β, deg	99.9740(10)	80.755(8)	103.174(11)
γ, deg	113.9930(10)	80.485(8)	90
V, Å^3	1107(2)	956.7(11)	1338.2(18)
Z	2	2	4
ρ_{calcd}, g/cm^{-3}	0.810	1.321	2.065
T, K	293	293	293
abs coeff, μ (Mo Kα), mm^{-1}	0.250	0.810	4.981
θ limits, deg	2.12 – 33.05	2.18 – 26.37	2.36 – 28.50
total no. of data	3958	3905	13723
no. of unique data	3158	2643	3380
no. of parameters	127	235	154
GOF on F^2	1.020	1.070	1.017
R_1,[a] %	4.18	8.89	4.50
wR_2,[b] %	11.39	26.74	13.38
max, min peaks e/Å^3	0.005, 0.001	0.010, 0.002	0.924, - 0.818

[a] $R_1 = \Sigma| |F_o| - |F_c| |/ \Sigma |F_o|$; [b] $wR_2 = \{\Sigma[w(F_o^2 - F_c^2)^2]/ \Sigma[w(F_o^2)^2]\}^{1/2}$

Table 6. Selected bond distances (Å) and bond angles (deg) for **L3·HCl**.

Bond distances		**Bond angles**	
C(1)-S(1)	1.778(2)	C(7)-C(2)-C(3)	117.29(14)
C(2)-C(7)	1.3978(19)	C(7)-C(2)-S(1)	118.96(10)
C(2)-C(3)	1.399(2)	C(3)-C(2)-S(1)	123.75(12)
C(2)-S(1)	1.7612(16)	C(4)-C(3)-C(2)	120.54(16)
C(3)-C(4)	1.376(3)	C(5)-C(4)-C(3)	121.46(15)
C(4)-C(5)	1.371(3)	C(4)-C(5)-C(6)	119.29(17)
C(5)-C(6)	1.392(2)	C(7)-C(6)-C(5)	119.44(16)
C(6)-C(7)	1.378(2)	C(6)-C(7)-C(2)	121.98(13)
C(7)-N(1)	1.4693(15)	C(6)-C(7)-N(1)	118.31(12)
C(8)-N(1)	1.4982(17)	C(2)-C(7)-N(1)	119.71(12)
C(8)-C(9)	1.5086(18)	N(1)-C(8)-C(9)	113.69(11)
C(9)-C(11)	1.3821(19)	C(11)-C(9)-C(10)	118.30(12)
C(9)-C(10)	1.384(2)	C(11)-C(9)-C(8)	117.18(12)
C(10)-C(11)	1.389(2)	C(10)-C(9)-C(8)	117.18(12)
C(11)-C(10)	1.389(2)	C(9)-C(10)-C(11)	120.68(13)
		C(9)-C(11)-C(10)	121.02(13)
		C(7)-N(1)-C(8)	113.08(10)
		C(2)-S(1)-C(1)	104.36(10)

Table 7. Selected bond distances (Å) and bond angles (deg) for [As(**L5**)I].

Bond distances		**Bond distances (contd.)**	
As(1)-I(1)	2.737(2)	C(5)-C(6)	1.378(9)
As(1)-N(1)	1.846(5)	C(7)-C(8)	1.488(9)
As(1)-S(1)	2.292(2)	C(8)-C(9)	1.397(8)
As(1)-N(2)	2.411(6)	C(9)-C(10)	1.373(9)
S(1)-C(1)	1.750(7)	C(10)-C(11)	1.378(1)
N(1)-C(6)	1.408(8)	C(11)-C(12)	1.379(1)
N(1)-C(7)	1.441(8)		
N(2)-C(8)	1.322(8)	**Bond angles**	
N(2)-C(12)	1.336(8)	N(1)-As(1)-S(1)	87.71(2)
C(1)-C(2)	1.375(9)	N(1)-As(1)-I(1)	97.86(2)
C(1)-C(6)	1.409(9)	S(1)-As(1)-I(1)	100.61(6)
C(2)-C(3)	1.356(1)	I(1)-As(1)-N(2)	88.98(1)
C(3)-C(4)	1.368(1)	S(1)-As(1)-N(2)	162.69(2)
C(4)-C(5)	1.370(1)	N(1)-As(1)-N(2)	76.64(2)

Table 8. Selected bond distances (Å) and bond angles (deg) for **L2**.

Bond distances		**Bond angles (contd.)**	
S(1)-C(13)	1.755(5)	C(15)-N(2)-C(16)	120.2(4)
S(1)-C(14)	1.787(7)	C(6)-C(1)-C(2)	120.1(4)
S(2)-C(21)	1.743(5)	C(1)-C(2)-C(3)	119.5(4)
S(2)-C(22)	1.789(6)	C(1)-C(2)-C(15)	119.3(4)
N(1)-C(7)	1.271(6)	C(3)-C(2)-C(15)	121.1(4)
N(1)-C(8)	1.404(6)	C(4)-C(3)-C(2)	119.9(4)
N(2)-C(15)	1.254(6)	C(3)-C(4)-C(5)	121.1(4)
N(2)-C(16)	1.410(6)	C(6)-C(5)-C(4)	118.3(4)
C(1)-C(6)	1.374(6)	C(6)-C(5)-C(7)	119.3(4)
C(1)-C(2)	1.389(6)	C(4)-C(5)-C(7)	122.4(4)
C(2)-C(3)	1.406(7)	C(1)-C(6)-C(5)	121.0(4)
C(2)-C(15)	1.457(6)	N(1)-C(7)-C(5)	122.3(4)
C(3)-C(4)	1.364(6)	C(9)-C(8)-C(13)	119.2(4)
C(3)-C(4)	1.364(6)	C(9)-C(8)-N(1)	122.9(5)
C(4)-C(5)	1.405(6)	C(13)-C(8)-N(1)	117.8(4)
C(5)-C(6)	1.397(6)	C(10)-C(9)-C(8)	121.5(6)
C(5)-C(7)	1.449(6)	C(11)-C(10)-C(9)	119.5(6)
C(8)-C(9)	1.382(7)	C(10)-C(11)-C(12)	120.4(5)
C(8)-C(13)	1.397(7)	C(11)-C(12)-C(13)	120.5(6)
C(9)-C(10)	1.375(8)	C(12)-C(13)-C(8)	118.9(5)
C(10)-C(11)	1.368(9)	C(12)-C(13)-S(1)	124.5(4)
C(11)-C(12)	1.382(9)	C(8)-C(13)-S(1)	116.6(3)
C(12)-C(13)	1.395(7)	N(2)-C(15)-C(2)	123.1(4)
C(16)-C(17)	1.387(7)	C(17)-C(18)-C(21)	119.9(4)
C(16)-C(21)	1.395(7)	C(17)-C(16)-N(2)	122.2(5)
C(17)-C(18)	1.371(8)	C(21)-C(16)-N(2)	117.8(4)
C(18)-C(19)	1.370(10)	C(18)-C(17)-C(16)	120.9(6)
C(19)-C(20)	1.370(9)	C(19)-C(18)-C(17)	119.6(6)
C(20)-C(21)	1.393(7)	C(18)-C(19)-C(20)	120.4(5)
		C(19)-C(20)-C(21)	121.2(5)
Bond angles		C(20)-C(21)-C(16)	118.0(5)
C(13)-S(1)-C(14)	103.4(3)	C(20)-C(21)-S(2)	125.4(4)
C(21)-S(2)-C(22)	103.9(3)	C(16)-C(21)-S(2)	116.6(4)
C(7)-N(1)-C(8)	118.3(4)		

CHAPTER 3

ARSENOFLUORS (AFs): DESIGN, SYNTHESIS AND PROPERTIES OF FLUORESCENT CHEMODOSIMETERS FOR As(III) UTILIZING BENZOTHIAZOLINE TO BENZOTHIAZOLE CONVERSIONS

3.1 Abstract

In a quest to develop fluorescent probes for As(III) ions, two small molecules termed ArsenoFluors (**AF1** and **AF2**), were designed as As(III)-specific chemodosimeters. The design incorporated a coumarin fluorescent reporter into an As(III)-reactive benzothiazoline functional group. AFs react with As(III) to afford the highly fluorescent coumarin-6 dye analogs (C6-CF_3 and C6) resulting in a 20 – 25 fold fluorescence enhancement at λ_{em} ~ 500 nm with detection limits of 0.14 – 0.23 ppb in THF at 298 K. The AFs also react with common environmental As(III) sources such as sodium arsenite in a THF/CHES (1:1, pH 9, 298 K) mixture resulting in a modest fluorescence enhancement (1.5- to 3-fold) due to the quenched nature of coumarin-6 derivatives in high polarity solvents. The dyes are selective for As(III) over common ions, though Cu(II) and Co(II) are potential interferences. Bulk analysis of the reaction of AFs and As(III) revealed that the C6 and Schiff-base disulfide analogs are the products of the reaction.

3.2 Introduction

Analytical detection methods based on fluorescence are increasingly popular for the detection of environmental, chemical and biological analytes. The advantages include the high

sensitivity and the rapid low cost of fluorescence methods. Additionally, the opportunity to tune the selectivity and photophysical properties of fluorescent dyes has made this field an active research area.[203] While there are numerous examples of small-molecule fluorescent dyes for toxic ions such as Hg(II), Pb(II) and Cd(II),[204] the design of fluorescent dyes for As(III) is a recent endeavor.

The objective of this study was to design and synthesize a chemodosimeter for the selective detection of As(III) ions. The chemodosimeter approach is attractive because the design is based on a specific and usually irreversible reaction between the dye and analyte of interest that leads to the formation of a fluorescent or colored compound.[205-209] The concentration of analyte is then determined by monitoring the photophysical properties of the new fluorescent product. The dyes used in this study, **AF1** – **AF2** (Chart 12), are inspired by the reported As(III)-promoted redox rearrangement of the benzothiazoline functional group discussed in chapter 2.[188] The design incorporates a benzothiazoline functional group covalently linked to a coumarin fluorophore. The choice of coumarin as the fluorescence reporting group in this study is based on its desirable properties such as: visible light excitation and emission (blue-green region), large Stokes shift (approx. 100 nm), high quantum yield and photostability.[210-212] In fact, coumarin dyes are versatile and have been applied in biological assays (for example, N-[3-(2-benzothiazolyl)-6-[2-[2-bis(carboxymethyl)amino]-5-methylphenoxy]ethoxy]-2-oxo-2H-benzo pyran-7-yl]-N-(carboxymethyl)-glycine (BTC) is a coumarin based probe utilized for detecting Ca(II) in living cells), determining polarities of microenvironments, collection of solar energy and manufacture of light emitting diodes among other uses.[211, 213-217]Also, coumarin derivatives are relatively easy to synthesize and their photophysical properties can be modulated by the nature of the substituents.[212] The reaction of As(III) and **AF1/AF2** is expected to afford the

highly fluorescent benzothiazole analog, which is a common laser dye known as coumarin-6 (Scheme 8). The AF dyes presented in this work represent the first examples of fluorescent sensors of As(III) ions.

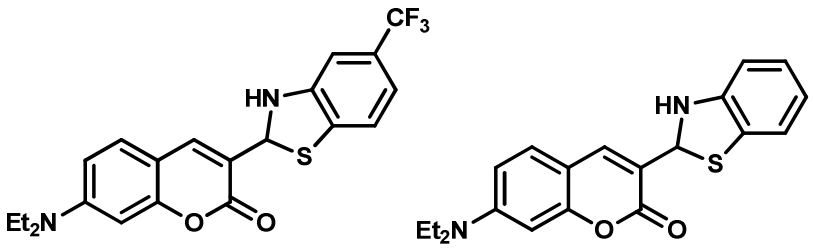

AF1 **AF2**

Chart 12. Fluorescence chemodosimeter **AF1** and **AF2**.

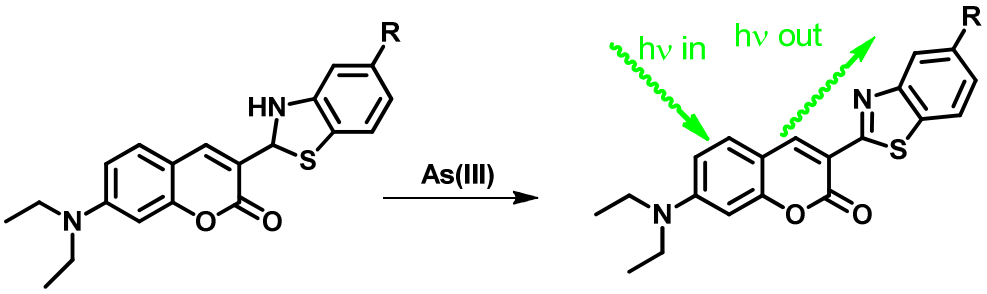

Scheme 8. Formation of fluorescent compound (Coumarin-6 analogs) upon reaction of AFs with As(III).

3.3 Results and Discussion

AF1 contains a $-CF_3$ group para to the benzothiazoline-S and the effect of this additional electron-withdrawing group on the photophysical properties of coumarin fluorophore will be evaluated. The synthesis of **AF1** was carried out in four steps that starts with the reaction of diethyl malonate and 4-(diethylamino)salicyladehyde in EtOH to give the fused-ring structure of the coumarin containing an ester functionality in the third position. Conversion to 7-(diethylamino)coumarin and eventually 7-(diethylamino)coumarin-3-aldehyde occurs via acid-

catalyzed hydrolysis of the ester group and decarboxylation followed by a formylation reaction with $POCl_3$ and DMF (Vilsmeier-Haack reaction) in 79% and 72% yield, respectively.[218-219] The **AF1** sensor was finally obtained by condensation of 7-(diethylamino)coumarin-3-aldehyde with 4-(trifluoromethyl)-2-aminothiophenol to afford **AF1** in 88% yield (Scheme 9). The chemical structure and purity of **AF1** was confirmed by ^{1}H and ^{13}C NMR, FTIR, ESI-MS, UV-vis, fluorescence and X-ray crystallography.

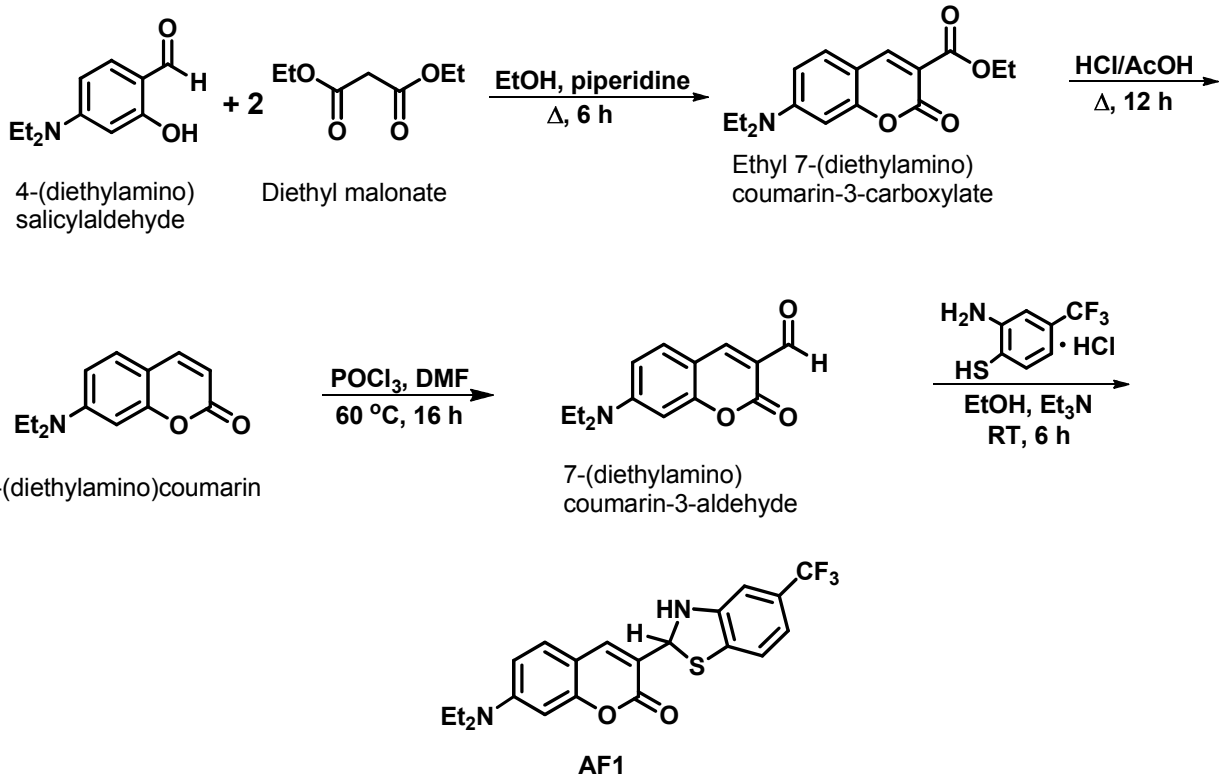

Scheme 9. Synthesis of **AF1**.

AF2 was synthesized following an analogous procedure and the characterization parameters corresponds with reported values.[218] In order to have a spectroscopic signature to compare with the reaction of As(III) and AF, the oxidized forms of **AF1** and **AF2**, namely C6-CF_3 and C6, were independently synthesized (or purchased in the case of coumarin-6) and characterized (Chart 13). Two strategies were used to synthesize the benzothiazole C6-CF_3; first

the compound was isolated from the reaction of **AF1** and As(III) after spectroscopic measurements. The second method involved air oxidation of **AF1** and recrystallization from hot EtOH to give C6-CF_3 in moderate yield (25%). Since the Schiff-base disulfide analogs of **AF1** and **AF2** were also potential products in the As(III) reaction, these were also synthesized. Thus, SB1 and SB2 were constructed by reaction of 7-(diethylamino)coumarin-3-aldehyde with the appropriate aromatic amine disulfide in modest yields. The purity of the synthesized compounds was verified by several spectroscopic techniques, which included ^{1}H and ^{13}C NMR, FTIR, ESI-MS, UV-vis, and fluorescence spectroscopies.

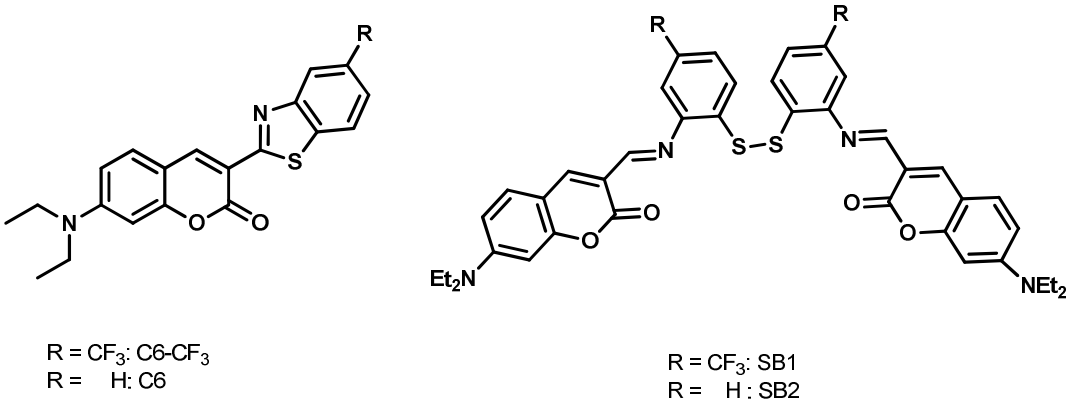

Chart 13. Oxidized analogs of **AF1** and **AF2.**

The **AF1** and **AF2** compounds are stable in the solid-state for weeks when stored under anaerobic conditions and in the dark as judged by ^{1}H NMR and UV-vis spectroscopies. However, organic solutions (THF, CH_2Cl_2) of **AF2** spontaneously oxidized to C6 (about 5% conversion to C6 for a solution left overnight as judged by changes in UV-vis) under normal laboratory (aerobic) environment, whereas solutions of **AF1** were stable to oxygen over several days. The stability of **AF1** in solution under aerobic conditions is likely due to the electron-withdrawing CF_3 group, which prevents the loss of hydride to form the benzothiazole.[220] The SBs are not as stable as the AFs, and slow (weeks) hydrolysis occurred resulting in reformation

of 7-(diethylamino)coumarin-3-aldehyde and the amine disulfide even in the solid-state. To determine if the solution of **AF1** and **AF2** undergoes tautomerization between the benzothiazoline and Schiff-base forms, the ^{1}H NMR was monitored over a period of one week. The resulting RT ^{1}H NMR spectrum of **AF1** or **AF2** in $CDCl_3$ display only one set of peaks indicating that these compounds exist only in the benzothiazoline form in both the solid- (X-ray structure of **AF1**) and solution-state. This conclusion is clearly evident in the D_2O-exchangeable NH proton resonance (4.89 ppm for **AF1**; 4.71 ppm for **AF2**) both in $CDCl_3$ and lack of a significantly downfield-shifted azomethine proton resonance that would be expected for the Schiff-base form.

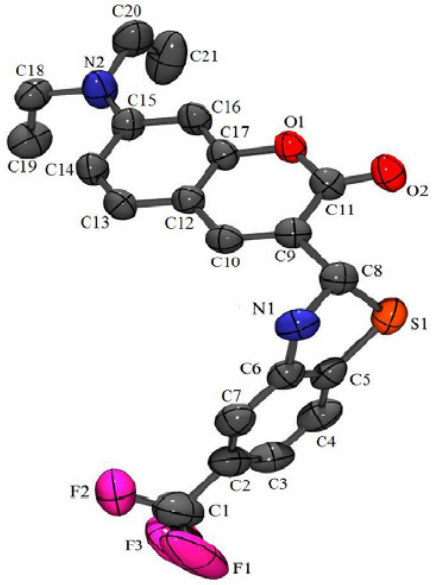

Figure 50. ORTEP view of **AF1** showing 50% thermal probability ellipsoids. H atoms are omitted for clarity. Selected bond distances (Å) and angles (deg) for **AF1**: C8-N1, 1.439(3); C8-S1, 1.869(3); C9-O2, 1.221(3); C9-O1, 1.366(3), N1-C6-S1, 107.09(18); O1-C9-O2, 116.0(2); C8-S1-C5, 88.48(3); C8-N1-C4, 110.6(2).

Orange single crystals of **AF1** were obtained by slow diffusion of hexanes into a $CDCl_3$ solution of **AF1** at RT. **AF1** crystallizes in the monoclinic system and $P2_1/n$ space group. The X-ray structure of **AF1** reveals the planes that define the coumarin and benzothiazoline moieties are

nearly perpendicular to each other (Figure 50). This is consistent with C8 being sp^3-hybridized as supported by the C8-N1 bond distance of 1.439(3) Å, which is typical for C – N single bonds and bond angles (N1-C8-C9: 111.5(2)º and C9-C8-S1: 106.82(17)º), which are typical for a tetrahedral geometry.

The electronic absorption properties of the dyes (**AF1** and **AF2**) and the oxidized analogs (C6-CF_3, C6, SB1 and SB2) were measured in THF at 298 K. **AF1** and **AF2** display broad intense maxima at 385 nm (ε: 29 000 M^{-1} cm^{-1}) and 379 nm (ε: 26 300 M^{-1} cm^{-1}), respectively (Figures 51 – 52). The bands are assigned as n–π* charge-transfer transitions from the Et_2N-group to the π cloud of the coumarin ring.[205, 210, 219, 221-223] There is a red-shift in the absorption band to 393 nm (ε: 29,500 $M^{-1}cm^{-1}$) when the absorption spectrum of **AF1** is measured in THF/CHES (1:1, pH 9, 298 K) (Figure 53). The C6 analogs exhibit a double-humped band between 440-464 nm at nearly double the molar absorptivity value (ε ~55,000 $M^{-1}cm^{-1}$) when compared to the AFs. The UV-vis spectra of the SB compounds are somewhat similar to C6 but with lower energy and more intense maxima (λ_{max}: 469 nm, ε: 85,000 $M^{-1}cm^{-1}$ for SB1; λ_{max}: 460 nm, ε: 65,000 $M^{-1}cm^{-1}$ for SB2). Analogous to **AF1**, the absorption spectra of C6-CF_3 and SB1 shift to lower energy in THF/CHES (λ_{max}: 473 nm, ε: 52,000 $M^{-1}cm^{-1}$ for C6-CF_3; λ_{max}: 482 nm, ε: 68,000 $M^{-1}cm^{-1}$ for SB1).

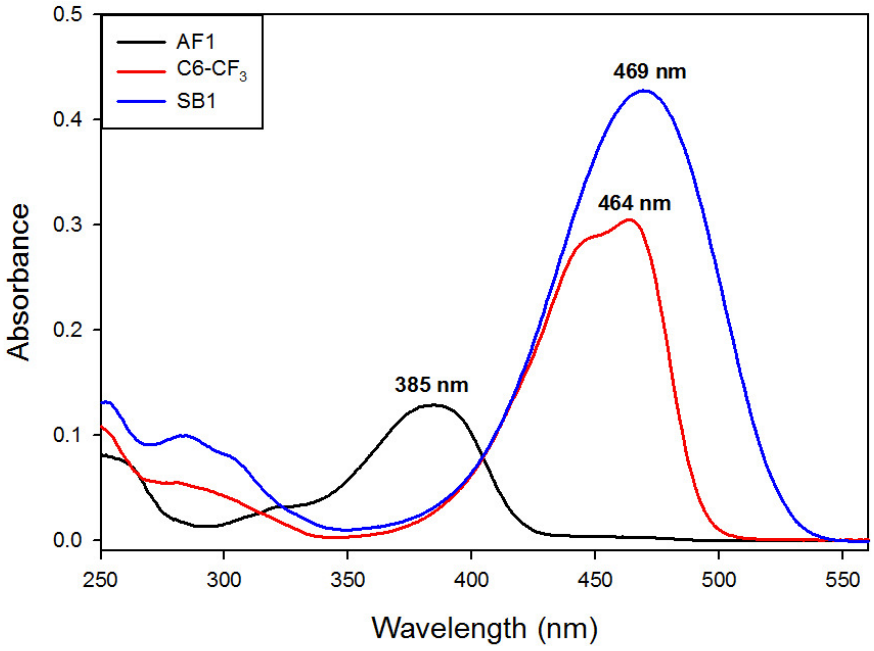

Figure 51. UV-vis spectra of **AF1** (black trace, 5.0 µM), C6-CF_3 (red trace, 5.7 µM), and SB1 (blue trace, 4.6 µM) in THF at 298 K.

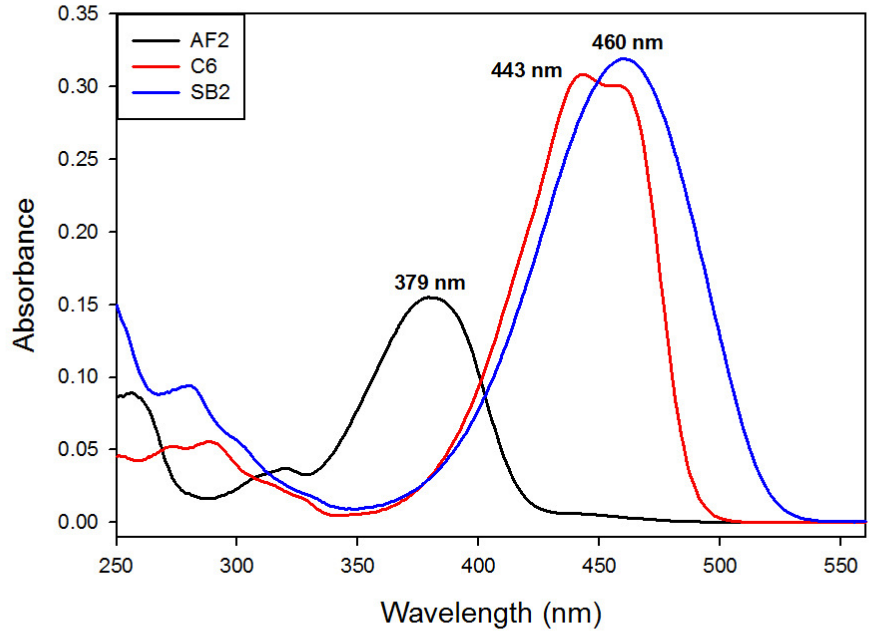

Figure 52. UV-vis spectra of **AF2** (black trace, 5.7 µM), C6 (red trace, 5.7 µM), and SB2 (blue trace, 4.9 µM) in THF at 298 K.

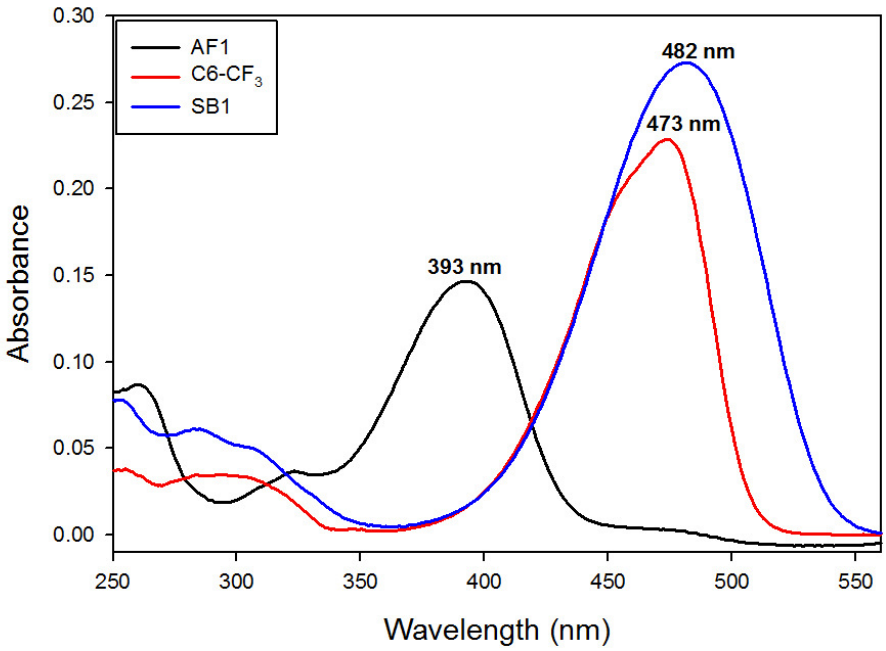

Figure 53. UV-vis spectra of **AF1** (black trace, 5.0 μM), C6-CF_3 (red trace, 4.8 μM), and SB1 (blue trace, 4.1 μM) in THF/CHES (1:1, pH 9) at 298 K.

In THF, **AF1** and **AF2** exhibit emission maxima (λ_{em}) at 496 nm and 492 nm, respectively, when excited at their absorption maxima (Figures 54 and 55). The AFs also have very low fluorescence quantum yield (Φ_f = 0.004; for **AF1** and 0.007; for **AF2**). The lack of emission from the dyes is likely due to the quenching by the thiazoline-N lone pair via a photoinduced-electron transfer mechanism.[218-219, 221] This property is ideal from the design standpoint as the dyes don't emit (OFF-state) before the analyte is added. However, the C6 analogs exhibit intense emission bands as seen from their high quantum yield (Φ_f = 0.88 for C6-CF_3 in THF). The quantum yield of SB1 and SB2 wasn't measured due to hydrolysis, but comparison of the fluorescence intensity of a similar concentration as the C6 analogs, shows that SB1 and SB2 exhibits minimal fluorescence intensity (Figures 54 – 55). The fluorescence properties of coumarin-containing dyes can be explained due to an intramolecular-charge-transfer (ICT) mechanism.[224] The presence of both an electron donating group (amino group) in

conjugation with an electron-withdrawing group (carbonyl group) in coumarin dyes leads to charge-transfer upon excitation by light.[221] Thus, the quantum yield and excited-state lifetime is affected by the solvent polarity because of the resulting change in dipole moment in the excited-state.[211] The ICT fluorescence mechanism is quite general and the fluorescence properties of the dyes can be modulated by varying parameters such as the nature of substituents or solvent polarity.

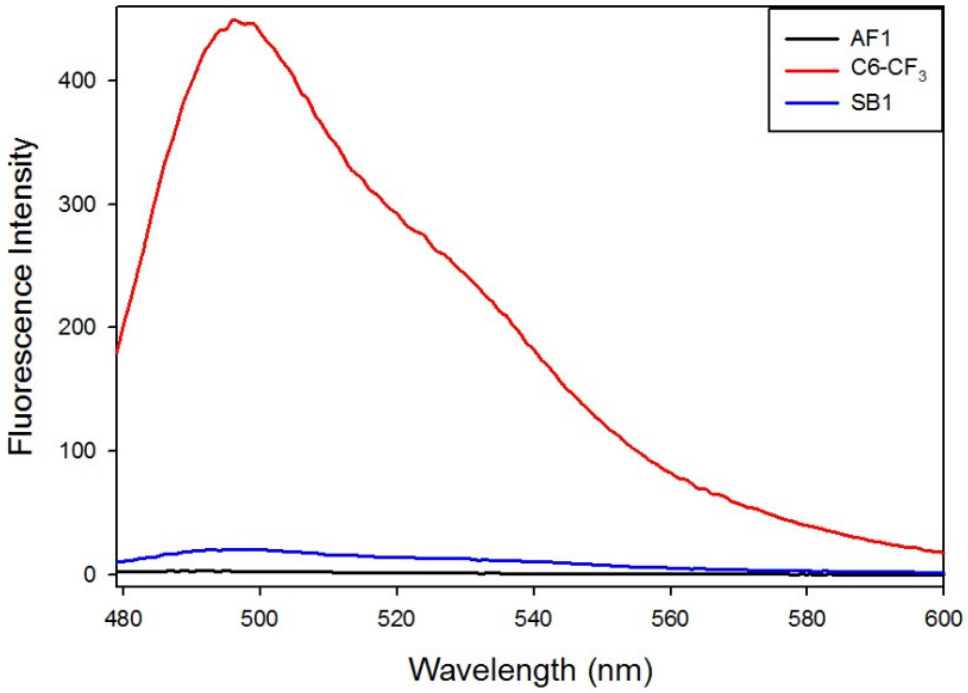

Figure 54. Fluorescence spectra of **AF1** (black trace, 0.45 μM, λ_{ex} = 385 nm), C6-CF_3 (red trace, 0.14 μM λ_{ex} = 464 nm) and SB1 (blue trace, 0.57 μM, λ_{ex} = 469 nm). Slit width = 5 nm. All spectra recorded in THF at 298 K.

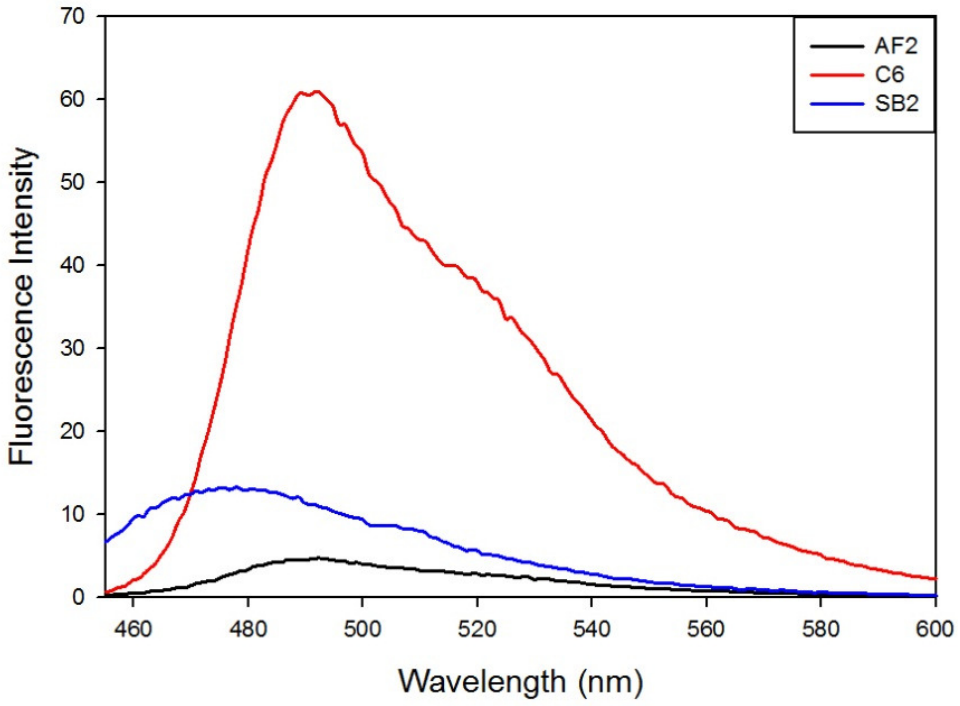

Figure 55. Fluorescence spectra of **AF2** (black trace, 0.57 μM), C6 (red trace, 0.57 μM) and SB2 (blue trace, 0.59 μM,). λ_{ex} = 443 nm, Slit width = 5 nm. All spectra recorded in THF at 298 K.

Addition of As(III) salts (either as $AsCl_3$ or AsI_3) to a THF solution of **AF1** or **AF2**, leads to the disappearance of the maxima peak and appearance of new peaks at 464 nm and 443 nm, respectively, in the UV-vis spectrum (Figures 56 – 57). This shows that **AF1** and **AF2** react with As(III) to form another species consistent with the chemodosimeter design. Monitoring the UV-vis spectra every five min shows that the reaction of **AF1** and **AF2** with As(III) is complete within 30 min. Hence, the incubation time for fluorescence experiments was set at 30 min to allow complete reaction. When As(III) salts are added to THF solutions of AFs, an increase in quantum yield to 0.101 (**AF1** reaction) and 0.121 (**AF2** reaction) is observed, resulting in an approximate 20 – 25-fold increase in fluorescence intensity of the dyes in the presence of As(III) (Figures 58 – 59). Thus, **AF1** and **AF2** perform as effective OFF-ON fluorescence sensors for As(III) in organic media at 298 K.

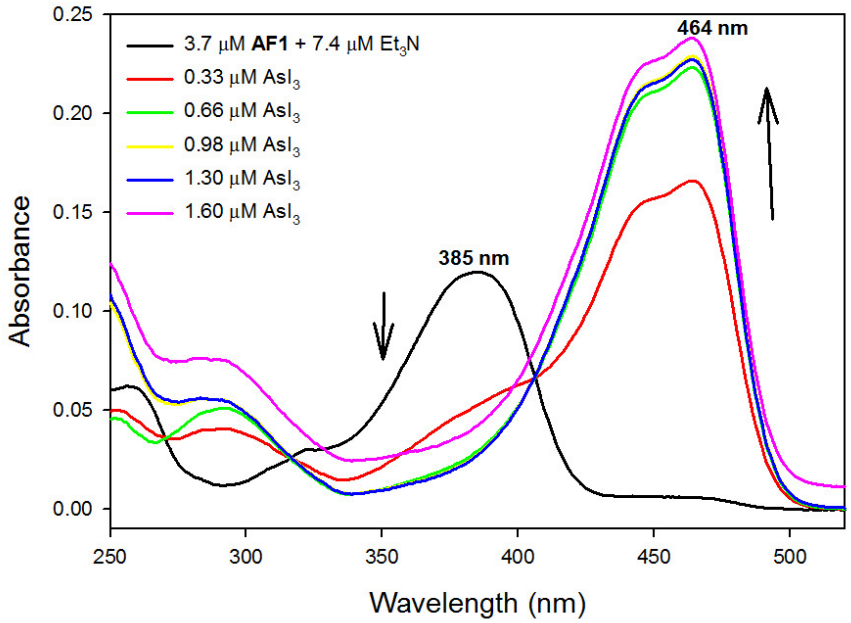

Figure 56. Absorption spectrum of 3.7 μM **AF1** in THF before and after adding 0.33 – 1.60 μM AsI_3 in THF at 298 K. Each scan was taken 30 mins after adding AsI_3. Arrows show direction of change.

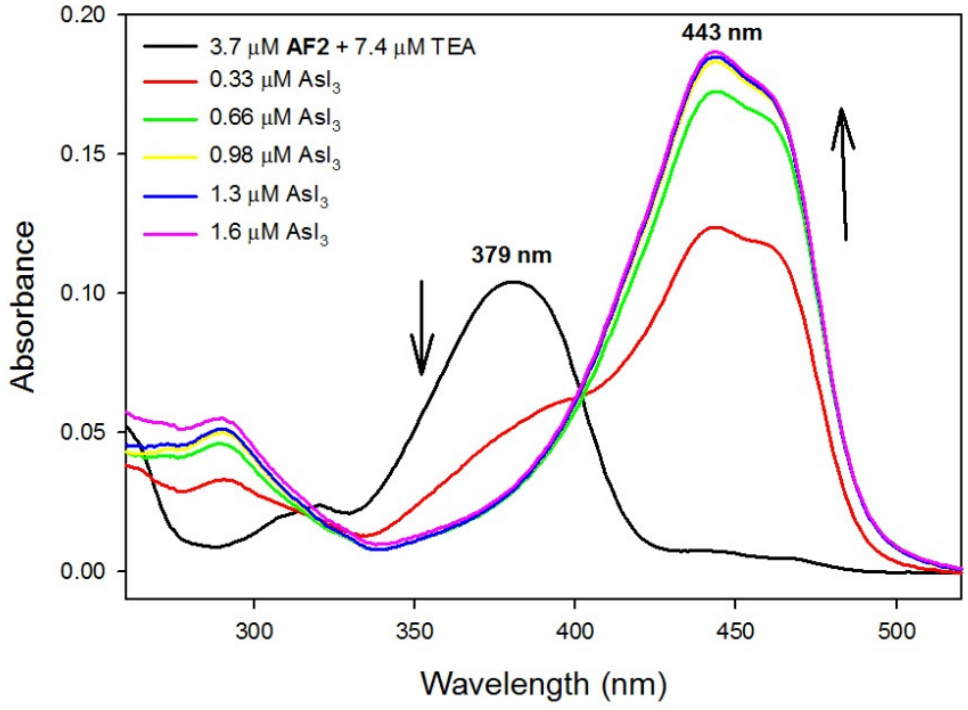

Figure 57. Absorption spectrum of 3.7 μM **AF2** in THF before and after adding 0.33 – 1.60 μM AsI_3 in THF at 298 K. Each scan was taken 30 mins after adding AsI_3. Arrows show direction of change.

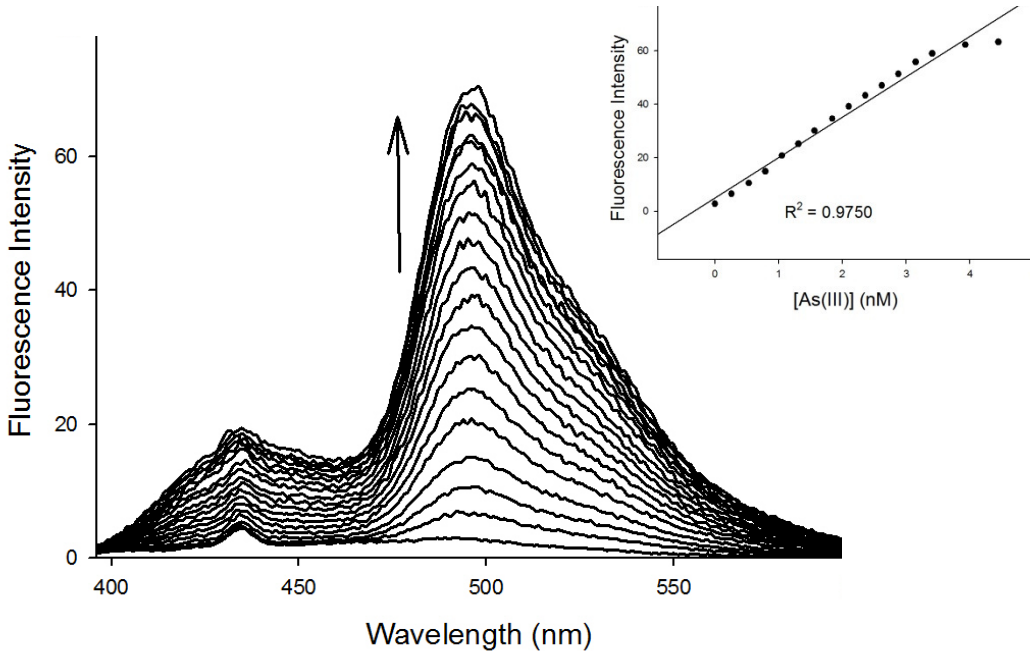

Figure 58. Fluorescence response of 0.45 μM **AF1** in THF at 298 K (λ_{ex} = 385 nm). Spectra shown are for [As(III)] of 0, 0.26, 0.53, 0.79, 1.05, 1.31, 1.56, 1.84, 2.10, 2.36, 2.62, 2.88, 3.15, 3.41, 3.93, 4.45, 4.97, 5.49 and 6.78 nM. Each reading was obtained 30 min after the addition of As(III). The arrow shows the direction of change. Inset: plot of fluorescence intensity change with [As(III)].

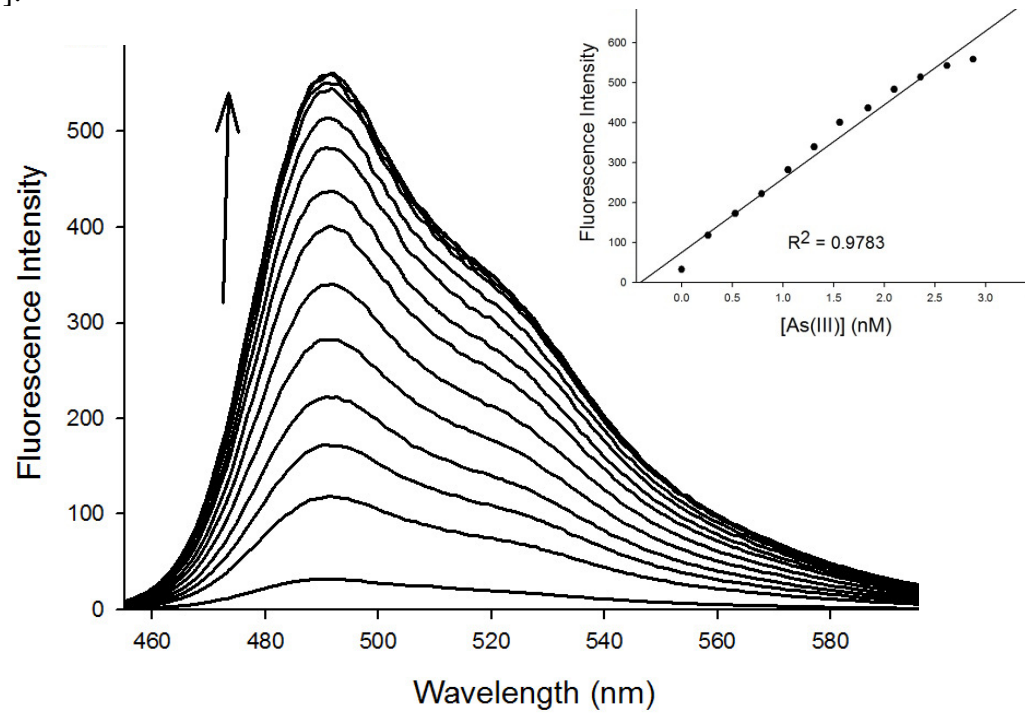

Figure 59. Fluorescence response of 0.45 μM **AF2** in THF at 298 K (λ_{ex} = 443 nm). Spectra shown are for [As(III)] of 0, 0.26, 0.53, 0.79, 1.05, 1.31, 1.56, 1.84, 2.10, 2.36, 2.62, 2.88, 3.15 and 3.41 nM. Each reading was obtained 30 min after the addition of As(III). The arrow shows direction of change. Inset: plot of fluorescence intensity change with [As(III)].

A desirable property of an As(III)-fluorescent dye is the ability to detect ppb-concentrations of As(III). Hence, the detection limit was determined by measuring [As(III)], which gave a signal-to-background ratio ≥ 3, a widely supported method of determination.[225-226] The detection limit was 0.53 nM (0.24 ± 0.13 ppb) and 0.31 nM (0.14 ± 0.03 ppb) for **AF1** and **AF2,** respectively. These detection limits are well below the established maximum contamination level (MCL) of 10 ppb for As compounds in drinking water. Therefore, **AF1** and **AF2** are highly sensitive fluorescent dyes for As(III). To determine if **AF1** and **AF2** will respond selectively to As(III) in the presence of other ions, the fluorescence response in THF was measured after adding 10 mol-equiv of the ion followed by 10 mol-equiv of As(III) (Figures 60 – 61). The competition studies show the fluorescence intensity of the dyes is unperturbed in the presence of alkali and alkali-earth metals such as Na(I), Mg(II), and Ca(II), indicating no reaction and excellent selectivity over these common environmentally encountered ions. Furthermore, the dyes are selective for As(III) over common first-row transition-metal ions like Mn(II), Fe(II)/(III), Ni(II) and Zn(II). Of the first-row metals tested, only Cu(II), and to a lesser extent Co(II), interferes with the As(III)-induced fluorescence increase. Analysis of the reaction product by ESI-MS and EPR, shows that Cu(II) promotes the exclusive formation of the Schiff-base, SB1 or SB2 and results in Cu(I). The use of a masking agent, one mol-equiv of cuprizone, didn't prevent the oxidation of **AF1** or **AF2** to Schiff-base (SB1 or SB2 respectively) by Cu(II) ions, which indicates an outer-sphere redox process. Overall, the chemoselectivity of **AF1** and **AF2** for As(III) is quite remarkable especially over other heavy metal toxic ions such as Hg(II), Pb(II) and Cd(II) (Figures 60 – 61).

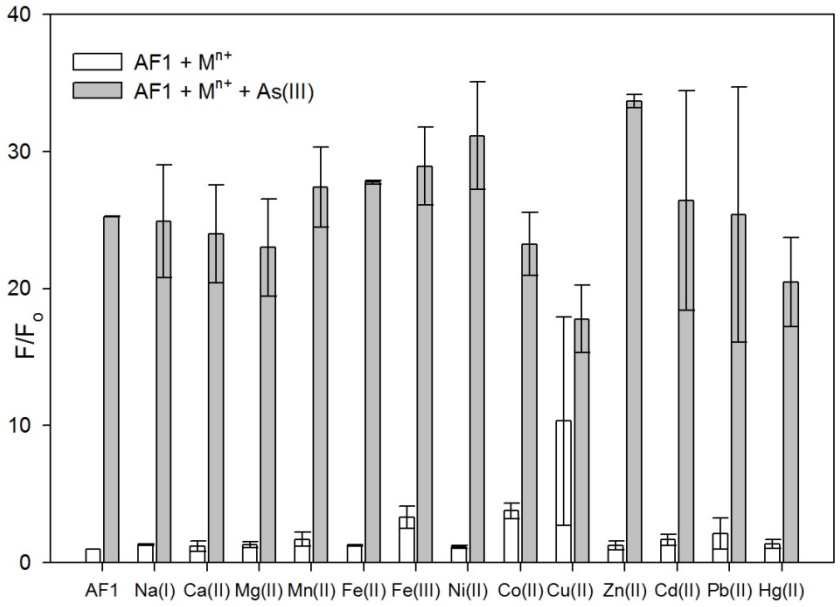

Figure 60. Fluorescence response of **AF1** to various ions (average of three trials) in THF at 298 K. Bars represent the final integrated fluorescence response (F) over the initial integrated emission (F_o). White bars represent the addition of the appropriate ion (4.5 μM) to a 0.45 μM solution of **AF1**. Gray bars represent the addition of 4.5 μM As(III) to the **AF1** + ion solutions.

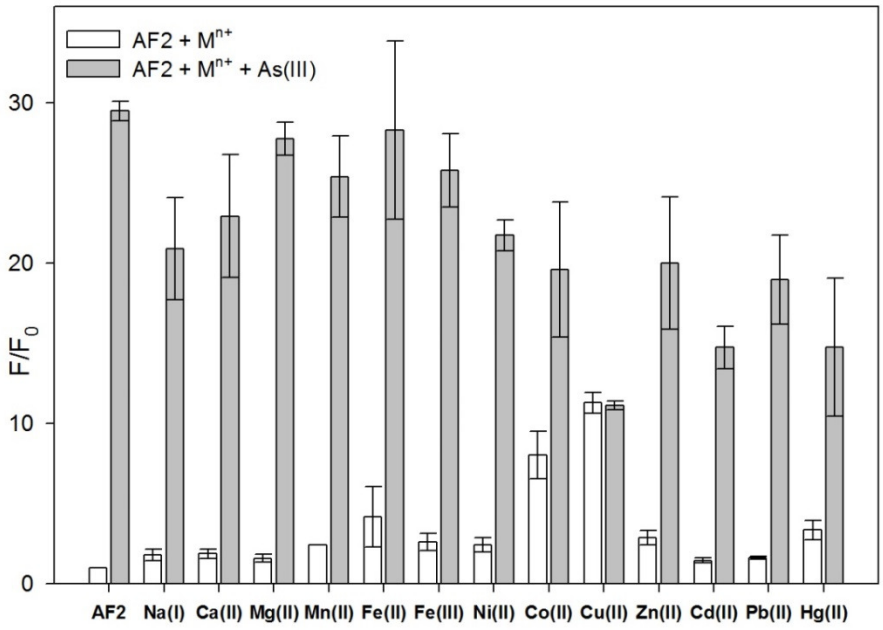

Figure 61. Fluorescence response of **AF2** to various ions (average of three trials) in THF at 298 K. Bars represent the final integrated fluorescence response (F) over the initial integrated emission (F_o). White bars represent the addition of the appropriate ion (4.5 μM) to a 0.45 μM solution of **AF2**. Gray bars represent the addition of 4.5 μM As(III) to the **AF2** + ion solutions.

While the AFs clearly react with As(III) in organic solvents such as THF, the aim was to use these constructs for monitoring environmental As(III) in the form of arsenite. Since the AFs are not entirely water-soluble, the reaction with arsenite was examined with **AF1** in a THF/H_2O mixture. **AF1** was selected due to its enhanced air stability and the reaction of **AF1** with As(III) salts (AsI_3 or $NaAsO_2$) was monitored by UV-vis and fluorescence spectroscopies in a THF/CHES (1:1, pH 9) mixed solvent at 298 K. In each case, the UV-vis maximum at ~390 nm disappeared with the formation of a new peak at ~470 nm (Figures 62 – 63) consistent with the reaction of **AF1** with As(III) in THF. An isobestic point at 420 nm is also observed in the mixed medium indicating a clean transformation. It should also be noted that the time required for complete transformation is slower in the aqueous THF mixture when compared to neat THF. The reaction is complete in 2.5 h or 5 h when either AsI_3 or $NaAsO_2$, respectively, is used compared to 0.5 h in THF. Addition of AsI_3 or $NaAsO_2$ to **AF1** in the aqueous mixture afforded a modest, but inconsistent increase in the fluorescence intensity (~1.2 – 3-fold increase) centered at 509 nm (λ_{ex}: 473 nm) (Figures 64 – 65). While this result is not ideal for fluorescence sensing, **AF1** does appear to react and report As(III)-ions in mixed aqueous media as demonstrated by the colorimetric response in the UV-vis. The decreased change in fluorescence intensity is explained by quenching of emission in a polar solvent possibly due to the stabilization of the polar excited state.[211]

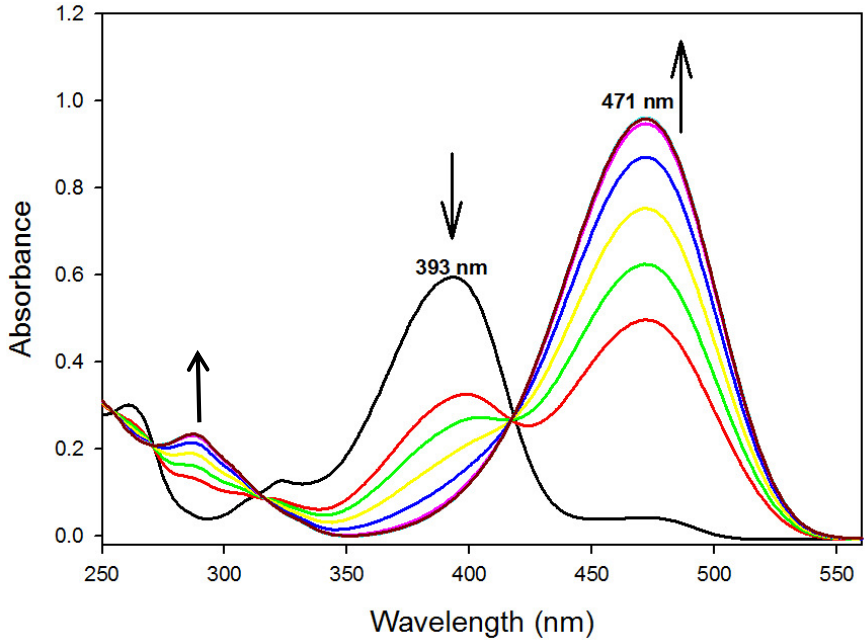

Figure 62. UV-vis spectral monitoring of the reaction of 19.0 μM **AF1** and 21.3 μM AsI_3 in THF/CHES (1:1, pH 9) at 298 K. Scan intervals are 30 min for 3 h total. Arrows display direction of change upon addition of As(III).

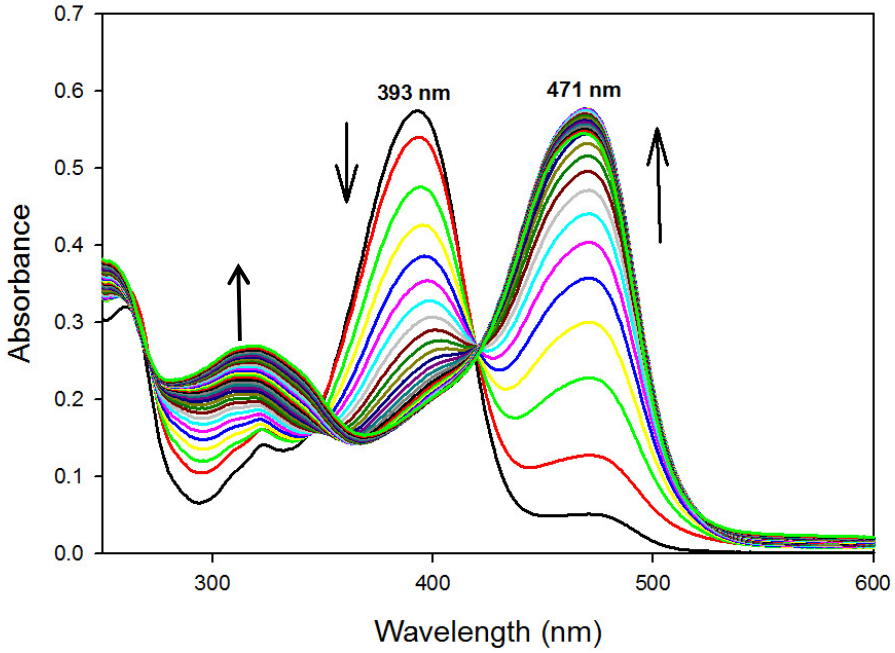

Figure 63. UV-vis spectral monitoring of the reaction of 17.1 μM **AF1** and 24.1 μM $NaAsO_2$ in THF/CHES (1:1, pH 9) at 298 K. Scan intervals are 30 min for 16 h total. Arrows display direction of change upon addition of As(III).

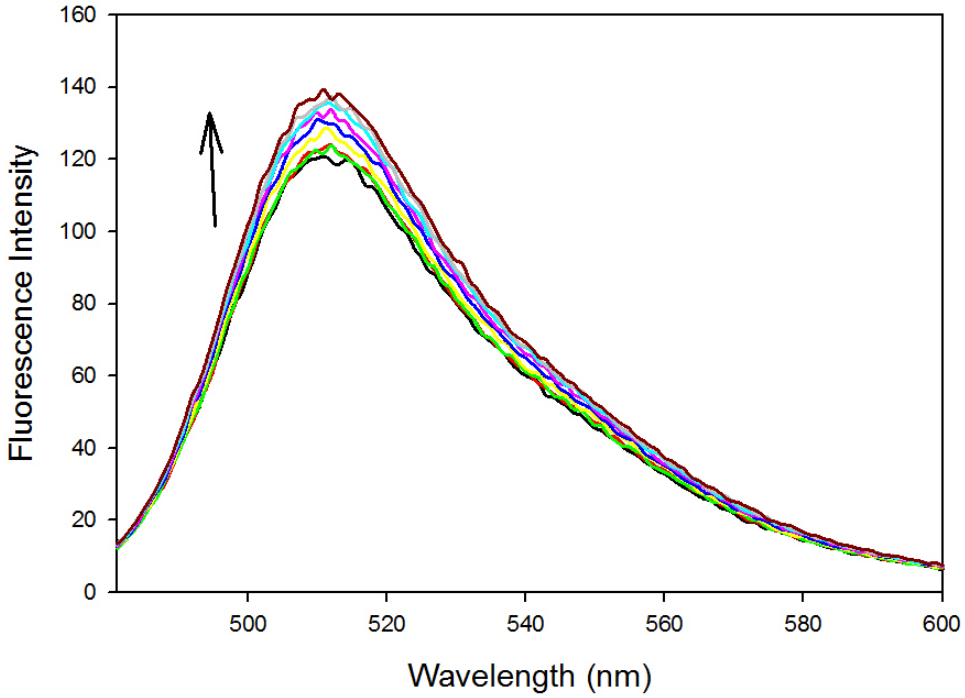

Figure 64. Fluorescence response of 0.98 μM **AF1** to 1.13 μM AsI_3 in THF/CHES (1:1, pH 9). Scan intervals are 30 min for 4 h total time. Arrow displays direction of change upon addition of As(III).

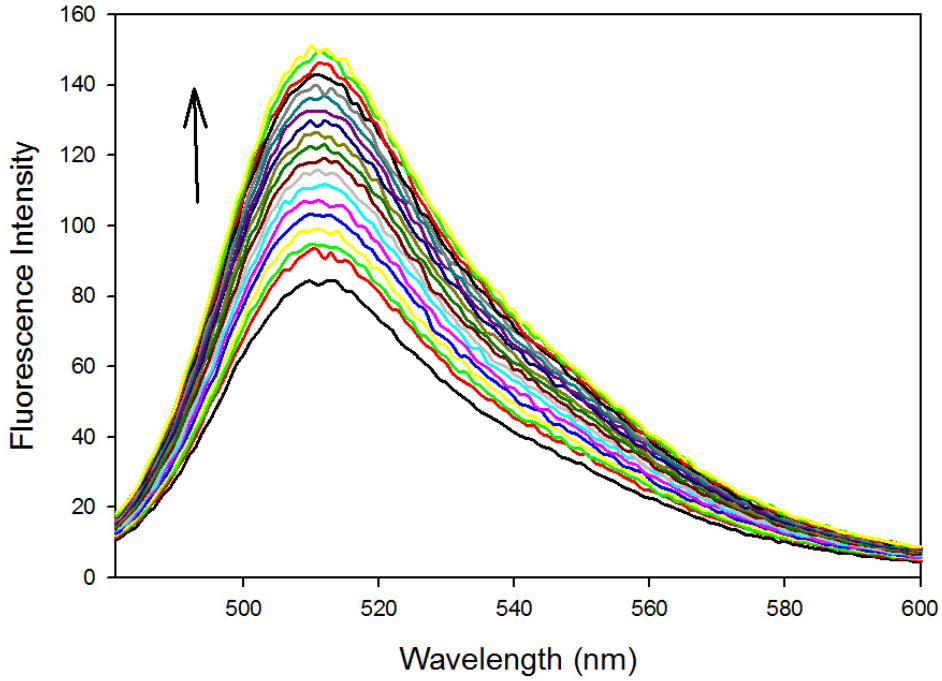

Figure 65. Fluorescence response of 0.98 μM **AF1** to 1.28 μM $NaAsO_2$ in THF/CHES (1:1, pH 9). Scan intervals are 10 min for 3 h total time. Arrow displays direction of change upon addition of As(III).

In an effort to determine the fluorescent species formed in the reaction of AFs and As(III), the spectroscopic data from the reactions reported above were compared to spectroscopic data of pure C6s and SBs. The addition of As(III) salts to THF solutions of AFs resulted in a new peak with a double-hump profile at 464 nm and 443 nm for the **AF1** and **AF2** reactions in THF respectively. This new UV-vis profile, which forms irrespective of As(III)/AF ratio, is consistent with the UV-vis profile of the C6 analogs (Figures 51, 52, 56, 57). A similar red-shift from 393 nm to 473 nm in THF/CHES (pH 9) is also in agreement with formation of C6-CF_3 (Figures 53, 62 & 63). These UV-vis changes support that the fluorescent species are the C6 analogs formed in the reaction. Further support for this assignment is the significant difference in the quantum yields of the analogs. For example, Φ_f (**AF1**) = 0.004 vs Φ_f (C6-CF_3) = 0.880 in THF. Although the C6 analogs are the main emissive compounds, the relatively low quantum yield (0.101 and 0.121 for **AF1** and **AF2** respectively) of the As(III) reaction products hints to the presence of other species or processes that reduces the fluorescence intensity of the highly emissive C6 analogs.

To gain further insight into the mechanism of the As(III)-promoted redox rearrangement of the benzothiazoline group in AFs, bulk synthesis and analysis of the products were performed. Analysis of the ^{1}H NMR spectrum of the bulk reaction product revealed peaks that can be assigned to the C6 and SB analogs in approximately equal amounts (based on proton integration) (Figure 66). Since the ^{1}H NMR spectrum of independently synthesized C6-CF_3, C6, SB1 and SB2 matches closely to the peaks in the reaction product, it can be inferred that the reaction of AFs with As(III) leads to oxidation of the AFs to form the C6 dyes with no evidence of an As(III) complex.

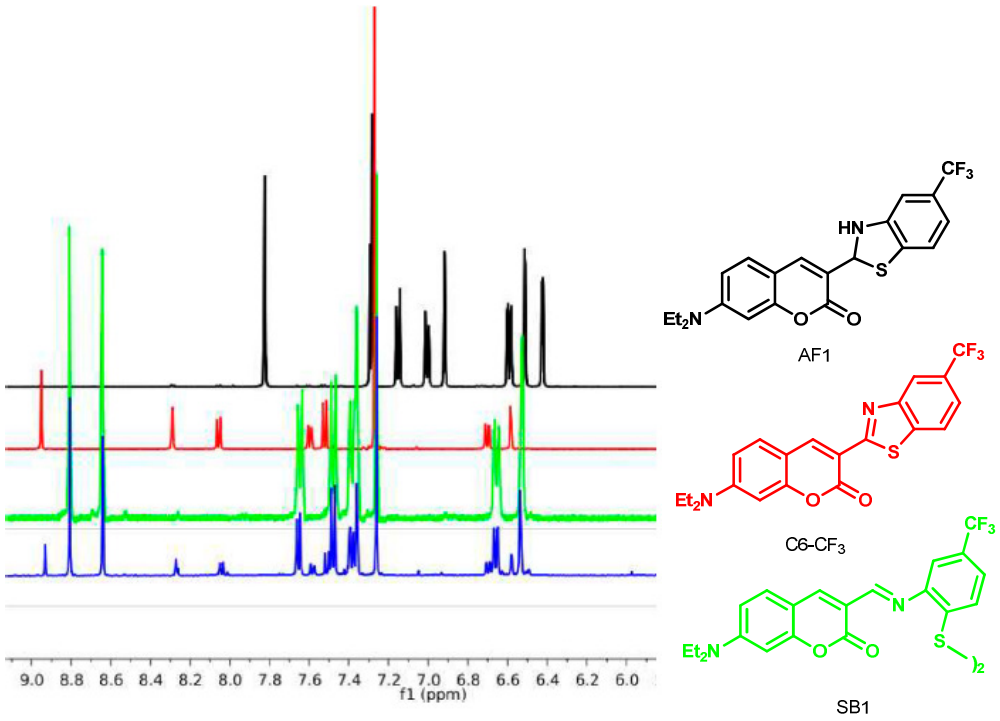

Figure 66. ^{1}H NMR spectrum (aromatic region) of the reaction of **AF1** + As(III) (blue), **AF1** (black), independently synthesized C6-CF_3 (red), independently synthesized SB1-disulfide (green) in $CDCl_3$ at 298 K.[227] Structural depiction of **AF1**, C6-CF_3 and SB1 (left).

The oxidation of AFs to form the oxidized analogs (C6 or SB) involve the loss of two electrons and one proton, which would imply the formation of an As(I) species. To test this hypothesis, a bulk reaction was performed by the addition of stoichiometric diphenylphosphinoethane (dppe), a chelating diphosphine ligand known to form a complex with As(I).[14, 228] The product obtained was characterized by ^{31}P NMR and ESI-MS. The observed peak at 61.63 ppm in the ^{31}P NMR spectrum has been reported for the formation $[As(dppe)]^+$, which is expected from the neutral dppe ligand and As(I) (Figure 67).[14, 228] Other peaks present in the ^{31}P NMR spectrum are assigned to phosphine oxide formation, which were observed in the reported synthesis of $[As(dppe)]^+$.[14] The ESI-MS further confirms the formation of $[As(dppe)]^+$ with a base peak at *m/z* = 473.0 (Figure 68). Other peaks present in the ESI-MS are as expected, i.e., *m/z* = 353.0 (AF2) and 703.2 (SB2). Collectively, these results indicate that a loosely bound

or free As(I) complex is present in the reaction mixture which is easily intercepted when the strong field dppe ligand is added to form $[As(dppe)]^+$.

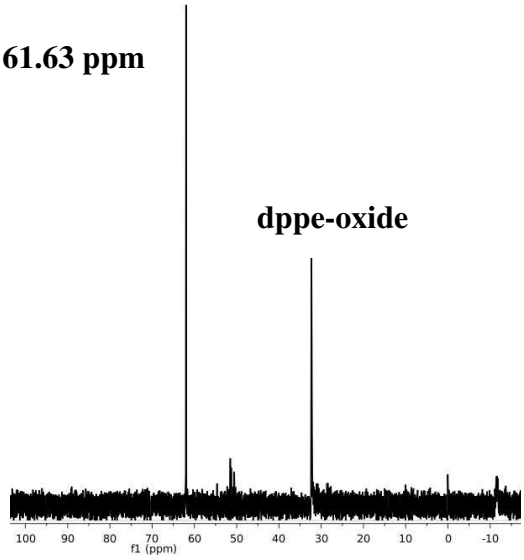

Figure 67. ^{31}P NMR spectrum of the reaction of **AF2** and AsI_3 under sensing conditions after the addition of dppe in CD_2Cl_2. The singlet peak at 61.63 ppm is assigned to $[As(dppe)]^+$ while the triplet at 31.91 ppm is assigned as phosphine oxide.[14]

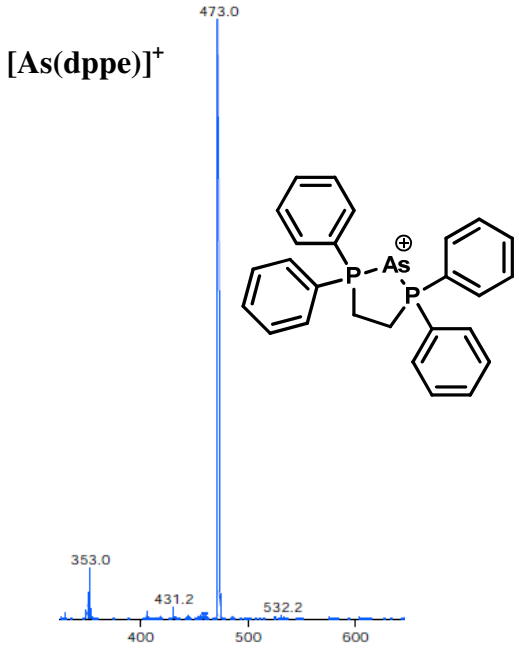

Figure 68. Positive mode LRMS-ESI-MS of the reaction of **AF2**, AsI_3 under sensing conditions after the addition of dppe showing parent peak at *m/z* = 473.0. Inset: structural depiction of $[As(dppe)]^+$.

Other insight into the reaction of AFs and As(III) was gained by carrying out cyclic voltammetry (CV) measurements under sensing conditions. The voltammogram of the **AF1**-As(III) reaction was compared to that of independently synthesized C6-CF_3 and SB1 (Figure 69). Two quasireversible waves ($E_{1/2}$: 0.97 V, ΔE_p: 0.11 V; $E_{1/2}$: 0.67 V, ΔE_p: 0.18 V vs Fc/Fc^+) and one irreversible wave (E_{ox}: 0.51 V vs Fc/Fc^+)) are observed in the CV of the reaction mixture. The quasireversible waves correspond to the events from the independently synthesized C6-CF_3 and SB1, which leaves the oxidation event at 0.51 V unassigned. This additional electroactive species is tentatively assigned as an As-ligated complex. This CV data further support the formation of C6 and SB analogs when AFs react with As(III).

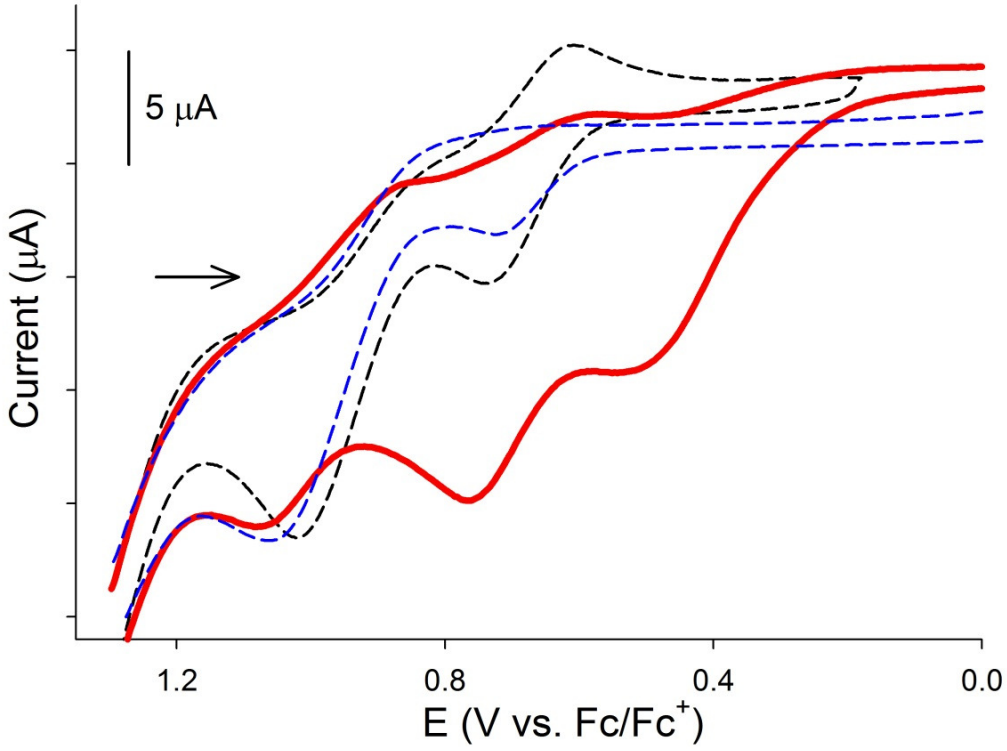

Figure 69. Cyclic voltammograms of THF solutions of the **AF1** and As(III) reaction mixture (red-solid trace), authentic C6-CF_3 (black-dashed trace), and authentic SB1 (blue-dashed trace) (0.1 M $^nBu_4NPF_6$ supporting electrolyte, glassy carbon working electrode, Pt-wire counter electrode, 100 mV/s scan speed, RT).[220] Arrow indicates direction of scan.

In summary, the reaction of AFs and As(III) lead to the formation of the highly emissive C6 analogs and the less emissive SBs with evidence that As(III) is reduced to As(I). In addition, the CV study hints to the formation of another species that is possibly transient in solution. Based on these studies and literature precedence for Cu(I/III) benzothiazoline reactions, the following mechanism is proposed (see Scheme 10). The first step likely involves a bis-coordination to the Schiff-base thiolate form of AFs, which is a reported mode of ligation of benzothiazoline groups with various metal ions.[184, 193] Then, rearrangement of one of the ligands to give an As(III)-amide bond via an attack of the thiolate on the imine-C, followed by a hydride transfer to form the benzothiazole (C6) and a proposed As(III)-hydride complex. Subsequently, reductive elimination from the hydride complex affords the As(I) and disulfide (SB). A similar rearrangement chemistry has been noted for the copper-mediated formation of benzothiazoles from an imine disulfide precursor utilizing the Cu(III/I) redox couple.[229-230] In that mechanism, an oxidative addition of Cu(I) across a disulfide bond affords the bis-coordinate Cu(III) Schiff – base complex similar to the first step in the As(III) mechanism discussed above. A hydride migration leads to the formation of the benzothiazole moiety and a transient Cu(III)-hydride complex. The hydride complex then dissociates to give Cu(I) and the benzothiazoline moiety. The hydride transfer step is feasible as observed in the use of benzothiazolines as hydride sources in the Brønsted acid catalyzed reduction of imines to chiral amines.[231-235] Finally, while precedence for As-hydride complexes with the exception of arsine and methylated As-hydride compounds is scarce, hydride-ligated intermediates with phosphorus have recently been reported.[236] All evidence (UV-vis, fluorescence, ^{1}H NMR, dppe reactivity) obtained in this work supports this mechanism.

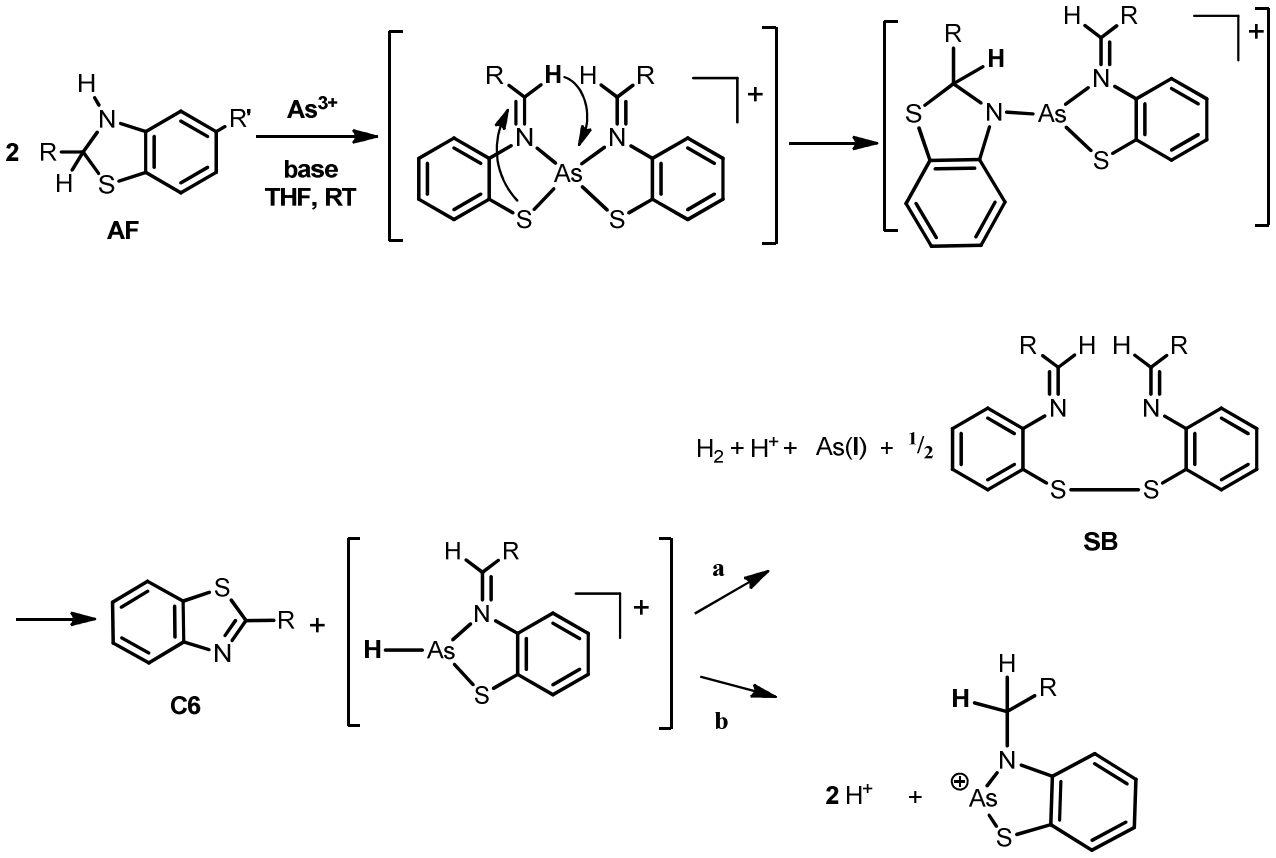

Scheme 10. Proposed mechanism for the reaction of As(III) with AF (route a) and **L5** (route b, chapter 2). Last step: reductive elimination (route a) and imine reduction (route b).

The products obtained from the reaction of benzothiazoline with As(III) in this study is different from that reported in chapter 2. In both examples the benzothiazole is a common product; but instead of an As(III)-ligated complex the Schiff-base disulfide was formed in the case of the AFs. The difference in product outcome is proposed to be the presence of the pyridine-N donor group, which enhances the stability of the As(III)-hydride complex and prevents reductive elimination. A general mechanism is proposed for the reaction of benzothiazoline functional group with As(III) based on the product distribution observed in these studies. The first step is likely the formation of bis-coordinate complex followed by hydride transfer to form the benzothiazole and As(III)-hydride complex. The fate of the transient As(III)-

hydride is the basis for the different products obtained. With **L5** (used in chapter 2), hydride transfer to the imine-C reduces the ligand and results in the four-coordinate As(III) complex. However, the As(III)-hydride complex in the AFs reaction decomposes to give Schiff-base disulfide and As(I).

3.4 Conclusion

Two chemodosimeters, **AF1** and **AF2**, containing a coumarin fluorophore appended to an As(III)-reactive benzothiazoline group were synthesized and characterized by spectroscopic methods. The oxidized analogs (C6-CF_3, C6 (commercially available), SB1 and SB2) were also synthesized and their spectroscopic characterization were used in analyzing and identifying the product of the AF and As(III) reaction. Indeed, the reaction of AFs with As(III) salts ($AsCl_3$ and AsI_3) resulted in a > 50 nm red-shift in the UV-vis experiment, which is consistent with the transformation of AFs to their oxidized species, C6 and SB. This reaction also elicited a 20 – 25 fold increase in fluorescence intensity in THF, in agreement to the highly emissive C6 analog being formed in the reaction. Thus, **AF1** and **AF2** act as OFF-ON fluorescent sensors for As(III). The dyes are sensitive to low concentration of As(III) with a detection limit range of 0.14 – 0.23 ppb, meaning they can be used for sensing [As(III)] below the accepted MCL of 10 ppb. Competition studies shows that formation of the C6 analog is selective for As(III), though ions such as Cu(II) and Co(II) that promote the formation of the SB analog could interfere with the sensing of As(III). AFs also react with $NaAsO_2$ in aqueous THF medium resulting in a UV-vis profile similar to C6 and SB analogs. However, the fluorescence of the C6 formed is quenched because of the high polarity of the aqueous THF medium. Bulk analysis, dppe reactivity and CV show that the reaction of AFs with As(III) results in formation of the

benzothiazole, Schiff-base disulfide and As(I) species. The reaction is proposed to go through a putative As(III)-hydride intermediate, which is transformed to the oxidized analogs of AFs. Collectively, this work shows that **AF1** and **AF2** are excellent fluorescent dyes for As(III) in organic media and can be used as colorimetric dyes for As(III) in mixed aqueous media.

3.5 Experimental Section

General Information. All reagents were purchased commercially and used as received unless otherwise noted. Acetonitrile (MeCN), methylene chloride (CH_2Cl_2), tetrahydrofuran (THF), diethyl ether (Et_2O) and pentane were purified by passage through activated alumina columns using an MBraun MB-SPS solvent purification system and stored over 4 Å molecular sieves under a dinitrogen (N_2) atmosphere before use. Triethylamine (Et_3N) was dried by storing over KOH and $CaSO_4$ in an N_2 atmosphere. Ethanol (EtOH) and methanol (MeOH) were dried by distilling from $Mg(OEt)_2$ and $Mg(OMe)_2$, respectively under N_2. A 50 mM CHES (*N*-cyclohexyl-2-aminoethanesulfonic acid) (pH = 9) solution was prepared by dissolving 1.0361 g of CHES in 100 mL of milli-Q water and the pH adjusted either with 1 M HCl or NaOH. Solvents were sufficiently degassed by at least three freeze-pump-thaw cycles before introduction into the glovebox. All solvents were filtered with a 0.45 μm nylon filter before spectroscopic measurements were recorded to remove particulates (primarily molecular sieves from anhydrous storage). Reactions performed in an MBraun Unilab glovebox was under an atmosphere of purified N_2. Stock solutions of ArsenoFluor1 (AF1) and ArsenoFluor2 (AF2) were freshly prepared before all spectroscopic studies. Ligands, 7-(diethylamino)-2-oxo-2*H*-chromene-3-carbaldehyde,[219, 221] AF2[218], 6,6′-disulfanediylbis(3-trifluoromethyl)aniline,[237] and

2,2'-disulfanediyldianiline,[238] were synthesized according to literature procedures. All fluorescence sensing experiments in THF contain 5 mol-equiv of Et_3N unless stated otherwise.

Physical Measurements. ^1H and ^{13}C NMR spectra were recorded in deuterated solvents on either a Varian Unity Inova 500 MHz or Varian Mercury plus 400 MHz NMR spectrometer at 298 K with chemical shifts referenced to tetramethylsilane (TMS) or residual protio signal of the deuterated solvent.[196] ^{31}P NMR spectra were recorded on a Varian Unity Inova 500 MHz NMR spectrometer at 298 K with chemical shifts referenced to external 85% H_3PO_4. FTIR spectra were collected on a ThermoNicolet 6700 spectrometer running the OMNIC software. Samples were run as solids either in a KBr matrix or ATR diamond transmission window. Electronic absorption spectra were run at 298 K using a Cary 50 spectrophotometer equipped with a Quantum Northwest TC 125 temperature control unit. Fluorescence spectra were run at 298 K using a Varian Eclipse spectrofluorometer also containing the Quantum Northwest TC 125 temperature controller. All UV-vis and fluorescence samples were prepared in gas-tight Teflon-lined screw cap quartz cells with an optical pathlength of 1 cm. The quartz cells were cleaned thoroughly before each measurement by soaking in 10% HNO_3 for at least 3 h to remove trace metals, then rinsing with saturated $NaHCO_3$ solution, DI water, and MeOH. Measurements of pH were performed on an Accumet pH meter from Fischer Scientific, model 25, with a combination electrode. A three point calibration with commercially available standards was performed before pH values were recorded. Cyclic Voltammetry (CV) measurements were performed with a PAR Model 273A potentiostat using a non-aqueous Ag/Ag^+ (0.01 M $AgNO_3$/0.1 M $^nBu_4NPF_6$ in MeCN) reference electrode, Pt counter electrode, and a glassy-carbon (2 mm diameter) milli-working electrode under an Ar atmosphere. Measurements were performed at ambient temperature using 0.8 – 8.0 mM analyte in THF containing 0.1 M $^nBu_4NPF_6$ as the supporting

electrolyte. The "Maximize Stability" mode was utilized in the PAR PowerCV software utilizing a low-pass 5.3 Hz filter. Ferrocene (Fc) was used as an internal standard and all potentials are reported relative to the Fc^+/Fc couple. Low Resolution ESI-MS data were collected using a Perkin-Elmer Sciex API I Plus quadrupole mass spectrometer and High Resolution ESI-MS data were collected using a Bruker Daltonics 9.4 T Apex Qh FT-ICR-MS. Elemental analysis was done by Quantitative Technologies Inc in Whitehouse, N.J. Uncorrected melting points were obtained with a Laboratory Device MEL-TEMP II. FTIR and UV-vis data were plotted using the SigmaPlot 10.0 software package and NMR data were plotted with MestReNova Lite.

Synthesis Safety Note. Caution! Compounds containing arsenic (As) are toxic and should be handled with extreme care.

Synthesis of AF1, 7-(diethylamino)-3-(5-(trifluoromethyl)-2,3-dihydrobenzothiazol-2-yl)-2*H*-chromen-2-one (racemic mixture). *Step 1:* **Synthesis of 7-diethylaminocoumarin.** A solid batch of 4-diethylaminosalicylaldehyde (1.9309 g, 9.992 mmol), diethylmalonate (3.2057 g, 20.014 mmol) and piperidine (1 mL) was dissolved in 30 mL of EtOH to give a dark red solution. The reaction was refluxed for 6 h, concentrated with the rotavap to remove EtOH and other volatiles to give a dark red oil. The oil was dissolved in HCl (20 mL) and acetic acid (20 mL) and refluxed for 12 h then further stirred at RT for 6 h. The flask was placed in an ice bath and 50 mL of DI water was added. A 40% NaOH solution was added dropwise until a pH ~ 5 was obtained. A light brown precipitate was obtained after stirring for 30 min, the mixture was filtered and the pale residue washed with DI water. The solid was dissolved in CH_2Cl_2, dried with $MgSO_4$, filtered and concentrated to give a yellow solid (1.7197, 79%). ^1H NMR (400

MHz, $CDCl_3$, δ from TMS): 1.22 (t, 6H), 3.42 (m, 4H), 6.04 (d, 1H), 6.50 (s, 1H), 6.57 (d, 1H), 7.25 (d, 1H), 7.54 (d, 1H). ^{13}C NMR (100.6 MHz, $CDCl_3$, δ from TMS): 12.4, 44.8, 97.5, 108.6, 109.2, 128.8, 143.7, 149.4, 150.7, 156.7, 162.3 (*C*=O). FTIR (KBr pellet), ν_{max} (cm^{-1}): 3391(w), 3067 (m), 2981 (m), 2931 (m), 1778 (m), 1704 (s,C=O), 1615 (s), 1519 (m), 1391 (m), 1286 (m), 1246 (s), 1221 (m), 1167 (m), 1126 (m), 1094 (m), 1070 (m), 1010 (m), 885 (m), 844 (s), 812 (s), 796 (m), 659 (m), 638 (s), 615 (s), 505 (vs), 462 (vs), 427 (s). *Step 2:* **Synthesis of 7-(diethylamino)-2-oxo-2*H*-chromen-3-carbaldehyde.** A solution of DMF (3 mL) was added dropwise to a batch of $POCl_3$ (3 mL) in a Schlenk flask placed in a water bath maintained at 40 – 50 ^oC to give a red-colored solution. Then a batch of the solid synthesized in step 1 (1.7197 g, 7.915 mmol) dissolved in 15 mL of DMF was added to the red $POCl_3$-DMF solution. The reaction was stirred at 60 ^oC for 16 h. The flask was placed in an ice-bath and 100 mL of DI water was added to give a dark-red mixture. A 50% NaOH was added dropwise until a pH ~ 5 was obtained. The mixture was filtered to give an orange solid and dark-red filtrate. The residue was dissolved in 30 mL of CH_2Cl_2 and dried with $MgSO_4$, filtered and concentrated to give an orange solid (1.4021 g, 72%). ^1H NMR (400 MHz, $CDCl_3$, δ from TMS): 1.25 (t, 6H), 3.47 (q, 4H), 6.47 (s, 1H), 6.67 (d, 1H), 7.41 (d, 1H), 8.25 (s, 1H), 10.12 (s, 1H). ^{13}C NMR (100.6 MHz, $CDCl_3$, δ from TMS): 12.5, 45.3, 97.2, 108.2, 110.2, 114.3, 132.5, 145.4, 153.5, 158.9, 161.9 (*C*=O), 187.0. FTIR (KBr pellet), ν_{max} (cm^{-1}): 3407 (w), 3060 (w), 2972 (m), 2928 (m), 2874 (w), 2847 (w), 1710 (vs), 1672 (s, C=O), 1622 (s), 1575 (s), 1540 (w), 1514 (s), 1486 (m), 1473 (m), 1456 (m), 1441 (m), 1426 (w), 1393 (m), 1378 (m), 1353 (s), 1306 (m), 1290 (m), 1277 (m), 1263 (s), 1189 (s), 1171 (m), 1149 (m), 1136 (m), 1093 (m), 1074 (m), 1006 (m), 973 (m), 945 (m), 821 (s), 798 (m), 776 (w), 760 (m), 653 (w), 647 (m), 618 (m), 505 (m), 525 (w). *Step 3:* **Synthesis of AF1.** A solid batch of 7-diethylaminocoumarin-3-aldehyde (0.5351 g, 2.182 mmol)

was dissolved in 10 mL of EtOH to give an orange colored solution. To this solution was then added a 10 mL EtOH solution of 2-amino-4-(trifluoromethyl)benzenethiol•HCl (0.6008 g, 2.616 mmol) containing Et_3N (0.2852 g, 2.818 mmol), which resulted in no immediate visible color change. The reaction was then stirred at RT for 6 h in the glovebox and a yellow precipitate was observed after 30 min. The reaction mixture was filtered to isolate the precipitated product and the solid was recrystallized from EtOH and dried under vacuum to afford 0.8040 g (1.912 mmol, 88%) of material. ^{1}H NMR (500 MHz, $CDCl_3$, δ from TMS): 1.21 (t, 6H), 3.42 (q, 4H), 4.88 (NH, d, 1H), 6.41 (methine CH, d, 1H), 6.49 (d, 1H), 6.57 (dd, 1H), 6.89 (s, 1H), 6.98 (d, 1H), 7.13 (d, 1H), 7.26 (d, 2H, integrates high due to overlap with solvent residual), 7.80 (s, 1H). ^{13}C NMR (100.6 MHz, $CDCl_3$, δ from TMS): 12.6, 45.0, 64.8, 97.3, 106.6, 108.2, 109.3, 117.8, 120.9, 121.9, 129.5, 139.4, 146.4, 149.6, 151.1, 156.1, 162.1 (*C*=O). FTIR (KBr pellet), ν_{max} (cm^{-1}): 3260 (m, N-H), 3084 (w), 2971 (m), 2930 (m), 2898 (w), 1681 (vs, C=O), 1605 (vs), 1522 (s), 1451 (m), 1418 (s), 1381 (w), 1354 (m), 1333 (s), 1261 (m), 1245 (s), 1190 (m), 1162 (m), 1134 (s), 1108 (s), 1071 (s), 1019 (w), 963 (w), 952 (w), 914 (w), 872 (m), 834 (s), 824 (s), 799 (w), 777 (s), 745 (w), 732 (w), 701 (w), 668 (m), 643 (w), 632 (w), 618 (w), 549 (w), 525 (w), 472 (w), 445 (w), 421 (w). LRMS-ESI (*m/z*): $[M + H]^+$ calcd for $C_{21}H_{20}F_3N_2O_2S$, 421.1; found, 421.0. UV-vis (THF, 298 K) λ_{max}, nm (ε, M^{-1} cm^{-1}): 385 (29,000).

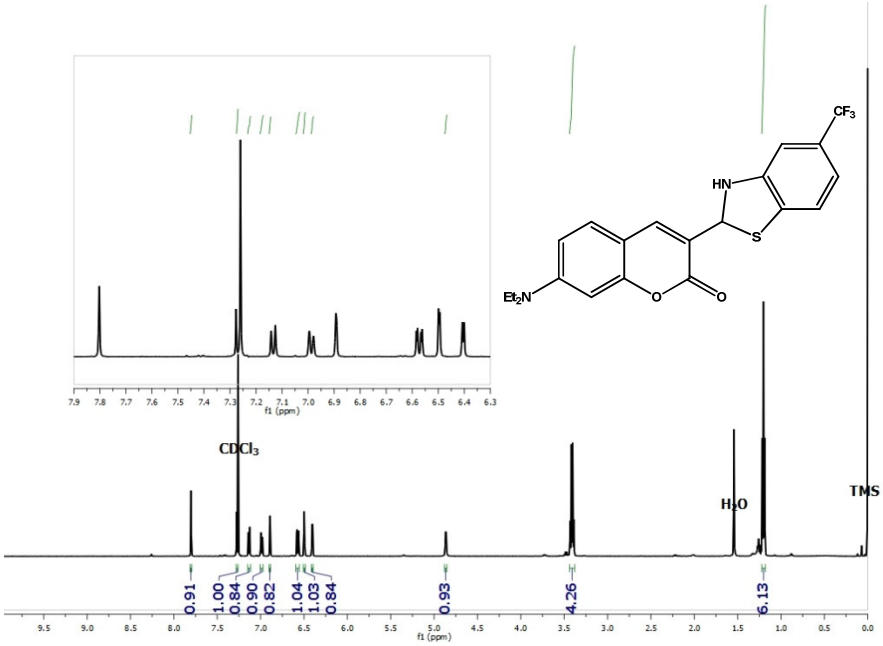

Figure 70. ^{1}H NMR spectrum of **AF1** in $CDCl_3$ at 298 K.

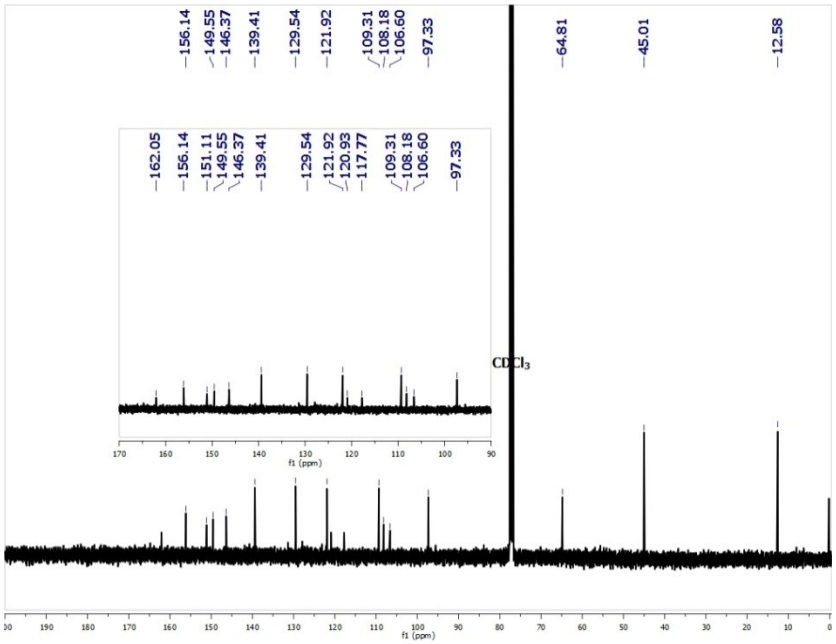

Figure 71. ^{13}C NMR spectrum of **AF1** in $CDCl_3$ at 298 K.

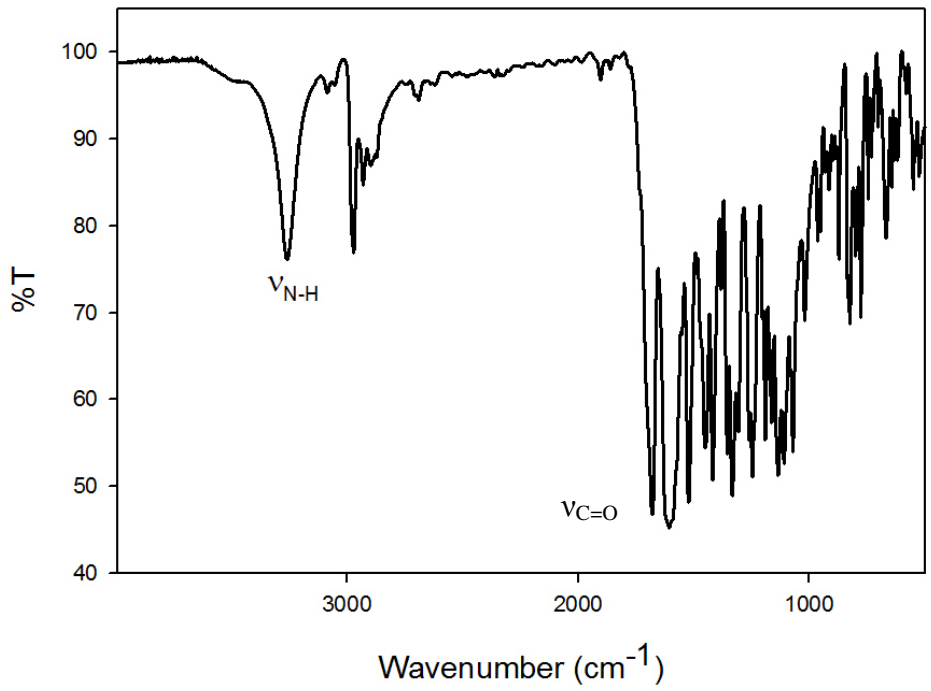

Figure 72. Solid-state FTIR-spectrum (ATR-diamond) of **AF1**.

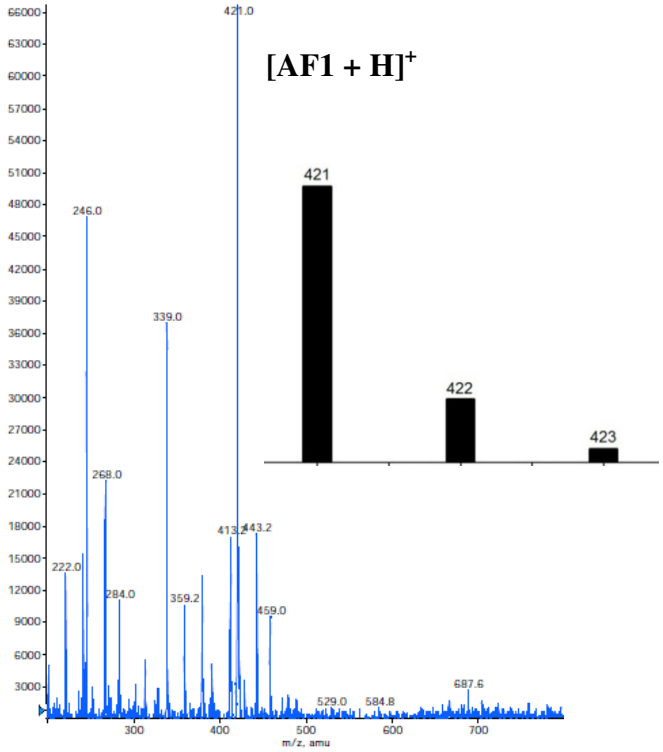

Figure 73. Positive mode LRMS-ESI-MS of **AF1** showing parent peak at *m/z* = 421.0. Inset: calculated molecular weight and isotopic distribution of **AF1**.

Synthesis of 7-(diethylamino)-3-(5-(trifluoromethyl)benzo[*d*]thiazol-2-yl)-2*H*-chromen-2-one (C6-CF_3). *Reaction A: using spectroscopic conditions*: To a 0.67 mM THF solution of AF1 containing 3.35 mM Et_3N was added a 6.5 mM THF solution of AsI_3 (excess As^{3+} to drive the oxidation reaction). The yellow-green solution was stirred for 30 min and the solvent was removed affording an orange-colored solid. The solid was then dissolved in CH_2Cl_2 and filtered through a bed of silica producing a bright green solution, which was concentrated to afford a brown solid. ^{1}H NMR (500 MHz, $CDCl_3$, δ from TMS): 1.33 (m, overlapping peaks), 3.49 (q, 4H), 6.58 (s, 1H), 6.70 (d, 1H), 7.51 (d, 1H), 7.59 (d, 1H), 8.04 (d, 1H), 8.27 (s, 1H), 8.93 (s, 1H). ^{13}C NMR (100.6 MHz, $CDCl_3$, δ from TMS): 11.48 (N-CH_2-*C*H_3), 44.15 (N-*C*H_2-CH_3), 96.08, 107.70, 109.15, 110.89, 118.28, 119.61, 121.18, 130.05, 138.66, 141.68, 151.23, 151.48, 156.31, 160.03 (*C*=N), 162.98 (*C*=O). FTIR (KBr pellet), ν_{max} (cm^{-1}): 2963 (m), 2926 (w), 1698 (m, C=O), 1620 (m, C=N), 1583 (m), 1519 (m), 1447 (w), 1417 (m), 1359 (w), 1332 (m), 1262 (s), 1008 (s), 950 (w), 863 (s), 789 (s), 704 (m), 662 (w), 500 (w). LRMS-ESI (*m/z*): $[M + H]^+$ calcd for $C_{21}H_{18}F_3N_2O_2S$, 419.1; found, 419.2. *Reaction B*: A solid mixture of 7-diethylaminocoumarin-3-aldehyde (0.0724 g, 0.2952 mmol), 4-(trifluoromethyl)-2-aminothiophenol hydrochloride (0.0679 g, 0.2952 mmol) and Et_3N (0.0851 g, 0.8409 mmol) was dissolved in 10 mL of EtOH to afford a light green solution. An orange colored precipitate formed in ~ 1 h after mixing and the reaction was left to stir exposed to air for 48 h. The solvent was then removed via rotovap and the ^{1}H NMR of the bulk orange residue revealed a mixture of AF1, C6-CF_3 (product of interest), and 7-diethylaminocoumarin-3-aldehyde. The desired C6-CF_3 compound was obtained from this mixture by recrystallization from hot EtOH to afford an orange solid (0.0303 g, 25%). m.p.: 242-243 °C. ^{1}H NMR (500 MHz, $CDCl_3$, δ from TMS): 1.27 (t, 6H, C*H*$_3$CH$_2$N-), 3.49 (q, 4H, CH$_3$C*H*$_2$N-), 6.58 (s, 1H), 6.69 (d, 1H), 7.51 (d, 1H), 7.59 (d,

1H), 8.04 (d, 1H), 8.27 (s, 1H), 8.93 (s, 1H). ^{13}C NMR (100.6 MHz, $CDCl_3$, δ from TMS): 12.64 (N-CH_2-CH_3), 45.31(N-CH_2-CH_3), 97.20, 108.83, 110.31, 111.98, 119.42 (q, J = 4.4 Hz), 120.76 (q, J = 3.0 Hz), 122.34, 127.29 (q, J = 273.8 Hz, CF_3), 128.82 (q, J = 32.4 Hz), 131.21, 139.79, 142.83, 152.37, 152.62, 157.45, 161.19 (*C*=N), 164.13 (*C*=O) unless noted ^{13}C peaks are singlets, splitting is due to coupling of the ^{13}C and ^{19}F nuclei. FTIR (KBr pellet), ν_{max} (cm^{-1}): 3083 (w), 2977 (w), 2931 (w), 2896 (w), 2872 (w), 1705 (s, C=O), 1697 (s, C=O), 1620 (vs, C=N), 1584 (vs), 1515 (vs), 1478 (w), 1419 (m), 1378 (w), 1352 (m), 1328 (vs), 1292 (w), 1277 (w), 1264 (w), 1228 (m), 1196 (s), 1150 (w), 1132 (s), 1112 (m), 1094 (w), 1070 (w), 1050 (w), 1015 (w), 977 (w), 950 (m), 884 (w), 821 (m), 811 (w), 799 (w), 770 (m), 708 (w), 679 (w), 669 (w), 636 (w), 530 (w), 512 (w), 472 (w), 442 (w). UV-vis (THF, 298 K) λ_{max}, nm (ε, M^{-1} cm^{-1}): 464 (52,900); UV-vis (THF/CHES (1:1, pH 9), 298 K) λ_{max}, nm (ε, M^{-1} cm^{-1}): 473 (52,000). LRMS-ESI (*m/z*): $[M + H]^+$ calcd for $C_{21}H_{18}F_3N_2O_2S$, 419.1; found, 419.2.

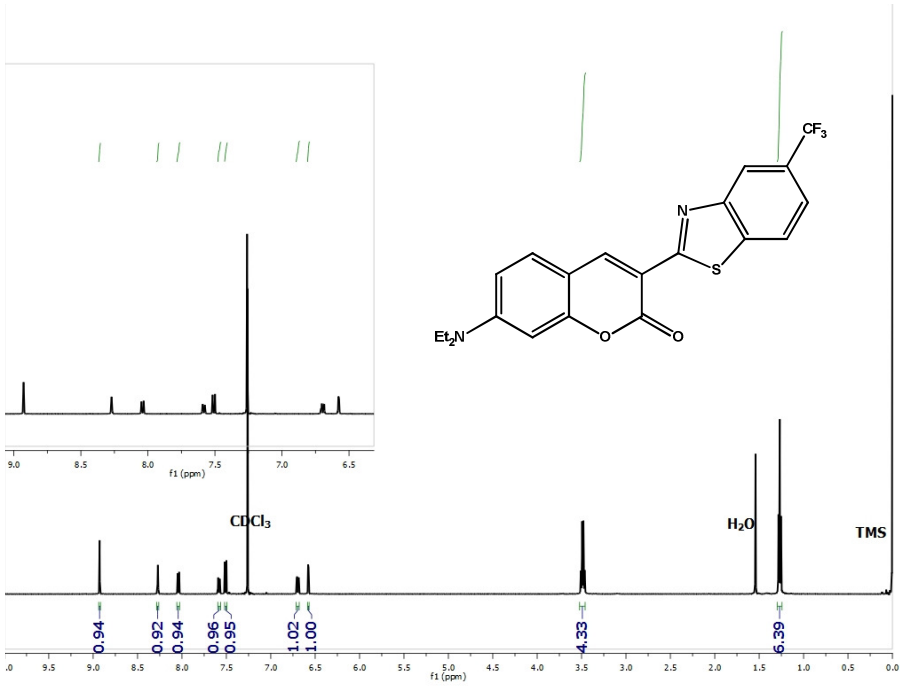

Figure 74. ^{1}H NMR spectrum of **C6-CF_3** in $CDCl_3$ at 298 K.

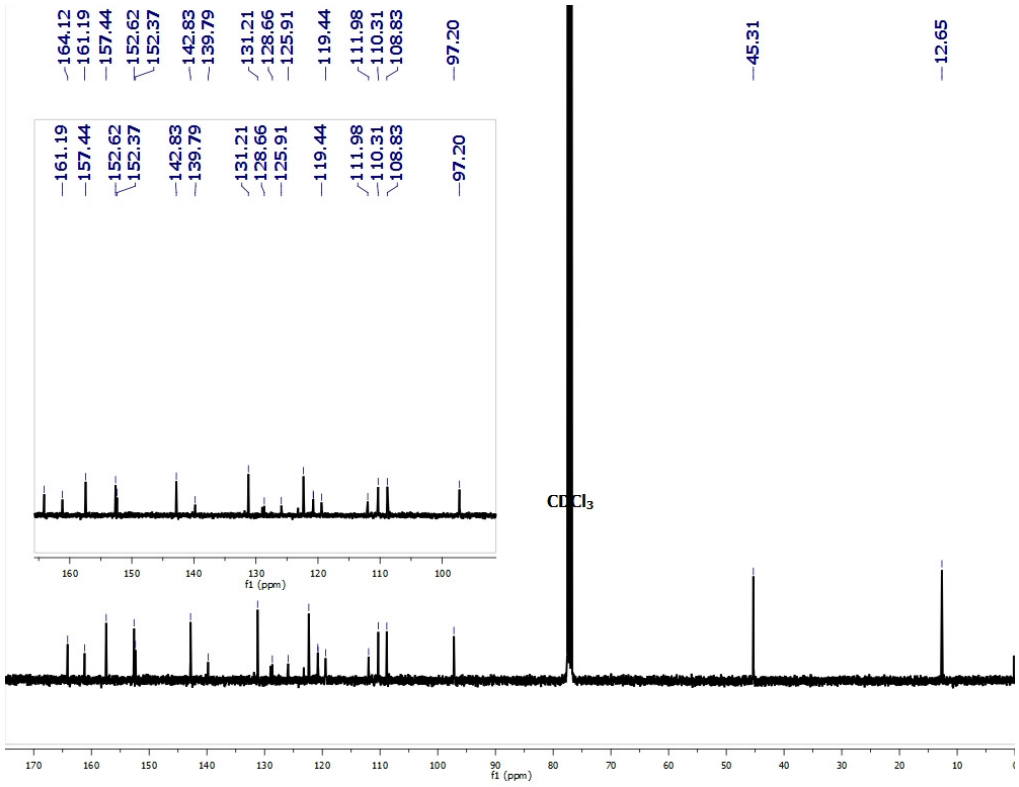

Figure 75. ^{13}C NMR spectrum of **C6-CF$_3$** in $CDCl_3$ at 298 K.

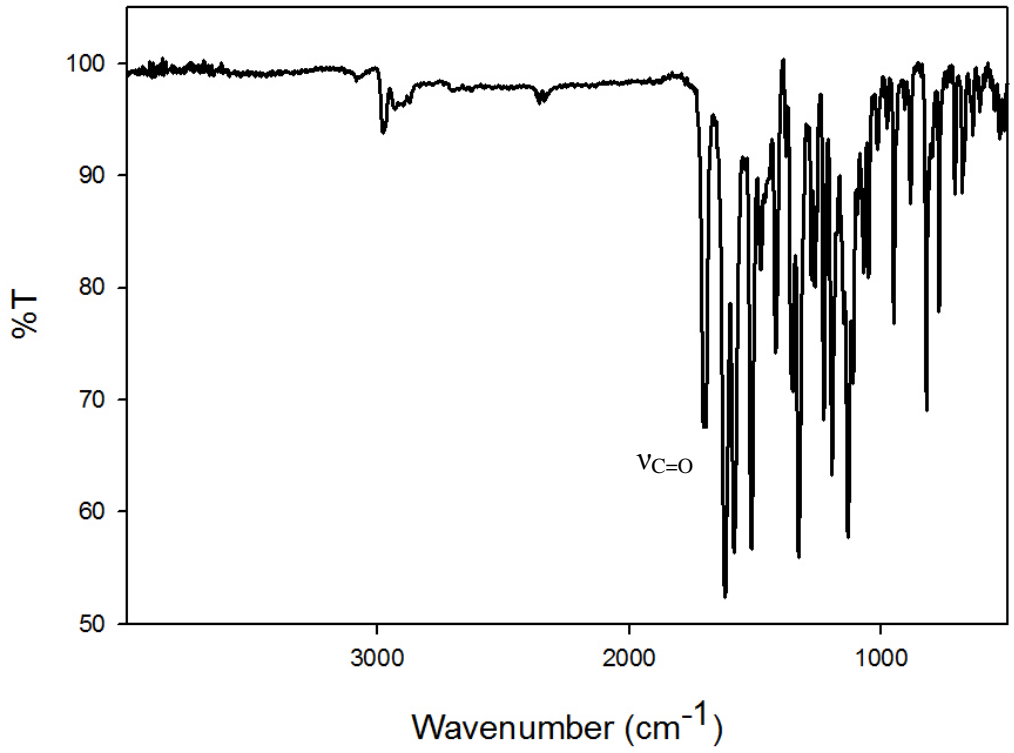

Figure 76. Solid-state FTIR-spectrum (ATR-diamond) of **C6-CF$_3$**.

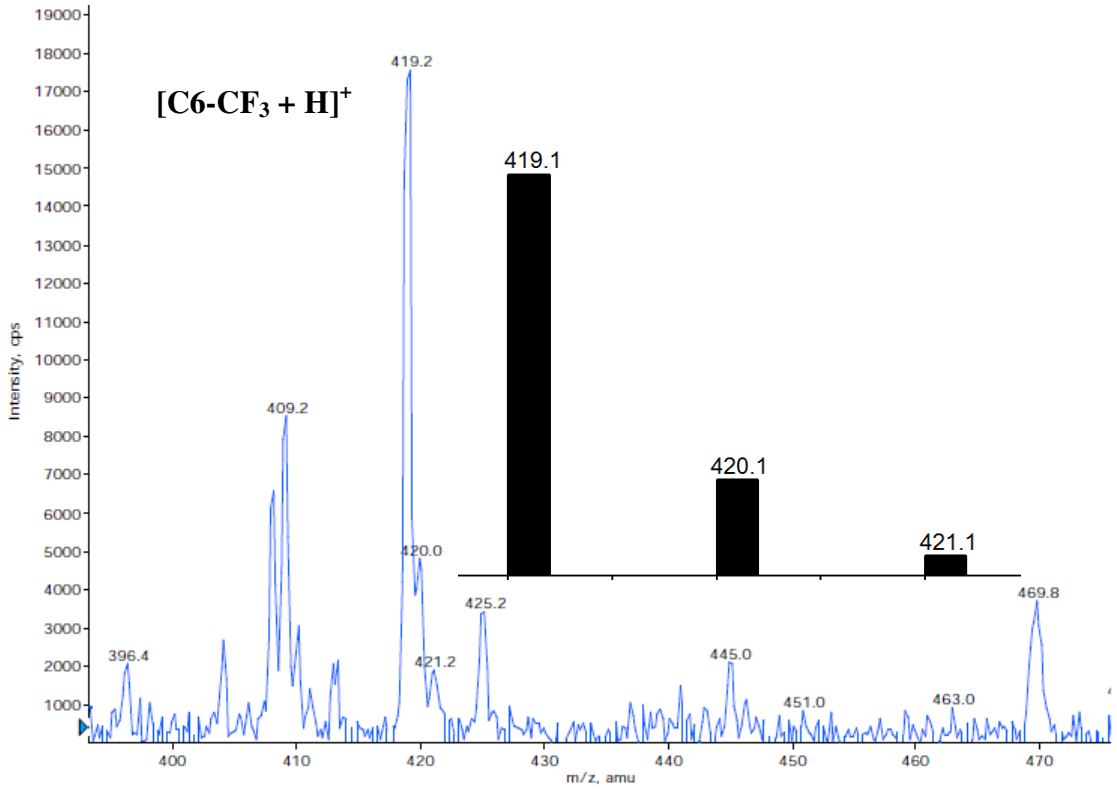

Figure 77. Positive mode LRMS-ESI-MS of **C6-CF$_3$** showing parent peak at *m/z* = 419.2. Inset: calculated molecular weight and isotopic distribution of **C6-CF$_3$**.

3,3'-((1*E*,1'*E*)-((disulfanediylbis(3-(trifluoromethyl)-6,1-phenylene))bis(azanylylidene)) bis(methanylylidene))bis(7-(diethylamino)-2*H*-chromen-2-one) (SB1). A solid batch of 7-diethylaminocoumarin-3-aldehyde (0.3924 g, 1.600 mmol) and 6,6′-disulfanediylbis(3-trifluoromethyl)aniline (0.3072 g, 0.7993 mmol) was dissolved in a mixture of propionitrile (6 mL), EtOH (3 mL), $CHCl_3$ (3 mL) and CH_2Cl_2 (5 mL) to give an orange colored slurry. The mixture was then refluxed for 7 h and stirred at RT for 12 h in the presence of 3 Å molecular sieves resulting in a bright orange colored mixture. A 20 mL portion of CH_2Cl_2 was added to the flask and the reaction was filtered to remove mol-sieves. The filtrate was then concentrated via rotovap to afford an orange solid, which was washed with 20 mL of Et_2O to remove unreacted aldehyde and dried to afford 0.1520 g (0.1812 mmol, 23%) of orange solid product. m.p.: 202-

204 °C. ^{1}H NMR (400 MHz, $CDCl_3$, δ from TMS): 1.25 (t, 12H, C*H*$_3$CH$_2$N-), 3.48 (q, 8H, CH$_3$C*H*$_2$N-), 6.53 (s, 2H), 6.65 (d, 2H), 7.37 (m, 4H), 7.48 (d, 2H), 7.64 (d, 2H), 8.64 (s, 2H), 8.81 (s, 2H). ^{13}C NMR (100.6 MHz, $CDCl_3$, δ from TMS): 12.67 (N-CH$_2$-*C*H$_3$), 45.32 (N-*C*H$_2$-CH$_3$), 97.45, 109.10, 110.11, 114.46 (q, 4.0 Hz), 114.63, 123.38 (q, 3.6 Hz), 124.09 (q, 272.0 Hz), 125.64, 129.68 (q, 33.2 Hz), 131.66, 136.39, 142.71, 149.09, 152.73, 156.15, 158.22 (*C*=N), 162.32 (*C*=O); unless noted ^{13}C peaks are singlets, splitting is due to coupling of the ^{13}C and ^{19}F nuclei. FTIR (KBr pellet), ν_{max} (cm^{-1}): 3082 (w), 2976 (m), 2930 (w), 2903 (w), 2871 (w), 1706 (s, C=O), 1621 (vs, C=N), 1582 (vs), 1519 (vs), 1484 (m), 1420 (m), 1378 (w), 1359 (s), 1331 (vs), 1276 (m), 1257 (m), 1229 (m), 1188 (s), 1111 (vs), 1072 (m), 1051 (m), 950 (w), 938 (w), 886 (w), 821 (m), 810 (m), 769 (w), 705 (w), 667 (w), 638 (w), 472 (w). LRMS-ESI (*m/z*): [M + H]$^+$ calcd for $C_{42}H_{37}F_6N_4O_4S_2$, 839.2; found, 839.2. UV-vis (THF, 298 K) λ_{max}, nm (ε, M^{-1} cm^{-1}): 469 (85,000); UV-vis (THF/CHES (1:1, pH 9), 298 K) λ_{max}, nm (ε, M^{-1} cm^{-1}): 482 (68,000).

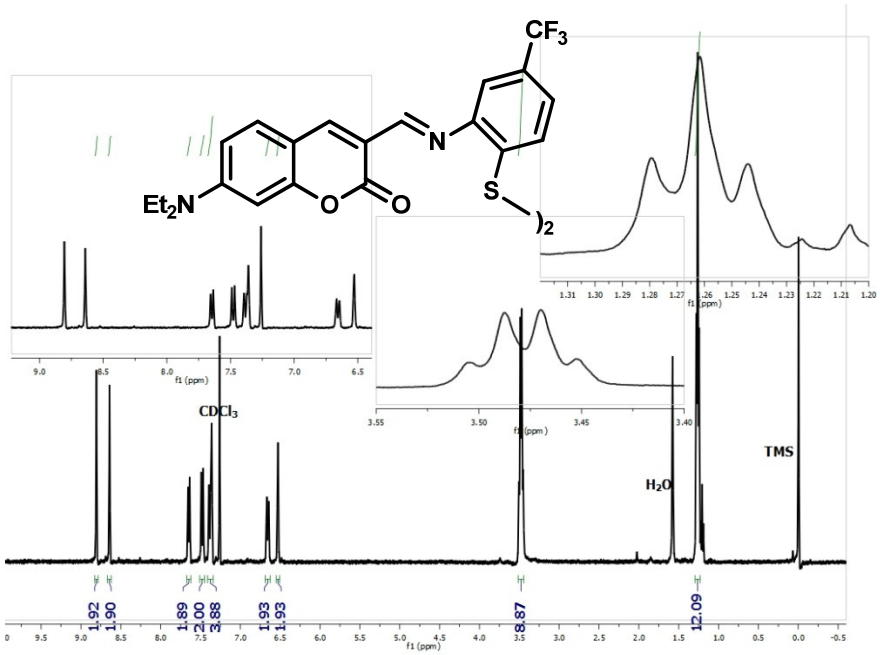

Figure 78. ^{1}H NMR spectrum of **SB1** in $CDCl_3$ at 298 K.

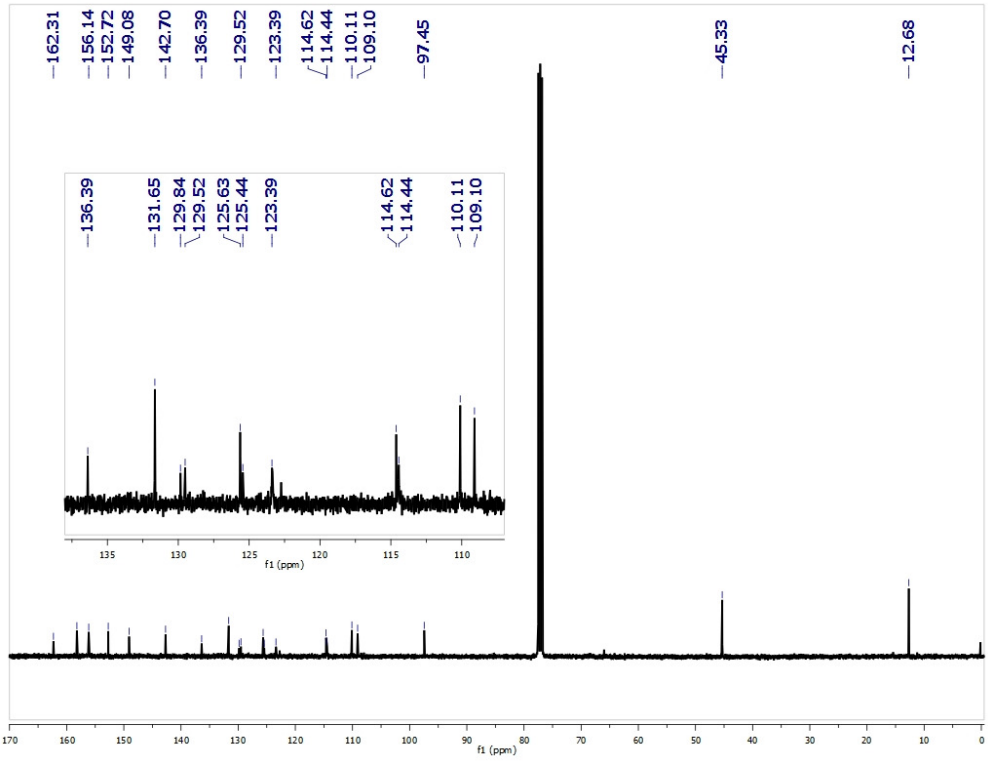

Figure 79. ^{13}C NMR spectrum of **SB1** in $CDCl_3$ at 298 K.

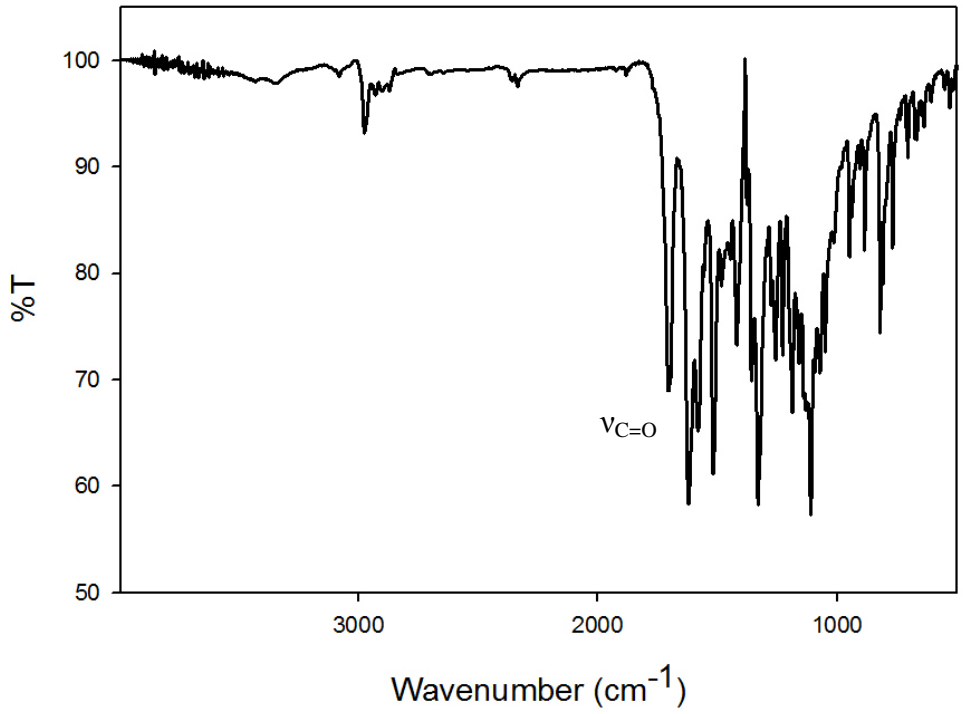

Figure 80. Solid-state FTIR-spectrum (ATR-diamond) of **SB1.**

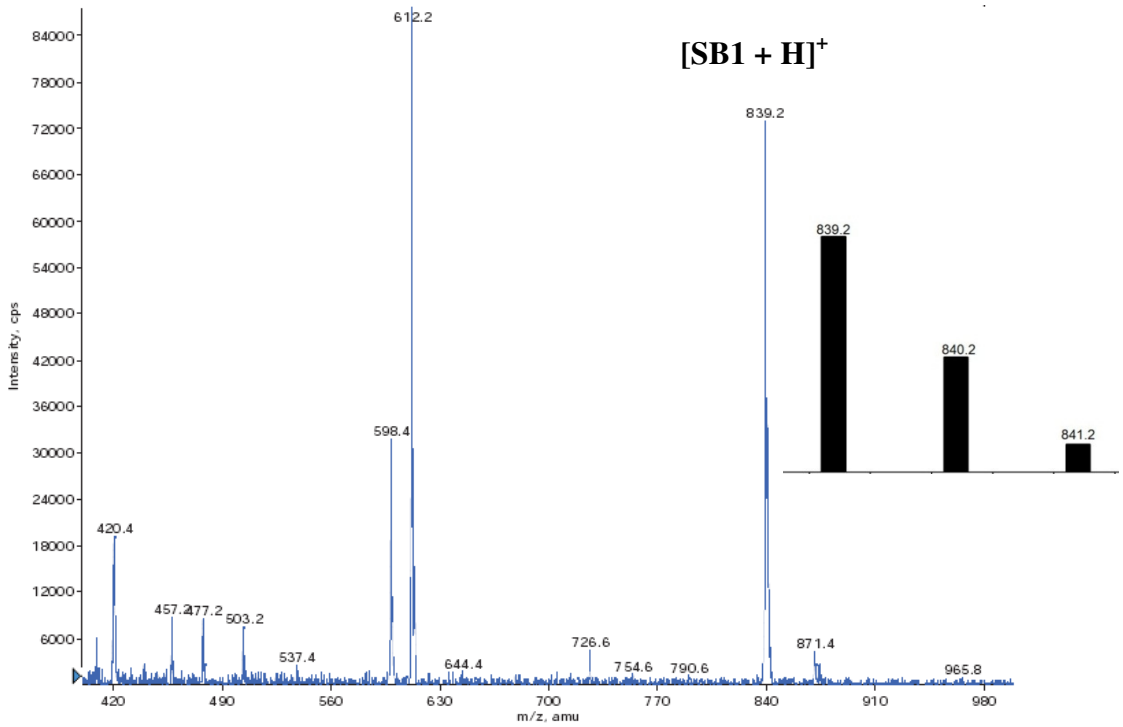

Figure 81. Positive mode LRMS-ESI-MS of **SB1** showing parent peak at *m/z* = 839.2. Inset: calculated molecular weight and isotopic distribution of **SB1**.

3,3'-(1*E*,1'*E*)-(2,2'-disulfanediylbis(2,1-phenylene)bis(azan-1-yl-1-ylidene))bis(methan-1-yl-1-ylidene)bis(7-(diethylamino)2*H*-chromen-2-one) (SB2). A solid batch of 2-aminothiophenol disulfide (0.0274 g, 0.110 mmol) and 7-diethylaminocoumarin-3-aldehyde (0.0569 g, 0.232 mmol) were dissolved in 12 mL of MeOH/CH_2Cl_2 (1:1) to afford a yellow colored solution. The reaction was then taken to reflux for 16 h resulting in no visible color change. Upon cooling to RT, the solvent was removed via rotovap to afford an orange residue, which was then washed with 10 mL of Et_2O and dried to afford a yellow solid product (0.0145 g, 0.0206 mmol, 19%). m.p.: 210 °C dec. ^{1}H NMR (400 MHz, $CDCl_3$, δ from TMS): 1.25 (t, 7H, C*H*$_3$CH$_2$N-, integrates slightly high due to overlap with trace Et_2O from workup), 3.48 (q, 5H, CH$_3$C*H*$_2$N-, integrates slightly high due to overlap with trace Et_2O from workup), 6.52 (s, 1H), 6.64 (d, 1H), 7.16 (m, 3H), 7.47 (d, 1H), 7.61 (d, 1H), 8.64 (s, 1H), 8.77 (s, 1H). ^{13}C NMR (100.6 MHz, $CDCl_3$, δ from

TMS): 12.67 (N-CH_2-CH_3), 45.23 (N-CH_2-CH_3), 97.38, 109.16, 109.90, 115.29, 117.57, 125.88, 127.12, 131.42, 132.43, 142.11, 148.96, 152.30, 154.40, 157.94 (*C*=N), 162.47 (*C*=O). FTIR (KBr pellet), ν_{max} (cm^{-1}): 3052 (w), 2970 (w), 2925 (w), 2868 (w), 1717 (s, C=O), 1618 (vs, C=N), 1583 (vs), 1560 (s), 1514 (vs), 1455 (m), 1418 (m), 1379 (m), 1354 (m), 1300 (w), 1258 (s), 1188 (s), 1169 (m), 1133 (s), 1076 (m), 912 (w), 820 (w), 795 (w), 741 (w), 685 (w), 654 (w), 601 (w), 468 (w). LRMS-ESI (*m/z*): $[M + H]^+$ calcd for $C_{40}H_{39}N_4O_4S_2$, 703.2; found, 703.2. UV-vis (THF, 298 K) λ_{max}, nm (ε, M^{-1} cm^{-1}): 460 (65,000).

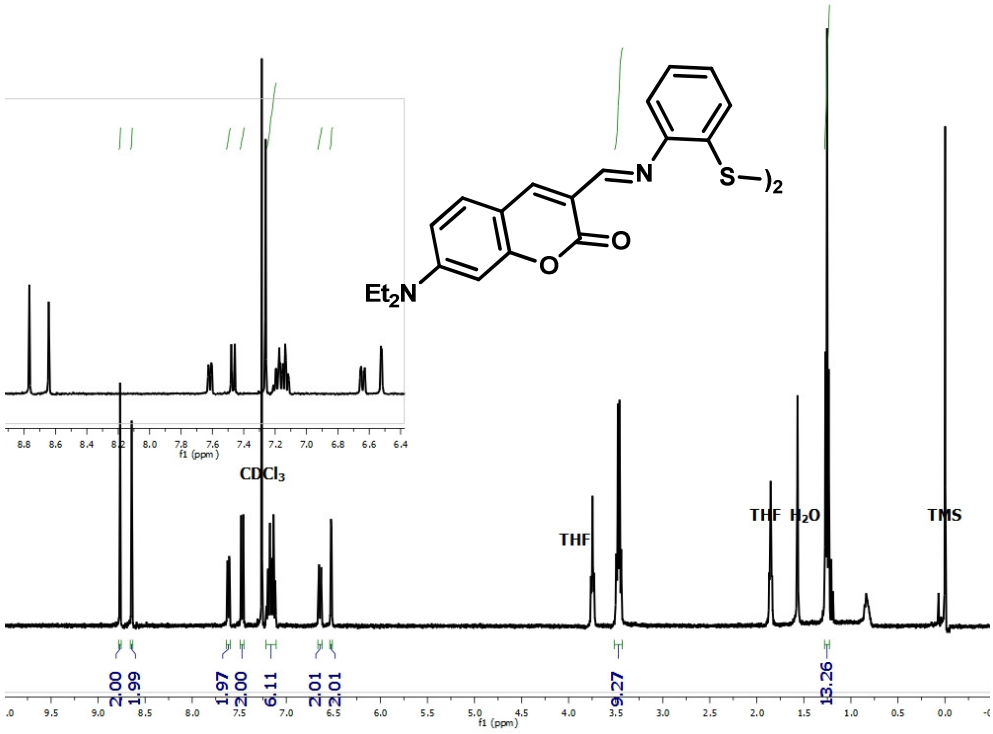

Figure 82. ^1H NMR spectrum of **SB2** in $CDCl_3$ at 298 K.

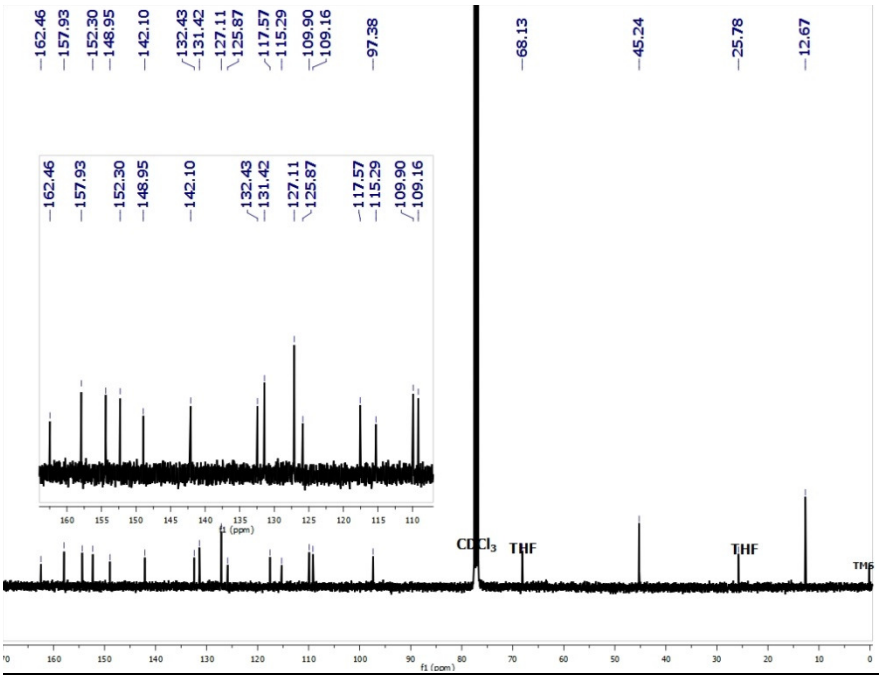

Figure 83. ^{13}C NMR spectrum of **SB2** in $CDCl_3$ at 298 K.

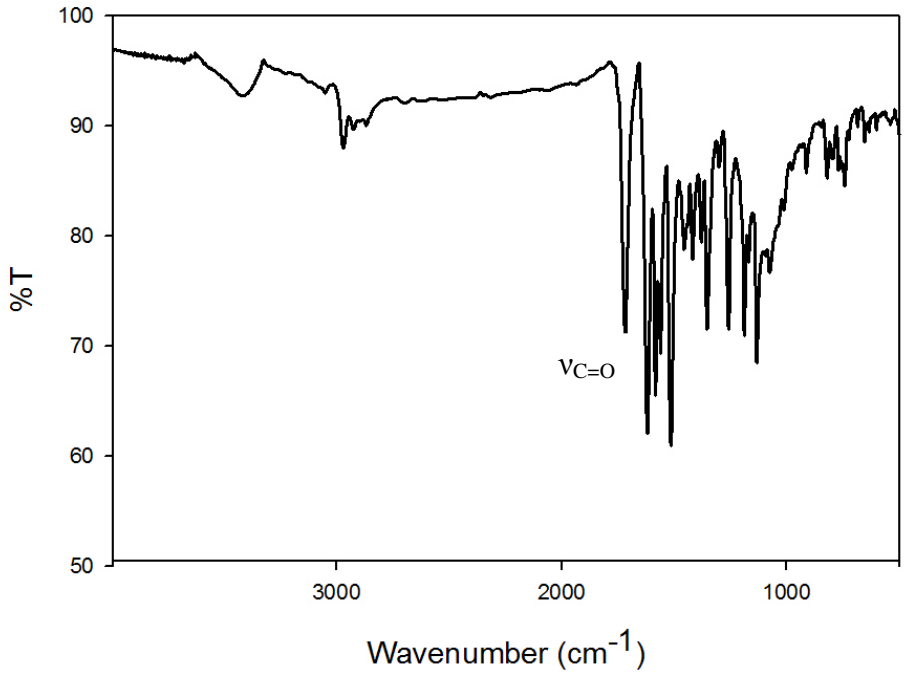

Figure 84. Solid-state FTIR-spectrum (ATR-diamond) of **SB2**.

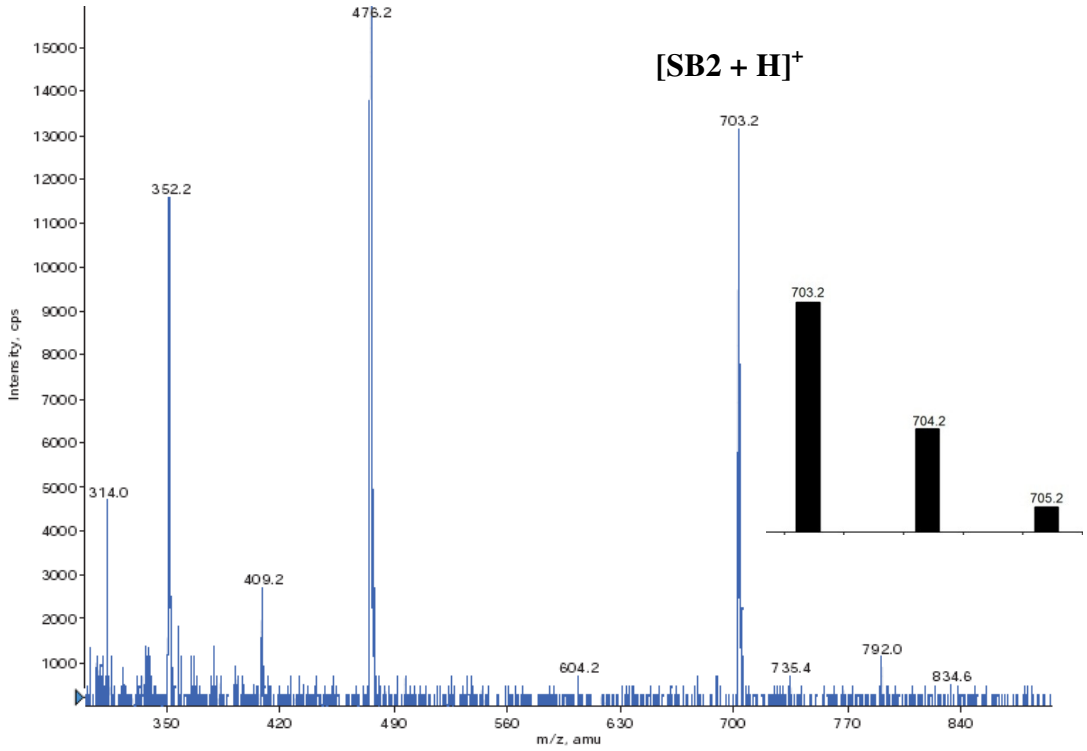

Figure 85. Positive mode LRMS-ESI-MS of **SB2** showing parent peak at *m/z* = 703.2. Inset: calculated molecular weight and isotopic distribution of **SB2**.

Reaction of AF1 and AsI_3. A solid batch of **AF1** (0.0154 g, 0.0367 mmol) was dissolved in 15 mL of THF containing 0.0038 g (0.0376 mmol) of Et_3N resulting in a light green homogeneous solution. To this mixture was then added a 15 mL THF solution of AsI_3 (0.0082 g, 0.0180 mmol) and the color changed instantaneously to red-orange with the formation of a pale precipitate (Et_3N•HI). After stirring at RT in the glovebox for 2 h, the off-white precipitate was filtered off to afford a red filtrate. The filtrate was then concentrated to afford a red solid and the ^1H NMR was taken, which revealed an equal mixture of C6-CF_3 and SB1 (there are peaks present in the aliphatic region that weren't identified). Both compounds are difficult to separate and thus yield of each compound is not reported: 0.0130 g of solid obtained (70% recovery).

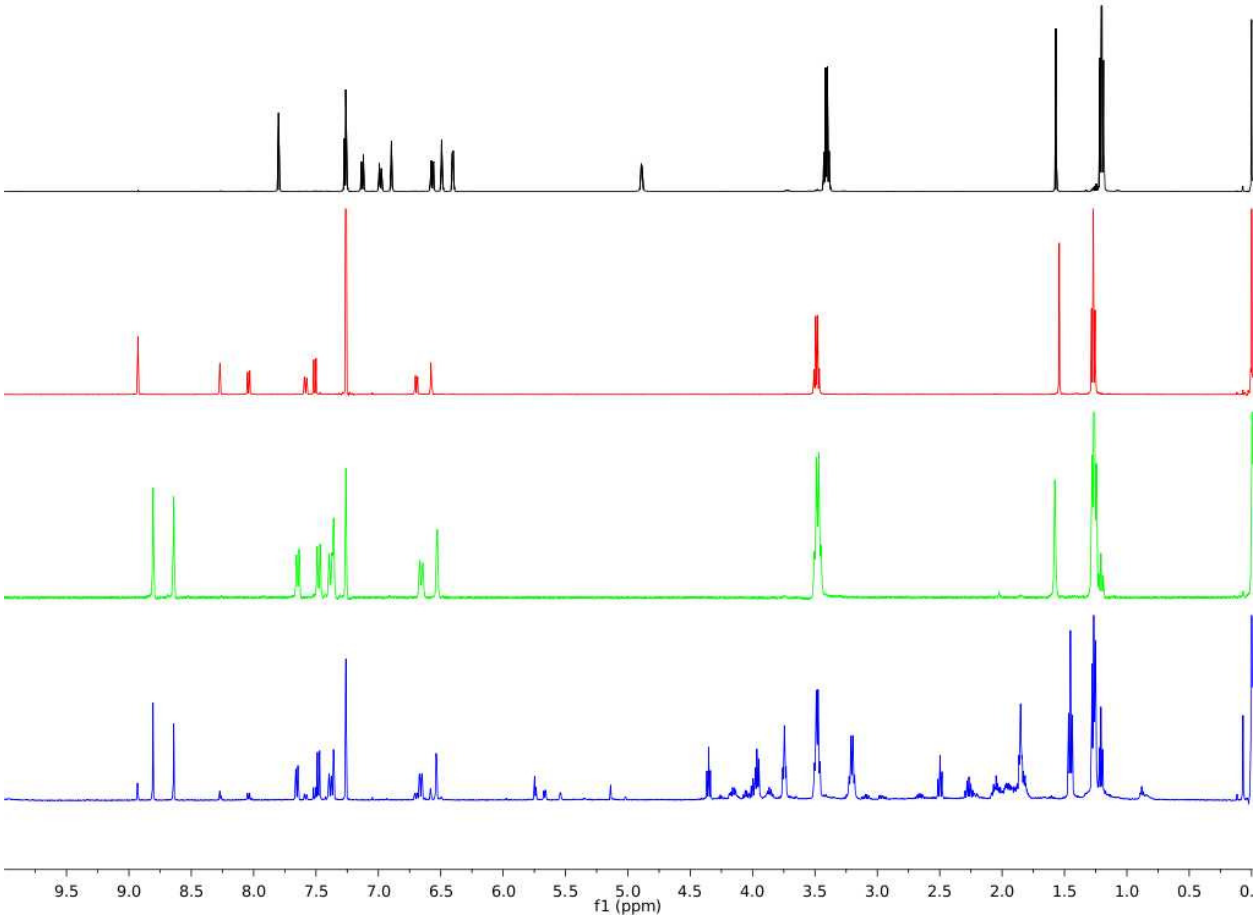

Figure 86. ^{1}H NMR spectra (full scale) of the reaction of **AF1** and AsI_3 (blue), **AF1** (black), C6-CF_3 (red) and SB1 (green trace) in $CDCl_3$. Peaks from THF (1.85, 3.76 ppm), Et_3N (1.03, 2.53 ppm), and Et_3N•HI (1.49, 3.18 ppm) are also present from workup. Peaks at 7.26 and 1.50 ppm are from residual $CHCl_3$ and H_2O in the NMR solvent.[220]

Reaction of AF2 and AsI_3. A solid batch of AF2 (0.0943 g, 0.2676 mmol) was dissolved in 6 mL of THF containing 0.0271 g (0.2678 mmol) of Et_3N resulting in a light green homogeneous solution. To this mixture was then added a 6 mL THF solution of AsI_3 (0.0615 g, 0.1350 mmol) and the color changed instantaneously to red-orange with the formation of a pale precipitate (Et_3N•HI). After stirring at RT in the glovebox for 2 h, the off-white precipitate was filtered off affording a red filtrate. This filtrate was concentrated to yield a red solid (0.1950 g, slightly

greater than 100% recovery presumably due to workup conditions) and the ^{1}H NMR was taken, which revealed a mixture of **AF2**, C6 and the Schiff-base disulfide SB2.

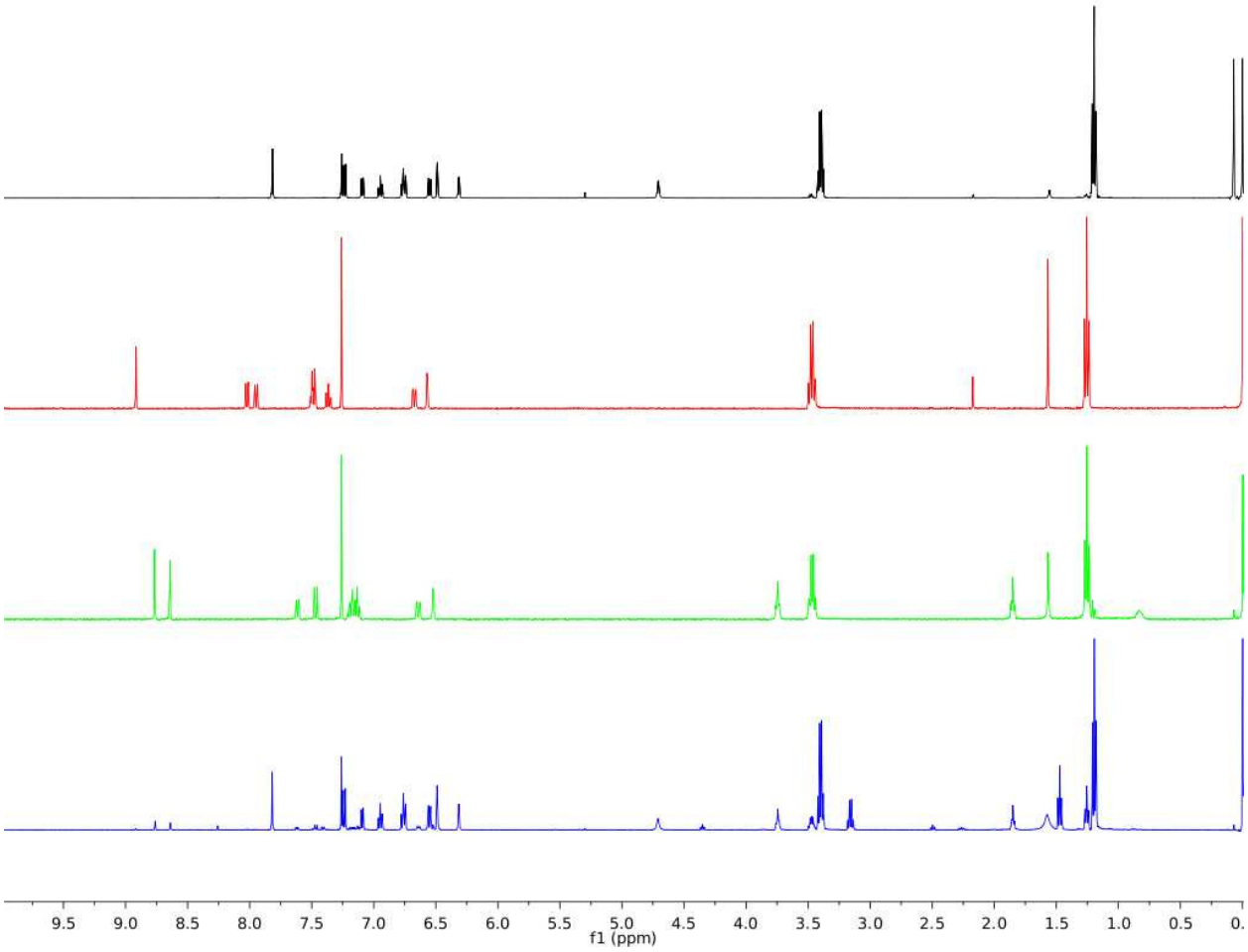

Figure 87. ^{1}H NMR spectra (full scale) of the reaction of **AF2** and AsI_3 (blue), **AF2** (black), C6 (red) and SB2 (green trace) in $CDCl_3$. Peaks from THF (1.85, 3.76 ppm), Et_3N (1.03, 2.53 ppm), and Et_3N•HI (1.49, 3.18 ppm) are also present from workup. Peaks at 7.26 and 1.50 ppm are from residual $CHCl_3$ and H_2O in the NMR solvent.

Reaction of AF2, AsI_3 and diphenylphosphinoethane (dppe). A solid batch of **AF2** (0.0279 g, 0.0792 mmol) was dissolved in 3 mL of THF containing Et_3N (0.0400 g, 0.3953 mmol) to afford a light green solution. To this solution was then added a 3 mL THF solution of AsI_3 (0.0360 g, 0.0790 mmol) that instantaneously generated a dark red heterogeneous mixture. After 30 min

stirring at RT, a clear and colorless 3 mL THF solution of dppe (0.0315 g, 0.0791 mmol) was added, which resulted in no visible color change. The reaction was left to stir for 1 h at RT before the solvent was removed *in vacuo* to afford a red oily solid. A 5 mL solution of Et_2O was added to the solid to remove any unreacted dppe and the solution was left to stir for 30 min. This mixture was then filtered to remove the insoluble dark red solid (0.0840 g), and the resulting red filtrate was concentrated to dryness to afford an orange colored solid (0.0485 g). Red solid characterization: LRMS-ESI (*m/z*) (positive mode): 353.0 (AF2 + H^+); 473.0 ($[As(dppe)]^+$); 703.2 (SB2 + H^+); (negative mode) 126.8 (I^-). ^{31}P NMR (202 MHz, CD_2Cl_2, δ from H_3PO_4): major peak, 61.63 (s) ($[As(dppe)]^+$); minor peaks, 51.00 (d) (appear within 30 min of sample preparation when precipitate starts forming in the NMR tube) and 31.91 (t) (assigned as phosphine oxide).[14] Orange solid characterization: 31.44 (t) (phosphine oxide), 27.60 (d) (not assigned), -12.17 (t) (unreacted dppe). NB: The compound formed is stable only for a short time in CD_2Cl_2 at RT, after a few min an unknown insoluble orange-colored decomposition product is formed and a doublet at ~50 ppm in the ^{31}P NMR appears. The appearance of these peaks are also observed in the original preparation of $[As(dppe)]^+$.[14]

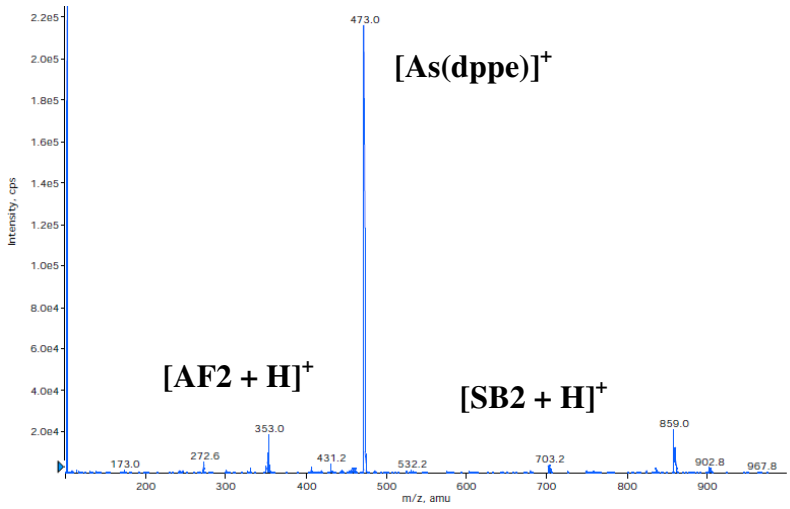

Figure 88. Positive mode LRMS-ESI-MS of the reaction of **AF2** and AsI_3 under sensing conditions after the addition of dppe. Selected peaks are labeled.

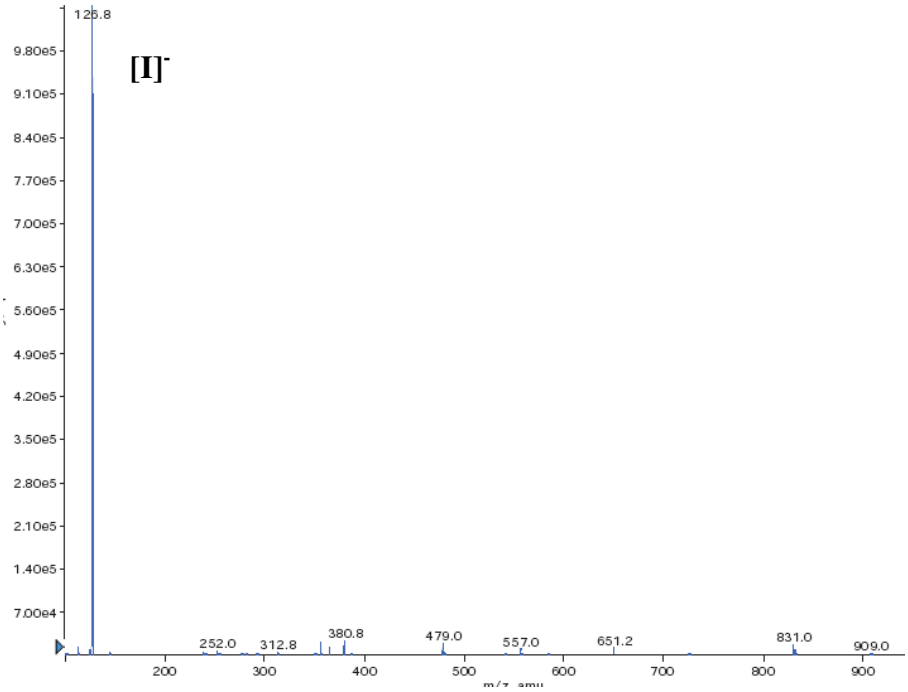

Figure 89. Negative mode LRMS-ESI-MS of the reaction of **AF2** and AsI_3 under sensing conditions after the addition of dppe. Selected peak is labeled.

Spectroscopic Measurements

UV-vis and fluorescence. Absorption and fluorescence samples were prepared in anhydrous THF in an N_2-filled glovebox at ambient temperatures for studies in organic media. Milli-Q grade water (18.2 MΩ·cm) was used to prepare samples for aqueous media studies. Stock solutions of **AF1**, **AF2**, $AsCl_3$, and AsI_3 were prepared fresh in degassed THF on the day of the experiment while stock solutions of $NaAsO_2$ were prepared in degassed Milli-Q water. The blank solution for the aqueous studies consists of THF/CHES (1:1, pH 9). The excitation wavelengths (λ_{ex}) were set at 460 nm (**AF1** in THF at 298 K), 471 nm (AF1 in THF/CHES (1:1) at 298 K), and 443 nm (AF2 in THF at 298 K) unless otherwise stated. The fluorescence readings were recorded 30 min after addition of As^{3+} to allow for complete reaction. All measurements were performed in triplicate, and we report the average.

Competition studies. AsI_3 was used to prepare the As^{3+} stock solutions in THF. THF solutions of Na^+, Ca^{2+}, Mg^{2+}, Mn^{2+}, Fe^{2+}, Ni^{2+}, Cu^{2+}, Zn^{2+}, Pb^{2+}, and Cd^{2+} were prepared from their perchlorate salts, solutions of Fe^{3+} and Hg^{2+} were prepared from their chloride salts, and a solution of Co^{2+} was prepared from $[Co(H_2O)_6](BF_4)_2$. A typical measurement contained 0.45 μM **AF1** or **AF2** containing 5 mol-equiv of base (Et_3N, 2.25 μM), while 10 mol-equiv of ion solution was used. The $[As^{3+}]$ in each competition study was 4.5 μM. As above, fluorescence readings were obtained 30 min after the addition of the ion aliquot.

Quantum yield (Φ_f). Coumarin 1 (Φ_f = 0.70 in EtOH)[239] and Coumarin 153 (Φ_f = 0.38 in EtOH)[240] were used as a standard in the calculation of the quantum yield of **AF1**, **AF2**, their As(III) reaction products, C6-CF_3 and C6 in THF. Solutions of the samples and standards with absorbance values in the range of 0.010 – 0.018 at the excitation maxima of the sample were prepared. The corrected emission spectra were obtained at 298 K with an excitation and emission slit width of 5 nm and integrated value was obtained by measuring the area under the corrected emission spectrum from 395-600 nm. The quantum yield was calculated by the comparative method with the following equation:

$$\mathbf{QY_x = QY_s \bullet [A_x/A_s] \bullet [F_s/F_x] \bullet [n_x/n_s]^2}$$

*where **QY**: Quantum yield; **A**: integrated area under the corrected fluorescence spectrum; **F**: fraction of light absorbed ($1 - 10^{-D}$); **D**: absorbance (optical density); **n** = refractive indices of the solvent (EtOH = 1.3614; THF = 1.4072); **subscript x:** sample; **subscript s:** standard*

Fluorescence readings were obtained 30 min after the addition of the As^{3+} aliquot. All measurements were performed at least in triplicate, and we report the average.

Detection Limit. Detection limits were calculated based on the signal-to-background (S/B) ratio method that describes a S/B $\geq$ 3 as a reliable detection limit.[225-226] The concentration of **AF1** or **AF2** used to determine the detection limit was the same as in the fluorescence measurements (0.45 μM). Various stock solutions (0.79 μM and 0.18 μM) of AsI_3 were prepared by serial dilution. The ratio was obtained by comparing the fluorescence intensity of As^{3+}-containing solutions from 0.061 nM – 17 nM to the fluorescence intensity without As^{3+}.

X-ray Data Collection and Structure Refinement. Orange single crystals of **AF1** were grown by slow diffusion of hexane into a saturated solution of **AF1** in $CDCl_3$ at RT. A suitable crystal was mounted and sealed inside a glass capillary. All geometric and intensity data were measured at 293 K on a Bruker SMART APEX II CCD X-ray diffractometer equipped with graphite-monochromatic Mo Kα radiation (λ = 0.71073 Å) with increasing ω (width 0.5° per frame) at a scan speed of 10 s/frame controlled by the SMART software package.[197] The intensity data were corrected for Lorentz-polarization effects and for absorption[198] and integrated with the SAINT software. Empirical absorption corrections were applied to structures using the SADABS program.[199] The structures were solved by direct methods with refinement by full-matrix least-squares based on F^2 using the SHELXTL-97 software[200] incorporated in the SHELXTL 6.1 software package.[201] The hydrogen atoms were fixed in their calculated positions and refined using a riding model. All non-hydrogen atoms were refined anisotropically. Selected crystal data and metric parameters for **AF1** are summarized in Tables 9 – 10. Perspective views of the molecules were obtained using ORTEP.[202] In **AF1**, the four atoms (C(18), C(19), C(20), C(21)) from the two ethyl groups on atom N(2) and the three fluorine atoms (F(1), F(2), F(3)) on the CF_3 group were found disordered in two sets and labeled accordingly for the two ethyl groups: C(18), C(19), C(20), C(21) for one set and C(18'), C(19'), C(20'), C(21') for the other set. For

the three fluorine atoms: F(1), F(2), F(3) comprise one set and F(1'), F(2'), F(3') are the other set). Each of these two sets is divided using the PART commands and proper restraints. The set of C(18), C(19), C(20), C(21) has 72% occupancy while the other (C(18'), C(19'), C(20'), C(21')) has 28% occupancy. The set of F(1), F(2), F(3) has 49% occupancy while the other (F(1'), F(2'), F(3')) has 51% occupancy.

Table 9. Summary of crystal data and intensity collection and structure refinement parameters for **AF1**.

Parameters	**AF1**
Formula	$C_{21}H_{19}N_2O_2F_3S$
Formula weight	420.44
Crystal system	Monoclinic
Space group	P $2_1/n$
Crystal color, habit	Orange, rectangle
a, Å	9.0134(6)
b, Å	18.0329(12)
c, Å	12.8011(8)
α, deg	90
β, deg	107.774(1)
γ, deg	90
V, Å^3	1981.3(2)
Z	4
ρ_{calcd}, g/cm^{-3}	1.409
T, K	296
abs coeff, μ (Mo Kα), mm^{-1}	0.211
θ limits, deg	2.259 – 22.661
total no. of data	26527
no. of unique data	4726
no. of parameters	331
GOF on F^2	1.027
R_1,[a] %	5.81
wR_2,[b] %	14.64
max, min peaks e/Å^3	0.432, -0.269

[a] $R_1 = \Sigma| |F_o| - |F_c| |/ \Sigma |F_o|$; [b] $wR_2 = \{\Sigma[w(F_o^2 - F_c^2)^2]/ \Sigma[w(F_o^2)^2]\}^{½}$

Table 10. Selected bond distances (Å) and bond angles (deg) for **AF1**.

Bond distances		**Bond angles (contd.)**	
H-bonding:		F(2)-C(1)-F(1)	112.1(10)
N(1)···O(2)#1	3.016(3)		
S(1)-C(5)	1.745(3)	F(2)-C(1)-F(3)	102.8(7)
S(1)-C(8)	1.869(3)	F(1)-C(1)-F(3)	103.8(9)
O(1)-C(11)	1.366(3)	F(2)-C(1)-C(2)	114.9(5)
O(1)-C(17)	1.383(3)	F(1)-C(1)-C(2)	111.2(5)
O(2)-C(11)	1.221(3)	F(3)-C(1)-C(2)	111.2(6)
N(1)-C(6)	1.415(3)	C(3)-C(2)-C(7)	121.4(3)
N(1)-C(8)	1.439(3)	C(3)-C(2)-C(1)	118.8(3)
N(2)-C(15)	1.361(3)	C(7)-C(2)-C(1)	119.8(3)
N(2)-C(18)	1.467(10)	C(2)-C(3)-C(4)	120.5(3)
N(2)-C(20)	1.496(7)	C(3)-C(4)-C(5)	119.1(3)
C(1)-F(1)	1.307(8)	C(4)-C(5)-C(6)	119.6(3)
C(1)-F(2)	1.280(8)	C(4)-C(5)-S(1)	127.8(2)
C(1)-F(3)	1.358(9)	C(6)-C(5)-S(1)	112.6(2)
C(1)-C(2)	1.477(5)	C(7)-C(6)-C(5)	120.5(3)
C(2)-C(3)	1.368(4)	C(7)-C(6)-N(1)	125.0(2)
C(2)-C(7)	1.377(4)	C(5)-C(6)-N(1)	114.4(2)
C(3)-C(4)	1.379(4)	C(6)-C(7)-C(2)	118.9(3)
C(4)-C(5)	1.396(4)	N(1)-C(8)-C(9)	111.5(2)
C(5)-C(6)	1.395(4)	N(1)-C(8)-S(1)	107.09(18)
C(6)-C(7)	1.379(4)	C(9)-C(8)-S(1)	106.82(17)
C(8)-C(9)	1.510(4)	C(10)-C(9)-C(11)	119.6(2)
C(9)-C(10)	1.345(4)	C(10)-C(9)-C(8)	123.9(2)
C(9)-C(11)	1.444(3)	C(11)-C(9)-C(8)	116.4(2)
C(10)-C(12)	1.418(3)	C(9)-C(10)-C(12)	121.5(2)
C(12)-C(17)	1.392(3)	O(2)-C(11)-O(1)	116.0(2)
C(12)-C(13)	1.404(4)	O(2)-C(11)-C(9)	125.7(2)
C(13)-C(14)	1.356(4)	O(1)-C(11)-C(9)	118.3(2)
C(14)-C(15)	1.416(4)	C(17)-C(12)-C(13)	115.9(2)
C(15)-C(16)	1.408(4)	C(17)-C(12)-C(10)	118.5(2)
C(16)-C(17)	1.365(3)	C(13)-C(12)-C(10)	125.6(2)
C(18)-C(19)	1.491(9)	C(14)-C(13)-C(12)	122.1(2)
C(20)-C(21)	1.499(8)	C(13)-C(14)-C(15)	121.4(2)
Bond angles		N(2)-C(15)-C(16)	121.8(3)
H-bonding:		N(2)-C(15)-C(14)	121.2(2)
N(1)-H(1A)...O(2)#1	168(3)		
C(5)-S(1)-C(8)	88.48(13)	C(16)-C(15)-C(14)	117.0(2)
C(11)-O(1)-C(17)	122.02(19)	C(17)-C(16)-C(15)	120.0(2)
C(6)-N(1)-C(8)	110.6(2)	C(16)-C(17)-O(1)	116.5(2)
C(15)-N(2)-C(18)	122.8(8)	C(16)-C(17)-C(12)	123.6(2)
C(15)-N(2)-C(20)	122.0(3)	C(18)-N(2)-C(20)	114.9(8)

CHAPTER 4

CONCLUSIONS AND FUTURE DIRECTIONS

4.1 Conclusions

We have successfully synthesized and studied two small molecule fluorescent sensors for As(III) compounds. A two-pronged approach was utilized in this work; (i) study of the coordination chemistry of As(III) with ligands containing different donor ability and (ii) incorporating the donor preference of As(III) to design the receptor portion of the fluorescent dyes. All the ligands used in this study contained a minimum of one S-based donor group because of the affinity of As(III) for S-based ligands. Ligands with thiolate-S groups were better at forming complexes with As(III) compared to the thioether-S groups. For example, the reaction with a monodentate thiolate ligand, N-acetyl-L-cysteine methyl ester ($SNAc^{OMe}$), resulted in a tri-coordinate As(III) complex based on spectroscopic evidence; while no reaction was observed with the thioether-S based ligands. Furthermore, a ligand containing thiolate-S groups protected in a benzothiazoline functional group also reacted with As(III). A disproportionation reaction was observed with 2-(pyridine-2-yl)-2,3-dihydrobenzo[*d*]thiazoline resulting in the oxidized (benzothiazole) and reduced analogs of the ligand. A four-coordinate complex with the reduced analog exhibits thiolate-S, amide-N, pyridine-N and iodide binding to As(III) in a Ψ-trigonal-bipyramidal geometry. This interesting complex was also robust as evidenced from the stability in aerobic conditions.

Based on the reaction of As(III) with the benzothiazoline functional group, a first generation fluorescent sensor for As(III) was designed by incorporating a coumarin fluorophore.

The fluorescent dyes are described as chemodosimeters because the reaction with As(III) will irreversibly form the benzothiazole analog which is a highly emissive dye. As expected, AFs react with As(III) salts in organic media to afford the C6 analogs (benzothiazole functional group) and result in significant changes in spectroscopic properties. The presence of As(III) resulted in a complete reaction with AFs as seen from the disappearance of the peak in the UV-vis and appearance of new peaks. A remarkable 20 – 25 fold fluorescence intensity increase was also obtained in the presence of As(III). This remarkable change means that the fluorescent dyes can be utilized as a detection method for As(III). Furthermore, AFs are sensitive and selective for As(III), two desirable properties in a fluorescent dye. This can be seen from the low-ppb detection limit and minimal interference from common and toxic ions present in water. Additionally, AFs reacts with a form of As(III) prevalent in the environment, $NaAsO_2$, and results in a dramatic change in absorption properties of the dyes.

The chemodosimeter design utilized in this study is a good proof of principle for obtaining a sensitive fluorescent sensor for As(III) ions. However, some improvements will be needed before such constructs can be used in environmental samples. For example the fluorescence response in aqueous media needs to be improved by possibly utilizing receptor groups that will minimize interference from other analytes in the environment. Also, designing a convenient dye delivery system will make this method amenable to environmental application.

4.2 Future Directions

One challenge encountered in the reported coumarin chemodosimeter fluorescent constructs is the quenched fluorescence intensity in aqueous media. To improve on this design, an iminocoumarin unit is proposed as the fluorescent reporting group in future constructs. The

iminocoumarin dyes contain an imine functional group in the second position of the coumarin ring. This simple exchange of the carbonyl group with an imine group changes the solubility and photophysical properties of the dye. Iminocoumarins were just recently introduced to the field of extrinsic dyes and they have most of the desirable properties of coumarin dyes such as large Stokes shift and excellent photostability. In addition, they absorb and emit at longer wavelength (λ_{em} > 500 nm) compared to coumarins and importantly they exhibit high quantum yield in aqueous media (Φ_f = 0.63 in sodium phosphate buffer, pH 7).[224] A proposed fluorescent construct based iminocoumarin is presented in Scheme 11. The dye is expected to exhibit low fluorescence intensity as observed in the AFs and then form a highly emissive analog upon reaction with arsenite in aqueous media. It will be interesting to see if the presence of the imino group will lead to an As(III) complex.

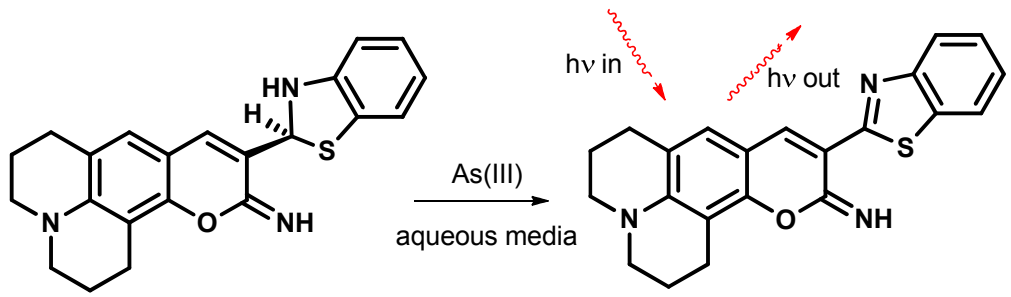

Scheme 11. Iminocoumarin-appended benzothiazoline fluorescent dyes proposed for the detection of As(III) in aqueous media.

The benzothiazoline functional group in AFs reacts slowly with arsenite (> 5 h) which is not desirable for field application. The receptor portion of the dye can be changed to improve the rate of reaction of the dyes with arsenite and water solubility of the dye. Inspired by the high affinity of arsenite for dihydrolipoic acid (log $\beta_{2:3}$ = 18.6),[89] a dithiolate receptor can be incorporated unto the iminocoumarin fluorophore (Chart 14). Binding with arsenite is expected

to affect the fluorescence properties that will aid the direct detection of arsenite in environmental samples.

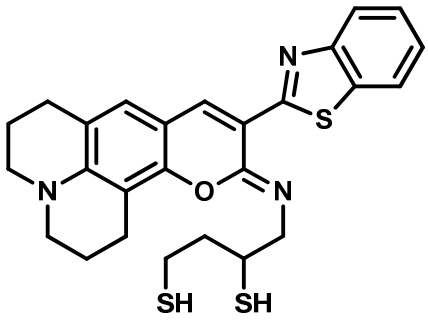

Chart 14. Iminocoumarin functionalized with a dithiol receptor group proposed for the detection of arsenite in aqueous media.

A convenient way to utilize these dyes in environmental applications is to immobilize them on paper strips in a similar way to the commercial test kits. Such a strategy has been used for Hg(II) fluorescent dyes, where solutions of the dyes were coated on strips of Whatmann 1 filter paper and were used to detect Hg(II) ions directly.[241] Fluorescence-based detection methods are poised to become a method of choice for arsenical compounds because of its sensitivity and ease of use.

REFERENCES

(1) Nriagu, J. O., Arsenic Poisoning Through the Ages. In *Environmental Chemistry of Arsenic*, Frakenberger, W. T. J., Ed. Marcel Dekker: New York, **2002**.

(2) Lechtman, H. *J. Field Archaeol.* **1996,** *23*, 477.

(3) Emsley, J., *Nature's Building Block: an A-Z Guide to the Elements*. Oxford University Press: Oxford, **2001**.

(4) Mellor, J. W., *A Comprehensive Treatise on Inorganic and Theoretical Chemistry*. Longman: London, **1929**; Vol. 9.

(5) Carmalt, C. J.; Norman, N. C., Arsenic, antimony and bismuth: some general properties and aspects of periodicity. In *Chemistry of Arsenic, Antimony and Bismuth*, Norman, N. C., Ed. Blackie Academic & Professional: London, **1998**.

(6) Audi, G.; Bersillon, O.; Blachot, J.; Wapstra, A. H. *Nucl. Phys. A* **2003,** *729*, 3.

(7) Greenwood, N. N.; Earnshaw, A., *Chemistry of the Elements*. 2nd ed.; Elsevier Science: **1997**.

(8) Francesconi, K. A.; Kuehnelt, D., Arsenic Compounds in the Environment. In *Environmental Chemistry of Arsenic*, Frakenberger, W. T. J., Ed. Marcel Dekker: New York, **2002**.

(9) O'Day, P. A. *Elements* **2006,** *2*, 77.

(10) Heslop, R. B.; Jones, K., *Inorganic Chemistry - A Guide to Advanced Study*. Elsevier Scientific: Amsterdam, **1976**.

(11) Hitchcock, P. B.; Lappert, M. F.; Li, G.; Protchenko, A. V. *Chem. Commun.* **2009**, 428.

(12) Reeske, G.; Hoberg, C. R.; Hill, N. J.; Cowley, A. H. *J. Am. Chem. Soc.* **2006,** *128*, 2800.

(13) Reeske, G.; Cowley, A. H. *Chem. Commun.* **2006**, 1784.

(14) Ellis, B. D.; Macdonald, C. L. B. *Inorg. Chem.* **2004,** *43*, 5981.

(15) Burford, N.; Carpenter, Y.-Y.; Eamonn, C.; Saunders, C. D. L., The Chemistry of Arsenic, Antimony and Bismuth. In *Biological Chemistry of Arsenic, Antimony and Bismuth*, Hongzhe, S., Ed. Wiley: Hoboken, NJ, **2010**.

(16) Cotton, F. A.; Wilkinson, G., *Advanced Inorganic Chemistry*. 3rd ed.; Wiley Interscience Publishers: New York, **1972**.

(17) Muñoz-Hernández, M.-Á., Arsenic: Inorganic Chemistry. In *Encyclopedia of Inorganic and Bioinorganic Chemistry*, John Wiley & Sons, Ltd: **2011**.

(18) Clementi, E.; Raimondi, D. L. *J. Chem. Phys.* **1963,** *38*, 2686.

(19) Cordero, B.; Gomez, V.; Platero-Prats, A. E.; Reves, M.; Echeverria, J.; Cremades, E.; Barragan, F.; Alvarez, S. *Dalton Trans.* **2008**, 2832.

(20) Cullen, W. R.; Reimer, K. J. *Chem. Rev.* **1989,** *89*, 713.

(21) Kutzelnigg, W. *Angew. Chem., Int. Ed.* **1984,** *23*, 272.

(22) Bissen, M.; Frimmel, F. H. *Acta Hydrochim. Hydrobiol.* **2003,** *31*, 9.

(23) Andreae, M. O.; Klumpp, D. *Environ. Sci. Technol.* **1979,** *13*, 738.

(24) Aposhian, H. V.; Gurzau, E. S.; Le, X. C.; Gurzau, A.; Healy, S. M.; Lu, X.; Ma, M.; Yip, L.; Zakharyan, R. A.; Maiorino, R. M.; Dart, R. C.; Tircus, M. G.; Gonzalez-Ramirez, D.; Morgan, D. L.; Avram, D.; Aposhian, M. M. *Chem. Res. Toxicol.* **2000,** *13*, 693.

(25) Jolliffe, D. M. *J. Roy. Soc. Med.* **1993,** *86*, 287.

(26) Riethmiller, S. *Chemotherapy* **2005,** *51*, 234.

(27) Thorburn, A. L. *Brit. J. Vener. Dis.* **1983,** *59*, 404.

(28) Zhu, J.; Chen, Z.; Lallemand-Breitenbach, V.; de The, H. *Nat. Rev. Cancer* **2002,** *2*, 705.

(29) Bisser, S.; N'Siesi, F.-X.; Lejon, V.; Preux, P.-M.; Van Nieuwenhove, S.; Miaka Mia Bilenge, C.; Büscher, P. *J. Infect. Dis.* **2007,** *195*, 322.

(30) Peryea, F. J. *Historical Use of Lead Arsenate Insecticides, Resulting Soil Contamination and Implications for Soil Remediation*; 16th World Congress of Soil Science: Montpellier, France, **1998**.

(31) Walsh, P. A.; Keeney, D. R., Behaviour and phytotoxicity of inorganic arsenicals in soils. In *Arsenical Pesticides.*, Woolson, E. A., Ed. American Chemical Society: Washington D.C., **1975**.

(32) Garbarino, J. R.; Bednar, A. J.; Rutherford, D. W.; Beyer, R. S.; Wershaw, R. L. *Environ. Sci. Technol.* **2003,** *37*, 1509.

(33) Rutherford, D. W.; Bednar, A. J.; Garbarino, J. R.; Needham, R.; Staver, K. W.; Wershaw, R. L. *Environ. Sci. Technol.* **2003,** *37*, 1515.

(34) Hileman, B. *Chem. Eng. News* **2007,** *85*, 34.

(35) Bunnett, J. F.; Mikolajczyk, M., *Arsenic and Old Mustard: Chemical Problems in the Destruction of Old Arsenical and Mustard Munitions*. Kluwer: Boston, **1998**.

(36) Stellman, J. M.; Stellman, S. D.; Christian, R.; Weber, T.; Tomasallo, C. *Nature* **2003,** *422*, 681.

(37) Oremland, R. S.; Stolz, J. F. *Science* **2003,** *300*, 939.

(38) Carapella, S.; Kroschwitz, J. I.; Seidel, A., *Arsenic and Arsenic Alloys Kirk-Othmer Encyclopedia of Chemical Technology 5th ed*. **2004**; Vol. 3, p 262.

(39) Fang, S. F.; Adomi, K.; Iyer, S.; Morkoc, H.; Zabel, H.; Choi, C.; Otsuka, N. *J. Appl. Phys.* **1990,** *68*, R31.

(40) Blakemore, J. S. *J. Appl. Phys.* **1982,** *53*, R123.

(41) Hingston, J. A.; Collins, C. D.; Murphy, R. J.; Lester, J. N. *Environ. Pollut.* **2001,** *111*, 53.

(42) United States Environmental Protection Agency. http://www.epa.gov/oppad001/ reregistration/cca/ (accessed May 2013).

(43) Joshi, A. P.; Munshi, K. N. *Microchem. J.* **1973,** *18*, 277.

(44) Dorogi, P. L.; Santarius, U.; Neumann, E. *Anal. Biochem.* **1982,** *124*, 27.

(45) Michaylova, V.; Yoroukova, L. *Anal. Chim. Acta* **1974,** *68*, 73.

(46) Kiriyama, T.; Kuroda, R. *Anal. Chim. Acta* **1974,** *71*, 375.

(47) Kalifa, H.; Issa, Y. M. *Microchem. J.* **1975,** *20*, 287.

(48) Griffin, B. A.; Adams, S. R.; Tsien, R. Y. *Science* **1998,** *281*, 269.

(49) Adams, S. R.; Campbell, R. E.; Gross, L. A.; Martin, B. R.; Walkup, G. K.; Yao, Y.; Llopis, J.; Tsien, R. Y. *J. Am. Chem. Soc.* **2002,** *124*, 6063.

(50) Doerr, A. *Nat. Methods* **2008,** *5*, 6.

(51) Ferguson, J. F.; Gavis, J., *A Review Of The Arsenic Cycle In Natural Waters*. Pergamon Press: Great Britain, **1972**; Vol. 6.

(52) Inskeep, W. P.; McDermott, T. R.; Fendorf, S., Arsenic (V)/(III) Cycling in Soils and Natural Waters: Chemical and Microbiological Processes. In *Enviromental Chemistry of Arsenic*, Frakenberger, W. T. J., Ed. Marcel Dekker: New York, **2002**.

(53) Peterson, M. L.; Carpenter, R. *Mar. Chem.* **1983,** *12*, 295.

(54) Seyler, P.; Martin, J. M. *Environ. Sci. Technol.* **1989,** *23*, 1258.

(55) Stolz, J. F.; Oremland, R. S. *FEMS Microbiol. Rev.* **1999,** *23*, 615.

(56) Smith, E.; Naidu, R.; Alston, A. M., Arsenic in the Soil Environment: A Review. In *Advances in Agronomy*, Donald, L. S., Ed. Academic Press: **1998**; Vol. Volume 64, pp 149-195.

(57) Newman, D.; Ahmann, D.; Morel, F. M. M. *Geomicrobiol. J.* **1998,** *15*, 255.

(58) Smedley, P. L.; Kinniburgh, D. G. *Appl. Geochem.* **2002,** *17*, 517.

(59) Lovley, D. R. *Annu. Rev. Microbiol.* **1993,** *47*, 263.

(60) *Atlas of Eh-pH Diagrams Intercomparison of Thermodynamic Databases*; 419; National Institute of Advanced Industrial Science and Technology Research Center for Deep Geological Environments Naoto TAKENO, **2005**.

(61) O'Day, P. A.; Vlassopoulos, D.; Meng, X.; Benning, L., Advances in Arsenic Research: Introductory Remarks. In *Advances in Arsenic Research Integraton of Experimental and Observational Studies and Implications for Mitigation*, O'Day, P. A.; Vlassopoulos, D.; Meng, X.; Benning, L., Eds. American Chemical Society: Washington, DC, **2005**.

(62) Oremland, R. S.; Hoeft, S. E.; Santini, J. M.; Bano, N.; Hollibaugh, R. A.; Hollibaugh, J. T. *Appl. Environ. Microbiol.* **2002,** *68*, 4795.

(63) Thomas, D. J.; Li, J.; Waters, S. B.; Weiging., X.; Adair, B. M.; Drobna, Z. M.; Devesa, V.; Styblo, M. *Exp. Biol. Med.* **2007,** *232*, 3.

(64) Hall, L. L.; George, S. E.; Kohan, M. J.; Styblo, M.; Thomas, D. J. *Toxicol. Appl. Pharmacol.* **1997,** *147*, 101.

(65) Hanaoka, K.; Tagawa, S.; Kaise, T. *Hydrobiologia* **1992,** *235-236*, 623.

(66) Francesconi, K. A.; Edmonds, J. S., Arsenic and Marine Organisms. In *Advances in Inorganic Chemistry*, Sykes, A. G., Ed. Academic Press: **1996**; Vol. 44, pp 147-189.

(67) Hanaoka, K.; Fujita, T.; Matsuura, M.; Tagawa, S.; Kaise, T. *Comp. Biochem. Phys.* **1987,** *86*, 681.

(68) Edmonds, J. S.; Francesconi, K. A. *Appl. Organomet. Chem.* **1988,** *2*, 297.

(69) Mukhopadhyay, R.; Rosen, B. P.; Phung, L. T.; Silver, S. *FEMS Microbiol. Rev.* **2002,** *26*, 311.

(70) Henke, K. R., Arsenic in Natural Environment. In *Arsenic: Environmental Chemistry, Health Threats and Waste Management*, Henke, K., Ed. Wiley: New Jersey, **2009**.

(71) Nickson, R.; McArthur, J.; Burgess, W.; Ahmed, K. M.; Ravenscroft, P.; Rahman, M. *Nature* **1998,** *395*, 338.

(72) Saha, J. C.; Dikshit, A. K.; Bandyopadhyay, M.; Saha, K. C. *Crit. Rev. Environ. Sci. Technol.* **1999,** *29*, 281.

(73) WHO *Environmental Health Criteria 224*; **2004**.

(74) Sadler, R.; Olszowy, H.; Shaw, G.; Biltoft, R.; Connell, D. *Water Air Soil Poll.* **1994,** *78*, 189.

(75) Williams, M. *Environ. Geol.* **2001,** *40*, 267.

(76) Welch, A. H.; Westjohn, D. B.; Helsel, D. R.; Wanty, R. B. *Ground Water* **2000,** *38*, 589.

(77) Christen, K. *Environ. Sci. Technol. A Pages* **2001,** *35*, 184A.

(78) Bednar, A. J.; Garbarino, J. R.; Ferrer, I.; Rutherford, D. W.; Wershaw, R. L.; Ranville, J. F.; Wildeman, T. R. *Sci. Total Environ.* **2003,** *302*, 237.

(79) Bentley, R.; Chasteen, T. G. *Microbiol. Mol. Biol. Rev.* **2002,** *66*, 250.

(80) Cortinas, I.; Field, J. A.; Kopplin, M.; Garbarino, J. R.; Gandolfi, A. J.; Sierra-Alvarez, R. *Environ. Sci. Technol.* **2006,** *40*, 2951.

(81) Stolz, J. F.; Perera, E.; Kilonzo, B.; Kail, B.; Crable, B.; Fisher, E.; Ranganathan, M.; Wormer, L.; Basu, P. *Environ. Sci.Technol.* **2007,** *41*, 818.

(82) Arai, Y.; Lanzirotti, A.; Sutton, S.; Davis, J. A.; Sparks, D. L. *Environ. Sci. Technol.* **2003,** *37*, 4083.

(83) Le, C. X., Arsenic Speciation in the Environment and Humans. In *Environmental Chemistry of Arsenic*, Frakenberger, W. T. J., Ed. Marcel Dekker: New York, **2002**.

(84) Mandal, B. M.; Suzuki, K. T. *Talanta* **2002,** *58*, 201.

(85) Shih, C.-J.; Lin, C.-F. *Chemosphere* **2003,** *53*, 691.

(86) Johnson, D. L. *Nature* **1972,** *240*, 44.

(87) USGS Arsenic in Groundwater of the United States. http://water.usgs.gov/nawqa /trace/arsenic/ (accessed May 2013).

(88) *National Research Council, Arsenic in Drinking Water: 2001 Update*. The National Academies Press: Washington, DC, **2001**.

(89) Spuches, A. M.; Kruszyna, H. G.; Rich, A. M.; Wilcox, D. E. *Inorg. Chem.* **2005,** *44*, 2964.

(90) Rosen, B. P. *FEBS Lett.* **2002,** *529*, 86.

(91) Liu, Z.; Shen, J.; Carbrey, J. M.; Mukhopadhyay, R.; Agre, P.; Rosen, B. P. *Proc. Natl. Acad. Sci. U.S.A.* **2002,** *99*, 6053.

(92) Rosen, B. P.; Tamas, M. J., Arsenic Transport in Prokaryotes and Eukaryotic Microbes. In *MIPs & Their Role in the Exchange of Metalloids*, Jahn, T. P.; Bienert, G. P., Eds. Landes Bioscience/ Springer Science + Business Media: **2010**.

(93) Bienert, G. P.; Jahn, T. P., Major Intrinsic Proteins and Arsenic Transport in Plants: New Players and Their Potential Role. In *MIPs and Their Role in the Exchange of Metalloids*, Jahn, T. P.; Bienert, G. P., Eds. Landes Bioscience/ Springer Science + Business Media: **2010**.

(94) Mukhopadhyay, R.; Beitz, E., Metalloid Transport by Aquaglyceroporins: Consequences in the Treatment of Human Diseases. In *MIPs and Their Role in the Exchange of Metalloids*, Jahn, T. P.; Bienert, G. P., Eds. Landes Bioscience/ Springer Science + Business Media: **2010**.

(95) Ramírez-Solís, A.; Mukopadhyay, R.; Rosen, B. P.; Stemmler, T. L. *Inorg. Chem.* **2004,** *43*, 2954.

(96) Scott, N.; Hatlelid, K. M.; MacKenzie, N. E.; Carter, D. E. *Chem. Res. Toxicol.* **1993,** *6*, 102.

(97) Szinicz, L.; Forth, W. *Arch. Toxicol.* **1988,** *61*, 444.

(98) Hu, Y.; Su, L.; Snow, E. T. *Mut. Res. / DNA Repair* **1998,** *408*, 203.

(99) Styblo, M.; Serves, S. V.; Cullen, W. R.; Thomas, D. J. *Chem. Res. Toxicol.* **1997,** *10*, 27.

(100) Ramadan, D.; Rancy, P. C.; Nagarkar, R. P.; Schneider, J. P.; Thorpe, C. *Biochemistry* **2009,** *48*, 424.

(101) Kitchin, K. T.; Wallace, K. *J. Inorg. Biochem.* **2008,** *102*, 532.

(102) Lin, S.; Cullen, W. R.; Thomas, D. J. *Chem. Res. Toxicol.* **1999,** *12*, 924.

(103) Ellis, D. R.; Gumaelius, L.; Indriolo, E.; Pickering, I. J.; Banks, J. A.; Salt, D. E. *Plant Physiol.* **2006,** *141*, 1544.

(104) Dhankher, O. P.; Rosen, B. P.; McKinney, E. C.; Meagher, R. B. *Proc. Natl. Acad. Sci. U.S.A.* **2006,** *103*, 5413.

(105) Delnomdedieu, M.; Basti, M. M.; Otvos, J. D.; Thomas, D. J. *Chem-Biol. Interact.* **1994,** *90*, 139.

(106) Delnomdedieu, M.; Basti, M. M.; Otvos, J. D.; Thomas, D. J. *Chem. Res. Toxicol* **1993,** *6*, 598.

(107) Nemeti, B.; Gregus, Z. *Toxicol. Sci.* **2004,** *82*, 419.

(108) Tokar, E. J.; Diwan, B. A.; Waalkes, M. P. *Environ. Health Perspect.* **2010,** *118*, 108.

(109) *International Agency for Research on Cancer. IARC Monographs on the Evaluation of Carcinogenic Risks to Humans: Some Metals and Metallic Compounds*; **2012**.

(110) Kinniburgh, D. G.; Kosmus, W. *Talanta* **2002,** *58*, 165.

(111) Maheshwari, S.; Drake, J. E.; Kori, K.; Light, M. E.; Ratnani, R. *Polyhedron* **2009,** *28*, 689.

(112) Silin', E. Y.; Belyakov, S. V.; Ashaks, Y. V.; Pech, L. Y.; Zaruma, D. E. *Russ. J. Inorg. Chem.* **2012,** *57*, 373.

(113) Burford, N.; Parks, T. M.; Royan, B. W.; Borecka, B.; Cameron, S. T.; Richardson, J. F.; Gabe, E. J.; Hynes, R. *J. Am. Chem. Soc.* **1992,** *114*, 8147.

(114) Burford, N.; Parks, T. M.; Royan, B. W.; Richardson, J. F.; White, P. S. *Can. J. Chem.* **1992,** *70*, 703.

(115) Burford, N.; Macdonald, C. L. B.; Parks, T. M.; Wu, G.; Borecka, B.; Kwiatkowski, W.; Cameron, S. T. *Can. J. Chem.* **1996,** *74*, 2209.

(116) Carmalt, C. J.; Lomeli, V.; McBurnett, B. G.; Cowley, A. H. *Chem. Commun.* **1997**, 2095.

(117) Johnson, J. M.; Voegtlin, C. *J. Biol. Chem.* **1930,** *89*, 27.

(118) Farrer, B. T.; McClure, C. P.; Penner-Hahn, J. E.; Pecoraro, V. L. *Inorg. Chem.* **2000,** *39*, 5422.

(119) Cea-Olivares, R.; Garcıa-Montalvo, V.; Moya-Cabrera, M. M. *Coord. Chem. Rev.* **2005,** *249*, 859.

(120) González-Montiel, S.; Andrade-López, N.; Alvarado-Rodríguez, J. G. *Eur. J. Inorg. Chem.* **2006**, 3762.

(121) Kolozsi, A.; Lakatos, A.; Galbács, G.; Madsen, A. Ø.; Larsen, E.; Gyurcsik, B. *Inorg. Chem.* **2008,** *47*, 3832.

(122) Alonzo, G.; Bertazzi, N.; Consiglio, M. *Inorg. Chim. Acta* **1984,** *85*, L35.

(123) Alonzo, G. *Inorg. Chim. Acta* **1983,** *73*, 141.

(124) Rey, N. A.; Howarth, O. W.; Pereira-Maia, E. C. *J. Inorg. Biochem.* **2004,** *98*, 1151.

(125) Zahler, W. L.; Cleland, W. W. *J. Biol. Chem.* **1968,** *243*, 716.

(126) Ioannou, P. V.; Tsivgoulis, G. M. *Main Group Chem.* **2012,** *11*, 89.

(127) Cruse, W. B. T.; James, M. N. G. *Acta Cryst.* **1972,** *B28*, 1325.

(128) Landrum, G. A.; Hoffmann, R. *Angew. Chem., Int. Ed.* **1998,** *37*, 1887.

(129) Starbuck, J.; C. Norman, N.; Guy Orpen, A. *New J. Chem.* **1999,** *23*, 969.

(130) Carter, T. G.; Healey, E. R.; Pitt, M. A.; Johnson, D. W. *Inorg. Chem.* **2005,** *44*, 9634.

(131) Vickaryous, J. W.; Herges, R.; Johnson, D. W. *Angew. Chem., Int. Ed.* **2004,** *43*, 5831.

(132) Vickaryous, J. W.; Healey, E. R.; Berryman, O. B.; Johnson, D. W. *Inorg. Chem.* **2005,** *44*, 9247.

(133) United States Environmental Protection Agency Publication. EPA816-F-01-004 http://www.epa.gov/safewater/arsenic/compliance.html (accessed May 2013).

(134) Erickson, B. E. *Environ. Sci. Technol. A Pages* **2003,** *37*, 35A.

(135) Goessler, W.; Kuehnelt, D., Analytical Methods for the Determination of Arsenic and Arsenic Compounds in the Environment. In *Environmental Chemistry of Arsenic*, Frakenberger, W. T. J., Ed. Mercel Dekker Inc.: New York, **2002**.

(136) Marsh, J. *Eddin. New Philos. J.* **1836,** *21*, 229.

(137) Melamed, D. *Anal. Chim. Acta* **2005,** *532*, 1.

(138) Dhar, R. K.; Zheng, Y.; Rubenstone, J.; van Geen, A. *Anal. Chim. Acta* **2004,** *526*, 203.

(139) Arsenic Quick II Test Kit. http://www.sensafe.com/481303.php (accessed June 2013).

(140) Frisbie, S.; Mitchell, E.; Yusuf, A. Z.; Siddiq, M. Y.; Sanchez, R.; Ortega, R.; Maynard, D.; Sarkar, B. *Environ. Health Persp.* **2005,** *113*, 1196.

(141) Klaue, B.; Blum, J. D. *Anal. Chem.* **1999,** *71*, 1408.

(142) Lin, Y.-F.; Walmsley, A. R.; Rosen, B. P. *Proc. Natl. Acad. Sci. U.S.A.* **2006,** *103*, 15617.

(143) Shi, W.; Dong, J.; Scott, R. A.; Ksenzenko, M. Y.; Rosen, B. P. *J. Biol. Chem.* **1996,** *271*, 9291.

(144) Liao, V. H.-C.; Ou, K.-L. *Environ. Toxicol. Chem.* **2005,** *24*, 1624.

(145) Stocker, J.; Balluch, D.; Gsell, M.; Harms, H.; Feliciano, J.; Daunert, S.; Malik, K. A.; van der Meer, J. R. *Environ. Sci. Technol.* **2003,** *37*, 4743.

(146) Ramanathan, S.; Shi, W.; Rosen, B. P.; Daunert, S. *Anal. Chem.* **1997,** *69*, 3380.

(147) Tauriainen, S.; Karp, M.; Chang, W.; Virta, M. *Appl. Environ. Microbiol.* **1997,** *63*, 4456.

(148) Wells, M.; Gösch, M.; Harms, H.; van der Meer, J. R. *Microchim. Acta* **2005,** *151*, 209.

(149) Tani, C.; Inoue, K.; Tani, Y.; Harun-ur-Rashid, M.; Azuma, N.; Ueda, S.; Yoshida, K.; Maeda, I. *J. Biosci. Bioeng.* **2009,** *108*, 414.

(150) Prindle, A.; Samayoa, P.; Razinkov, I.; Danino, T.; Tsimring, L. S.; Hasty, J. *Nature* **2012,** *481*, 39.

(151) Siegfried, K.; Endes, C.; Bhuiyan, A. F. M. K.; Kuppardt, A.; Mattusch, J.; van der Meer, J. R.; Chatzinotas, A.; Harms, C. *Environ. Sci. Technol.* **2012,** *46*, 3281.

(152) Soignet, S. L.; Frankel, S. R.; Douer, D.; Tallman, M. S.; Kantarjian, H.; Calleja, E.; Stone, R. M.; Kalaycio, M.; Scheinberg, D. A.; Steinherz, P.; Sievers, E. L.; Coutre, S.; Dahlberg, S.; Ellison, R.; Warrell, R. P. J. *J. Clin. Oncol.* **2001,** *19*, 3852.

(153) Zhang, X.; Uroic, M. K.; Xie, W.-Y.; Zhu, Y.-G.; Chen, B.-D.; McGrath, S. P.; Feldmann, J.; Zhao, F.-J. *Environ. Poll.* **2012,** *165*, 18.

(154) Grynkiewicz, G.; Poenie, M.; Tsien, R. Y. *J. Biol. Chem.* **1985,** *260*, 3440.

(155) Parker, K. J.; Kumar, S.; Pearce, D. A.; Sutherland, A. J. *Tetrahedron Lett.* **2005,** *46*, 7043.

(156) Satofuka, H.; Fukui, T.; Takagi, M.; Atomi, H.; Imanaka, T. *J. Inorg Biochem.* **2001,** *86*, 595.

(157) Baglan, M.; Atlgan, S. *Chem. Commun.* **2013,** *49*, 5325.

(158) Lakowicz, J. R., *Principle of Fluorescence Spectroscopy*. Kluwer Academic/Plenum: **2006**; p 960.

(159) Franck, J.; Dymond, E. G. *Trans. Faraday Soc.* **1926,** *21*, 536.

(160) Condon, E. U. *Phys. Rev.* **1928,** *32*, 858.

(161) Chasteen, T. G. Jablonski Diagram. http://www.shsu.edu/~chm_tgc/chemilumdir/JABLONSKI.html (accessed 05-27-2013).

(162) Stokes, G. G. *Phil. Trans. R. Soc.* **1852,** *142*, 463.

(163) Kasha, M. *Disc. Faraday Soc.* **1950,** *9*, 14.

(164) Cammann, K. *Phys. Chem. Chem. Phys.* **2003,** *5*, 5159.

(165) Rich, R. L.; Myszka, D. G. *J. Mol. Recognit.* **2002,** *15*, 352.

(166) de Silva, A. P.; Fox, D. B.; Moody, T. S.; Weir, S. M. *Trends Biotechnol.* **2001,** *19*, 29.

(167) Harvey, D., *Modern Analytical Chemistry*. McGraw-Hills Companies, Inc: Boston, **2000**.

(168) Pluth, M. D.; Tomat, E.; Lippard, S. J. *Annu. Rev. Biochem.* **2011,** *80*, 333.

(169) Tomat, E.; Lippard, S. J. *Curr. Opin. Chem. Biol.* **2010,** *14*, 225.

(170) Nolan, E. M.; Lippard, S. J. *Acc. Chem. Res.* **2009,** *42*, 193.

(171) Lim, M. H.; Lippard, S. J. *Acc. Chem. Res.* **2007,** *40*, 41.

(172) Miller, E. W.; Chang, C. J. *Curr. Opin. Chem. Biol.* **2007,** *11*, 620.

(173) Anderson, D. J.; Guo, B.; Xu, Y.; Ng, L. M.; Kricka, L. J.; Skogerboe, K. J.; Hage, D. S.; Schoeff, L.; Wang, J.; Sokoll, L. J.; Chan, D. W.; Ward, K. M.; Davis, K. A. *Anal. Chem.* **1997,** *69*, 165.

(174) Domaille, D. W.; Que, E. L.; Chang, C. J. *Nat. Chem. Biol.* **2008,** *4*, 168.

(175) Zhang, J. F.; Kim, J. S. *Anal. Sci.* **2009,** *25*, 1271.

(176) Que, E. L.; Domaille, D. W.; Chang, C. J. *Chem. Rev.* **2008,** *108*, 1517.

(177) Wang, J. S.; Wai, C. M. *J. Chem. Educ.* **2004,** *81*, 207.

(178) Carter, T. G.; Vickaryous, J. W.; Cangelosi, V. M.; Johnson, D. W. *Comments Inorg. Chem.* **2007,** *28*, 97.

(179) Hamaker, C. G.; Oberts, B. P. *J. Chem. Crystallogr.* **2006,** *36*, 735.

(180) Efremov, V. A.; Potolokov, V. N.; Nikolashin, S. V.; Fedorov, V. A. *Inorg. Mater.* **2002,** *38*, 837.

(181) Kniep, R.; Reski, H. D. *Inorg. Chim. Acta* **1982,** *64*, L83.

(182) Stetter, H. *Angew. Chem. Int. Ed.* **1954,** *66*, 217.

(183) Hill, N. J.; Levason, W.; Reid, G. *Inorg. Chem.* **2002,** *41*, 2070.

(184) Lindoy, L. F.; Livingstone, S. E. *Inorg. Chim. Acta* **1967,** *1*, 365.

(185) Touw, D. S.; Nordman, C. E.; Stuckey, J. A.; Pecoraro, V. L. *Proc. Natl. Acad. Sci. U.S.A.* **2007,** *104*, 11969.

(186) Raston, C. L.; Skelton, B. W.; Tolhurst, V.-A.; White, A. H. *Dalton Trans.* **2000**, 1279.

(187) Burford, N.; Landry, J. C.; Ferguson, M. J.; McDonald, R. *Inorg. Chem.* **2005,** *44*, 5897.

(188) Ezeh, V. C.; Patra, A. K.; Harrop, T. C. *Inorg. Chem.* **2010,** *49*, 2586.

(189) Bott, R. C.; Smith, G.; Sagatys, D. S.; Lynch, D. E.; Kennard, C. H. L. *Aust. J. Chem.* **2000,** *53*, 917.

(190) Klapötke, T. M.; Nöth, H.; Schütt, T.; Suter, M. *Eur. J. Inorg. Chem.* **2002**, 2511.

(191) Green, S. P.; Jones, C.; Jin, G.; Stasch, A. *Inorg. Chem.* **2007,** *46*, 8.

(192) Zhou, T.; Radaev, S.; Rosen, B. P.; Gatti, D. L. *EMBO J.* **2000,** *19*, 4838.

(193) Noveron, J. C.; Herradora, R.; Olmstead, M. M.; Mascharak, P. K. *Inorg. Chim. Acta* **1999,** *285*, 269.

(194) Zhang, C.; Guzei, I. A.; Espenson, J. H. *Inorg. Chem.* **2001,** *40*, 2437.

(195) Koley, A. P.; Nirmala, R.; Prasad, L. S.; Ghosh, S.; Manoharan, P. T. *Inorg. Chem.* **1992,** *31*, 1764.

(196) Fulmer, G. R.; Miller, A. J. M.; Sherden, N. H.; Gottlieb, H. E.; Nudelman, A.; Stoltz, B. M.; Bercaw, J. E.; Goldberg, K. I. *Organometallics* **2010,** *29*, 2176.

(197) *Smart v5.625: Software for the CCD Detector System*; Bruker AXS: Madison, WI, **2000**.

(198) Walker, N.; Stuart, D. *Acta Cryst.* **1983,** *A39*, 158.

(199) Sheldrick, G. M. *SADABS: Area Detector Absorption Correction*; University of Gottingen: Gottingen, Germany, **2001**.

(200) Sheldrick, G. M. *SHELX-97: Program for Refinement of Crystal Structures*; University of Gottingen: Gottingen, Germany, **1997**.

(201) Sheldrick, G. M. *SHELXTL 6.1, Crystallographic Computing Systems*; Siemens Analytical XRay Instruments: Madison, WI, **2000**.

(202) Johnson, C. K. *ORTEP III, Report ORNL-5138*; Oak Ridge National Laboratory: Oak Ridge, TN, **1976**.

(203) Quang, D. T.; Kim, J. S. *Chem. Rev.* **2010,** *110*, 6280.

(204) Kim, H. N.; Ren, W. X.; Kim, J. S.; Yoon, J. *Chem. Soc. Rev.* **2012,** *41*, 3210.

(205) Ma, W.; Xu, Q.; Du, J.; Song, B.; Peng, X.; Wang, Z.; Li, G.; Wang, X. *Spectrochim. Acta A* **2010,** *76*, 248.

(206) Kim, J. H.; Kim, H. J.; Kim, S. H.; Lee, J. H.; Do, J. H.; Kim, H.-j.; Lee, J. H.; Kim, J. S. *Tetrahedron Lett.* **2009,** *50*, 5958.

(207) Yang, Y.-K.; Yook, K.-J.; Tae, J. *J. Am. Chem. Soc.* **2005,** *127*, 16760.

(208) Song, F.; Watanabe, S.; Floreancig, P. E.; Koide, K. *J. Am. Chem. Soc.* **2008,** *130*, 16460.

(209) Ros-Lis, J. V.; Marcos, M. D.; Mártinez-Máñez, R.; Rurack, K.; Soto, J. *Angew. Chem., Int. Ed.* **2005,** *44*, 4405.

(210) Zhou, S.; Jia, J.; Gao, J.; Han, L.; Li, Y.; Sheng, W. *Dyes Pigm.* **2010,** *86*, 123.

(211) Barik, A.; Nath, S.; Pal, H. *J. Chem. Phys.* **2003,** *119*, 10202.

(212) Jones, G. I.; Jackson, W. R.; Choi, C.-Y.; Bergmark, W. R. *J. Phys. Chem.* **1985,** *89*, 294.

(213) Mizukami, S.; Okada, S.; Kimura, S.; Kikuchi, K. *Inorg. Chem.* **2009,** *48*, 7630.

(214) Iatridou, H.; Foukaraki, E.; Kuhn, M. A.; Marcus, E. M.; Haugland, R. P.; Katerinopoulos, H. E. *Cell Calcium* **1994,** *15*, 190.

(215) Sarkar, N.; Datta, A.; Das, S.; Bhattacharyya, K. *J. Phys. Chem.* **1996,** *100*, 15483.

(216) Swanson, S. A.; Wallraff, G. M.; Chen, J. P.; Zhang, W.; Bozano, L. D.; Carter, K. R.; Salem, J. R.; Villa, R.; Scott, J. C. *Chem. Mater.* **2003,** *15*, 2305.

(217) Wang, Z. S.; Cui, Y.; Hara, K.; Dan-oh, Y.; Kasada, C.; Shinpo, A. *Adv. Mater.* **2007,** *19*, 1138.

(218) Sheng, R.; Ma, J.; Wang, P.; Liu, W.; Wu, J.; Li, H.; Zhuang, X.; Zhang, H.; Wu, S. *Biosens. Bioelectron.* **2010,** *26*, 949.

(219) Wu, J.-S.; Liu, W.-M.; Zhuang, X.-Q.; Wang, F.; Wang, P.-F.; Tao, S.-L.; Zhang, X.-H.; Wu, S.-K.; Lee, S.-T. *Org. Lett.* **2007,** *9*, 33.

(220) Ezeh, V. C.; Harrop, T. C. *Inorg. Chem.* **2013,** *52*, 2323.

(221) Kim, T.-K.; Lee, D.-N.; Kim, H.-J. *Tetrahedron Lett.* **2008,** *49*, 4879.

(222) Suresh, M.; Das, A. *Tetrahedron Lett.* **2009,** *50*, 5808.

(223) Hu, M.; Fan, J.; Li, H.; Song, K.; Wang, S.; Cheng, G.; Peng, X. *Org. Biomol. Chem.* **2011,** *9*, 980.

(224) Komatsu, K.; Urano, Y.; Kojima, H.; Nagano, T. *J. Am. Chem. Soc.* **2007,** *129*, 13447.

(225) Shiraishi, Y.; Sumiya, S.; Hirai, T. *Chem. Commun.* **2011,** *47*, 4953.

(226) Garner, A. L.; Koide, K. *J. Am. Chem. Soc.* **2008,** *130*, 16472.

(227) Ezeh, V. C.; Harrop, T. C. *Inorg. Chem.* **2012,** *51*, 1213.

(228) Ellis, B. D.; Carlesimo, M.; Macdonald, C. L. B. *Chem. Commun.* **2003**, 1946.

(229) Šrogl, J.; Hývl, J.; Révész, Á.; Schröder, D. *Chem. Commun.* **2009**, 3463.

(230) Rokob, T. A.; Rulíšek, L.; Šrogl, J.; Révész, Á.; Zins, E. L.; Schröder, D. *Inorg. Chem.* **2011,** *50*, 9968.

(231) Zhu, C.; Akiyama, T. *Synlett* **2011,** *2011*, 1251.

(232) Henseler, A.; Kato, M.; Mori, K.; Akiyama, T. *Angew. Chem., Int. Ed.* **2011,** *50*, 8180.

(233) Zhu, C.; Akiyama, T. *Org. Lett.* **2009,** *11*, 4180.

(234) Saito, K.; Akiyama, T. *Chem. Commun.* **2012,** *48*, 4573.

(235) Zhu, C.; Akiyama, T. *Adv. Synth. Catal.* **2010,** *352*, 1846.

(236) Dunn, N. L.; Ha, M.; Radosevich, A. T. *J. Am. Chem. Soc.* **2012,** *134*, 11330.

(237) Iranpoor, N.; Zeynizadeh, B. *Synthesis* **1999**, 49.

(238) Obtained by treating 2-aminothiophenol with NaOH and 50% hydrogen peroxide

(239) Quantum Yield was determined by absolute measurement made by Nanoco with an integrating sphere setup.

(240) Brouwer, A. M. *Pure Appl. Chem.* **2011,** *83*, 2213.

(241) Hatai, J.; Pal, S.; Jose, G. P.; Bandyopadhyay, S. *Inorg. Chem.* **2012,** *51*, 10129.

APPENDIX A

DESIGN, SYNTHESIS AND PROPERTIES OF DANSYL-APPENDED CHEMOSENSORS FOR As(III) FLUORESCENCE DETECTION

A.1. Abstract

The arsenic concentration in the environment is dynamic and requires constant monitoring to ensure that levels in drinking water doesn't exceed 10 ppb as set by the U. S. EPA. We have developed five dansyl-based fluorescent dyes (**DNS1 – 5**) and tested their ability to report the presence of As(III) ions in solution. The dyes were designed to have a dansyl fluorophore appended to different receptor groups with known affinity for As(III). As expected for dansyl-based dyes, **DNS 1 – 5** have absorption maxima between 330 – 360 nm and emission maxima within 400 – 600 nm in organic media such as CH_2Cl_2 and MeOH. The fluorescence changes upon adding As(III) ions were modest and were not suitable to reliably detect As(III) ions.

A. 2. Introduction

A common strategy in the design of fluorescent dyes is the chemosensor approach. Chemosensors are molecules capable of transforming chemical information such as the presence of a particular analyte into a useful analytical signal.[1] A chemosensor is comprised of an analyte recognition unit and a signal transduction domain that is triggered upon analyte binding.[2-7] The fluorophore-spacer-receptor construct (Chart A.1), where the fluorescent group is separated from

the analyte receptor portion by a covalent bond or functional group will be utilized in the design for As(III) fluorescent dyes. Five dyes, **DNS1 – 5** (Chart A.2) were designed containing dansyl group as the fluorophore and their utility as As(III) fluorescent dyes were be examined.

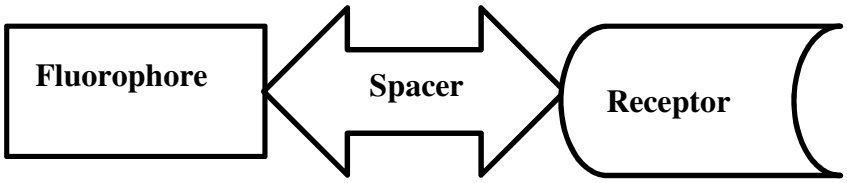

Chart A.1. Fluorophore-spacer-receptor construct for chemosensors.

The dansyl group is a well-known fluorophore usually attached to a receptor via a sulfonamide bond. Dansyl derivatives typically exhibit intense emission bands in the 400 – 600 nm region.[8] These bands are due to charge-transfer from the lone pair electron on the dimethylamino group into the π-antibonding orbital of the naphthalene ring.[9] The fluorescence properties of dansyl-labeled compounds are highly sensitive to the polarity of its microenvironment,[10] which has resulted in its extensive use as an extrinsic dye in protein folding studies.[11-12] The choice of dansyl as the fluorescence reporter unit is basically due to its high sensitivity and the ease of synthesizing a variety of analogs. Therefore, the objective of this study was to take advantage of the aforementioned properties of dansyl reporters and incorporate them into molecules with receptors for As(III) ions.

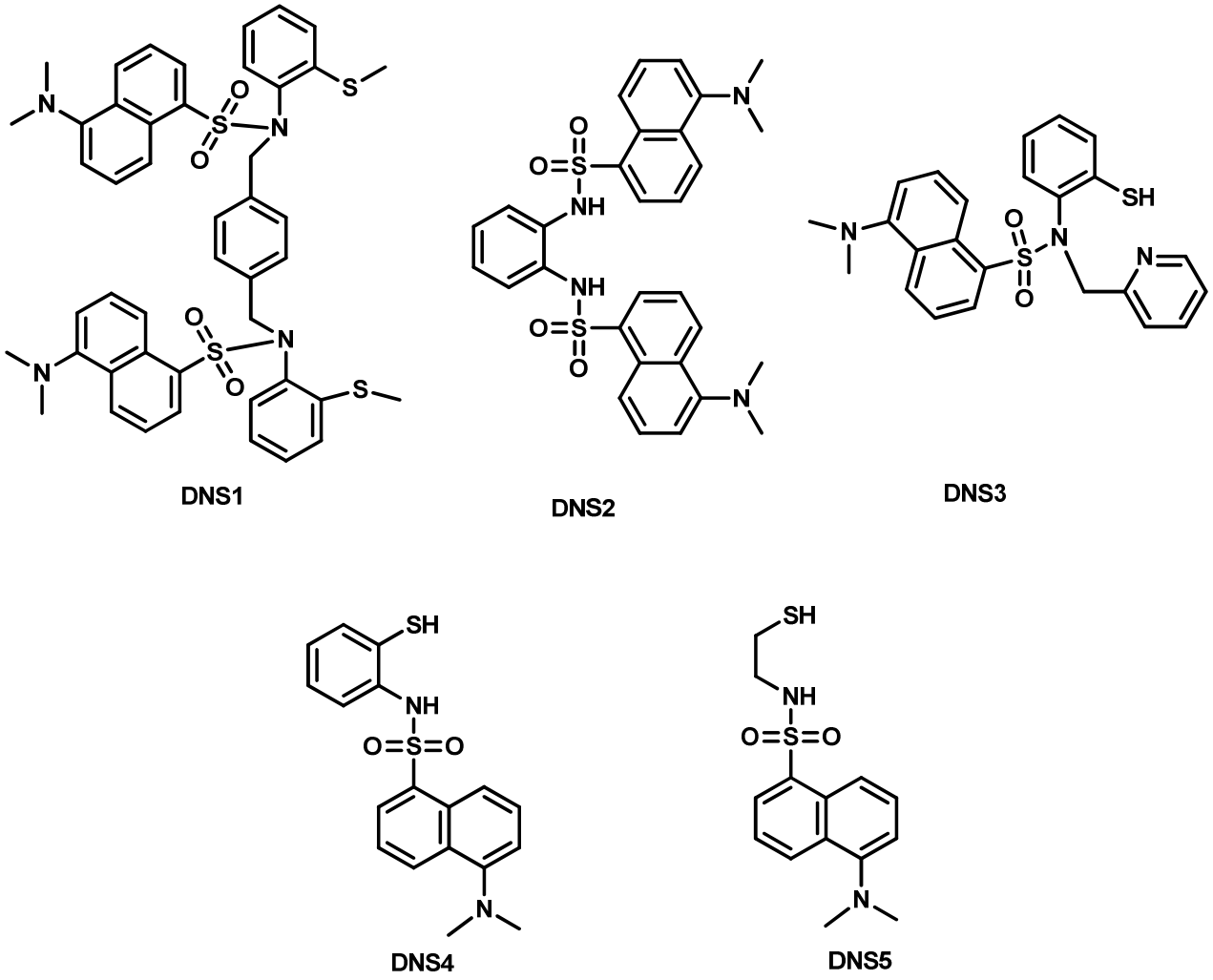

Chart A.2. Fluorescence chemosensors containing dansyl fluorescent group.

Several dansyl-based As(III) probes were designed based on variable donor capability. The design for **DNS1** is based on appending the dansyl fluorescent group to **L3** (Chapter 2), which was used in the coordination chemistry study of As(III) with thioether donors. We envisioned a [As_2(**DNS1**)$_3$] type complex where As(III) binds via a thioether-S bond with further complex stability through SBIs to the tertiary –N group. A change in fluorescence properties is expected upon complexation which will bring the dansyl group in close proximity and result in a change of its microenvironment. The receptor group in **DNS2** is 1,2-phenylenediamine and is

inspired from the ability of As(III) to form two-coordinate complexes.[13] This dye has been reported for the extraction of Pb(II) from aqueous samples into organic solvents.[14] **DNS2** forms a two-coordinate complex with Pb(II) and results in a 1.5-fold decrease in the fluorescence intensity upon binding Pb(II). **DNS2** is expected to react with As(III) and result in a measurable change in fluorescence properties. The receptor in **DNS3** is inspired by the four-coordinate As(III) complex reported in chapter 2, where the reduced 2-(pyridine-2-yl)-2,3-dihydrobenzo[*d*]thiazoline forms a stable complex with As(III). **DNS3** is expected to bind to As(III) with the thiolate-S, sulfonamide and pyridine-N donor groups. Both **DNS4** and **DNS5** contain thiolate-S and sulfonamide-N donor groups known to form a five-membered chelate with As(III).[15-17] While **DNS4** contains an aromatic group, the thiolate in **DNS5** is aliphatic and both compounds are expected to react with As(III) and give a change in fluorescence properties. These dyes were synthesized and their ability to report As(III) by changes in fluorescence properties were evaluated.

A.3. Results and Discussion

DNS1 was synthesized in one step by the reaction of **L3** (thioether ligand from chapter 2) and dansyl chloride in MeCN using K_2CO_3 as base (Scheme A.1). After purification, a green solid was obtained in modest yield (27%) and the purity of the dye was confirmed by $^{1}H/^{13}C$ NMR and ESI-MS. The ^{1}H NMR shows thirteen signals which integrates slightly higher than the expected forty-six hydrogen atoms due to overlapping solvent peaks. The parent peak at *m/z* = 847 in the ESI-MS confirms the formation of **DNS1**. **DNS2** was synthesized following a literature procedure by the reaction of 1,2-phenylenediamine and dansyl chloride in CH_2Cl_2 using

Et_3N as base.[14] Characterization by $^1H/^{13}C$ NMR, FTIR and ESI-MS confirms the formation of **DNS2**.

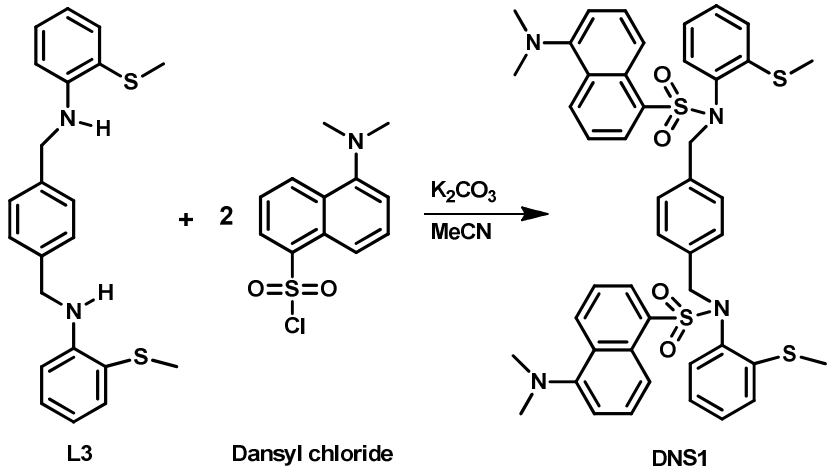

Scheme A.1. Synthesis of **DNS1**.

Synthesis of **DNS3** was carried out in four-steps (Scheme A.2), starting from the reduction of **L5** (used in chapter 2 to study the coordination chemistry of As(III)) with $NaBH_4$ in MeOH to afford the ring-open aminothiol compound **1**. The thiol group in **1** was then protected by air oxidation to afford the disulfide, **2** in 67% yield. The fluorescent reporter group was appended by the reaction of **2** and dansyl chloride in MeCN using K_2CO_3 as base to give **3** in 15% yield. Compounds 1 – 3 were characterized by $^1H/^{13}C$ NMR, FTIR and ESI-MS and shows that the expected compounds were formed. Finally, the disulfide bond in **3** was reduced by the reaction with $NaBH_4$ in THF to give **DNS3** as a green oil in 79% yield. ^1H NMR spectrum of **DNS3** shows a broad peak at 2.13 ppm which integrates for one hydrogen and is assigned to the thiol group. This assignment is supported by a weak peak at 2378 cm^{-1} in the FTIR. Synthesis of **DNS4** was carried out in two-steps (Scheme A.3), starting from the reaction of the disulfide of 2-aminothiophenol and dansyl chloride in MeCN to give **4** in 18% yield. ^1H NMR of **4** integrates slightly higher than the expected thirty-four hydrogen atom possibly due to contamination with

mono-dansylated species. The peaks at 3455 cm^{-1} and 3360 cm^{-1} in the FTIR indicates the presence of N-H groups which is the point of attachment to the dansyl group. Further support for the formation of **4** is obtained from the ESI-MS where a peak at *m/z* = 714.6 which can be assigned to $[\mathbf{4} + H]^+$ is present. The second step, which would have entailed the reduction of the disulfide bond to afford **DNS4** wasn't attempted because of a shift to developing coumarin-based chemodosimeters for As(III).

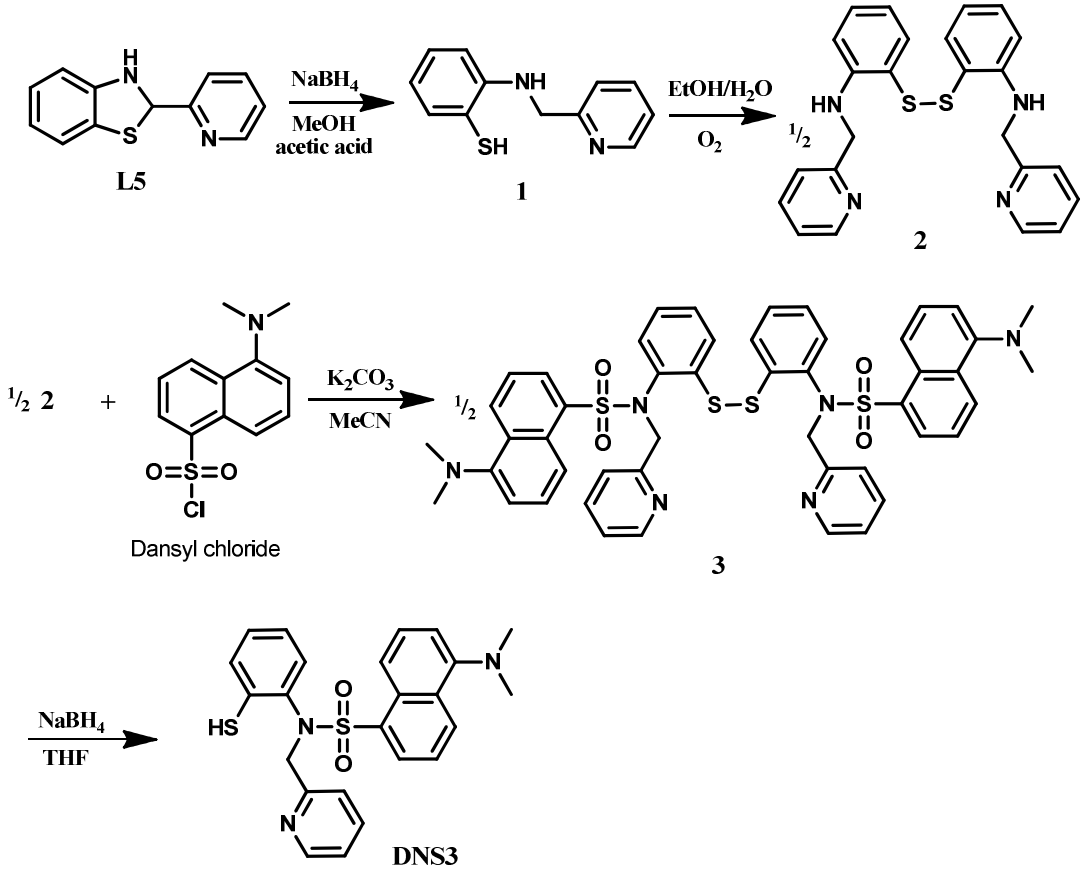

Scheme A.2. Synthesis of **DNS3**.

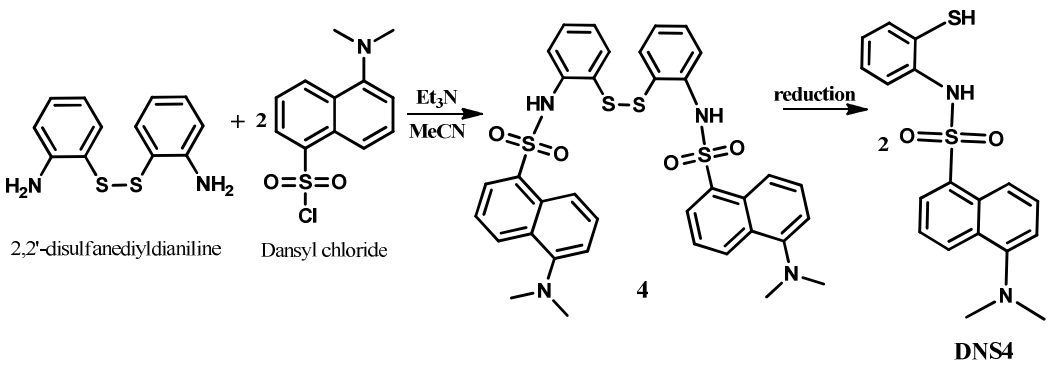

Scheme A.3. Synthesis of **DNS4**.

While a previous synthesis has been reported for **DNS5**, we report a different and more efficient procedure in this work. **DNS5** was synthesized in a three-step procedure (Scheme A.4): (i) protection of the thiol group of cysteamine by reaction with triphenylmethanol in TFA to generate S-trityl-cysteamine;[18] (ii) reaction of the protected S-trityl-cysteamine with the fluorescent reporting group dansyl chloride to give **5**; and finally (iii) removal of the trityl protecting group by reaction with Et_3SiH in TFA/CH_2Cl_2 (1:1) to generate pure **DNS5** in high yield (70%) as confirmed by $^1H/^{13}C$ NMR, FTIR, ESI-MS, elemental analysis, and X-ray crystallography. Pale-yellow single crystals of **DNS5** were obtained by slow diffusion of hexanes into a CH_2Cl_2 solution of **DNS5** at RT. **DNS5** crystallizes in the monoclinic system and $P2_1/c$ space group. An ORTEP diagram of **DNS5** reveals a cis-like geometry between the HN-CH_2-CH_2-SH ligating atoms, which appears poised for binding As(III)-ions to form a stable five-member chelate ring (Figure A.1). The determined bond lengths and angles are similar to other reported dansyl-sulfonamide structures.[10, 19]

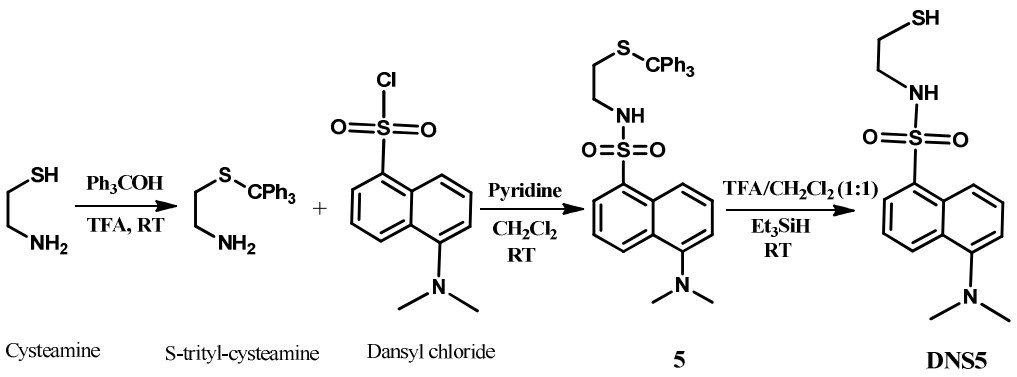

Scheme A.4. Synthesis of **DNS5**.

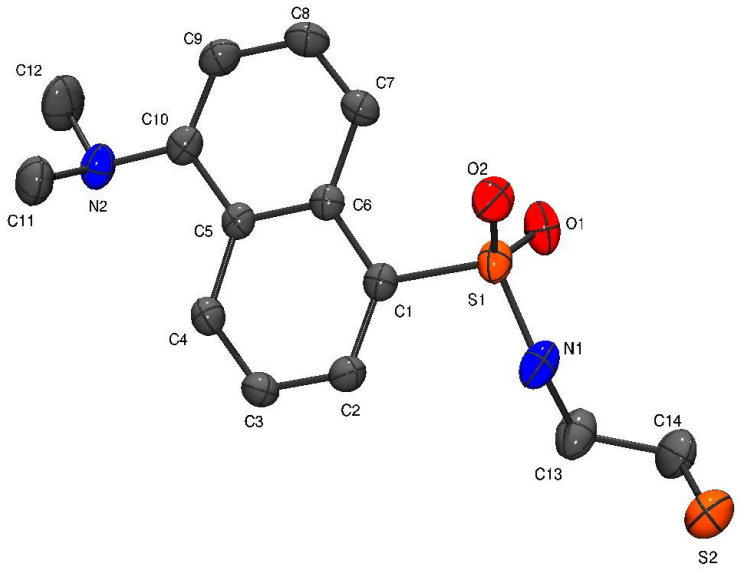

Figure A.1. ORTEP of **DNS5** showing 30% thermal probability ellipsoids. H atoms are omitted for clarity. Selected bond distances (Å) and angles (deg) for **DNS5**: S1-O1, 1.4267(19); S1-O2, 1.4343 (17); S1-N1, 1.598(2); S2-C14, 1.818(3); N1-C13, 1.473(3); O1-S1-O2, 118.65(12); O1-S1-N1, 108.45(12); O2-S1-N1, 106.34(11); N1-S1-C1, 108.20(19); C13-N1-S1, 124.02(19); N1-C13-C14, 111.5(2); C13-C14-S2, 114.5(2).

The dyes are soluble in common organic solvents such as THF and CH_2Cl_2. They are also stable for months when stored in the dark and in an inert atmosphere at room temperature. Study of their absorption and emission properties were carried out in organic media and the fluorescence change in the presence of As(III) was also evaluated. The UV-vis spectra of the

dyes exhibit similar absorption maxima irrespective of the solvent polarity. The λ_{max} in **DNS1** – **DNS3** are 345 nm (CH_2Cl_2), 340 nm (DCE) and 340 nm (CH_2Cl_2) respectively at 298 K. The electronic absorption properties of **DNS5** were studied in MeOH and MeOH/Et_3N. The UV-vis spectrum of **DNS5** exhibits two absorption maxima at 249 nm (ε = 12,900 M^{-1} cm^{-1}) and 336 nm (ε = 4,100 M^{-1} cm^{-1}) in MeOH at 298 K. It does not appear that the presence of excess Et_3N (5 mol-equiv; a general base present during metal complexation studies) effects λ_{max}, but a small increase in ε was observed (ε = 14,700 and 4,700 M^{-1} cm^{-1} at 248 and 336 nm, respectively), possibly the dianionic form of **DNS5**. The absorption property of **DNS1** – **5** is similar to other reported dansyl-based dyes.[8, 20] Hence, the peaks are assigned to the charge-transfer from the dimethylamino group to the π–antibonding orbital of the naphthalene ring of the dansyl group.[8-9, 21]

The dyes exhibits fluorescence with emission peak within the range of 400 – 600 nm observed for other dansyl-based dyes.[22-24] **DNS1** emits at 513 nm in CH_2Cl_2 (λ_{ex} = 345 nm) and a slight blue-shift to λ_{em} = 507 nm is observed for **DNS2** in DCE (λ_{ex} = 340 nm) at 298 K. Two fluorescence maxima is observed for **DNS3**, λ_{em} = 437 nm and 526 nm (λ_{ex} = 340 nm) in CH_2Cl_2 at 298 K. The 437 nm emission peak is tentatively assigned to the receptor portion of **DNS3** since the oxidized 2-(pyridine-2-yl)-2,3-dihydrobenzo[*d*]thiazoline is known to exhibit fluorescence.[25] Finally, the fluorescence spectrum of **DNS5** exhibits a maximum at λ_{em} = 501 nm with a measured quantum yield (Φ_f) of 0.36 in MeOH/Et_3N at 298 K upon excitation at λ_{ex} = 336 nm. In summary, the electronic and emission properties of **DNS1** – **5** are dominated by the appended dansyl fluorophore and is expected to be perturbed by the presence of As(III).

The ability of the dyes to report the presence of As(III) was evaluated by changes in fluorescence properties of the dyes. Changes that are acceptable for sensing purposes include a

significant increase or decrease in fluorescence intensity or a shift in emission maxima. Figure A.2 shows the fluorescence profile of **DNS1** upon adding aliquots of As(III) (as $AsCl_3$). The fluorescence maximum and intensity remained the same; which means that the presence of As(III) doesn't affect the fluorescence properties of **DNS1**. This observation is consistent with the lack of complexation with As(III) when **L3** was used as a ligand. Addition of As(III) (as $AsCl_3$) to a solution of **DNS2** in DCE resulted in a slight shift in the emission maxima from 507 nm to ~ 511 nm with no significant change in fluorescence intensity (Figure A.3). However, this slight red-shift of the emission maxima is not significant for use in sensing As(III). Fluorescence intensity decrease (quenching) is observed on adding As(III) (as $AsCl_3$) aliquots to a CH_2Cl_2 solution of **DNS3** (Figure A.4). The peak at 437 nm disappears with the first aliquot of As(III) (0.5 mol-equiv of As(III)) and a modest two-fold decrease in the 526 nm peaks is observed after two mol-equiv of As(III) is added. The immediate quenching of the 437 nm peak supports the assignment to the receptor portion of **DNS3** and binding As(III) prevents the emission pathway. However, the binding event does not perturb the dansyl fluorescence in a significant way. When aliquots of As(III) (as $AsCl_3$) are added to **DNS5** in MeOH/Et_3N at 298 K (Figure A.5), the fluorescence maximum blue-shifts to 496 nm from 501 nm with a modest increase in fluorescence intensity. In summary, the changes in the fluorescence properties of the dyes upon adding As(III) ions were not significant for sensing purposes. The weak donor ability of the thioether-S and lack of preference for amines can be attributed to the weak binding of As(III) to **DNS1** and **DNS2**. The thiol group in **DNS3** and **DNS5** enhances their affinity for As(III) though the binding doesn't translate to a significant fluorescence change. A design improvement will involve removing the spacer bond and incorporating the receptor group directly onto the

fluorophore, this will ensure that any binding event will results in a significant fluorescence change.

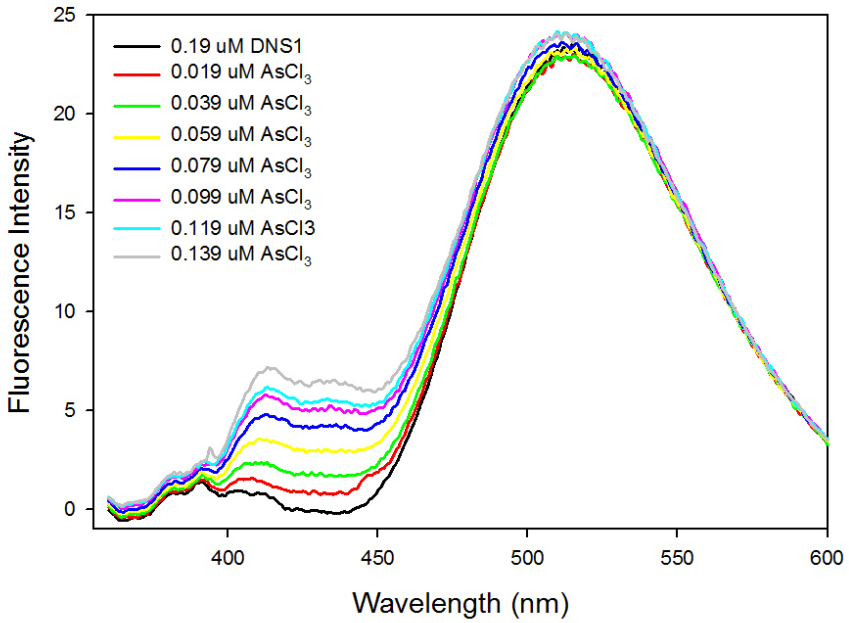

Figure A.2. Fluorescence titration of **DNS1** and $AsCl_3$ in CH_2Cl_2 at 298 K. The fluorescence intensity increase between 400 – 450 nm is possibly due to light scattering by the solvent.

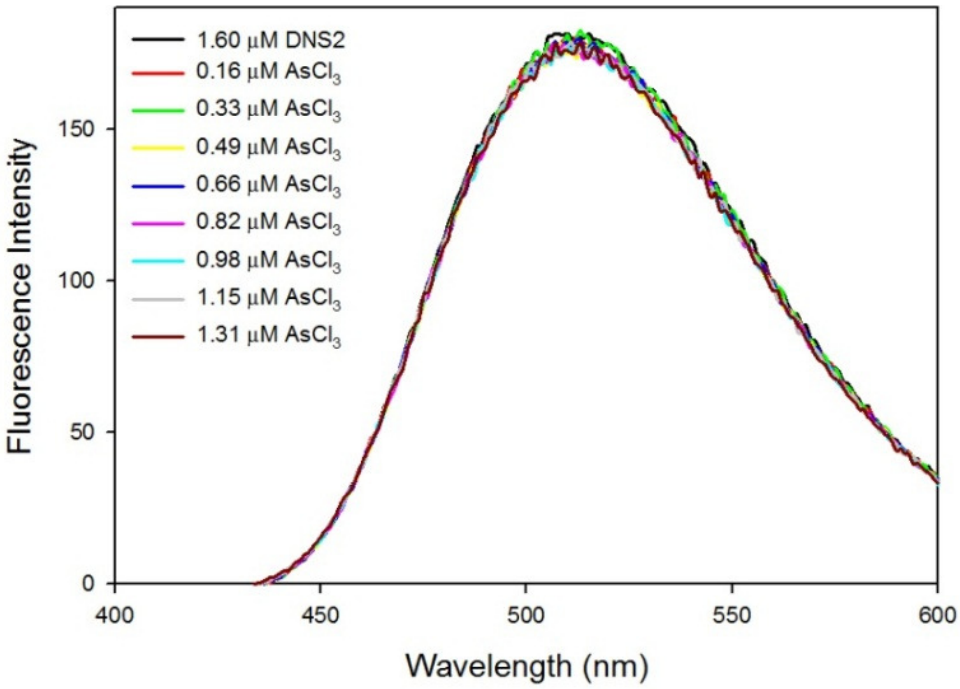

Figure A.3. Fluorescence titration of **DNS2** and $AsCl_3$ in DCE at 298 K.

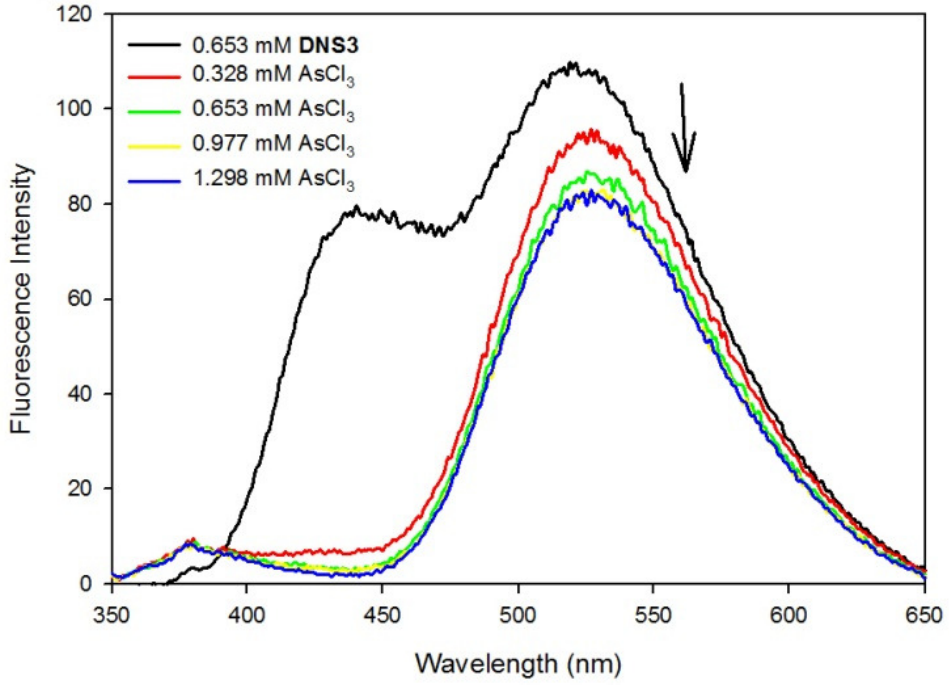

Figure A.4. Fluorescence titration of **DNS3** with $AsCl_3$ in CH_2Cl_2 at 298 K. Arrow shows direction of change.

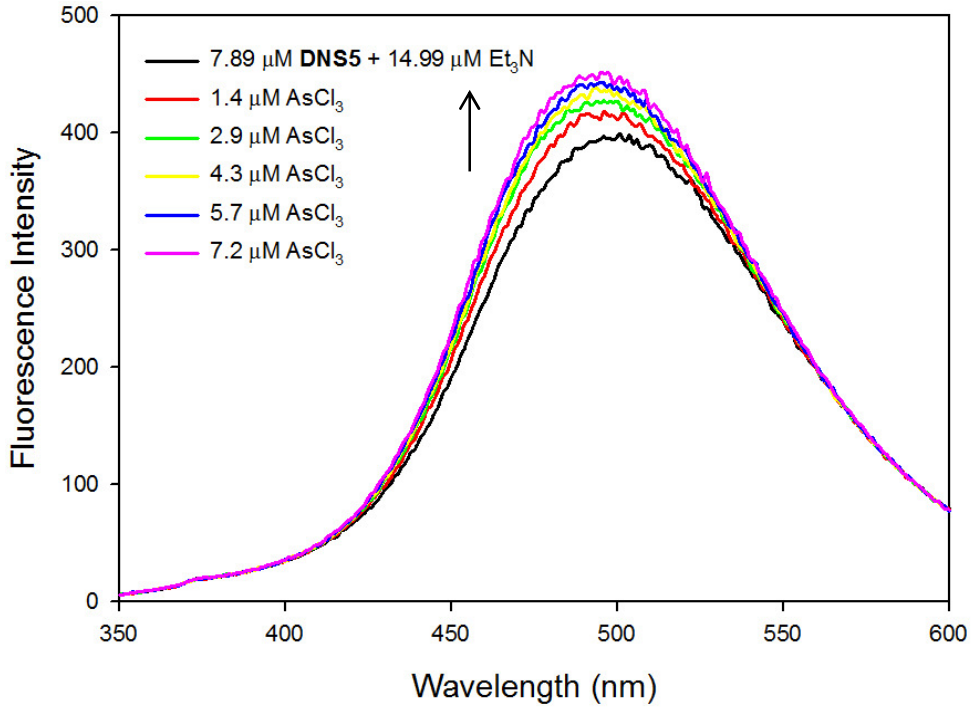

Figure A.5. Fluorescence titration of **DNS5** and $AsCl_3$ in MeOH at 298 K. Arrow shows direction of change.

Despite the lack of a significant fluorescence turn-on in the As(III), we tested the capability of **DNS5** to sense other analytes. Addition of Zn(II) (as $[Zn(H_2O)_6](ClO_4)_2$) leads to ~ 2-fold fluorescence enhancement in integrated emission intensity (Φ_f = 0.59), and the emission spectrum blue-shifts from 506 nm to 487 nm suggestive of Zn(II) complexation (Figure A.6). In general, **DNS5** doesn't have much utility as a chemosensor for cationic analyte, as the fluorescence properties don't change much in the presence of common ions (Figure A.6 inset). The only changes observed is with Zn(II) and Hg(II), which promotes a two-fold increase and decrease respectively in fluorescence intensity.

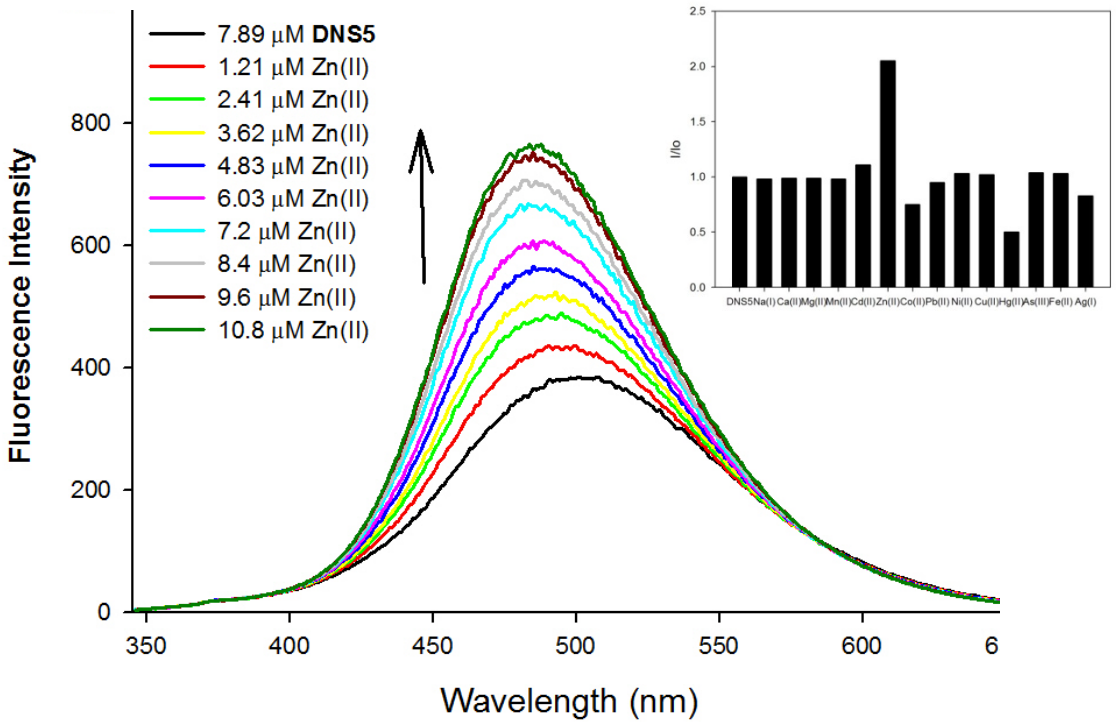

Figure A.6. Fluorescence titration of **DNS5** and Zn(II) in MeOH at 298 K. Inset: fluorescence response of 3.3 μM **DNS5** in the presence of 33.0 μM of the listed ions. Arrow shows direction of change.

A.4 Conclusion

The chemosensor approach studied in this work utilized the dansyl fluorophore as the fluorescent reporting unit. Various receptor groups were used in the dyes due to their reported

affinity for As(III). The photophysical properties of the dyes shows the electronic and emission properties were mostly controlled by the dansyl group. Therefore, the presence of As(III) was expected to affect the emission properties of the dansyl group in the dyes. The changes observed in this study were modest and indicates that these fluorescent construct are unsuitable for As(III) sensing.

A.5 Experimental section

General Information. All reagents were purchased commercially and used as received unless otherwise noted. Acetonitrile (MeCN), methylene chloride (CH_2Cl_2), tetrahydrofuran (THF), diethyl ether (Et_2O) and pentane were purified by passage through activated alumina columns using an MBraun MB-SPS solvent purification system and stored over 4 Å molecular sieves under a dinitrogen (N_2) atmosphere before use. Triethylamine (Et_3N) was dried by storing over KOH and $CaSO_4$ in an N_2 atmosphere. Ethanol (EtOH) and methanol (MeOH) were dried by distilling from $Mg(OEt)_2$ and $Mg(OMe)_2$, respectively under N_2. Dichloroethane (DCE) was dried by distilling over $CaCl_2$ under N_2. Solvents were sufficiently degassed by at least three freeze-pump-thaw cycles before introduction into the glovebox. All solvents were filtered with a 0.45 μm nylon filter before spectroscopic measurements were recorded to remove particulates (primarily molecular sieves from anhydrous storage). Reactions performed in an MBraun Unilab glovebox was under an atmosphere of purified N_2. Stock solutions of chemosensors were freshly prepared before all spectroscopic studies. Ligands, S-trityl-cysteamine,[18] DNS2,[14] and racemic 2-(pyridine-2-yl)-2,3-dihydrobenzo[*d*]thiazoline[26] were synthesized according to literature procedures. All fluorescence sensing experiments in THF contain 5 mol-equiv of Et_3N unless stated otherwise.

Physical Measurements. ^{1}H and ^{13}C NMR spectra were recorded in deuterated solvents on either a Varian Unity Inova 500 MHz or Varian Mercury plus 400 MHz NMR spectrometer at 298 K with chemical shifts referenced to tetramethylsilane (TMS) or residual protio signal of the deuterated solvent.[27] FTIR spectra were collected on a ThermoNicolet 6700 spectrometer running the OMNIC software. Samples were run as solids either in a KBr matrix or ATR diamond transmission window. Electronic absorption spectra were run at 298 K using a Cary 50 spectrophotometer equipped with a Quantum Northwest TC 125 temperature control unit. Fluorescence spectra were run at 298 K using a Varian Eclipse spectrofluorometer also containing the Quantum Northwest TC 125 temperature controller. All UV-vis and fluorescence samples were prepared in gas-tight Teflon-lined screw cap quartz cells with an optical pathlength of 1 cm. The quartz cells were cleaned thoroughly before each measurement by soaking in 10% HNO_3 for at least 3 h to remove trace metals, then rinsing with saturated $NaHCO_3$ solution, DI water, and MeOH. Low Resolution ESI-MS data were collected using a Perkin-Elmer Sciex API I Plus quadrupole mass spectrometer and High Resolution ESI-MS data were collected using a Bruker Daltonics 9.4 T Apex Qh FT-ICR-MS. Elemental analysis was done by Quantitative Technologies Inc in Whitehouse, N.J. Uncorrected melting points were obtained with a Laboratory Device MEL-TEMP II. FTIR and UV-vis data were plotted using the SigmaPlot 10.0 software package and NMR data were plotted with MestReNova Lite.

Synthesis Safety Note. Caution! Compounds containing arsenic (As) are toxic and should be handled with extreme care.

***N*,*N*'-(1,4-phenylenebis(methylene))bis(5-(dimethylamino)-*N*-(2-(methylthio)phenyl) naphthalene-1-sulfonamide (DNS1)**. A solid mixture of **L3** (used as a ligand in chapter 2) (0.7078 g, 1.85 mmol), dansyl chloride (1.0164 g, 3.76 mmol) and K_2CO_3 (0.5756 g, 4.16 mmol) was dissolved in 30 mL of MeCN to give an orange colored mixture. The flask was wrapped in foil to prevent photodegradation[28] and refluxed under an atmosphere of N_2 for 7.5 h. The color changed from orange to brown during the course of the reaction. The reaction was filtered to give a dirty white solid (0.4792 g) and a brown colored filtrate. The filtrate was concentrated with the rotavap to give brown-colored oil. The oil was dissolved in 15 mL CH_2Cl_2 and washed twice with saturated $NaHCO_3$ solution, once with DI water, and once with saline solution. The organic layer was dried with $MgSO_4$, filtered and concentrated with the rotavap to give a brown-colored oil. The oil was treated with 10 mL Et_2O to remove unreacted dansyl chloride. The Et_2O insoluble oil was purified by flash chromatography with a silica stationary phase (mobile phase = 3:1 hexane: ethyl acetate + 10% Et_3N) into two components – the product of interest and the mono-dansylated product. The fraction with the product of interest was concentrated and a green solid was obtained (0.4300 g, 27%). ^{1}H NMR (400 MHz, $CDCl_3$, δ from TMS): 2.02 (s, 6H), 2.88 (s, 12H), 4.59 (dd, 2H), 4.87 (dd, 2H), 6.67 (t, 2H), 6.89 (d, 4H), 7.00 (d, 2H), 7.13 (m, 6H), 7.35 (t, 2H), 7.43 (t, 2H), 8.12 (d, 2H), 8.23 (d, 2H), 8.52 (d, 2H)-higher integration is due to impurities from the monodansylated species and overlapping solvent peaks. ^{13}C NMR (100 MHz, $CDCl_3$, δ from TMS): 15.6, 45.7, 53.9, 103.4, 104.8, 115.1, 120.8, 123.1, 124.6, 126.2, 127.5, 128.9, 129.3, 130.1, 130.4, 130.5, 130.7, 135.4, 151.5. LRMS-ESI (*m/z*), $[M + H]^+$ calcd for $C_{46}H_{46}N_4O_4S_4$, 847.2; found, 847.2. UV-vis (CH_2Cl_2, 298 K) λ_{max}, nm: 345 nm.

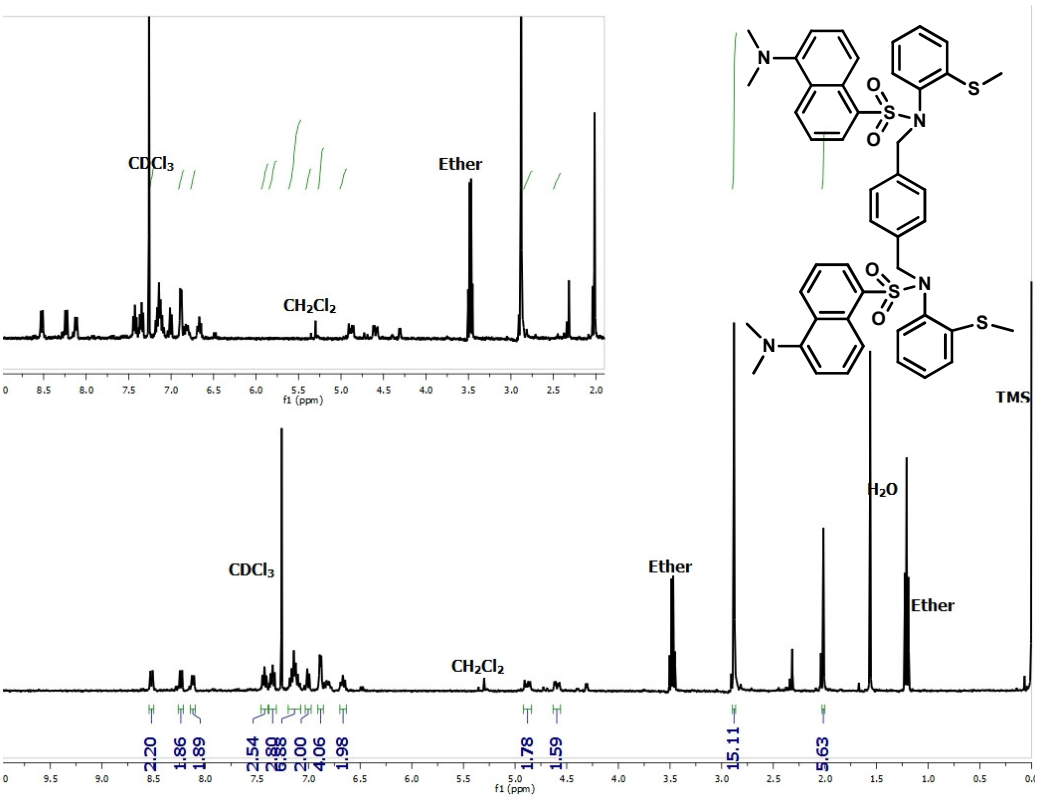

Figure A.7. ^{1}H NMR spectrum of **DNS1** in $CDCl_3$ at 298 K.

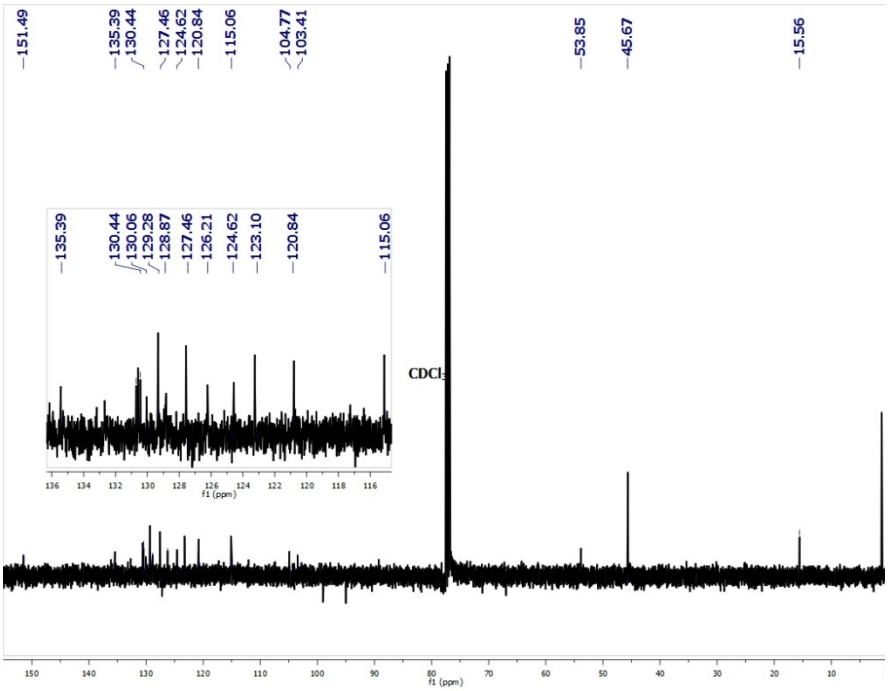

Figure A.8. ^{13}C NMR spectrum of **DNS1** in $CDCl_3$ at 298 K.

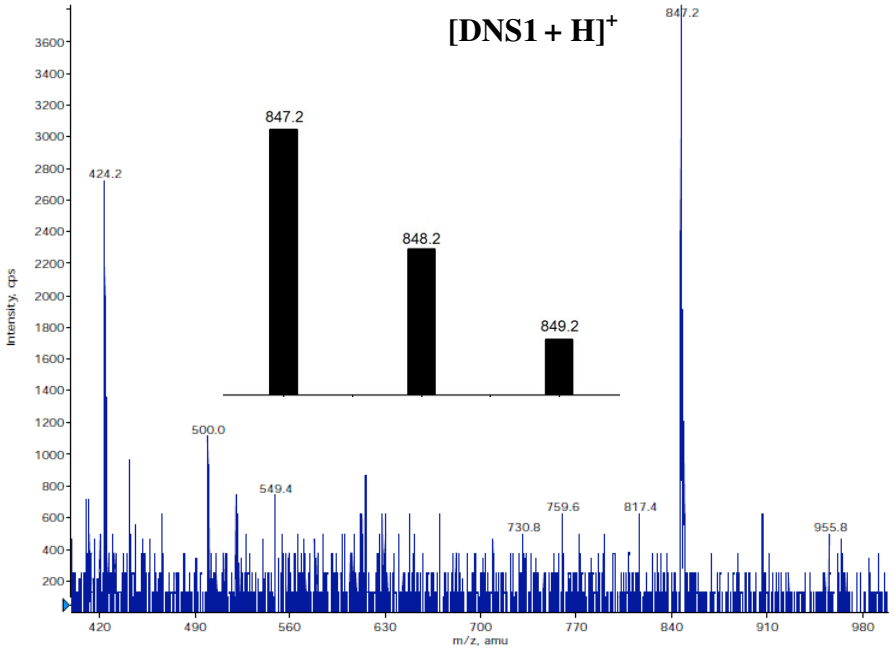

Figure A.9. Positive mode LRMS-ESI-MS of **DNS1** showing parent peak at *m/z* = 847.2. Inset: calculated molecular weight and isotopic distribution of **DNS1**.

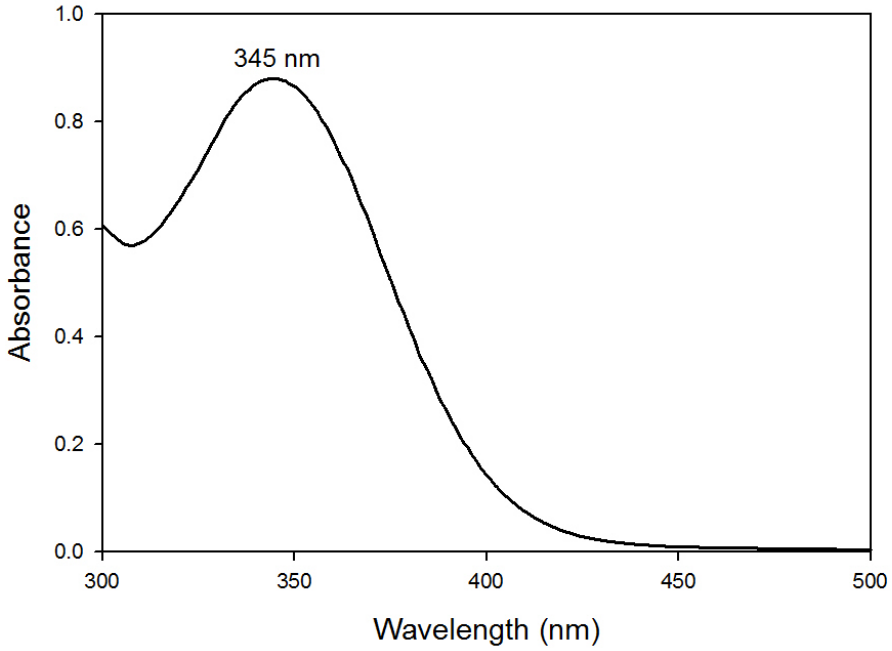

Figure A.10. UV-vis spectrum of a 1.0 μM solution of **DNS1** in CH_2Cl_2 at 298 K

5-(dimethylamino)-*N*-(2-mercaptophenyl)-*N*-(pyridine-2-ylmethyl)naphthalene-1-sulfonamide (DNS3). *Step 1*: **Synthesis of 2-((pyridine-2-ylmethyl)amino)benzenethiol (1).** A

solid batch of a racemic mixture of 2-(pyridine-2-yl) -2,3-dihydrobenzo[*d*]thiazoline (0.5548 g, 2.59 mmol) was dissolved in 25 mL of MeOH to give a light yellow solution. $NaBH_4$ (1.0536 g, 27.8 mmol) was added in small portions while the reaction was stirring, effervescence was observed but no color change. The reaction was left to stir for 1 h at RT before the MeOH was removed via rotavap to give a yellow solid. 40 mL of cold (0 ^oC) DI water was added to quench the excess $NaBH_4$ and 6 mL of acetic acid was added to neutralize the reaction (final pH = 5). The emulsion obtained was left to stir for 30 min and the color turned greenish-yellow. The oil was extracted by adding 50 mL of CH_2Cl_2, the organic layer was then washed with DI water and dried with Na_2SO_4. After filtration, CH_2Cl_2 was removed using the rotavap to give a greenish-yellow oil. *Step 2*: **Synthesis of 2,2'-disulfanediylbis(*N*-(pyridine-2-ylmethyl)aniline) (2).** The greenish-yellow oil obtained from step 1 was dissolved in 30 mL of EtOH/H_2O (1:1) mixture and air was bubbled through the solution for 48 h. CH_2Cl_2 (50 mL) was added to the reaction to extract the oily portion and the organic layer was dried with $MgSO_4$, filtered and concentrated to give a brown oil. Flash chromatography using silica gel stationary phase and a mobile phase of 4:1 hexane:ethyl acetate + drops of TEA, then pure ethyl acetate gave two fractions. Fraction 2 was collected and concentrated to give a yellow-colored oil (0.3756 g, 67%). ^1H NMR (400 MHz, $CDCl_3$, δ from TMS): 4.40 (d, 4H), 5.88 (t, 2H), 6.49 (m, 4H), 7.13 (m, 4H), 7.24 (t, 3H), 7.58 (t, 2H), 8.56 (d, 2H). ^{13}C NMR (100 MHz, $CDCl_3$, δ from TMS): 49.2, 111.0, 116.9, 118.8, 121.0, 122.1, 132.0, 136.6, 137.2, 149.0, 149.4, 158.6. FTIR (ATR-diamond, powder) ν_{max} (cm^{-1}): 3404 (w, ν_{N-H}), 3048 (w), 3012 (w), 2979 (w), 2925 (w), 2850 (w), 1584 (s), 1569 (s), 1496 (s), 1474 (m), 1448 (m), 1430 (m), 1353 (w), 1318 (m), 1263 (s), 1162 (m), 1148 (m), 1137 (m), 1104 (w), 1088 (w), 1047 (w), 1034 (m), 995 (m), 981 (w), 895 (w), 786 (w), 729 (vs), 700 (vs), 617 (m), 572 (w). LRMS-ESI (*m/z*), $[M + H]^+$ calcd for $C_{24}H_{22}N_4S_2$, 431.1; found, 431.2. *Step*

3: **Synthesis of *N*,*N*'-disulfanediylbis(2,1-phenylene))bis(5-(dimethylamino)-*N*-(pyridine-2-ylmethyl)naphthalene-1-sulfonamide) (3).** A batch of the oil synthesized in step II (0.7075 g, 1.64 mmol), dansyl chloride (1.3182 g, 4.88 mmol) and K_2CO_3 (0.6838 g, 4.94 mmol) were combined in 30 mL of MeCN to give an orange colored mixture. The mixture was refluxed under an atmosphere of N_2 for 9 h and the color turned dark green with the appearance of a white precipitate. The white solid was removed by filtration and the filtrate obtained was concentrated to give a greenish-black oil. The oil was triturated with 10 mL of Et_2O and filtered to give a blue-colored precipitate (0.0299 g) and yellow-colored filtrate. The filtrate was concentrated to give a yellow oil and purified using flash chromatography (SiO_2 as stationary phase and 1:1 CH_2Cl_2:hexane + TEA as mobile phase). Fraction 2 was collected and concentrated to give a yellow crystalline solid (0.2213 g, 15%). ^{1}H NMR (400 MHz, $CDCl_3$, δ from TMS): 2.85 (s, 12H), 6.67 (s, 2H), 6.86 (d, 2H), 7.07 (m, 4H), 7.17 (m, 4H), 7.26 (m, 4H, integrates higher due to overlap of $CDCl_3$), 7.46 (t, 2H), 7.53 (d, 2H), 7.64 (t, 2H), 7.80 (d, 2H), 8.02 (d, 2H), 8.20 (d, 2H), 8.56 (m, 4H). ^{13}C NMR (100 MHz, $CDCl_3$, δ from TMS): 45.5 ($N(CH_3)_2$, 70.4, 115.4, 119.1, 119.9, 120.4, 122.7, 123.1, 123.2, 125.5, 127.1, 128.1, 130.1, 130.6, 130.8, 131.6, 132.2, 133.2, 137.3, 137.8, 149.8, 151.6, 159.7. FTIR (ATR-diamond, powder) ν_{max} (cm^{-1}): 3055 (w), 2961 (m), 2924 (m), 2849 (m), 2830 (m), 2779 (m), 1610 (w), 1585 (m), 1568 (m), 1502 (m), 1456 (m), 1450 (m), 1433 (m), 1406 (m), 1393 (m), 1347 (m), 1307 (m), 1258 (s), 1231 (m), 1199 (m), 1162 (m), 1144 (s), 1091 (s), 1074 (s), 1056 (vs, $\nu_{S=Oasy}$), 1045 (vs), 1021 (vs, $\nu_{S=Osy}$), 994 (s), 940 (m), 837 (w), 786 (vs), 761 (s), 742 (s), 722 (s), 705 (s), 691 (s), 677 (s), 623 (s), 600 (m), 577 (s), 535(m). LRMS-ESI (*m/z*), $[M + 2H/2]^+$ calcd for $C_{48}H_{44}N_6O_4S_4$, 448.2; found, 448.0. M.pt: 65 – 70 ^{o}C (uncorrected). *Step IV*: Reduction to give **DNS3.** A batch of the solid synthesized in step 3 (0.0475 g, 0.05 mmol) was dissolved in 10 mL of THF to give a

yellow colored solution. A slurry of $NaBH_4$ (0.0315 g, 0.83 mmol) in 5 mL of THF was added dropwise, effervescence was observed but no color change. The reaction was stirred at RT and monitored with the aid of TLC (1:1 acetone: hexane + drops of Et_3N as mobile phase). One fluorescent spot was observed after stirring the reaction for 49 h. THF was removed and the oil obtained was treated with 10% acetic acid to quench unreacted $NaBH_4$. CH_2Cl_2 was added to extract the product, and then the solution was washed twice with DI water and concentrated to give a yellowish green oil (0.0189 g, 79%). ^{1}H NMR (400 MHz, CD_3CN, δ from TMS): 2.13 (m, 1H), 2.83 (s, 6H), 6.93 (s, 1H), 7.10 (d, 1H), 7.21 (t, 1H), 7.31 (m, 2H), 7.40 (m, 1H), 7.51 (t, 1H), 7.57 (d, 1H), 7.71 (t, 2H), 7.84 (m, 2H), 8.19 (d, 1H), 8.47 (d, 1H), 8.65 (d, 1H), 8.72 (d, 1H). FTIR (ATR-diamond, powder) ν_{max} (cm^{-1}): 3058 (w), 2943 (m), 2867 (m), 2789 (w), 2378 (w), 2260 (m), 1718 (m), 1611 (w), 1586 (s), 1570 (s), 1503 (m), 1459 (s), 1434 (s), 1406 (m), 1394 (m, 1352 (vs), 1309 (m), 1231 (m), 1200 (m), 1164 (vs, $\nu_{S=Oasy}$), 1147 (vs, $\nu_{S=Osy}$), 1058 (vs), 994 (m), 941 (m), 836 (m), 789 (vs), 777 (s), 747 (vs), 723(s), 625 (vs), 579 (s). LRMS-ESI (*m/z*), $[M + H]^+$ calcd for $C_{24}H_{24}N_3O_2S_2$, 450.1; found, 448.0.

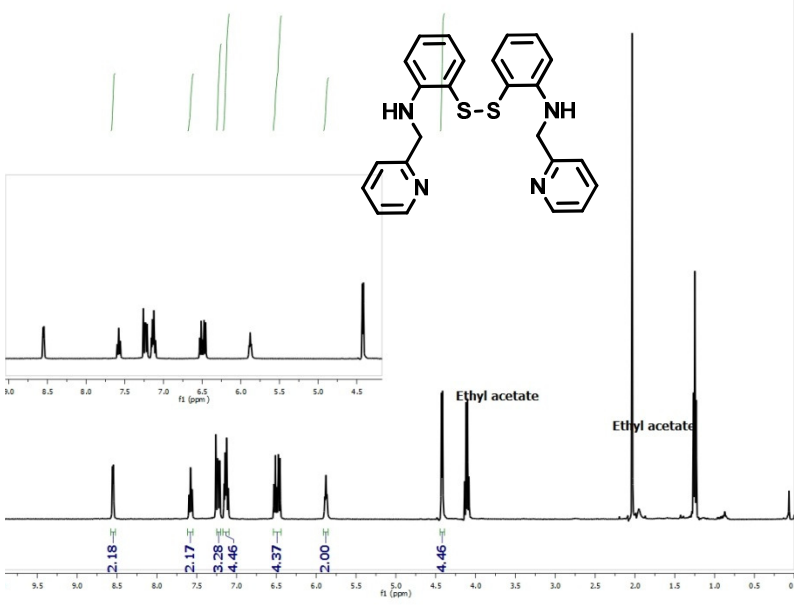

Figure A.11. ^{1}H NMR spectrum of **2** in $CDCl_3$ at 298 K.

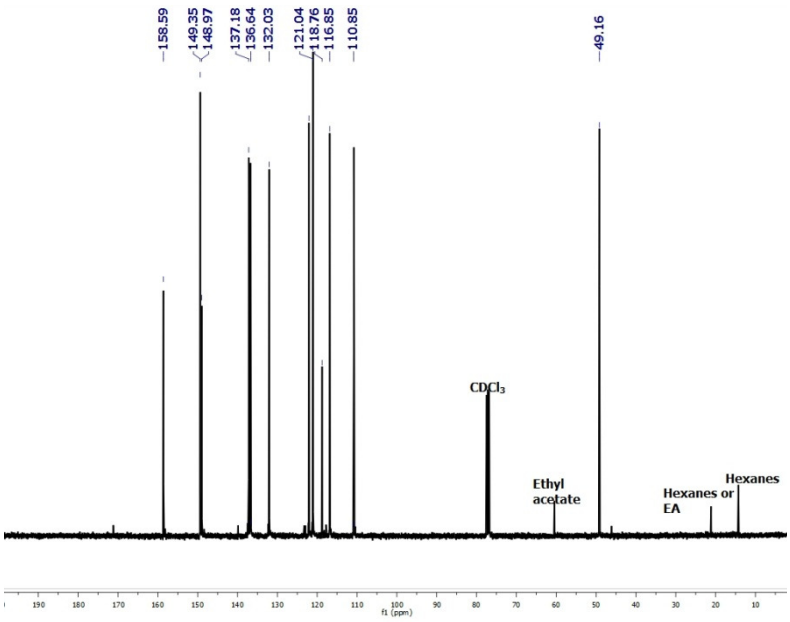

Figure A.12. ^{13}C NMR spectrum of **2** in $CDCl_3$ at 298 K.

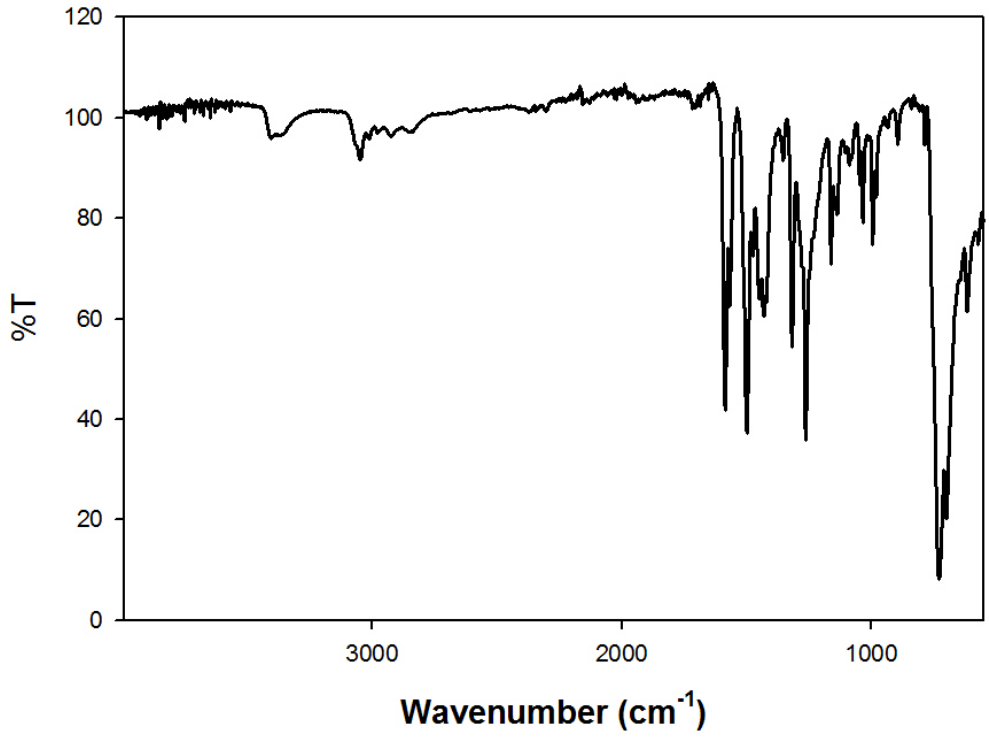

Figure A.13. Solid-state FTIR-spectrum (ATR-diamond) of **2**.

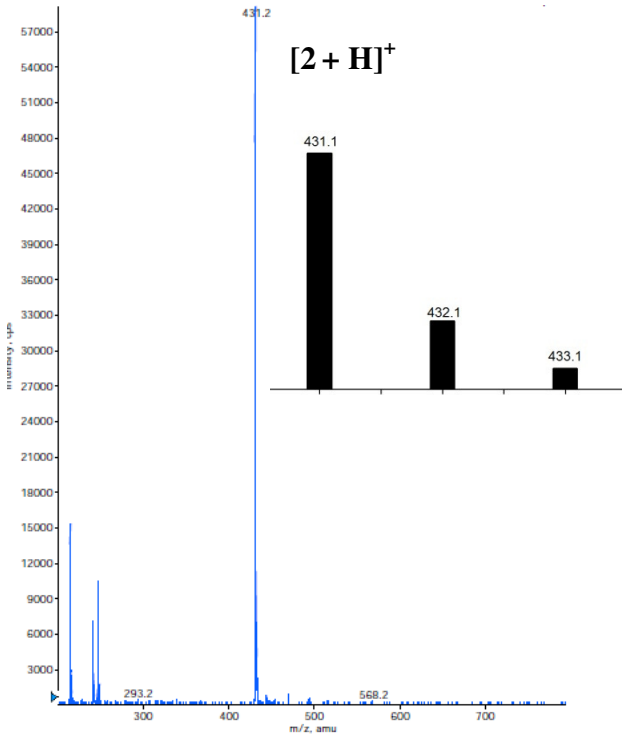

Figure A.14. Positive mode LRMS-ESI-MS of **2** showing parent peak at *m/z* = 431.2. Inset: calculated molecular weight and isotopic distribution of **2**.

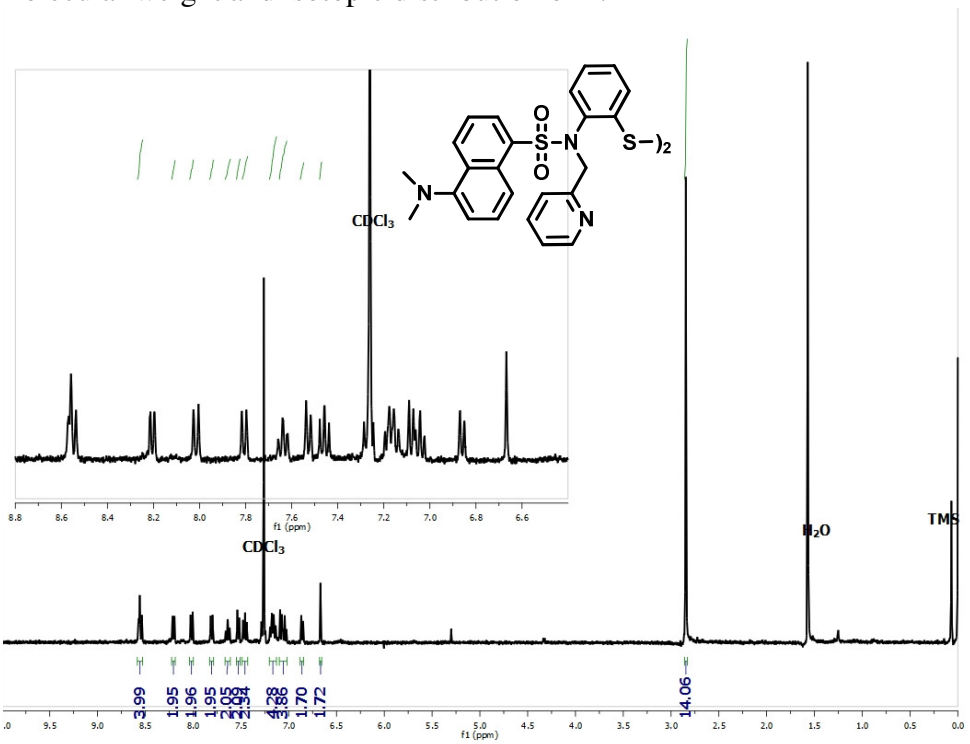

Figure A.15. ^{1}H NMR spectrum of **3** in $CDCl_3$ at 298 K.

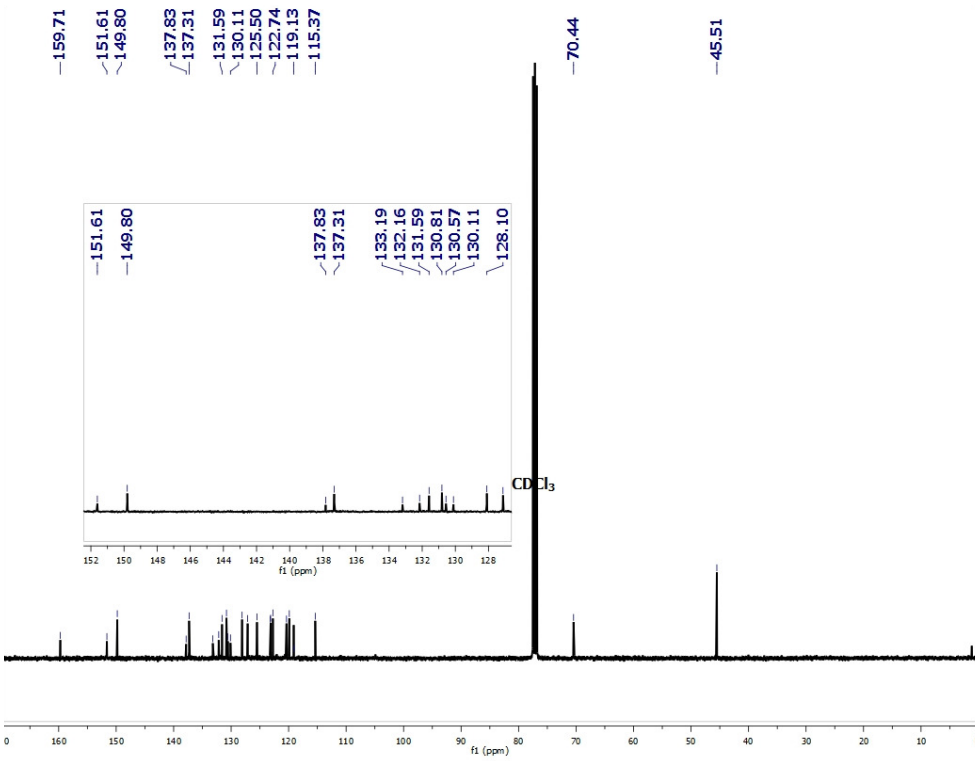

Figure A.16. ^{13}C NMR spectrum of **3** in $CDCl_3$ at 298 K.

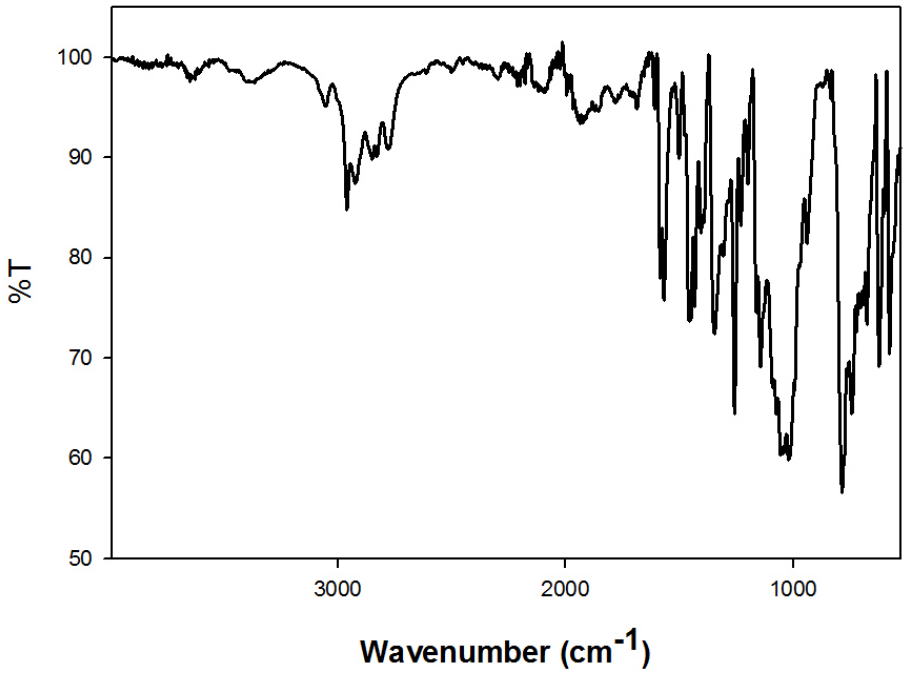

Figure A.17. Solid-state FTIR-spectrum (ATR-diamond) of **3**.

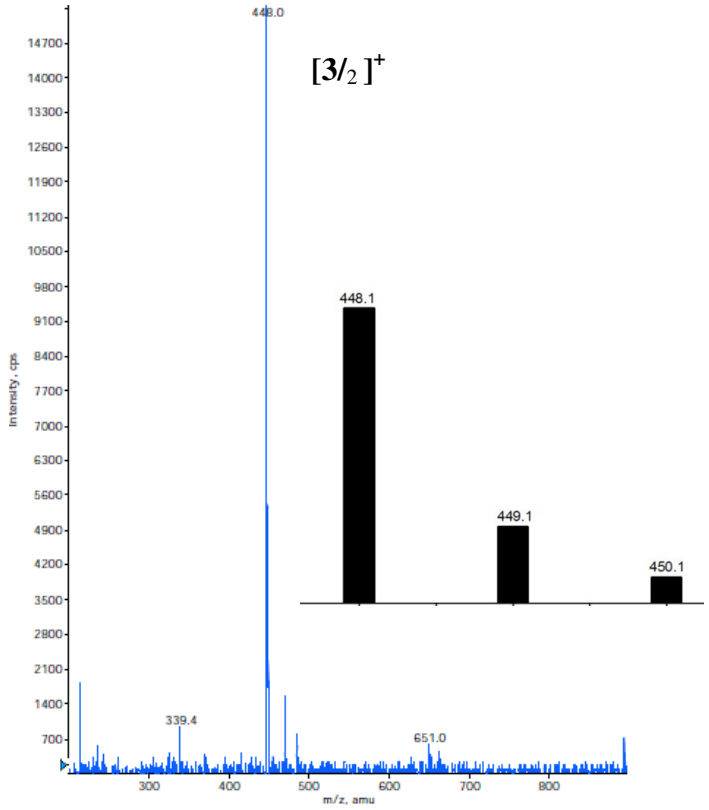

Figure A.18. Positive mode LRMS-ESI-MS of **3** showing base peak at *m/z* = 448.0. Inset: calculated molecular weight and isotopic distribution of $[\mathbf{3}/_2]^+$.

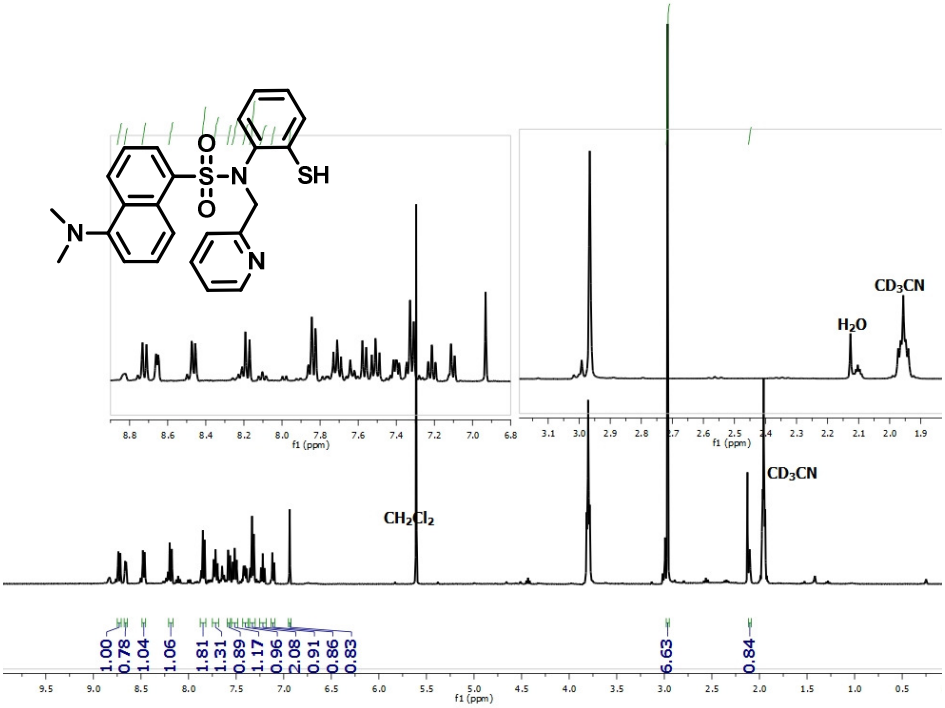

Figure A.19. ^{1}H NMR spectrum of **DNS3** in CD_3CN at 298 K.

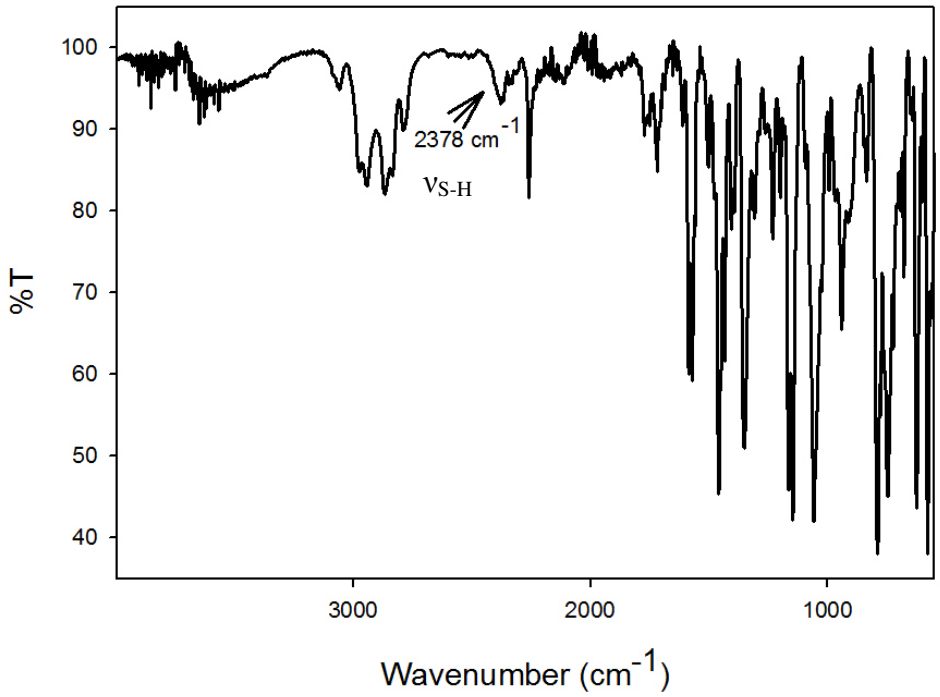

Figure A.20. Solid-state FTIR-spectrum (ATR-diamond) of **DNS3**.

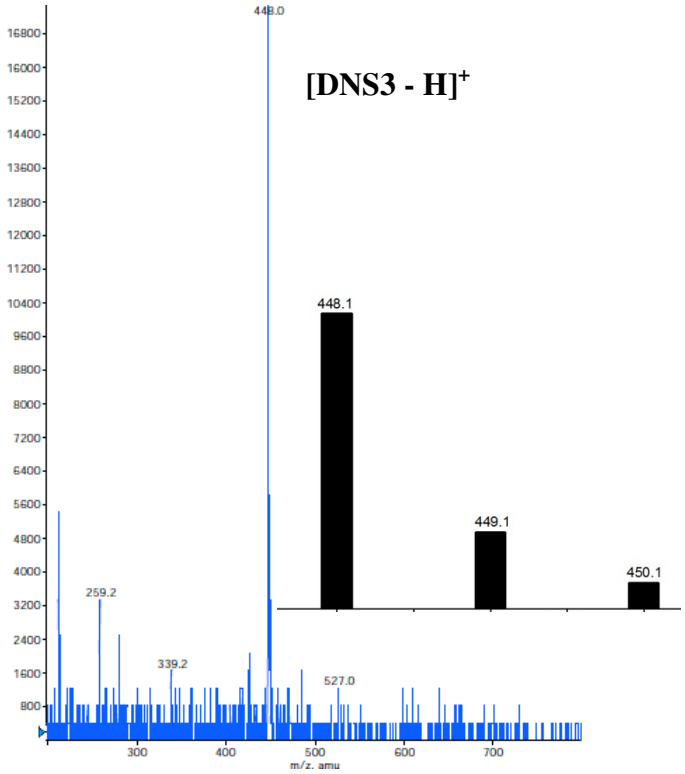

Figure A.21. Positive mode LRMS-ESI-MS of **DNS3** showing base peak at *m/z* = 448.0. Inset: calculated molecular weight and isotopic distribution of [**DNS3-H**]$^+$.

5-(dimethylamino)-*N*-(2-mercaptophenyl)naphthalene-1-sulfonamide (DNS4). *Step 1*: **Synthesis of N,N'-(disulfanediylbis(2,1-phenylene))bis(5-dimethylamino)naphthalene-1-sulfonamide (4).** A solid batch of 2,2'-disulfanediyldianiline (0.4699 g, 1.89 mmol), dansyl chloride (1.0503 g, 3.89 mmol) and Et_3N (1.089 g, 10.76 mmol) was dissolved in 30 mL of MeCN to give an orange solution. The solution was stirred at RT in the glovebox for 83 h and then concentrated to give a dark-red colored oil. The oil was treated with THF to cause the formed TEA·HCl to precipitate and the filtrate was then concentrated to give a reddish-brown oil. The oil was dissolved in 30 mL of CH_2Cl_2 and washed twice with saturated $NaHCO_3$, once with DI water and dried with $MgSO_4$, the organic layer was then filtered and concentrated to give a brown-colored oil. The oil was purified by flash chromatography (SiO_2 as stationary phase and 1:1 acetone:hexane + TEA as mobile phase). Fraction 2 was concentrated to give a reddish-brown solid (0.2475 g, 18%). ^{1}H NMR (400 MHz, $CDCl_3$, δ from TMS, higher integration of peaks due to solvent): 2.88 (s, 12H), 4.33 (s, 2H), 6.64 (m, 4H), 7.14 (m, 4H), 7.21 (m, 4H), 7.53 (m, 2H), 7.95 (m, 2H), 8.40 (m, 2H), 8.61 (t, 2H). FTIR (ATR-diamond, powder) ν_{max} (cm^{-1}): 3455 (m), 3360 (m), 3056 (m), 2937 (m), 2863 (m), 2828 (m), 2775 (m), 1604 (vs), 1583 (vs), 1563 (vs), 1507 (m), 1474 (vs), 1444 (vs), 1406 (s), 1366 (s), 1347 (s), 1305 (s), 1249 (m), 1232 (m), 1199 (m), 1158 (s, $\nu_{S=Oasy}$), 1143 (s, $\nu_{S=Osy}$), 1092 (m), 1075 (m), 1055 (m), 1019 (m), 942 (m), 886 (s), 848 (s), 836 (s), 787 (s), 743 (s), 704 (s) 675 (m), 655 (m), 615 (m), 594 (w), 570 (w), 59 (m). LRMS-ESI (*m/z*), $[M + H]^+$ calcd for $C_{36}H_{34}N_4O_4S_4$, 714.9; found, 714.6. M.pt: 68-75 ^oC (uncorrected).

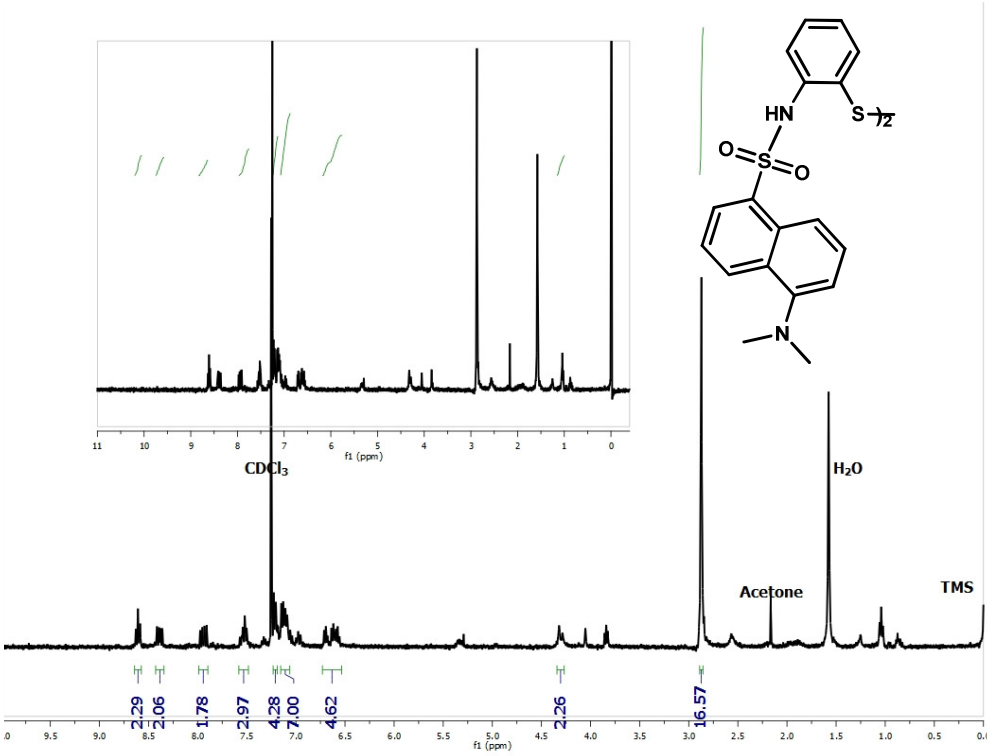

Figure A.22. ^{1}H NMR spectrum of **4** in $CDCl_3$ at 298 K.

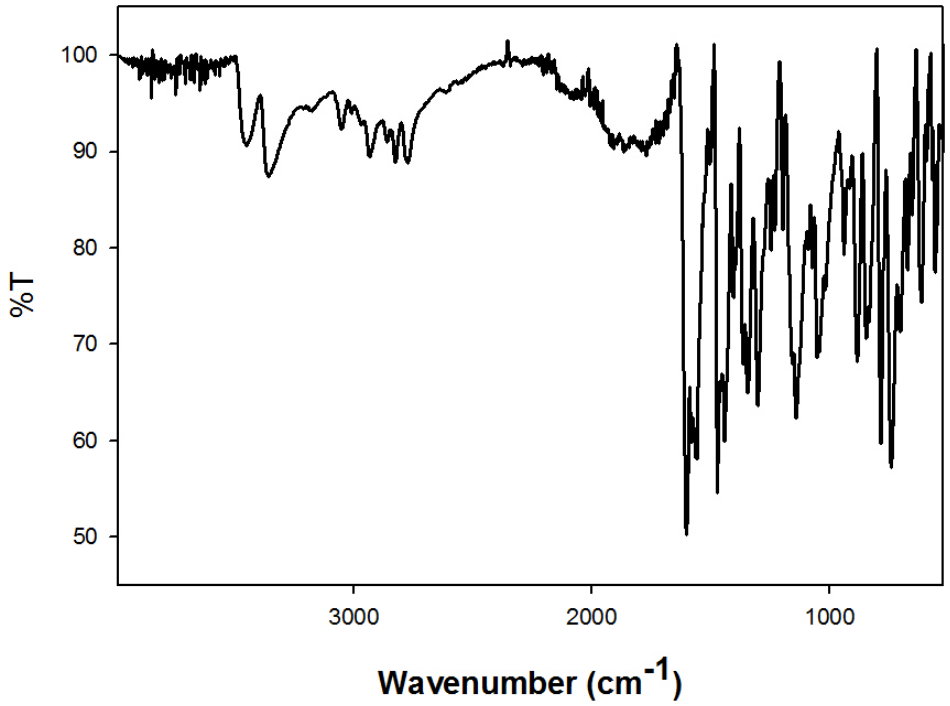

Figure A.23. Solid-state FTIR-spectrum (ATR-diamond) of **4**.

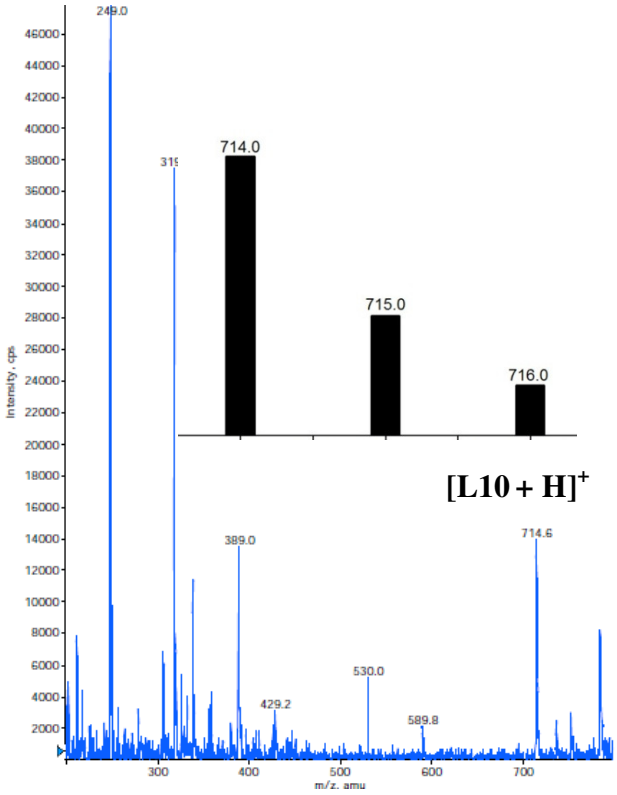

Figure A.24. Positive mode LRMS-ESI-MS of **4** showing parent peak at *m/z* = 714.6. Inset: calculated molecular weight and isotopic distribution of **4**.

Synthesis 5-(dimethylamino)-N-(2-mercaptoethyl)naphthalene-1-sulfonamide (DNS5). *Step 1*: **Synthesis of 5-(dimethylamino)-*N*-(2-(tritylthio)ethyl)naphthalene-1-sulfonamide (5).** A batch of S-trityl-cysteamine (1.3173 g, 4.1235 mmol) was dissolved in 5 mL of CH_2Cl_2 containing pyridine (0.5334 g, 6.7434 mmol) to afford a clear solution. To this solution was added a 5 mL CH_2Cl_2 solution of dansyl chloride (1.1204 g, 4.1535 mmol) affording a yellow slightly heterogeneous solution that was left to stir at room temperature (RT) in the glovebox for 16 h. An additional 20 mL of CH_2Cl_2 was then added to dissolve the insolubles and the reaction was washed with dilute HCl (pH ~ 2). Basic workup of the organic layer was carried out by washing twice with a saturated $NaHCO_3$ solution and once with saline. After drying with $MgSO_4$, the organic layer was filtered and concentrated on a rotary evaporator to yield a yellow oil. Purification by column chromatography (silica, 3:1 hexanes/ethyl acetate)

afforded the compound as a light green solid (2.238 g, 4.049 mmol, 98%). ^{1}H NMR (400 MHz, $CDCl_3$, δ from TMS): 2.32 (m, 2H), 2.54 (q, 2H), 2.90 (s, 6H), 4.69 (t, 1H, NH), 7.16 (m, trityl-H, 10H), 7.28 (m, trityl-H, dansyl-H, 14 H, integrates high because this peak overlaps with the solvent residual peak), 7.48 (t, 1H), 7.55 (t, 1H), 8.11 (d, 1H), 8.18 (d, 1H), 8.54 (d, 1H). ^{13}C NMR (100 MHz, $CDCl_3$, δ from TMS): 32.1, 42.1, 45.6, 67.0, 115.4, 118.9, 123.3, 126.9, 127.4, 128.1, 128.6, 129.5, 129.7, 129.8, 130.1, 130.6, 134.7, 144.5, 152.2. FTIR (ATR-diamond, solid), ν_{max} (cm^{-1}): 3282 (m, ν_{NH}), 3054 (m), 2939 (m), 2830 (m), 2784 (m), 1719 (m), 1612 (w), 1588 (m), 1573 (m), 1486 (m), 1443 (m), 1407 (m), 1316 (m), 1231 (w), 1201 (w), 1159 (m), 1140 (s), 1073 (m), 1034 (m), 944 (w), 904 (w), 839 (w), 788 (s), 766 (w), 741 (s), 698 (s), 621 (m), 568 (m). LRMS-ESI (*m/z*), $[M + H]^+$ calcd for $C_{33}H_{33}N_2O_2S_2$, 553.2; found, 553.0. mp: 143-144 °C. *Step 2*: **Synthesis of 5-(dimethylamino)-*N*-(2-mercaptoethyl)naphthalene-1-sulfonamide (DNS5).** A portion of **5** (0.9173 g, 1.6595 mmol) was dissolved in a 14 mL solution of TFA/CH_2Cl_2 (1:1) to give an orange colored homogeneous solution. Upon adding Et_3SiH (0.2032 g, 1.7475 mmol), the reaction mixture instantly turned pale-yellow and was left to stir further for 2 h at RT. The volume of the reaction was then reduced to half with the aid of a double trap short path distillation apparatus and the resulting white precipitate (Ph_3CH) was filtered out. The filtrate was then dissolved in CH_2Cl_2, washed once with a $NaHCO_3$ solution, dried with $MgSO_4$, filtered and concentrated to afford a yellow oil. The oil was triturated with hexanes to remove excess Ph_3CH and Et_3SiH. Drying the oil in vacuo resulted in a yellow solid product (0.3533 g, 1.138 mmol, 69%). ^{1}H NMR (400 MHz, $CDCl_3$, δ from TMS): 1.21 (t, 1H, SH), 2.52 (m, 2H), 2.89 (s, 6H), 3.08 (m, 2H), 5.21 (m, 1H, NH), 7.21 (d, 1H), 7.55 (m, 2H), 8.27 (m, 2H), 8.55 (d, 1H). ^{13}C NMR (100 MHz, $CDCl_3$, δ from TMS): 25.0, 45.6, 46.1, 115.5,

118.8, 123.4, 128.7, 129.7, 129.8, 130.1, 130.9, 134.9, 152.3. FTIR (ATR-diamond, solid), ν_{max} (cm^{-1}): 3261 (m, ν_{NH}), 2992 (w), 2933 (m), 2862 (m), 2827 (m), 2779 (m), 2566 (w, ν_{SH}), 1611 (m), 1587 (m), 1576 (m), 1503 (w), 1478 (w), 1460 (m), 1436 (s), 1405 (m), 1353 (m), 1307 (s), 1233 (m), 1201 (m), 1179 (m), 1160 (s), 1136 (s), 1093 (m), 1073 (s), 971 (w), 947 (m), 907 (m), 885 (m), 851 (m), 823 (w), 783 (s), 679 (m), 621 (m), 569 (m), 540 (m). LRMS-ESI (*m/z*), $[M + H]^+$ calcd for $C_{14}H_{19}N_2O_2S_2$, 311.1; found, 311.0. Anal. calcd for $C_{14}H_{18}N_2O_2S_2$: C, 54.17; H, 5.84; N, 9.02. Found: C, 54.34; H, 5.53; N, 8.76. mp: 109–111 ^oC (uncorrected). UV-vis (MeOH, 298 K) λ_{max}, nm (ε, M^{-1} cm^{-1}): 249 (12,856), 336 (4,131). UV-vis (MeOH + TEA, 298 K) λ_{max}, nm (ε, M^{-1} cm^{-1}): 249 (14,698), 336 (4,660).

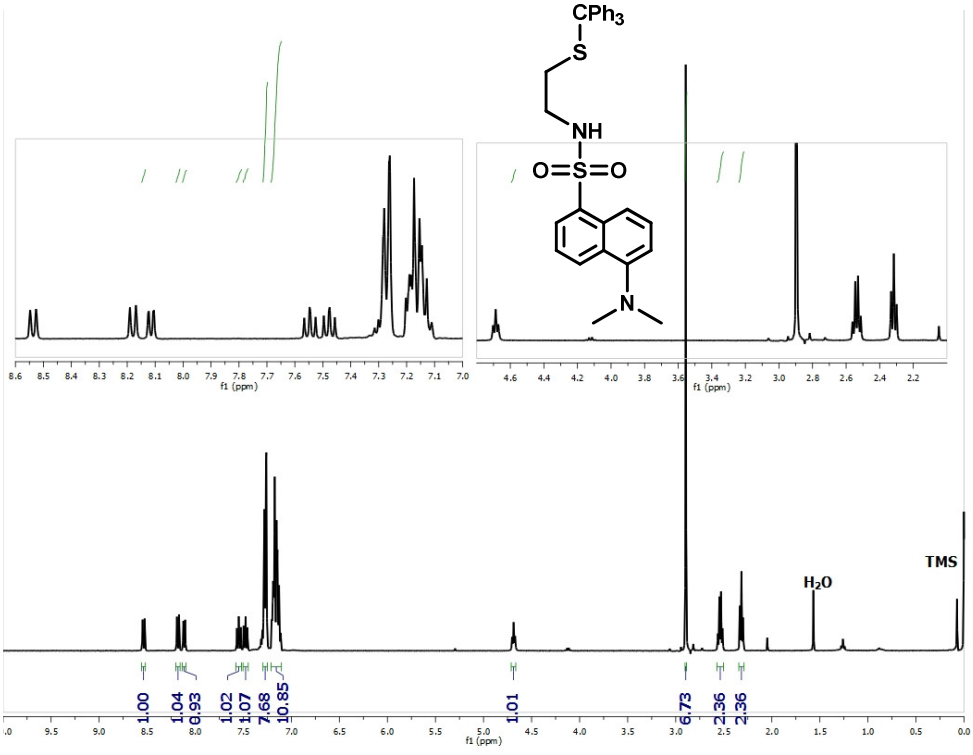

Figure A.25. ^1H NMR spectrum of **5** in $CDCl_3$ at 298 K.

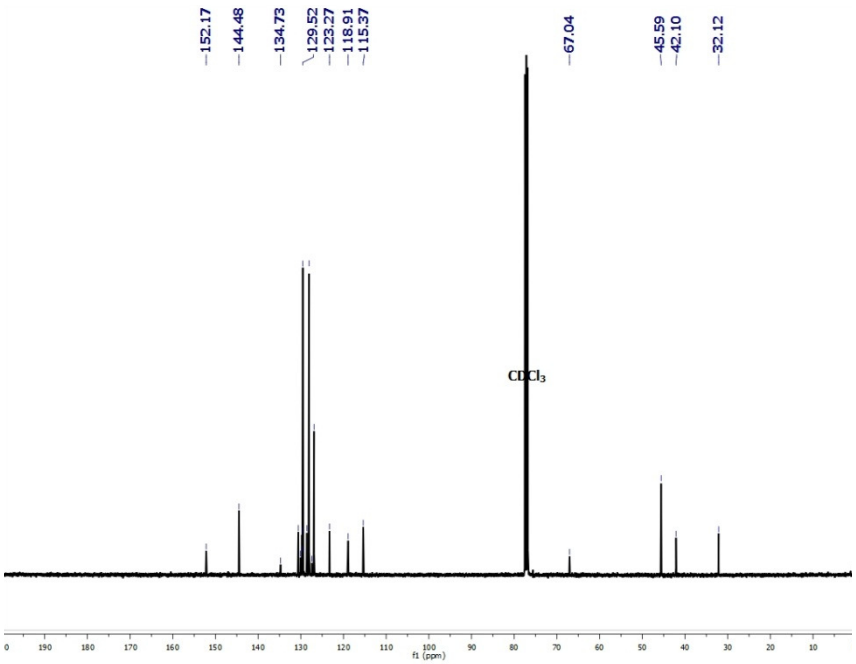

Figure A.26. ^{13}C NMR spectrum of **5** in $CDCl_3$ at 298 K.

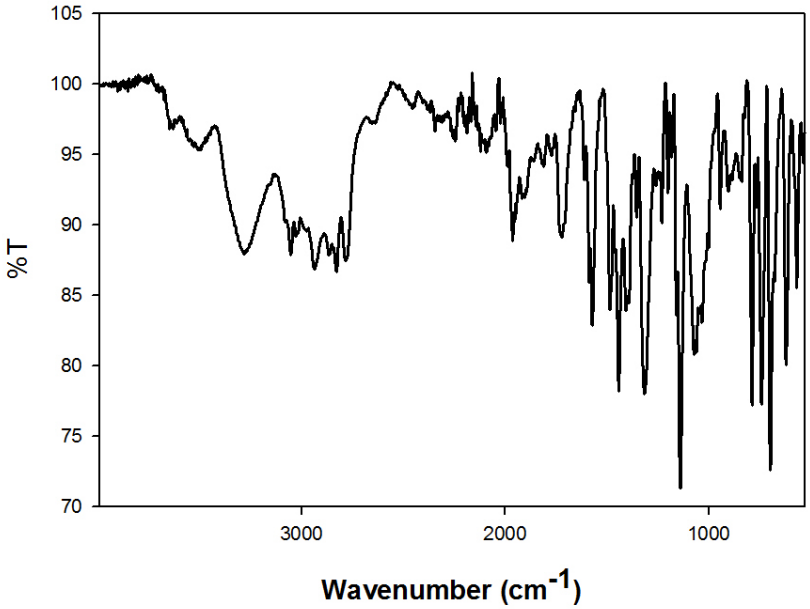

Figure A.27. Solid-state FTIR-spectrum (ATR-diamond) of **5**.

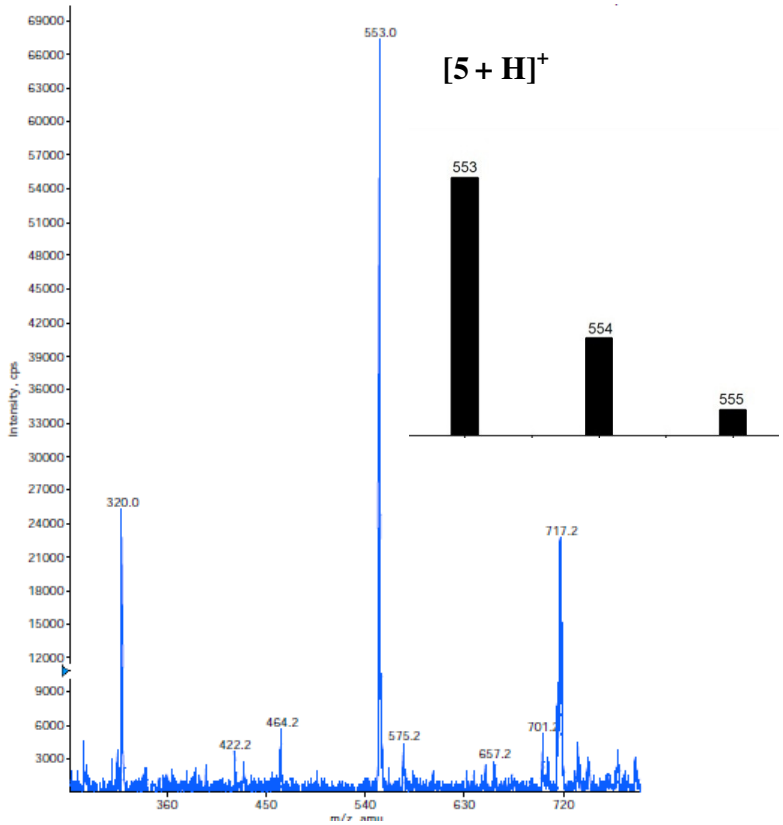

Figure A.28. Positive mode LRMS-ESI-MS of **5** showing parent peak at *m/z* = 553.0. Inset: calculated molecular weight and isotopic distribution of **5**.

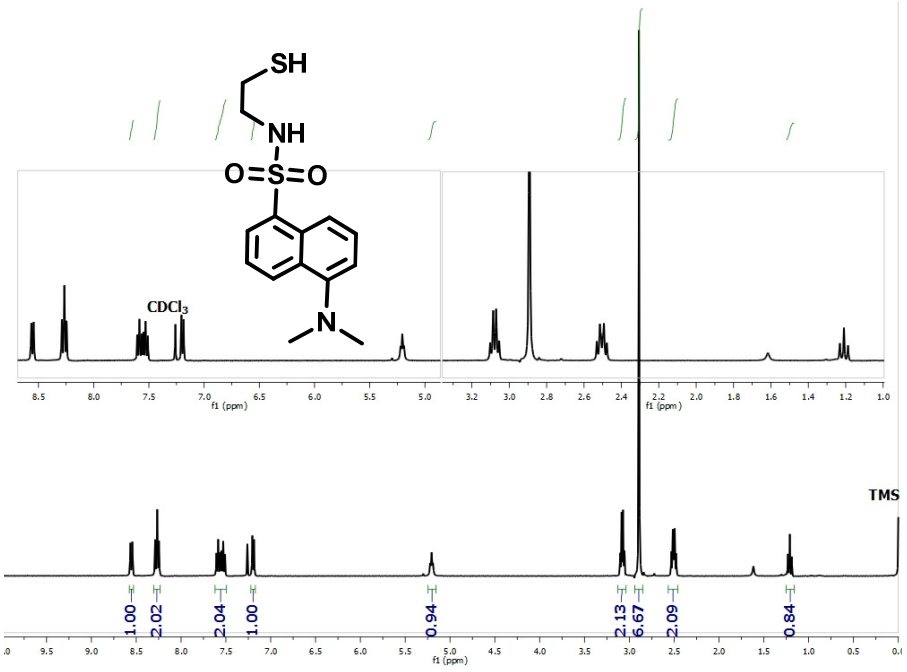

Figure A.29. ^{1}H NMR spectrum of **DNS5** in $CDCl_3$ at 298 K.

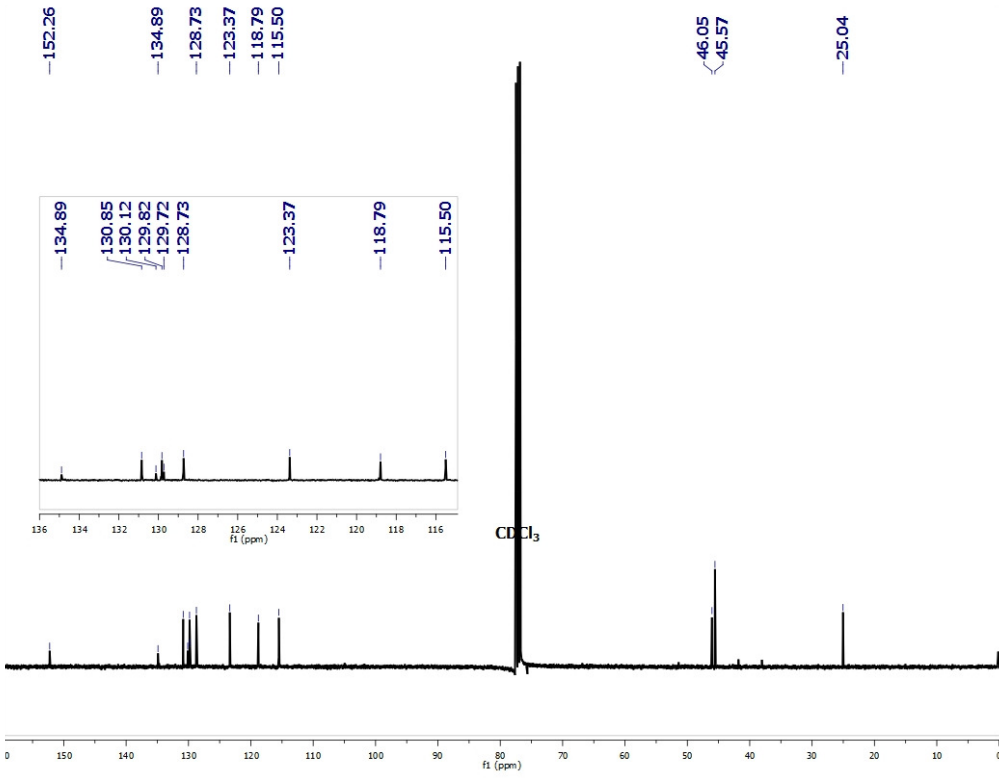

Figure A.30. ^{13}C NMR spectrum of **DNS5** in $CDCl_3$ at 298 K.

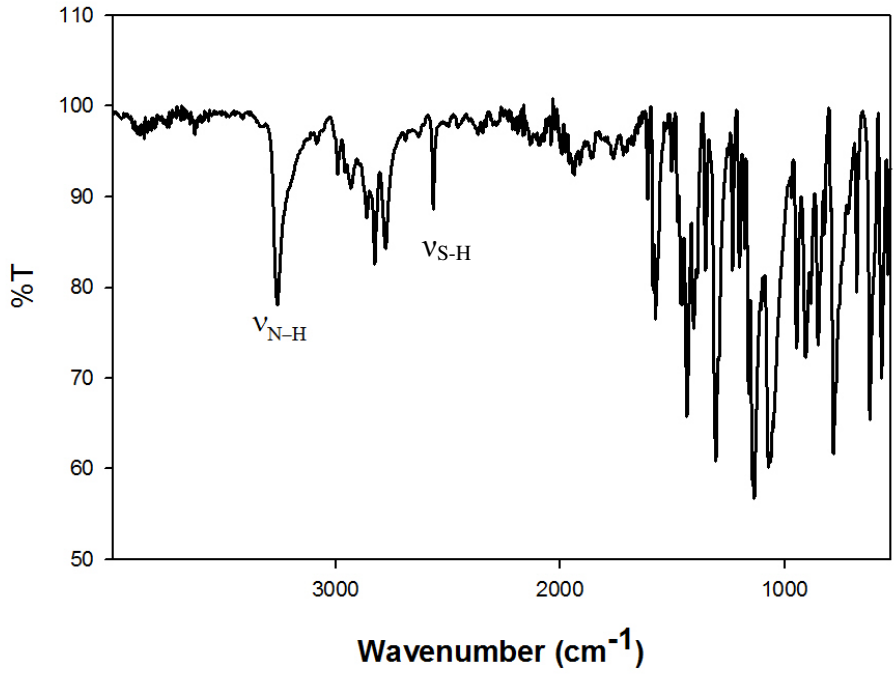

Figure A.31. Solid-state FTIR spectrum (ATR-diamond) of **DNS5**.

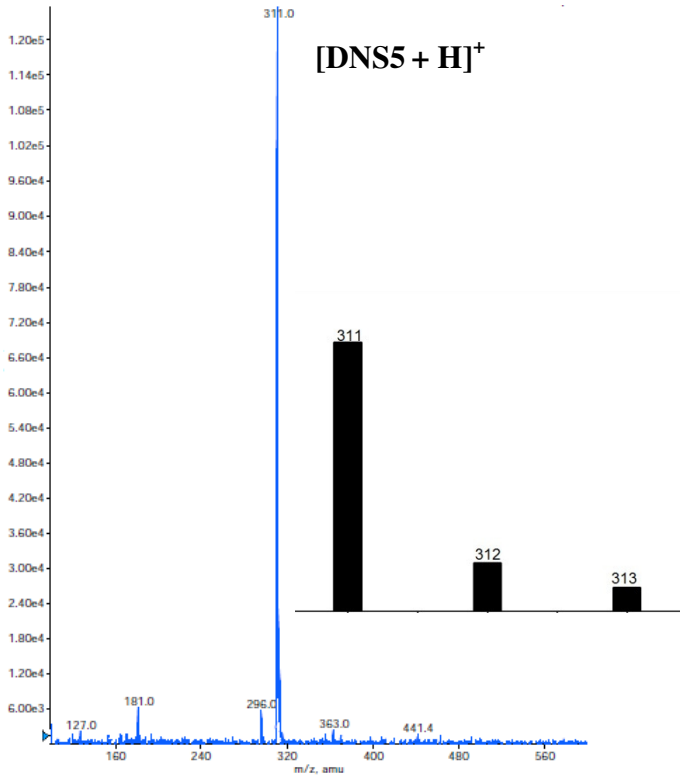

Figure A.32. Positive mode LRMS-ESI-MS of **DNS5** showing parent peak at *m/z* = 311.0. Inset: calculated molecular weight and isotopic distribution of **DNS5**.

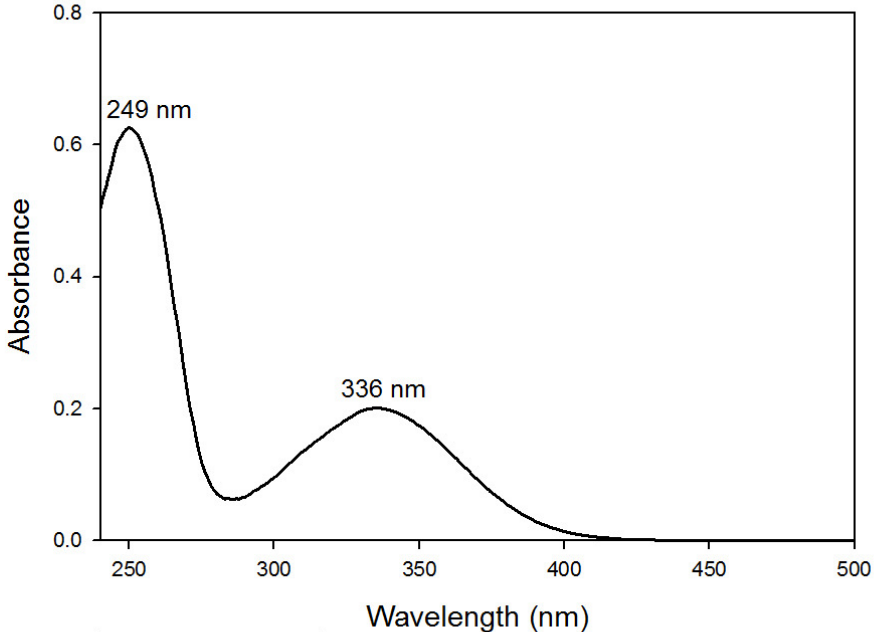

Figure A.33. UV-vis spectrum of 49.7 μM of **DNS5** in MeOH at 298 K.

Spectroscopic Measurements

Competition studies. $AsCl_3$ and AsI_3 were used to prepare the As^{3+} stock solutions. MeOH solutions of Na^+, Ca^{2+}, Mg^{2+}, Mn^{2+}, Fe^{2+}, Ni^{2+}, Cu^{2+}, Zn^{2+}, Pb^{2+}, and Cd^{2+} were prepared from their perchlorate salts, solutions of Fe^{3+} and Hg^{2+} were prepared from their chloride salts, and a solution of Co^{2+} was prepared from $[Co(H_2O)_6](BF_4)_2$. A typical measurement contained 3.3 μM **DNS5** containing 5 mol-equiv of base (Et_3N, 16.5 μM), while 10 mol-equiv of metal ions was used.

Quantum yield (Φ_f). Coumarin 1 (Φ_f = 0.70 in EtOH)[29] was used as a standard in the calculation of the quantum yield of **DNS5** and its reaction with Zn(II). Solutions of the samples and standards with absorbance values in the range of 0.010 – 0.018 at excitation maxima of the sample were prepared. The corrected emission spectra were obtained at 298 K with an excitation and emission slit width of 5 nm, an integrated value was obtained by measuring the area under the corrected emission spectrum from 346-600 nm. The quantum yield was calculated by the comparative method with the following equation:

$$\mathbf{QY_x = QY_s \bullet [A_x/A_s] \bullet [F_s/F_x] \bullet [n_x/n_s]^2}$$

*where **QY**: Quantum yield; **A**: integrated area under the corrected fluorescence spectrum; **F**: fraction of light absorbed ($1 - 10^{-D}$); **D**: absorbance (optical density); **n** = refractive indices of the solvent (EtOH = 1.3614; THF = 1.4072); **subscript x:** sample; **subscript s:** standard*

Fluorescence readings were obtained 30 min after the addition of the As^{3+} aliquot. All measurements were performed at least in triplicate, and we report the average.

X-ray Data Collection and Structure Refinement. Yellow single crystals of **DNS5** were grown by slow diffusion of hexane into a saturated solution of **DNS5** in CH_2Cl_2 at RT. A

suitable crystal was mounted and sealed inside a glass capillary. All geometric and intensity data were measured at 293 K on a Bruker SMART APEX II CCD X-ray diffractometer equipped with graphite-monochromatic Mo Kα radiation (λ = 0.71073 Å) with increasing ω (width 0.5° per frame) at a scan speed of 10 s/frame controlled by the SMART software package.[30] The intensity data were corrected for Lorentz-polarization effects and for absorption[31] and integrated with the SAINT software. Empirical absorption corrections were applied to structures using the SADABS program.[32] The structures were solved by direct methods with refinement by full-matrix least-squares based on F^2 using the SHELXTL-97 software[33] incorporated in the SHELXTL 6.1 software package.[34] The hydrogen atoms were fixed in their calculated positions and refined using a riding model. All non-hydrogen atoms were refined anisotropically. Selected crystal data and metric parameters for **DNS5** are summarized in Tables A.1 – A.2. Perspective views of the molecules were obtained using ORTEP.[35]

Table A.1. Summary of crystal data and intensity collection and structure refinement parameters for **DNS5**.

Parameters	**DNS5**
Formula	$C_{14}H_{18}N_2O_2S_2$
Formula weight	310.42
Crystal system	Monoclinic
Space group	P $2_1/_c$
Crystal color, habit	Yellow, rectangle
a, Å	11.0143(7)
b, Å	18.8381(12)
c, Å	7.4955(5)
α, deg	90
β, deg	102.356(1)
γ, deg	90
V, Å^3	1519.21(17)
Z	4
ρ_{calcd}, g/cm^{-3}	1.357
T, K	293
abs coeff, μ (Mo Kα), mm^{-1}	0.353
θ limits, deg	2.16 – 30.90
total no. of data	24598
no. of unique data	4779
no. of parameters	182
GOF on F^2	1.024
R_1,[a] %	5.90
wR_2,[b] %	15.73
max, min peaks e/Å^3	0.405, - 0.354

[a] $R_1 = \Sigma| |F_o| - |F_c| |/ \Sigma |F_o|$; [b] $wR_2 = \{\Sigma[w(F_o^2 - F_c^2)^2]/ \Sigma[w(F_o^2)^2]\}^{1/2}$

Table A.2. Selected bond distances (Å) and bond angles (deg) for **DNS5**.

Bond distances		**Bond angles (contd.)**	
H-bond S=O---N-H	2.965		
S(1)-O(1)	1.4267(19)	O(2)-S(1)-C(1)	106.79(10)
S(1)-O(2)	1.4343(17)	N(1)-S(1)-C(1)	108.20(10)
S(1)-N(1)	1.598(2)	C(2)-C(1)-C(6)	121.67(19)
S(1)-C(1)	1.776(2)	C(2)-C(1)-S(1)	119.31(16)
S(2)-C(14)	1.810(3)	C(6)-C(1)-S(1)	119.02(15)
C(1)-C(2)	1.367(3)	C(7)-C(6)-C(5)	118.97(18)
C(1)-C(6)	1.431(3)	C(7)-C(6)-C(1)	123.42(18)
C(6)-C(7)	1.417(3)	C(5)-C(6)-C(1)	117.57(17)
C(6)-C(5)	1.424(3)	C(4)-C(5)-C(6)	118.79(17)
C(5)-C(4)	1.421(3)	C(4)-C(5)-C(10)	121.64(18)
C(5)-C(10)	1.431(3)	C(6)C(5)-C(10)	119.50(17)
C(4)-C(3)	1.352(3)	C(3)-C(4)-C(5)	121.37(19)
N(2)-C(10)	1.420(3)	C(10)-N(2)-C(11)	113.08(19)
N(2)-C(11)	1.455(3)	C(10)-N(2)-C(12)	114.9(2)
N(2)-C(12)	1.457(3)	C(11)-N(2)-C(12)	110.5(2)
C(7)-C(8)	1.356(3)	C(8)-C(7)-C(6)	119.8(2)
C(10)-C(9)	1.368(3)	C(9)-C(10)-N(2)	123.07(19)
C(2)-C(3)	1.401(3)	C(9)-C(10)-C(5)	119.1(2)
C(8)-C(9)	1.402(3)	N(2)-C(10)-C(5)	117.79(19)
N(1)-C(13)	1.473(3)	C(1)-C(2)-C(3)	119.68(19)
C(13)-C(14)	1.492(4)	C(7)-C(8)-C(9)	121.7(2)
Bond angles		C(10)-C(9)-C(8)	120.7(2)
O(1)-S(1)-O(2)	118.65(12)	C(13)-N(1)-S(1)	124.02(19)
O(1)-S(1)-N(1)	108.45(12)	C(4)-C(3)-C(2)	120.82(19)
O(2)-S(1)-N(1)	106.34(11)	N(1)-C(13)-C(14)	111.5(2)
O(1)-S(1)-C(1)	108.03(10)	C(13)-C(14)-S(2)	114.5(2)

A.6 References

(1) Lim, N. C.; Schuster, J. V.; Porto, M. C.; Tanudra, M. A.; Yao, L.; Freake, H. C.; Brücker, C. *Inorg. Chem.* **2005,** *44*, 2018.

(2) Czarnik, A. W., Fluorescent Chemosensors for cations, anions and neutral analytes. In *Topics in Fluorescence Spectroscopy*, Lakowicz, J. R., Ed. Plenum Press: New York, **1994**; Vol. 4, pp 49 -70.

(3) Czarnik, A. W. *Acc. Chem. Res.* **1994,** *27*, 302.

(4) Fabbrizzi, L.; Poggi, A. *Chem. Soc. Rev.* **1995,** *24*, 197.

(5) de Silva, P. A.; Nimal Gunaratne, H. Q.; Gunnlaugsson, T.; Huxley, A. J. M.; McCoy, C. P.; Rademacher, J. T.; Rice, T. E. *Chem. Rev.* **1997,** *97*, 1515.

(6) Rurack, K.; Resch-Genger, U. *Chem. Soc. Rev.* **2002,** *31*, 116.

(7) de Silva, A. P.; Fox, D. B.; Huxley, A. J. M.; Moody, T. S. *Coord. Chem. Rev.* **2000,** *205*, 41.

(8) Prodi, L.; Bolletta, F.; Montalti, M.; Zaccheroni, N. *Eur. J. Inorg. Chem.* **1999**, 455.

(9) Li, Y.-H.; Chan, L.-M.; Tyer, L.; Moody, R. T.; Hirnel, C. M.; Hercules, D. M. *J. Am. Chem. Soc.* **1975,** *97*, 3118.

(10) Aoki, S.; Kawatani, H.; Goto, T.; Kimura, E.; Shiro, M. *J. Am. Chem. Soc.* **2001,** *123*, 1123.

(11) Walkup, G. K.; Imperiali, B. *J. Am. Chem. Soc.* **1997,** *119*, 3443.

(12) Bartzatt, R. *J. Pharmacol. Toxicol.* **2001,** *45*, 247.

(13) Burford, N.; Macdonald, C. L. B.; Parks, T. M.; Wu, G.; Borecka, B.; Kwiatkowski, W.; Cameron, S. T. *Can. J. Chem.* **1996,** *74*, 2209.

(14) Kavallieratos, K.; Rosenberg, J. M.; Chen, W.-Z.; Ren, T. *J. Am. Chem. Soc.* **2005,** *127*, 6514.

(15) Burford, N.; Parks, T. M.; Royan, B. W.; Borecka, B.; Cameron, S. T.; Richardson, J. F.; Gabe, E. J.; Hynes, R. *J. Am. Chem. Soc.* **1992,** *114*, 8147.

(16) Alonzo, G. *Inorg. Chim. Acta* **1983,** *73*, 141.

(17) Burford, N.; Parks, T. M.; Royan, B. W.; Richardson, J. F.; White, P. S. *Can. J. Chem.* **1992,** *70*, 703.

(18) Gale, E. M.; Patra, A. K.; Harrop, T. C. *Inorg. Chem.* **2009,** *48*, 5620.

(19) Koike, T.; Watanabe, T.; Aoki, S.; Kimura, E.; Shiro, M. *J. Am. Chem. Soc.* **1996,** *118*, 12969.

(20) Prodi, L.; Montalti, M.; Zaccheroni, N.; Dallavalle, F.; Folesani, G.; Lanfranchi, M.; Corradini, R.; Pagliari, S.; Marchelli, R. *Helv. Chim. Acta* **2001,** *84*, 690.

(21) Parola, J. A.; Lima, J. C.; Pina, F.; Pina, J.; de Melo, J. S.; Soiano, C.; García-España, E.; Aucejo, R.; Alarcón, J. *Inorg. Chim. Acta* **2007,** *360*, 1200.

(22) Branchi, B.; Ceroni, P.; Bergamini, G.; Balzani, V.; Maestri, M.; van Heyst, J.; Lee, S.-K.; Luppertz, F.; Vögtle, F. *Chem. Eur. J.* **2006,** *12*, 8926.

(23) Vögtle, F.; Gestermann, S.; Kauffmann, C.; Ceroni, P.; Vicinelli, V.; De Cola, L.; Balzani, V. *J. Am. Chem. Soc.* **1999,** *121*, 12161.

(24) Vögtle, F.; Gestermann, S.; Kauffmann, C.; Ceroni, P.; Vicinelli, V.; Balzani, V. *J. Am. Chem. Soc.* **2000,** *122*, 10398.

(25) Zhang, L.; Tang, B.; Ding, Y. *J. Agric. Food Chem.* **2005,** *53*, 549.

(26) Koley, A. P.; Nirmala, R.; Prasad, L. S.; Ghosh, S.; Manoharan, P. T. *Inorg. Chem.* **1992,** *31*, 1764.

(27) Fulmer, G. R.; Miller, A. J. M.; Sherden, N. H.; Gottlieb, H. E.; Nudelman, A.; Stoltz, B. M.; Bercaw, J. E.; Goldberg, K. I. *Organometallics* **2010,** *29*, 2176.

(28) Zanetta, J. P.; Vincendon, G.; Mandel, P.; Gombos, G. *J. Chrom. A* **1970,** *51*, 441.

(29) Quantum Yield was determined by absolute measurement made by Nanoco with an integrating sphere setup.

(30) *Smart v5.625: Software for the CCD Detector System*; Bruker AXS: Madison, WI, **2000**.

(31) Walker, N.; Stuart, D. *Acta Cryst.* **1983,** *A39*, 158.

(32) Sheldrick, G. M. *SADABS: Area Detector Absorption Correction*; University of Gottingen: Gottingen, Germany, **2001**.

(33) Sheldrick, G. M. *SHELX-97: Program for Refinement of Crystal Structures*; University of Gottingen: Gottingen, Germany, **1997**.

(34) Sheldrick, G. M. *SHELXTL 6.1, Crystallographic Computing Systems*; Siemens Analytical XRay Instruments: Madison, WI, **2000**.

(35) Johnson, C. K. *ORTEP III, Report ORNL-5138*; Oak Ridge National Laboratory: Oak Ridge, TN, **1976**.